COLD COLLISIONS OF METASTABLE NEON ATOMS

Kalte Stöße metastabiler Neon Atome

TECHNISCHE
UNIVERSITÄT
DARMSTADT

Vom Fachbereich Physik
der Technischen Universität Darmstadt

zur Erlangung des Grades
eines Doktors der Naturwissenschaften (Dr. rer. nat.)

genehmigte Dissertation von
M. Sc. Christian Cop
aus Bensheim

Referent: Prof. Dr. Reinhold Walser
Korreferent: Prof. Dr. Gerhard Birkl

Tag der Einreichung: 18.04.2017
Tag der Prüfung: 24.05.2017

Darmstadt 2017
D 17

In liebendem Gedenken
an meinen Vater
Fryderyk Cop

ABSTRACT

In this thesis we investigate theoretically the cold collision properties of metastable neon (Ne*). The collisions of metastable rare gases (Rg*) exhibit a plethora of interesting phenomena: Due to the high internal excitation energies of the metastable atoms ionization processes are very likely. The produced ions can be detected with single-ion efficiency in the experiment. In experiments with atomic Rg* gases at cold temperatures $T \simeq 1$ mK, this allows for *in-situ* monitoring of the real-time dynamics of the atomic gas and for example for the study of two-particle correlations. Furthermore, in cold Rg* gases one can examine the prospects of creating a Bose-Einstein condensate or a degenerate Fermi gas of Rg*. Ne* is a promising candidate for Bose-Einstein condensation and in the group of *G. Birkl* the properties of cold gases of Ne* are investigated experimentally. Two-body loss rate coefficients due to the ionization processes and elastic cross sections have been measured [1–5]. It is useful to complement the experimental measurements with a theoretical study in order to obtain a better understanding of the cold Ne* gases and the collision physics of Ne*.

At the low temperatures of the atomic gases, these gases are dilute with particle number densities of $n \simeq 10^9$ cm^{-3}. For these low densities, the behavior of the gas is determined mainly by two-body collision physics which is solved by quantum scattering theory in terms of the S matrix. The collision physics is given by short-range interactions and long-range interactions of the atoms. The short-range interaction potentials of Ne* have been calculated in [6] and the long-range interaction potentials in [7–9] in the molecular basis of Ne_2.

In this thesis we first calculate short-range and long-range interactions of atoms and molecular basis states of diatomic molecules with a simpler electronic structure than Ne* and Ne_2 in order to introduce the notation and to discuss the characteristics of the calculated molecular interaction potentials and in order to employ them in the scattering calculations for Ne*. Instead of solving the full scattering equations by taking into account all the molecular interaction potentials, we demonstrate that the collision physics of Ne* can be described in terms of a coupled two-channel model with a single interaction potential only which describes the elastic scattering of Ne*. In this model, ionization in Ne* collisions is described by the transition of the upper elastic interaction channel to the lower channel, representing the loss or ionization channel. We introduce two versions of the two-channel model in this work.

In the first version, the two channels are given by square-well potentials. We can solve the scattering equations analytically and for complex wave numbers k and study the solutions in the complex k plane. With an expansion of the S matrix in terms of its poles in the complex k plane we find a parametrization of the two-body loss rate coefficients. We show that these coefficients describe ionizing collisions of Ne* by comparing them to the experimental measurements and to the numerical results obtained by the two-channel model in the second version.

In this second version of the two-channel model, the elastic scattering channel is given by a realistic interaction potential of Ne*, consisting of a calculated short-range and long-range molecular potential, and the loss channel by a model ionization potential. For this model we calculate the two-body loss rate coefficients and the elastic cross sections for the isotope mixtures of Ne* which have been measured experimentally and demonstrate that the free potential parameters can be optimized to the experimental data to achieve very good agreement of the numerical results with the experimental measurements. We discuss the validity of the two-channel model by comparing the results to existing models for cold Rg* collisions and find that the two-channel model of this work is a useful extension to these models.

ZUSAMMENFASSUNG

In dieser Arbeit untersuchen wir theoretisch die kalten Stoßeigenschaften von metastabilem Neon (Ne*). Stöße von metastabilen Edelgasen (Rg*) zeigen eine Vielzahl interessanter physikalischer Phänomene: Durch die hohe Anregungsenergie der metastabilen Atome kommt es bei Stößen mit hoher Wahrscheinlichkeit zu Ionisation. Die entstehenden Ionen können im Experiment mit Einzelionen-Sensitivität detektiert werden. In kalten atomaren Rg* Gasen mit Temperaturen $T \simeq 1$ mK wird es dadurch möglich, die Dynamik des Gases in Echzeit zu beobachten und zum Beispiel Zwei-Teilchen-Korrelationen zu untersuchen. Ebenfalls kann man in den kalten atomaren Rg* Gasen die Möglichkeit untersuchen, Bose-Einstein Kondensate oder entartete Fermi-Gase zu erzeugen. Ne* ist ein vielversprechender Kandidat für Bose-Einstein Kondensation und die Arbeitsgruppe von *G. Birkl* untersucht daher experimentell die Eigenschaften kalter atomarer Ne* Gase. Im Experiment wurden Zwei-Körper-Verlustraten-Koeffizienten durch Ionisationsprozesse und elastische Streuquerschnitte gemessen [1–5]. Die vorliegende Arbeit soll die experimentellen Messungen mit einer theoretischen Untersuchung komplementieren, um ein besseres Verständnis der Eigenschaften der Ne* Gase und der Stoßeigenschaften von Ne* zu erhalten.

Bei den niedrigen Temperaturen der atomaren Gase sind diese mit Teilchenzahldichten von $n \simeq 10^9$ cm^{-3} stark verdünnt. Deren Verhalten ist dann durch die Zwei-Körper-Stoßphysik bestimmt, die in der Streutheorie durch die S Matrix beschrieben wird. Die Stoßphysik ist zum einen gegeben durch kurzreichweitige Wechselwirkungen und zum anderen durch langreichweitige Wechselwirkungen der Atome. Die kurz- und langreichweitigen Wechselwirkungspotenziale für Ne* wurden in der molekularen Basis von Ne_2 in [6] und in [7–9] bestimmt.

Um die Notation dieser Wechselwirkungspotenziale einzuführen, deren Charakteristiken zu diskutieren und um diese Potenziale in den Streurechnungen für Ne* zu verwenden, berechnen wir in der vorliegenden Arbeit zunächst kurzreichweitige und langreichweitige Wechselwirkungen von Atomen und molekulare Zustände von diatomaren Molekülen die eine einfachere elektronische Struktur als Ne* und Ne_2 aufweisen. Wir werden in dieser Arbeit zeigen, dass man anstatt die vollen Streugleichungen inklusive aller Wechselwirkungspotenziale lösen zu müssen, die Streuphysik von Ne* durch ein Zwei-Kanal-Modell beschreiben kann, indem nur ein einziges Wechselwirkungspotenzial zur Beschreibung der elastischen Streuung von Ne* verwendet wird. In diesem Modell werden die Ionisationsprozesse in Stößen von Ne* durch den Übergang von oberem elastischen Streukanal zu unterem Kanal, der den Ionisations- oder Verlustkanal darstellt, beschrieben. Wir stellen dieses Modell in zwei verschiedenen Varianten vor.

In der ersten Variante sind die zwei Kanäle durch Kastenpotenziale gegeben. Wir können die Streugleichungen für dieses Modell analytisch und für komplexe Wellenzahlen k lösen und die Lösungen in der komplexen k Ebene untersuchen. Mit einer Entwicklung der S Matrix durch ihre Pole in der komplexen k Ebene parametrisieren wir die Zwei-Körper-Verlustraten-Koeffizienten. Wir zeigen, dass diese Koeffizienten die Ionisation in Ne* Stößen beschreiben, indem wir sie mit den experimentellen Messungen und den Resultaten des Zwei-Kanal-Modells in seiner zweiten Variante vergleichen.

In dieser zweiten Variante des Zwei-Kanal-Modells ist der elastische Streukanal durch ein realistisches Potenzial für Ne*, bestehend aus bekanntem kurz- und langreichweitigen Wechselwirkungspotenzial, und der Verlustkanal durch ein Modell-Ionisationspotenzial gegeben. Für dieses Modell berechnen wir die Zwei-Körper-Verlustraten-Koeffizienten und elastischen Streuquerschnitte für die im Experiment untersuchten Isotopen-Mischungen von Ne*. Eine Optimierung der freien Potenzial-Parameter an die experimentellen Daten führt zu einer sehr guten Übereinstimmung der berechneten und gemessenen Streuraten. Wir diskutieren die Gültigkeit des Zwei-Kanal-Modells, indem wir es mit bereits vorhandenen Modellen zur Beschreibung von Rg* Stößen vergleichen und zeigen, dass das Zwei-Kanal-Modell der vorliegenden Arbeit eine nützliche Erweiterung der vorhandenen Modelle darstellt.

CONTENTS

1

INTRODUCTION

At very low temperatures of atomic gases of bosons a phase transition of the thermal gas to a Bose-Einstein Condensate (BEC) was predicted in 1924/1925 by Bose and Einstein [10, 11]. The BEC is a peculiar state where all bosons reside in the same quantum state [12]. The critical temperature for the phase transition of a uniform three-dimensional gas with non-interacting bosons reads [12]

$$T_c = \frac{2\pi}{(\zeta(3/2))^{2/3}} \frac{\hbar n^{3/2}}{m k_B}, \tag{1.1}$$

where ζ is the Riemann zeta function [13], n is the particle number density and m is the particle mass. A typical value of T_c is given for sodium, by $T_c \simeq 2\ \mu\text{K}$ for a particle density of $n = 10^{14}\ \text{cm}^{-3}$ [14]. Due to new methods of cooling and trapping atoms with laser light developed in the seventies and eighties and due to the invention of evaporative cooling [15,16] it became possible to cool gases of alkali atoms close to T_c [17]. This triggered much experimental effort to investigate the prospects to achieve a Bose-Einstein condensate of alkali atoms. The first BECs were created and observed experimentally in 1995 for ^{87}Rb and ^{23}Na [14, 18]. The invention of the new methods of cooling and trapping were rewarded in 1997 [19–21] and the first experimental observations of a BEC in 2001 [22, 23] with the noble prize of physics.

Besides the investigation of the prospects of cooling cold gases of alkali atoms below T_c, exciting physics emerged from cooling atomic gases of metastable rare gases (Rg*). These experiments have been started in the 1980s with the lightest elements of this species namely with He* [24] and Ne* [25]. The Rg* atoms possess large internal energies (~ 20 eV) which stands in contrast to their relative kinetic energies at very low temperatures ($\sim 10^{-10}$ eV). Due to the high internal energies, ionization collisions become very likely and the dominant processes are Penning Ionization (PI) and Associative Ionization (AI) which are given by [26,27]

$$\begin{aligned} \text{PI}: &\quad \text{Rg}^* + \text{Rg}^* \longrightarrow \text{Rg} + \text{Rg}^+ + \text{e}^-, \\ \text{AI}: &\quad \text{Rg}^* + \text{Rg}^* \longrightarrow \text{Rg}_2^+ + \text{e}^-. \end{aligned} \tag{1.2}$$

Typically in the experiment, there is no discrimination between PI and AI processes so that we refer to both as PI. Ions originated from PI can be easily detected spatially and temporally and therefore experiments with metastable rare gases allow for *in-situ* monitoring of dynamics of the cold gases and of two-particle correlations. The two-particle correlation *Hanbury Brown and Twiss* (HBT) effect has been demonstrated for Ne* [28] for thermal bosons and for He* for both thermal bosons and fermions [29].

In 2001 the first BEC of the metastable rare gases was demonstrated for He* [30–32] and a few years later also a degenerate Fermi gas of He* was observed [33] which is the analog of a BEC for fermions. This success for He* was achieved by spin-polarizing the atoms. This is an efficient technique as due to the *Wigners spin conservation rule*, spin is conserved during the collision [34]. Therefore, the PI process is forbidden for spin-polarized atoms as can be seen by the reaction equation for PI

$$\begin{array}{ccccccccc} \text{Rg}^* & + & \text{Rg}^* & \longrightarrow & \text{Rg} & + & \text{Rg}^+ & + & e^-, \\ s=1 & + & s=1 & \longrightarrow & s=0 & + & s=\frac{1}{2} & + & s=\frac{1}{2}, \end{array} \tag{1.3}$$

where the total spin S of the left-hand side of the PI reaction for spin-polarized atoms is $S = 2$ but on the right-hand side can only be $S \leq 1$ and spin is not conserved. This suppression of PI due to spin-polarization of the atoms was demonstrated in the experiment early for

He* [35] and later for Ne* [2]. The possibility of suppressing the ionization processes in Ne* collisions triggered the experimental investigation of the possibility to condense Ne* to quantum degeneracy. The group of *G. Birkl* [1] at the TU Darmstadt has collected a large amount of experimental data on the collisions properties of the three different stable isotopes of ^{20}Ne, ^{21}Ne and ^{22}Ne [1–5]. A major goal of this work is the theoretical study of the collision properties of Ne* by taking into account the experimental results in order to describe the properties of the cold atomic Ne* gases.

THEORETICAL WORK ON METASTABLE RARE GAS COLLISIONS

The theoretical work on metastable rare gas collisions is based on quantum scattering theory [36–38] as the magneto-optically, magnetically or optically trapped atoms are in a very dilute gas phase. In dilute gases, the properties of the gas are mainly dominated by two-body interactions. In order to understand these two-body interactions one has to start by studying the single atom physics and the diatomic molecular physics on a microscopic level [39–43]. The two-body scattering states are expanded in molecular states in molecular theory [44–46] and in the resulting *coupled-channel equations* the interaction potentials of the diatomic molecules appear. These potentials consist of a short-range part given by the exchange forces in the diatomic molecule [47] and a long-range part governed by the interaction of the multipoles of the electrostatic interaction potential between the atoms [48]. At low relative collision energies of the atoms only a few partial waves contribute to the scattering rates [49–53]. For these partial-wave contributions the *Bethe-Wigner threshold laws* [54,55] apply which have been studied for collisions in cold atomic gases in [50]. Instead of solving the full *coupled-channel equations* by taking into account the multitude of molecular potentials occurring due to the atom–atom interactions, models have been developed to parametrize cold collisions of atoms.

A widely used model to describe cold collisions of metastable rare gases is the *quantum reflection model* [56–59]. The colliding atoms possess high internal energies and therefore the probability of undergoing the highly exothermic PI process is very high when the electron orbitals of the colliding atoms overlap. The basic assumption of the *quantum reflection model* is a 100 % ionization probability at short-range. In this case, the short-range part of the potential does not influence the scattering physics which then is solely determined by the long-range potential. As the long-range part is not very sensitive to changes in isotopic mass, the scattering rates become universal and independent of the specific isotope or of the scattering length. Therefore, the *quantum reflection model* is also called the *universal model* [60]. It was suggested by the experiment that Ne* collisions are not universal [2] which was also addressed in [5].

In [61, 62] the *quantum reflection model* was generalized to the case where the ionization probability at short-range is assumed to be less than unity. In this case, the short-range part of the potentials becomes important and is dependent on reduced mass and scattering length and the scattering rates are non-universal. This so-called *non-universal model* parametrizes the scattering rates in the threshold limit $T \to 0$ in two parameters only. The results of [60–62] are based on an analysis of *Multichannel Quantum Defect Theory* (MCQDT) [63–66] which has been evolved in the recent years to be applicable for slow atomic collisions [67, 68] and molecular collisions [69] and serves as an alternative to the standard approach of solving the full *coupled-channel equations*.

In the experiment, the collision properties of Ne* have been measured experimentally for cold Ne* gases at temperatures $T \simeq 1$ mK which is not in the threshold limit. In order to describe these properties we introduce as an alternative approach to these models a coupled two-channel model with a single interaction channel and a single ionization channel. Elastic scattering is described by the interaction channel and ionizing collisions are given by the transition of interaction channel to ionization channel. We introduce this two-channel model for Ne* collisions in two variations. In the first model the two channels are given by square-well potentials and in the second model by a realistic molecular interaction potential of Ne* and a model ionization potential. Molecular interaction potentials are classified due to five *Hund's coupling cases* $(a) - (e)$ [47, 70, 71]. The molecular interaction potentials of Ne* have

1 http://www.iap.tu-darmstadt.de/apq/

been calculated at short-range in the molecular *Hund's case* (a) basis [6] and at long-range in the molecular *Hund's case* (c) basis [7–9] of Ne_2. In order to employ a molecular interaction potential of Ne* in the scattering calculation we first have to introduce these molecular basis states and illustrate the origin of these potentials. We structure the work as follows.

OUTLINE

In chapter 2 we start with the discussion of one-electron atoms. Complex and real solutions to the Schrödinger equation are given which are the atomic orbitals. These one-electron atomic orbitals will be employed throughout this thesis in order to calculate interaction energies of atoms at short-range and long-range. Furthermore, we introduce in this chapter the *Hartree-Fock equations* and the numerical methods we use to solve them in order to obtain molecular interaction potentials.

In chapter 3 we discuss the short-range interactions of atoms which are given by the molecular potentials of the diatomic system. In order to introduce the molecular potentials of Ne* we give the *Born-Oppenheimer approximation* and the Linear Combination of Atomic Orbitals (LCAO) method which is an important approximation method to calculate the potential energies. With the solutions for H_2^+ and H_2 we introduce the symmetries and the notation for the molecular states and potentials and the different *Hund's cases*. Furthermore, we introduce the *Heitler-London* (HL) method as an alternative approach to calculate molecular orbitals and potential energies and discuss the advantages and disadvantages of the LCAO and HL method with regard to their applicability at short-range and long-range.

In chapter 4 we derive the different types of long-range interactions between atoms by a multipole expansion of the electrostatic interaction energy. In Ne* collisions, the *van der Waals* interaction dominates the long-range physics. We introduce this type of interaction by calculating the *van der Waals* energy explicitly for ground state interactions of hydrogen and helium in an atomic basis. This introduces the *van der Waals* coefficient c_6.

In chapter 5 we give an overview of the basic concepts of quantum scattering theory as the atomic collision process is solved by quantum scattering theory. Of particular importance for this work are the analytic properties of the S matrix for complex wave numbers as in the two-channel model with square-well potentials we will parametrize the inelastic processes of Ne* in terms of a pole expansion of the S matrix in the complex k plane. Equally important is the derivation of the inelastic cross sections and two-body loss rate coefficients for identical and non-identical bosons/fermions with spin into a loss channel as this is used in the two-channel model with the realistic interaction potential to calculate homonuclear and heteronuclear collision properties of Ne*.

In chapter 6 we introduce the molecular potentials of Ne*. First, we study the atomic properties of Ne* and then the diatomic properties. We set up the scattering equations for Ne* in terms of the molecular basis and derive expressions for the two-body loss rate coefficients in this basis.

In chapter 7 we introduce the coupled two-channel model with square-well potentials. For weak couplings, the two-channel solutions are given in terms of the uncoupled single-channel solutions. Therefore, we first study the single-channel S matrix in terms of its poles the complex k plane before we generalize the results to the two-channel case. From the pole-expansion of the S matrix we derive a parametrization of the two-body loss rate coefficients.

In chapter 8 we introduce the two-channel model for Ne* collisions with a realistic interaction potential and a model ionization potential. We fit the free parameters of this model to the experimental data points and calculate elastic cross sections and two-body loss rate coefficients for both homonuclear and heteronuclear collisions of Ne* of the different isotope mixtures available in the experiment. The results are compared to the results of the *quantum reflection model*, the *non-universal model* and the two-channel model with square-well potentials.

In chapter 9 we conclude and discuss the results of this thesis and the future prospects of the theoretical work as well as of the experimental work on Ne*.

2

SINGLE-ATOM PHYSICS

In this chapter we investigate the properties of single atoms in order to understand the atomic properties of Ne*. We start with the simplest case, the one-electron atoms, with the special case of hydrogen. The solutions of the Schrödinger equation are the well-known hydrogen-like orbitals which can be complex or real. These orbitals will be employed throughout this work in order to calculate interaction energies of atoms. We then introduce the spin in the system as the spin-orbit coupling is important in Ne*. For many-electron systems we explain the spectroscopic notation in *Russel-Saunders* notation which is applicable for some atomic states of Ne*. For the calculation of molecular interaction potential energies of many-electron systems we introduce at the end of this chapter the *Hartree-Fock equations* and discuss briefly the numerical methods which we apply throughout this thesis for calculating molecular potential energies.

2.1 ONE-ELECTRON ATOMS

The simplest one-electron atom is the hydrogen atom which has been object to intense theoretical and experimental studies. Its properties, including non-relativistic and relativistic effects, are well-understood [72–74]. The analytic solutions of the Schrödinger equation hold generally for hydrogen-like atoms in the Coulomb field of the nucleus with charge Z. In this work, we study the solutions of the hydrogen-like atoms not only as an example to illustrate the idea of spin-orbitals and to explain the spin-orbit coupling but also as a starting point for examining the properties of the more complex system Ne*.

2.1.1 *Hydrogen-like orbitals*

For solving the Schrödinger equation for hydrogen-like atoms we follow [40]. The time-independent Schrödinger equation for hydrogen-like atoms in position space reads

$$H_0(\mathbf{r})\varphi(\mathbf{r}) = E\varphi(\mathbf{r}), \tag{2.1}$$

with E the energy of the system. Here, $H_0(\mathbf{r})$ in atomic units (see appendix A) is given by

$$H_0(\mathbf{r}) = -\frac{1}{2}\nabla_{\mathbf{r}}^2 - \frac{Z}{r}, \tag{2.2}$$

with Z the nuclear charge. Note that this equation is general for a single-electron atom with nuclear charge Z. For $Z = 1$ we recover the solutions of hydrogen. The Laplace operator in spherical coordinates reads

$$\nabla_{\mathbf{r}}^2 = \frac{1}{r^2}\frac{\partial}{\partial r}\left(r^2\frac{\partial}{\partial r}\right) + \frac{1}{r^2\sin\theta}\frac{\partial}{\partial\theta}\left(\sin\theta\frac{\partial}{\partial\theta}\right) + \frac{1}{r^2\sin^2\theta}\left(\frac{\partial^2}{\partial\varphi^2}\right). \tag{2.3}$$

The angular dependence of the Laplacian on the polar angle θ and on the azimuthal angle ϕ is given by the square of the orbital angular momentum operator $\mathbf{L}$, reading

$$\mathbf{L}^2 = -\left(\frac{1}{\sin\theta}\frac{\partial}{\partial\theta}\left(\sin\theta\frac{\partial}{\partial\theta}\right) + \frac{1}{\sin^2\theta}\frac{\partial^2}{\partial\varphi^2}\right). \tag{2.4}$$

After inserting this expression for $\mathbf{L}^2$ in (2.3) and the result in the Schrödinger equation (2.1) we obtain

$$\left(-\frac{1}{2r^2}\frac{\partial}{\partial r}\left(r^2\frac{\partial}{\partial r}\right) + \frac{\mathbf{L}^2}{2r^2} - \frac{Z}{r}\right)\varphi(\mathbf{r}) = E\varphi(\mathbf{r}). \tag{2.5}$$

This differential equation can be transformed in a radial Schrödinger equation by separating radial and angular coordinates. The separation ansatz reads

$$\varphi_{nlm_l}(r,\theta,\varphi) = R_{nl}(r)Y_{lm_l}(\theta,\varphi). \tag{2.6}$$

with the radial wave function R_{nl} and the spherical harmonics Y_{lm_l} [13]. The wave functions φ_{nlm_l} are the so-called hydrogen-like orbitals. For the principal quantum number $n = 0, 1, 2, 3$ they are called s, p, d, f-orbitals, respectively. The radial wave function R_{nl} fulfills the boundary condition

$$\lim_{r\to 0} rR_{nl}(r) = 0. \tag{2.7}$$

The spherical harmonics are eigenfunctions of the square of the angular momentum operator $\mathbf{L}^2$ and of the z-component L_z and the eigenvalue equations reads

$$\mathbf{L}^2 Y_{lm_l} = l(l+1)Y_{lm_l}, \quad L_z Y_{lm} = m_l Y_{lm_l} \tag{2.8}$$

with the eigenvalues $l(l+1)$ and m_l. The projection m_l is the projection of the orbital angular momentum on the quantization axis. Note that the spherical harmonics have definite parity under the inversion operation i on the electron coordinates at the origin. They transform as

$$\mathcal{P}_i Y_{lm_l}(\theta,\varphi) = Y_{lm_l}(\pi-\theta,\varphi+\pi) = (-1)^l Y_{lm_l}(\theta,\varphi), \tag{2.9}$$

In general, the spherical harmonics are complex functions and read [40]

$$Y_{lm_l}(\theta,\varphi) = \sqrt{(-1)^{m_l+|m_l|}}\sqrt{\frac{2l+1}{4\pi}\frac{(l-m_l)!}{(l+m_l)!}}P_l^{|m_l|}(\cos\theta)e^{im_l\varphi}, \tag{2.10}$$

where $P_l^{m_l}(\cos\theta)$ are the associated Legendre polynomials [13].

Reduced radial Schrödinger equation

If we introduce the radial function ψ_{nl} by the relation

$$R_{nl}(r) = \frac{\psi_{nl}(r)}{r}, \tag{2.11}$$

and use the ansatz (2.6) we can transform the Schrödinger equation (2.5) into the reduced radial Schrödinger equation for ψ_{nl}. Elimination of the angular part by using the eigenvalue equation (2.8) leads to

$$\frac{1}{2}\psi_{nl}''(r) + \left(E + \frac{Z}{r} - \frac{l(l+1)}{r^2}\right)\psi_{nl}(r) = 0. \tag{2.12}$$

For hydrogen-like systems, the reduced radial Schrödinger equation can be solved analytically. We do not carry out the detailed calculation but simply give the result for $\psi_{nl}(r)$ which reads [40]

$$\psi_{nl}(r) = \sqrt{\frac{(n-l-1)!Z}{n^2[(n+l)!]^3}}\left(\frac{2Zr}{n}\right)^{l+1}e^{-Zr/n}L_{n+l}^{2l+1}\left(\frac{2Zr}{n}\right), \tag{2.13}$$

where L_{n+l}^{2l+1} are the Laguerre polynomials [40]. With the explicit forms of the Laguerre polynomials we give in table 2.1 the expressions for the hydrogen-like orbitals $\varphi_{nlm_l}(r,\theta,\varphi)$ for all quantum numbers (nlm_l) up to $n \leq 3$. The energy of the hydrogen only depends on the principal quantum number n, reading [72]

$$E_n = -Z^2/2n^2. \tag{2.14}$$

The energy eigenvalues are independent of the orbital quantum numbers l and m_l and thus degenerate for a given n. The orbital angular momentum number takes the values $l = 0, \ldots, n-1$ while its projection on the quantization axis m_l can take the values $-l, \ldots, +l$.

n	l	m_l	spectroscopic notation	wave functions orbitals	energy
1	0	0	$1s$	$Z^{3/2}\frac{1}{\sqrt{\pi}}\cdot e^{-q}$	$-Z^2/2$
2	0	0	$2s$	$Z^{3/2}\frac{1}{\sqrt{32\pi}}\cdot e^{-q/2}\cdot(2-q)$	$-Z^2/8$
2	1	0	$2p_0$	$Z^{3/2}\frac{1}{\sqrt{32\pi}}\cdot e^{-q/2}\cdot q\cos\theta$	
2	1	±1	$2p_{\pm1}$	$\mp Z^{3/2}\frac{1}{\sqrt{64\pi}}\cdot e^{-q/2}\cdot q\sin\theta\, e^{\pm i\varphi}$	
3	0	0	$3s$	$Z^{3/2}\frac{1}{81\sqrt{3\pi}}\cdot e^{-q/3}\cdot\left(27-18q+2q^2\right)$	$-Z^2/18$
3	1	0	$3p_0$	$Z^{3/2}\frac{1}{81}\sqrt{\frac{2}{\pi}}\cdot e^{-q/3}\cdot\left(6q-q^2\right)\cos\theta$	
3	1	±1	$3p_{\pm1}$	$Z^{3/2}\frac{1}{81\sqrt{\pi}}\cdot e^{-q/3}\cdot\left(6q-q^2\right)\sin\theta\, e^{\pm i\varphi}$	
3	2	0	$3d_0$	$Z^{3/2}\frac{1}{81\sqrt{6\pi}}\cdot e^{-q/3}\cdot q^2\left(3\cos^2\theta-1\right)$	
3	2	±1	$3d_{\pm1}$	$\mp Z^{3/2}\frac{1}{81\sqrt{\pi}}\cdot e^{-q/3}\cdot q^2\sin\theta\cos\theta\, e^{\pm i\varphi}$	
3	2	±2	$3d_{\pm2}$	$Z^{3/2}\frac{1}{162\sqrt{\pi}}\cdot e^{-q/3}\cdot q^2\sin^2\theta\, e^{\pm 2i\varphi}$	

Table 2.1: Hydrogen-like orbitals $\varphi_{nlm}(r,\theta,\varphi)$ for $n\leq 3$, with $q\equiv Zr$ [40]. The energy eigenvalues only depend on the principal quantum number n and are given in E_h (see appendix A).

Real hydrogen-like orbitals

In general, the hydrogen-like orbitals are complex because the spherical harmonics defined in equation (2.10) are complex functions. By a suitable linear superposition of the hydrogen-like orbitals we can generate real orbitals. As an example, we construct real p-orbitals by [72]

$$np_x(\mathbf{r}) = \frac{1}{\sqrt{2}}\left[\varphi_{n,1,-1}(\mathbf{r}) - \varphi_{n,1,1}(\mathbf{r})\right], \tag{2.15a}$$

$$np_y(\mathbf{r}) = \frac{i}{\sqrt{2}}\left[\varphi_{n,1,-1}(\mathbf{r}) + \varphi_{n,1,1}(\mathbf{r})\right], \tag{2.15b}$$

$$np_z(\mathbf{r}) = \varphi_{n,1,0}(\mathbf{r}), \tag{2.15c}$$

where x, y and z designate the symmetry axes of the orbitals. Figure 2.1 shows the contour surfaces for the p_x-orbital and p_y-orbital for $n=2$. The parity of p-orbitals under inversion i of the coordinates is given by equation (2.9) as odd which can be directly seen from the figure. An additional symmetry is given by reflection σ_v of coordinates of the p_x-, p_y-orbital in a plane including the x-axis, y-axis, respectively. Explicit expressions for the real hydrogen-like orbitals are given in table 2.2. The table also includes the d-orbitals.

As was shown in this subsection, the Schrödinger equation for the hydrogen atom can be solved analytically. For heavier atoms, diatomic molecules or even polyatomic molecules this is not the case anymore. Approximations have to be introduced like the *central field approximation* for an n-electron atom or the *Born-Oppenheimer approximation* for polyatomic molecules. Even with these approximations, the resulting equations remain complicated and the solutions rely on numerical methods. The nobel prize for the development of computational methods in quantum chemistry was awarded in 1998 to *J.A. Pople* and *W. Kohn* [75,76]. Many electronic-structure codes are available and most of them employ real orbitals in their calculations. The example of p_x-, p_y- and p_z-orbitals of hydrogen illustrates this idea of real orbitals as a result of superposing complex orbitals.

2.1.2 *Total angular momentum states*

Throughout this work we will often use states with definite orbital angular momentum **L** and spin **S** in a coupled basis with total angular momentum **J**. The ground state of Ne* is given in

n	l	spectroscopic notation	wave functions orbitals
2	1	$2p_x$	$Z^{3/2}\frac{1}{\sqrt{32\pi}}\cdot x\cdot e^{-q/2}$
2	1	$2p_y$	$Z^{3/2}\frac{1}{\sqrt{32\pi}}\cdot y\cdot e^{-q/2}$
2	1	$2p_z$	$Z^{3/2}\frac{1}{\sqrt{32\pi}}\cdot z\cdot e^{-q/2}$
3	1	$3p_x$	$Z^{3/2}\frac{1}{\sqrt{32\pi}}\cdot x\cdot(6-q)\cdot e^{-q/3}$
3	1	$3p_y$	$Z^{3/2}\frac{1}{\sqrt{32\pi}}\cdot y\cdot(6-q)\cdot e^{-q/3}$
3	1	$3p_z$	$Z^{3/2}\frac{1}{\sqrt{32\pi}}\cdot z\cdot(6-q)\cdot e^{-q/3}$
3	2	$3d_{z^2}$	$Z^{3/2}\frac{1}{81\sqrt{6\pi}}\cdot(2z^2-x^2-y^2)\cdot e^{-q/3}$
3	2	$3d_{xz}$	$Z^{3/2}\frac{1}{81}\sqrt{\frac{2}{\pi}}\cdot xz\cdot e^{-q/3}$
3	2	$3d_{yz}$	$Z^{3/2}\frac{1}{81}\sqrt{\frac{2}{\pi}}\cdot yz\cdot e^{-q/3}$
3	2	$3d_{xy}$	$Z^{3/2}\frac{1}{81}\sqrt{\frac{2}{\pi}}\cdot xy\cdot e^{-q/3}$
3	2	$3d_{x^2-y^2}$	$Z^{3/2}\frac{1}{81\sqrt{2\pi}}\cdot(x^2-y^2)\cdot e^{-q/3}$

Table 2.2: p- and d-type real hydrogen-like orbitals, with $q \equiv Zr$.

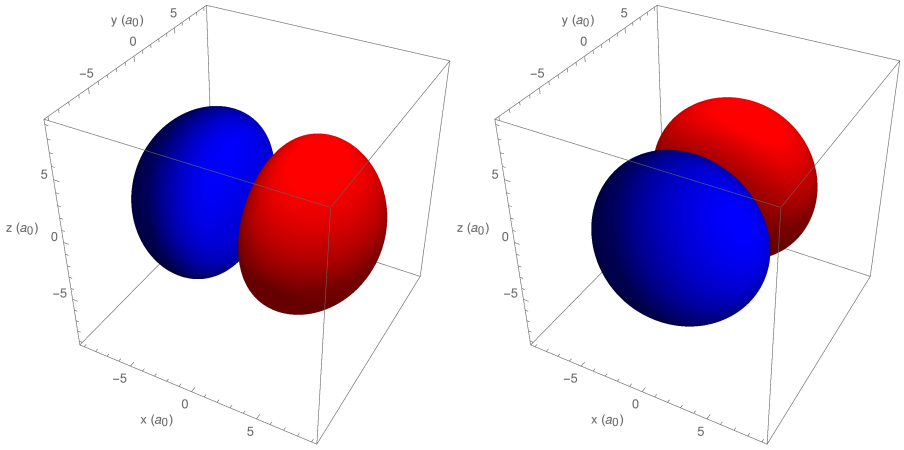

(a) $|2p_x(x,y,z)|^2 = 0.0001$ (b) $|2p_y(x,y,z)|^2 = 0.0001$

Figure 2.1: Contour surfaces of probability densities $|2p_x|^2$, $|2p_y|^2$ for the real hydrogen p_x- and p_y-orbitals. The red surfaces indicate $2p_x, 2p_y > 0$ while the blue surfaces indicate $2p_x, 2p_y < 0$.

this basis. To understand these states, we introduce the spin in our discussion of hydrogen-like systems. Consider the product state

$$|lsm_l m_s\rangle = |nlm_l\rangle \otimes |sm_s\rangle\,, \tag{2.16}$$

where $|sm_s\rangle$ describes the spin-part of the electron and $|nlm_l\rangle$ the spatial part. The spin-state $|sm_s\rangle$ is an eigenstate of the spin operator $\mathbf{S}^2$ and of the projection on the quantization axis S_z. We have

$$\mathbf{S}^2\,|sm_s\rangle = s(s+1)\,|sm_s\rangle\,, \quad S_z\,|sm_s\rangle = m_s\,|sm_s\rangle\,. \tag{2.17}$$

For a single electron we have $s = 1/2$ and $m_s = -1/2, +1/2$. The spatial state $|nlm_l\rangle$ fulfills the eigenvalue equations

$$\mathbf{L}^2\,|nlm_l\rangle = l(l+1)\,|nlm_l\rangle\,, \quad L_z\,|nlm_l\rangle = m_l\,|nlm_l\rangle\,, \tag{2.18}$$

where $\mathbf{L}$ is the orbital angular momentum operator and L_z is the projection operator on the z-axis. The operators H_0, $\mathbf{S}^2$, S_z, $\mathbf{L}^2$, L_z form a complete set of commuting observables [72].

Therefore, the product state $|lsm_l m_s\rangle$ is a simultaneous eigenstate to all of these operators. These states are orthonormal

$$\langle l's'm_l'm_s'|lsm_l m_s\rangle = \delta_{ll'}\delta_{m_l m_l'}\delta_{m_s m_s'}. \tag{2.19}$$

In this thesis we will also write the product state $|lsm_l m_s\rangle$ in position space. For a single electron we have

$$\psi_{nlm_l sm_s}(\mathbf{r}) = \varphi_{nlm_l}(\mathbf{r}) \cdot \chi_{m_s}, \tag{2.20}$$

where φ_{nlm_l} is the spatial part of the system and χ_{m_s} is the spin function which can be denoted by α for $m_s = +1/2$ and by β for $m_s = -1/2$. This notation is used in the quantum chemistry literature [77–79] and $\psi_{nlm_l sm_s}$ is known as a spin-orbital. For hydrogen-like systems, the spatial orbitals φ_{nlm_l} are given in table 2.1.

Now we construct total angular momentum states. The total angular momentum operator is given by

$$\mathbf{J} = \mathbf{L} + \mathbf{S}, \qquad \mathbf{J}^2 = \mathbf{L}^2 + \mathbf{S}^2 + 2\mathbf{L}\cdot\mathbf{S}, \tag{2.21}$$

where the operator $\mathbf{L}\cdot\mathbf{S}$ is given by the inverse relation

$$\mathbf{L}\cdot\mathbf{S} = \frac{1}{2}\left(\mathbf{J}^2 - \mathbf{L}^2 - \mathbf{S}^2\right). \tag{2.22}$$

The operators $\mathbf{J}^2$ and J_z commute with H_0. The operator $\mathbf{L}\cdot\mathbf{S}$ commutes with $\mathbf{L}^2$, $\mathbf{S}^2$, $\mathbf{J}^2$, J_z, but we have

$$[\mathbf{L}\cdot\mathbf{S}, L_z] \neq 0, \quad [\mathbf{L}\cdot\mathbf{S}, S_z] \neq 0. \tag{2.23}$$

Thus, the states $|lsm_l m_s\rangle$ cannot be eigenfunctions of $\mathbf{L}\cdot\mathbf{S}$. Therefore, we construct total orbital angular momentum states

$$|lsjm\rangle = \sum_{m_l m_s} |lsm_l m_s\rangle \langle lsm_l m_s|lsjm\rangle, \tag{2.24}$$

where $\langle lsm_l m_s|lsjm\rangle$ is a Clebsch-Gordan coefficient (see appendix B). These states are eigenstates of $\mathbf{J}^2$, $\mathbf{J}_z$, $\mathbf{L}^2$, $\mathbf{S}^2$, fulfilling the eigenvalue equations

$$\mathbf{J}^2|lsjm\rangle = j(j+1)|lsjm\rangle, \quad J_z|lsjm\rangle = m|lsjm\rangle, \tag{2.25}$$

$$\mathbf{L}^2|lsjm\rangle = l(l+1)|lsjm\rangle, \quad \mathbf{S}^2|lsjm\rangle = s(s+1)|lsjm\rangle, \tag{2.26}$$

with $m = -j, \ldots, +j$ and $j = |l-s|, \ldots, l+s$, and also of $\mathbf{L}\cdot\mathbf{S}$.

2.1.3 *Spin-orbit coupling*

After the introduction of the spin of the electron in hydrogen-like systems we can discuss the spin-orbit coupling. This is important, because spin-orbit coupling is present in Ne* and influences the collision physics. So far we have considered the non-relativistic Schrödinger equation (2.1) for a single electron in the field of the proton. The spin-orbit interaction describes the interaction of the spin of the electron with the magnetic field created by the movement of the nucleus. This spin-orbit interaction modifies the system Hamiltonian to

$$H = H_0 + H_{\mathrm{SO}}, \tag{2.27}$$

where H_0 is the non-relativistic Hamiltonian for the one-electron system. The spin-orbit term H_{SO} stems from the relativistic Dirac equation for an electron moving in the vector potential $\mathbf{A}$ and in the electrostatic potential φ generated by the nucleus [80]. For small velocities up to an order v^2/c^2 the spin-orbit term appears in the Dirac equation as

$$H_{\mathrm{SO}} = -\frac{1}{4c^2}\boldsymbol{\sigma}\cdot\nabla\varphi\times\boldsymbol{p}, \tag{2.28}$$

where c is the speed of light and $\mathbf{p}$ is the momentum of the electron. The Pauli matrices $\boldsymbol{\sigma}$ describe the spin of the system and are related to the spin operator by $\mathbf{s} = \frac{1}{2}\boldsymbol{\sigma}$. If the electrostatic potential φ is isotropic, the spin-orbit term can be written as [40]

$$H_{\mathrm{SO}} = \xi(r)\mathbf{L}\cdot\mathbf{S}, \quad \xi(r) = -\frac{1}{2c^2}\frac{1}{r}\frac{d\varphi}{dr}, \tag{2.29}$$

Given the electrostatic potential of hydrogen-like atoms, $\varphi(r) = Z/r$, we can calculate the radial function $\xi(r)$ as

$$\xi(r) = Z/2c^2r^3. \tag{2.30}$$

As the spin-orbit coupling in hydrogen is orders of magnitude smaller than the Coulomb interaction we can apply a perturbational approach in order to calculate the spin-orbit energies [81]. As the eigenvalues of H_0 are degenerate [see equation 2.14] the energy of the spin-orbit coupling is retrieved from the secular equation of first-order perturbation theory [40]

$$|H_{ij}^{\mathrm{SO}} - E_{njls}^{(1)}\delta_{ij}| = 0, \quad \text{with } H_{ij}^{\mathrm{SO}} = \langle\psi_{ni}^{(0)}|\, H_{\mathrm{SO}}\, |\psi_{nj}^{(0)}\rangle\,, \tag{2.31}$$

where $E_{njls}^{(1)}$ is the 1st order spin-orbit energy and where the state $|\psi_{nj}^{(0)}\rangle$ is the unperturbed total angular momentum state, given by equation (2.24). The matrix element $\langle\psi_{ni}^{(0)}|\, H_{\mathrm{SO}}\, |\psi_{nj}^{(0)}\rangle$ factorizes in a part only depending on the quantum numbers l, s, j and in a radial part. The part depending only on the quantum numbers l, s, j reads

$$\begin{aligned}\langle l'sj'm'|\,\mathbf{L}\cdot\mathbf{S}\,|lsjm\rangle =& \frac{1}{2}\,\langle l'sj'm'|\,(\mathbf{J}^2 - \mathbf{L}^2 - \mathbf{S}^2)\,|lsjm\rangle \\ =& \frac{1}{2}\,(j(j+1) - l(l+1) - s(s+1))\,\delta_{j'j}\delta_{l'l}\delta_{m'm},\end{aligned} \tag{2.32}$$

where we used that the total angular momentum states $|lsjm\rangle$ are orthonormal. The radial part is given by the integral

$$\langle\xi(r)\rangle = \langle nlm_l|\,\xi(r)\,|nlm_l\rangle \equiv \xi_{nl} = \int \xi(r)|\psi_{nl}(r)|^2 dr, \tag{2.33}$$

where the radial functions ψ_{nl} are given by equation (2.13). The spin-orbit radial function $\xi(r)$ is given by equation (2.30) and insertion in equation (2.33) results in

$$\xi_{nl} = \frac{Z}{2c^2}\left\langle\frac{1}{r^3}\right\rangle. \tag{2.34}$$

Expectation values of the type $\langle 1/r^k\rangle$ can be solved analytically for hydrogen-like wave functions and the results are tabulated in the literature [82]. We simply give the result for $k = 3$ which reads

$$\left\langle\frac{1}{r^3}\right\rangle = \frac{Z^3}{n^3(l+1)(l+\frac{1}{2})l}. \tag{2.35}$$

By inserting equation (2.35) in equation (2.34) and combining the result with the expectation value of the $\mathbf{l}\cdot\mathbf{s}$ operator (2.32) we finally obtain the spin-orbit energy

$$E_{njls}^{(1)} = \frac{Z^4}{4c^2}\frac{j(j+1) - l(l+1) - s(s+1)}{n^3(l+1)(l+\frac{1}{2})l}. \tag{2.36}$$

This result shows a Z^4 dependency of the spin-orbit coupling. Thus, for heavier atoms, the spin-orbit coupling becomes much more dominant and the perturbation approach of this subsection may break down. For many-electron systems such as Ne* the calculation of spin-orbit energies is more complicated. The coupling scheme is more complex and energy splittings have to be evaluated carefully. We will discuss the spin-orbit coupling and the fine-structure of Ne* in chapter 6. We now generalize the discussion of atoms to many-electron atoms.

2.2 MANY-ELECTRON ATOMS

Ne* is a many-electron system. In order to understand its atomic properties we need to introduce the spectroscopic notation of atoms and discuss the construction of many-electron states. The many-electron states can be represented by Slater determinants which will be introduced in this section. With the help of the Slater-Condon rules we then calculate the *Hartree-Fock equations* which result from the minimization of the non-relativistic many-electron energy expectation value in terms of the electron orbitals. We start with the spectroscopic notation of many-electron atomic states.

2.2.1 *Spectroscopic notation for atomic states*

Here, we explain the *Russel-Saunders* or (LS) coupling in many-electron system [83]. This is important because the ground state of Ne* is given in Russel-Saunders notation even though the general coupling mechanisms in Ne* are given by intermediate states of LS coupling and jj coupling.

Consider an n-electron system. Each electron is a spin-1/2 system and may has non-zero orbital angular momentum. If the Coulomb interactions of the electrons and the nucleus is strong compared to the spin-orbit coupling, which was discussed in the previous section, it is likely that the individual orbital angular momenta and spins of the electrons couple to a total orbital momentum $\mathbf{L}$ and a total electronic spin $\mathbf{S}$, reading

$$\mathbf{L} = \sum_i \mathbf{L}_i, \quad \mathbf{S} = \sum_i \mathbf{S}_i, \tag{2.37}$$

where $\mathbf{L}_i$, $\mathbf{S}_i$ are orbital angular momentum and spin operators of electron i. In equation (2.21) the coupling of $\mathbf{L}$ and $\mathbf{S}$ to a total orbital angular momentum was shown for a one-electron system. If the one-electron operators $\mathbf{L}$, $\mathbf{S}$ in equation (2.21) are replaced by the operators in equation (2.37) we obtain the total orbital angular momentum $\mathbf{J}$ of the n-electron system in *Russel-Saunders* or LS-coupling [83]. The z-components of $\mathbf{L}$ and $\mathbf{S}$ in this coupling scheme are given by

$$L_z = \sum_i L_{z,i}, \quad S_z = \sum_i S_{z,i}, \tag{2.38}$$

with $L_{z,i}$, $S_{z,i}$ the z-components of $\mathbf{L}$, $\mathbf{S}$, respectively. The spectroscopic notation for an n-electron state $|lsjm\rangle$ in Russel-Saunders coupling is given by

$$^{2s+1}l_j, \tag{2.39}$$

where $2s+1$ is called the multiplicity of the state. For $s = 0, 1, 2, \ldots$ the state is a singlet, triplet, quintet state, ..., respectively. For $l = 0, 1, 2, \ldots$ the state is designated as S, P, D, ... state as opposed to the lowercase letters for single-electron systems.

2.2.2 *Slater determinants*

In contrast to one-electron systems, the Schrödinger equation for many-electron atoms cannot be solved analytically. The Coulomb repulsion H_1 of the electrons makes the electronic wave function non-separable. However, H_1 contains a large spherical symmetric component. This large spherical symmetric component makes it possible to introduce the *central field approximation* which we discuss in this section. We start with the non-relativistic Hamiltonian for a single atom with n electrons [40]

$$H = H_0 + H_1 = \sum_{i=1}^{n} h_0(\mathbf{r}_i, \mathbf{p}_i) + \sum_{i<j}^{n} h_1(\mathbf{r}_i, \mathbf{r}_j). \tag{2.40}$$

with

$$h_0(\mathbf{r}_i, \mathbf{p}_i) = -\frac{\nabla^2_{\mathbf{r}_i}}{2} - \frac{Z}{r_i}, \quad h_1(\mathbf{r}_i, \mathbf{r}_j) = \frac{1}{|\mathbf{r}_i - \mathbf{r}_j|}. \tag{2.41}$$

H_0 describes the kinetic energy of the electrons and the Coulomb attraction between nucleus and electrons while H_1 describes the Coulomb repulsion between the electrons. In general, the electron repulsion energy H_1 is not a small contribution to the total energy so that the system cannot be treated in a perturbation approach. The operator H_1 is a sum over the two-electron operators h_1 which makes it difficult to solve the Schrödinger equation for the full n-electron system. However, it contains a large spherically symmetric part so that the effect of the Coulomb repulsion for the ith electron by all the other electrons can be described in terms of an averaged, spherically symmetric potential energy $V(r_i)$ which acts on the ith electron. Assume, that we split the Hamiltonian (2.40) into

$$H = H_0' + H_1', \tag{2.42}$$

where

$$H_0' = \sum_{i=1}^{n} h_0'(\mathbf{r}_i, \mathbf{p}_i) = -\sum_{i=1}^{n} \frac{\nabla_{\mathbf{r}_i}^2}{2} + V(r_i), \quad H_1' = \sum_{i<j}^{n} h_1(\mathbf{r}_i, \mathbf{r}_j) - \frac{1}{2}\left\langle \sum_{i,j\neq i}^{n} h_1(\mathbf{r}_i, \mathbf{r}_j) \right\rangle, \tag{2.43}$$

and where we have introduced the one-electron potential

$$V(r_i) = -\frac{Z}{r_i} + \frac{1}{2}\left\langle \sum_{j\neq i}^{n} h_1(\mathbf{r}_i, \mathbf{r}_j) \right\rangle. \tag{2.44}$$

The term $1/2\langle\sum_{j\neq i}^{n} h_1(\mathbf{r}_i, \mathbf{r}_j)\rangle$ denotes the average over a sphere of the electron repulsion for electron i and is independent of angular coordinates [40]. Often, H_1' is only a small contribution to the total energy of the system. This term describes the electron correlation energy E_{corr}. One has to be careful in neglecting H_1' as in some cases E_{corr} can become very large. Keeping this in mind we assume in the following that the total energy of the electronic system is described by H_0' only. This is the *central field approximation*. The time-independent Schrödinger equation for H_0' reads

$$H_0'\Phi(\{\mathbf{r}\}) = \left[\sum_{i=1}^{n} h_0'\right]\Phi(\{\mathbf{r}\}) = E\Phi(\{\mathbf{r}\}), \tag{2.45}$$

where $\{\mathbf{r}\} = \{\mathbf{r}_1, \ldots, \mathbf{r}_n\}$ is the set of all electron coordinates. As h_0' is a one-electron operator we can employ a single-electron product state ansatz for the wave function $\Phi(\{\mathbf{r}\})$, reading

$$\Phi(\{\mathbf{r}\}) = \varphi_1(\mathbf{r}_1) \cdot \varphi_2(\mathbf{r}_2) \cdot \ldots \cdot \varphi_n(\mathbf{r}_n), \tag{2.46}$$

and the Schrödinger equation becomes separable into n one-particle equations of the type

$$h_0'\varphi(\mathbf{r}) = \varepsilon\varphi(\mathbf{r}), \tag{2.47}$$

with ε the one-electron energy and where we omitted the subscript i for particle i. As in the simple case of the hydrogen-like atoms, this equation can be solved by separating the variables of the radial distance r and of the angular coordinates (θ, φ). The solutions are given by central field orbitals, where the angular part is given by the spherical harmonics $Y_{lm_l}(\theta, \varphi)$ and the radial part by a radial wave function $R_{nl}(r)$ so that we obtain

$$\varphi_{nlm_l}(\mathbf{r}) = R_{nl}(r)Y_{lm_l}(\theta, \varphi). \tag{2.48}$$

Note, that the radial functions $R_{nl}(r)$ are not the hydrogen-like solutions but functions whose exact shapes depend on the shape of the averaged potential $V(r)$ of the n-electron atom.

As electrons are fermions, the total wave function of the system needs to be antisymmetric under the exchange of two electrons. Two fermions cannot reside in the same quantum state. This is also known as the *Pauli exclusion principle* [84]. The total electronic wave function of the n-electron system which is totally antisymmetric can be written in form of the Slater determinant [40]

$$\Psi(\{\mathbf{r}\}) = \frac{1}{\sqrt{n!}}\begin{vmatrix} \psi_1(1) & \psi_2(1) & \cdots & \psi_n(1) \\ \psi_1(2) & \psi_2(2) & \cdots & \psi_n(2) \\ \vdots & \ddots & \ddots & \vdots \\ \psi_1(n) & \psi_2(n) & \cdots & \psi_n(n) \end{vmatrix}, \tag{2.49}$$

with $\psi_k(j)$ the spin-orbitals (2.20) with k denoting the set of quantum numbers $(nlsm_l m_s)$ and j denoting the coordinates of particle j. As the single-electron spin-orbitals have definite parity under the inversion of the electron coordinate, the n-electron Slater determinant also has definite parity under inversion i of all the electron coordinates, reading

$$\mathcal{P}_i \Psi(\{\mathbf{r}\}) = \Psi(\{-\mathbf{r}\}) = (-1)^{l_1}(-1)^{l_2}\dots(-1)^{l_n}\Psi(\{\mathbf{r}\}). \tag{2.50}$$

With the Slater determinant we introduce in section 2.2.4 the *Hartree-Fock equations* which we solve in this thesis in order to calculate molecular potential energies. In order to derive the *Hartree-Fock equations* we introduce the Slater-Condon rules for the Slater determinants in the next section.

2.2.3 *Slater-Condon rules*

The *Slater-Condon rules* have been derived in [85,86]. We assume two Slater determinants for n electrons, Ψ_A and Ψ_B, given by

$$\Psi_A = \frac{1}{\sqrt{n!}}\begin{vmatrix} \psi_{a_1}(1) & \psi_{a_2}(1) & \dots & \psi_{a_n}(1) \\ \psi_{a_1}(2) & \psi_{a_2}(2) & \dots & \psi_{a_n}(2) \\ \vdots & \ddots & \ddots & \vdots \\ \psi_{a_1}(n) & \psi_{a_2}(n) & \dots & \psi_{a_n}(n) \end{vmatrix}, \; \Psi_B = \frac{1}{\sqrt{n!}}\begin{vmatrix} \psi_{b_1}(1) & \psi_{b_2}(1) & \dots & \psi_{b_n}(1) \\ \psi_{b_1}(2) & \psi_{b_2}(2) & \dots & \psi_{b_n}(2) \\ \vdots & \ddots & \ddots & \vdots \\ \psi_{b_1}(n) & \psi_{b_2}(n) & \dots & \psi_{b_n}(n) \end{vmatrix}. \tag{2.51}$$

Here, $\psi_{a_k}(i)$ and $\psi_{b_{k'}}(i')$ are spin orbitals. As in the previous section, k and k' denote the quantum numbers n, l, m_l, m_s, while i and i' denote the coordinates of electron i and i', respectively.

One-electron operators

Furthermore, we assume an operator F which is given by

$$F = \sum_{i=1}^{n} f(i), \tag{2.52}$$

where f is a one-electron operator and i denotes coordinate r_i and momentum p_i of particle i. The Slater-Condon rule for the diagonal matrix element $\langle \Psi_A | F | \Psi_A \rangle$ reads

$$\langle \Psi_A | F | \Psi_A \rangle = \sum_{i=1}^{n} \langle \psi_{a_i}(1) | f(1) | \psi_{a_i}(1) \rangle . \tag{2.53}$$

Thus, the diagonal matrix element $\langle \Psi_A | F | \Psi_A \rangle$ is simply given by a sum of expectation values of the single electron operators in terms of the single-electron spin-orbitals. This result holds because of the orthonormality of the spin-orbitals. If A and B differ by more than one pair of spin-orbitals $\psi_{a_k} \neq \psi_{b_l}$, the Slater-Condon rule for the off-diagonal matrix element $\langle \Psi_A | F | \Psi_B \rangle$ reads

$$\langle \Psi_A | F | \Psi_B \rangle = 0. \tag{2.54}$$

If A and B only differ by one spin-orbital $\psi_{a_k} \neq \psi_{b_l}$, but all the other spin-orbitals are the same, the off-diagonal matrix element of F reads

$$\langle \Psi_A | F | \Psi_B \rangle = \pm \langle \psi_{a_k}(1) | f(1) | \psi_{b_l}(1) \rangle . \tag{2.55}$$

Here, a plus sign occurs when the parity of the permutation of ψ_{b_l} from the lth position to the kth position in the Slater determinant is positive/even and a minus sign occurs when the permutation is negative/odd.

Two-electron operators

We introduce the operator G, given by

$$G = \sum_{i<j}^{n} g(i,j), \tag{2.56}$$

where g is a two-electron operator and i and j denote the coordinates r_i, r_j and momenta p_i, p_j of the two particles i and j, respectively. The Slater-Condon rule for the diagonal matrix element in terms of the Slater determinant Ψ_A is given by

$$\begin{aligned}\langle \Psi_A | \, G \, | \Psi_A \rangle = \sum_{k<t} \big[&\langle \psi_{a_k}(1), \psi_{a_t}(2) | \, g(1,2) \, | \psi_{a_k}(1), \psi_{a_t}(2) \rangle \\ &- \langle \psi_{a_k}(1), \psi_{a_t}(2) | \, g(1,2) \, | \psi_{a_t}(1), \psi_{a_k}(2) \rangle \big] \,, \end{aligned} \tag{2.57}$$

where $|\psi_{a_k}(1), \psi_{a_t}(2)\rangle$ denotes the two-electron product state

$$|\psi_{a_k}(1), \psi_{a_t}(2)\rangle = |\psi_{a_k}(1)\rangle \otimes |\psi_{a_t}(2)\rangle \,. \tag{2.58}$$

If A and B differ by more than two pairs of spin orbitals, $\psi_{a_k} \neq \psi_{b_m}$ and $\psi_{a_l} \neq \psi_{b_n}$, the off-diagonal matrix element reads

$$\langle \Psi_A | \, G \, | \Psi_B \rangle = 0. \tag{2.59}$$

Consider the case, where Ψ_A and Ψ_B differ by two pairs of spin orbitals, i.e. $\psi_{a_k} \neq \psi_{b_m}$ and $\psi_{a_l} \neq \psi_{b_n}$, but all the other spin orbitals are the same. The Slater-Condon rule for the off-diagonal matrix element of G then reads

$$\langle \Psi_A | \, G \, | \Psi_B \rangle = \pm \left[\langle \psi_{a_k}, \psi_{a_t} | \, g \, | \psi_{b_m}, \psi_{b_n} \rangle - \langle \psi_{a_k}, \psi_{a_l} | \, g \, | \psi_{b_n}, \psi_{b_m} \rangle \right] , \tag{2.60}$$

where we have omitted the electron coordinates $1, 2$. The plus sign occurs when the permutations of ψ_{b_m} from the mth position to the kth position and of ψ_{b_l} from the lth position to the nth position are both even or both odd. The minus sign occurs otherwise. When the Slater determinants A and B differ only by one pair of spin orbitals $\psi_{a_k} \neq \psi_{b_l}$ and all the others are the same, we have

$$\langle \Psi_A | \, G \, | \Psi_B \rangle = \pm \sum_{t \neq k} \left[\langle \psi_{a_k}, \psi_{a_t} | \, g \, | \psi_{b_l}, \psi_{a_t} \rangle - \langle \psi_{a_k}, \psi_{a_t} | \, g \, | \psi_{a_t}, \psi_{b_l} \rangle \right] . \tag{2.61}$$

Here, the plus and minus sign occur to the same rule as in equation (2.60). Having established the Slater-Condon rules we can now introduce the *Hartree-Fock equations*.

2.2.4 *Hartree-Fock equations*

The *Hartree-Fock equations* are the basic equations which we solve in this work in order to obtain atomic and molecular potential energies. With the Slater-Condon rules we are able to derive the energy expectation value of the non-relativistic n-electron Hamiltonian (2.40) where the n-electron state is given by the single Slater determinant (2.49). Based on the minimization principle, variation of the energy with respect to the spin-orbitals leads to the *Hartree-Fock equations*.

We start by employing the Slater-Condon rules to derive the energy eigenvalue of the Hamiltonian (2.40). We identify the free Hamilton operator H_0 in equation (2.40) with F and h_0 in equation (2.41) with f, reading

$$F = H_0, \quad f = h_0 = -\frac{\nabla^2_{\mathbf{r}_i}}{2} - \frac{Z}{r_i}. \tag{2.62}$$

Furthermore, we identify the Coulomb repulsion term H_1 (2.40) with the operator G and h_1 in equation (2.41) with g, given by

$$G = H_1, \quad g = h_1 = \frac{1}{|\mathbf{r}_i - \mathbf{r}_j|}. \tag{2.63}$$

With the Slater-Condon rules of the diagonal matrix elements in the equations (2.53), (2.57) we derive the energy expectation value of the Hamiltonian H in terms of the Slater determinant (2.49) as

$$E = \langle \Psi | \, H \, | \Psi \rangle = \sum_k^n I_k + \frac{1}{2} \sum_{km}^n (J_{km} - K_{km}), \tag{2.64}$$

where the one-electron integral I_k and the two-electron integrals J_{km}, K_{km} are given by

$$I_k = \langle \psi_k | h_0 | \psi_k \rangle , \quad J_{km} = \langle \psi_k, \psi_m | h_1 | \psi_k, \psi_m \rangle , \quad K_{km} = \langle \psi_k, \psi_m | h_1 | \psi_m, \psi_k \rangle , \tag{2.65}$$

with J_{km} the Coulomb integral and K_{km} the exchange integral. The exchange integral K_{km} only exists if the two electrons in the orbitals ψ_k, ψ_m have spin projections in the same direction, i.e. if $m_{s_1} = m_{s_2}$.

So far we have not made any restrictions on the specific configuration of the n-electron system. We now assume the case of closed shells, i.e. the case where all spatial orbitals are doubly occupied respecting the Pauli exclusion principle so that for one spatial orbital one electron is in the spin-up state ($m_s = +1/2$) while the second electron of this spatial orbital is in the spin-down state ($m_{s'} = -1/2$). There are then $n/2$ electrons in spin-up configurations and $n/2$ electrons in spin-down configurations. The energy expectation value then can be written as

$$E = 2 \sum_{q}^{n/2} I_q + \sum_{qq'}^{n/2} \left(2J_{qq'} - K_{qq'} \right) , \tag{2.66}$$

where the summations q, q' are only over the spatial quantum numbers and the factor two arises from the double occupation of the spatial orbitals.

In order to derive the *Hartree-Fock equations* one has to minimize the energy expectation value with respect to a variation of the spin-orbitals. The *Hartree-Fock equations* resulting from the minimization of equation (2.66) for closed shell atoms, where all spatial orbitals are doubly occupied, are called *Restricted Hartree-Fock* (RHF) equations. For open-shell systems with at least one spatial orbital only singly occupied, different expressions are derived depending on the specific assumptions on the electronic state of the system. There exists the *Unrestricted Hartree-Fock* (UHF) equations which result from the assumption of no restrictions on the spins of the electrons. In the derivation of the *Restriced open-shell Hartree-Fock* (ROHF) equations it is assumed that only the spatial orbitals of the closed shells are restricted to be occupied by two electrons with opposite spins. Solving either the RHF, UHF or the ROHF equations has different advantages and disadvantages, for example the disadvantage of *spin contamination problem* for the UHF method where the electronic wave function is not restricted to be a pure spin state anymore. Another disadvantage is the *dissociation problem* of too large electronic energies at large separations of the RHF method which will be discussed in more detail in section 3.5.2. A detailed discussion of the different methods can be found in the literature [79, 87, 88].

We now derive the RHF equations and start with the energy expression (2.66). The derivation of the *Hartree-Fock equations* is based on the variational method of Ritz [72, 84]. The variational principle states that if one considers the energy expectation value as a functional of the states $|\Psi\rangle$, reading

$$E[|\Psi\rangle] = \frac{\langle \Psi | H | \Psi \rangle}{\langle \Psi | \Psi \rangle}, \tag{2.67}$$

the stationary value $\delta E[|\Psi\rangle] = 0$ is obtained if $|\Psi\rangle$ is an eigenvector of the discrete spectrum of H. It can be shown that for an arbitrary state $|\Psi\rangle$, it always holds

$$E[|\Psi\rangle] \geq E_0, \tag{2.68}$$

where E_0 is the ground state energy of the system. The energy eigenvalue of an arbitrary state $|\Psi\rangle$ is always bigger than or equal to the energy eigenvalue of the ground state of the system. In order to find a good approximation to the energy and wave function of the system, we have to minimize equation (2.67) with respect to the orbitals $|\varphi_q\rangle$ of $|\Psi\rangle$ under the condition that the orbitals are normalized

$$\langle \varphi_q | \varphi_q \rangle = 1, \quad \forall q. \tag{2.69}$$

Varying the RHF energy-expression (2.66) with respect to the orbitals $\{|\varphi_q\rangle\}$ under the condition (2.69) leads to the *Hartree-Fock equations* [40]

$$F(1)\varphi_q(1) = \varepsilon_q \varphi_q(1), \tag{2.70}$$

where ε_q is the orbital energy of the ψ_q orbital and where we have introduced the Fock operator [77]

$$F(1) = h_0(1) + \sum_{q'} \left[2J_{q'}(1) - K_{q'}(1) \right]. \tag{2.71}$$

The Coulomb operator $J_{q'}(1)$ and the exchange operator $K_{q'}(1)$ in the Fock operator are defined as follows

$$J_{q'}(1)\varphi_q(1) = \left[\int |\varphi_{q'}(2)|^2 \frac{1}{|\mathbf{r}_1 - \mathbf{r}_2|} d\mathbf{r}_2 \right] \varphi_q(1), \tag{2.72a}$$

$$K_{q'}(1)\psi_q(1) = \left[\int \varphi^*_{q'}(2) \frac{1}{|\mathbf{r}_1 - \mathbf{r}_2|} \varphi_q(2) d\mathbf{r}_2 \right] \varphi_{q'}(1). \tag{2.72b}$$

There is no method of solving the *Hartree-Fock equations* (2.70) directly. Equation (2.70) suggests that the problem consists of a simple eigenvalue problem but the Fock operator itself consists of the orbitals one is seeking for. Therefore, the *Hartree-Fock equations* have to be solved in a *self-consistent* manner. For more details regarding the *Hartree-Fock equations* we refer the interested reader to the literature [40, 78, 79].

Beyond Hartree-Fock

The *Hartree-Fock equations* (2.70) have been derived by assuming that the electron repulsion can be described in a *mean-field* approach. In this assumption, the correlation energy E_{corr} of the electrons is neglected. The exact total electronic energy of an n-electron system is given by

$$E_{\text{tot}} = E_{\text{HF}} + E_{\text{corr}}, \tag{2.73}$$

with E_{HF} the *Hartree Fock* energy of the system. There are many methods beyond *Hartree-Fock* to account for E_{corr} such as the *Configuration Interaction* (CI) methods, the *Multiconfigurational SCF* (MCSCF) methods or the *Møller-Plesset perturbation theory* (MP). With all of these methods, it is possible to obtain more accurate results for electronic energies of atoms or potential energies of molecules than with the standard *Hartree-Fock method*. The description of these methods is outside the scope of this work, the interested reader is referred to the literature [77, 79]. Modern electronic structure programs are available which include the standard *Hartree-Fock* , CI, MCSCF methods and the MP perturbation theory as well as alternative approaches as the *(Time-Dependent) Density Functional Theory* ((TD)DFT) and the *Coupled Cluster* (CC) methods [79].

In order to solve the *Hartree-Fock equations* we use in this work the *General Atomic and Molecular Electronic Structure System* (GAMESS) package [89, 90]. This package incorporates all the methods mentioned here and will be employed in this work to calculate molecular potential energies.

CONCLUSION

In this chapter we discussed the properties of atomic systems. We started with the hydrogen-like atoms, introduced complex and real orbitals and showed how the spin of the electrons leads to spin-orbit coupling. We then introduced the many-electron atoms, explained the spectroscopic notation for LS coupled states, showed how the Slater determinants are constructed as the properly antisymmetric electronic states of the system and introduced the Slater-Condon rules. With the Slater-Condon rules we introduced the *Hartree-Fock equations*. It is important to understand the physics of a single atom in order to understand the interaction properties of colliding atoms. This will be studied in the next section for short-range interactions in terms of the diatomic molecular states and potential energies.

3

SHORT-RANGE INTERACTIONS

In binary collisions of Ne* at short-range ($r \leq 20\ a_0$), the physics is given in terms of the diatomic molecular properties of the system. Therefore, it is of considerable interest for this work to investigate the properties of diatomic molecules in detail as also the interaction potentials of Ne* are given in a molecular basis. We start with the fundamental approximation of molecular physics, the *Born-Oppenheimer approximation*. The separation of electronic and nuclear motion in this approximation is a crucial point in order to obtain the molecular interaction potentials. We then introduce the Linear Combination of Atomic Orbitals (LCAO) method for the construction of molecular orbitals and show how the *Hartree-Fock equations* transform in this method to the *Roothaan equations* for molecular systems. In order to discuss the symmetries and to introduce the spectroscopic notation for electronic states of diatomic molecules, we calculate ground state molecular potential and the molecular orbitals of H_2^+ numerically by solving the *Roothaan equations* with the GAMESS package (see previous chapter). The molecular interaction potentials of Ne* were calculated in the molecular bases corresponding to *Hund's case* (a) and *Hund's case* (c). We introduce these bases by discussing the coupling mechanisms and the spectroscopic notation in many-electron diatomic molecules. As an example for many-electron molecules we introduce the H_2 molecule for which we construct fully anti-symmetrized electronic states in the *Hund's case* (a) basis and give general expressions for the lowest eigenenergies of H_2. Furthermore, we introduce the *Heitler-London* (HL) approximation which is an alternative approach to construct molecular orbitals and compare this approach to the LCAO by calculating the molecular potential energies of H_2.

3.1 BORN-OPPENHEIMER APPROXIMATION

The nonrelativistic Hamilton operator of polyatomic molecules consists of the nuclear kinetic energy T_{nuc} and the electronic part H_{el} and reads

$$H = T_{\text{nuc}} + H_{\text{el}}. \tag{3.1}$$

The electronic part includes the kinetic energy of the electrons and all the Coulomb interactions, conveniently also the Coulomb repulsion of the nuclei. As the masses of the nuclei M_α are typically much larger than the electron masses the term T_{nuc} is very often small compared to the electronic Hamiltonian H_{el}. This is what is exploited in the *Born-Oppenheimer approximation* [47], which we describe in this section.

Assume a polyatomic molecule with a total number of k nuclei and a total of n electrons. The time-independent Schrödinger equation for this system in atomic units reads [47]

$$\left(-\sum_{\alpha=1}^{k} \frac{\nabla^2_{\mathbf{R}_\alpha}}{2M_\alpha} - \sum_{i=1}^{n} \frac{\nabla^2_{\mathbf{r}_i}}{2} + V(\mathbf{r},\mathbf{R}) \right) \Psi(\mathbf{r},\mathbf{R}) = E\Psi(\mathbf{r},\mathbf{R}), \tag{3.2}$$

where $\mathbf{r} = \{\mathbf{r}_1, \mathbf{r}_2, \ldots, \mathbf{r}_n\}$ denotes the set of all $3n$ electron coordinates and $\mathbf{R} = \{\mathbf{R}_1, \mathbf{R}_2, \ldots, \mathbf{R}_k\}$ denotes the set of all $3k$ nuclei coordinates. The first term in the Schrödinger equation is the nuclei kinetic energy T_{nuc}. The potential $V(\mathbf{r},\mathbf{R})$ is the full Coulomb interaction term, consisting of the repulsion between the electrons and between the nuclei and of the attraction between the nuclei and the electrons. The energy E is the total energy of the molecular system. Given the splitting of the Hamiltonian (3.1) we can write a separation ansatz of the wave function as

$$\Psi(\mathbf{r},\mathbf{R}) = \sum_m \psi^{\text{nuc}}_m(\mathbf{R})\phi_m(\mathbf{r},\mathbf{R}), \tag{3.3}$$

where $\phi_m(\mathbf{r}, \mathbf{R})$ is the electronic part of the wave function depending on the electron coordinates $\mathbf{r}$ and parametrically on the nuclear coordinates $\mathbf{R}$. The nuclear part of the wave function, given by $\psi_m^{\text{nuc}}(\mathbf{R})$, depends on the nuclear coordinates only.

With the ansatz (3.3) we obtain a separate Schrödinger equation for the electronic wave function

$$H_{\text{el}}\phi_n(\mathbf{r}, \mathbf{R}) = V_n(\mathbf{R})\phi_n(\mathbf{r}, \mathbf{R}), \tag{3.4}$$

where the subscript n of the electronic wave function is the nth eigenstate of H_{el} and where we introduced V_n as the eigenenergies to the nth eigenstate of the electronic Schrödinger equation (3.4). Note that equation (3.4) is solved for given $\mathbf{R}$. As the electronic energy eigenvalues and the electronic eigenstates both change upon changing the position of the nuclei, they depend parametrically on $\mathbf{R}$. The eigenenergies $V_n(\mathbf{R})$ as a function of $\mathbf{R}$ are the potential energy curves and the *Born-Oppenheimer potentials* [47]. These are the potential energy surfaces entering the scattering equations in cold atom collisions. In slow atomic collisions, the colliding nuclei move adiabatically on these potential curves generated by the electrons [52, 91]. We show this more explicitly now.

If we use the ansatz (3.3) in the Schrödinger equation (3.2) and project the solution to the electronic state ϕ_n^* we obtain

$$\left(T_{\text{nuc}} + V_n(\mathbf{R})\right)\psi_n^{\text{nuc}}(\mathbf{R}) + \sum_m c_{nm}\psi_m^{\text{nuc}}(\mathbf{R}) = E\psi_n^{\text{nuc}}(\mathbf{R}), \tag{3.5}$$

where the coefficients c_{nm} are given

$$c_{nm} = \int \phi_n^* T_{\text{nuc}}\phi_m d\mathbf{r} - \frac{1}{2}\left[\int d\mathbf{r}\, \phi_n^* \sum_\alpha \frac{1}{M_\alpha}\frac{\partial}{\partial \mathbf{R}_\alpha}\phi_m\right]\frac{\partial}{\partial \mathbf{R}_\alpha}. \tag{3.6}$$

Thus, with the separation ansatz (3.3) for the Schroedinger equation (3.2) we obtain two separate differential equations for the electronic and nuclear part of motion,

$$H_{\text{el}}\phi_n(\mathbf{r}, \mathbf{R}) = V_n(\mathbf{R})\phi_n(\mathbf{r}, \mathbf{R}), \tag{3.7a}$$

$$\left(T_{\text{nuc}} + V_n(\mathbf{R})\right)\psi_n^{\text{nuc}}(\mathbf{R}) + \sum_m c_{nm}\psi_m^{\text{nuc}}(\mathbf{R}) = E\psi_n^{\text{nuc}}(\mathbf{R}). \tag{3.7b}$$

Solving these many-particle Schrödinger equations is not a simple matter. Approximation methods to solve the electronic Schrödinger equation (3.4), (3.7a) will be discussed in this chapter.

In order to solve the Schrödinger equation for the nuclei, we also need approximations, as the exact solution is only given for an infinite summation in equation (3.7b) which cannot be done in practice. The simplest approximation is to set $c_{nm} = 0$ for all n, m. This is the *Born-Oppenheimer approximation*. Equation (3.7b) then becomes

$$\left(T_{\text{nuc}} + V_n(\mathbf{R})\right)\psi_n^{\text{nuc}}(\mathbf{R}) = E\psi_n^{\text{nuc}}(\mathbf{R}). \tag{3.8}$$

In this approximation the nuclei move in the *Born-Oppenheimer potential* $V_n(\mathbf{R})$ of the electrons. Within this approximation, it is considered that the electrons react instantaneously on a change of nuclear coordinates. In reality, this is not quite true, the nuclei at distance $\mathbf{R}$ feel the potential of the electrons at a slightly "earlier" distance $\mathbf{R} - \Delta\mathbf{R}$. To account for this higher-order correction, we can set all off-diagonal terms $c_{n\neq m} = 0$ and keep only the diagonal terms. This is the *adiabatic approximation* [47]. Equation (3.7b) becomes

$$\left(T_{\text{nuc}} + \mathcal{V}_n(\mathbf{R})\right)\psi_n^{\text{nuc}}(\mathbf{R}) = E\psi_n^{\text{nuc}}(\mathbf{R}), \tag{3.9}$$

where the potential $\mathcal{V}_n(\mathbf{R})$ is given by the *Born-Oppenheimer potential* $V_n(\mathbf{R})$ plus an additional term, reading

$$\mathcal{V}_n(\mathbf{R}) = V_n(\mathbf{R}) + \sum_\alpha \frac{1}{2M_\alpha}\int d\mathbf{r}\left(\frac{\partial\phi_n(\mathbf{r}, \mathbf{R})}{\partial \mathbf{R}_\alpha}\right)^2, \tag{3.10}$$

where the derivative of the electronic wave function with respect to the nuclear coordinates is contained. Here, the response of the electron wave function to a change in nuclear positions

is a small correction, as the masses of the nuclei M_α are much bigger than the mass of the electron and also the derivative of the electronic wave function with respect to the nuclear coordinates is only a small number compared with the derivative of the electron wave function with respect to the electron coordinates. Within the *adiabatic approximation* the electrons follow the nuclei adiabatically, there is no non-adiabatic mixing of different electron configurations ϕ_n, ϕ_m with $n \neq m$. In order to account for the non-adiabatic effects beyond the *Born-Oppenheimer approximation* and the *adiabatic approximation* one also has to account for the off-diagonal terms $c_{n\neq m}$.

It was mentioned in the previous chapter for atomic systems that solving the many-electron Schrödinger equation is not a trivial task. This is even more true for molecular systems. As an approximation method to solve the electronic Schrödinger equation (3.4) for molecular systems we introduce in the next section the LCAO approximation.

3.2 LINEAR COMBINATION OF ATOMIC ORBITALS

The Linear Combination of Atomic Orbitals (LCAO) method is an approximation method for molecular orbitals [70]. This method assumes that the molecular orbitals can be constructed as a superposition of atomic orbitals. We show here, how the *Hartree-Fock equations*, derived in the previous chapter, transform under this approximation to the *Roothaan equations* for molecular systems [92]. Consider the electronic, non-relativistic Hamiltonian for the many-electron molecule in atomic units

$$H_{\text{el}} = H_0 + V = -\sum_i \frac{\nabla^2_{\mathbf{r}_i}}{2} + \sum_{i>j,j} \frac{1}{|\mathbf{r}_i - \mathbf{r}_j|} - \sum_{i,\alpha} \frac{Z_\alpha}{|\mathbf{r}_i - \mathbf{r}_\alpha|} + \sum_{\alpha>\beta,\beta} \frac{Z_\alpha Z_\beta}{|\mathbf{r}_\alpha - \mathbf{r}_\beta|}. \tag{3.11}$$

Here, the indices i, j refer to electron coordinates whereas α, β refer to the coordinates of the nuclei. Z_α is the nuclear charge of the atom α. The Hamiltonian H_0 without electron repulsion is given by

$$H_0 = \sum_i h_0(i) = \sum_i \left\{ -\frac{\nabla^2_{\mathbf{r}_i}}{2} - \sum_\alpha \frac{Z_\alpha}{|\mathbf{r}_i - \mathbf{r}_\alpha|} + \sum_{\alpha>\beta,\beta} \frac{Z_\alpha Z_\beta}{|\mathbf{r}_\alpha - \mathbf{r}_\beta|} \right\}, \tag{3.12}$$

where h_0 is a generalization of the one-electron operator h_0 (2.41) of the atomic case and conventionally includes the repulsions between the nuclei. Consider now the LCAO ansatz

$$|\phi_\mu\rangle = \sum_j c_{j\mu} |\varphi_j\rangle , \tag{3.13}$$

with $|\phi_\mu\rangle$ the molecular orbitals, $|\varphi_j\rangle$ the atomic orbitals and $c_{j\mu}$ the expansion coefficients. We note that the atomic orbitals are not necessarily orthogonal and the overlap integral is given by

$$S_{ij} = \langle \varphi_i | \varphi_j \rangle. \tag{3.14}$$

However, the molecular orbitals satisfy the orthogonality condition

$$\langle \phi_\mu | \phi_\nu \rangle = \delta_{\mu\nu}. \tag{3.15}$$

Inserting the LCAO ansatz (3.13) in the *Hartree-Fock equations* (2.70) leads to the *Hartree-Fock equations* in LCAO form which are called the *Roothaan equations*. The *Roothaan equations* read

$$\sum_j \left(F_{ij} - \varepsilon_\mu S_{ij} \right) c_{j\mu} = 0, \tag{3.16}$$

where we have introduced the Fock operator in LCAO form

$$F_{ij} = H_{ij} + \sum_{\nu lk} c^*_{l\nu} c_{k\nu} c_{j\mu} \left[2\langle ij|lk\rangle - \langle ik|lj\rangle \right], \tag{3.17}$$

with

$$H_{ij} = \langle \varphi_i | \, h_0 \, | \varphi_j \rangle , \tag{3.18}$$

where h_0 is defined in equation (3.12), and

$$\langle ij|lk\rangle \equiv \langle \varphi_i, \varphi_l| \frac{1}{|\mathbf{r}_1 - \mathbf{r}_2|} |\varphi_j, \varphi_k\rangle . \tag{3.19}$$

The energies ε_μ in the *Roothaan equations* are the molecular orbital energies of the molecular orbital ϕ_μ. The *Roothaan equations* have nontrivial solutions for the coefficients $c_{j\mu}$ only if

$$\det |F_{ij} - \varepsilon_\mu S_{ij}| = 0, \tag{3.20}$$

holds. The *Roothaan equations* (3.16) can be solved again by *self-consistent field* methods. Starting with an initial guess for the coefficients $\{c_{j\mu}\}$ one solves (3.16), (3.20) for a new set of $\{c_{j\mu}\}$ until they converge. With these coefficients one obtains the molecular orbitals ϕ_μ with equation (3.13). The total energy of a closed-shell system can be calculated by

$$E = 2\sum_\mu I_\mu + \sum_{\mu\nu} \left[2J_{\mu\nu} - K_{\mu\nu}\right], \tag{3.21}$$

where the one-electron integral I_μ and the Coulomb and exchange integrals [see equations (2.65)] are given by

$$I_\mu = \sum_{ij} c^*_{i\mu} c_{j\mu} H_{ij}, \tag{3.22a}$$

$$J_{\mu\nu} = \sum_{ijkl} c^*_{i\mu} c^*_{l\nu} c_{j\mu} c_{k\nu} \langle ij|lk\rangle, \tag{3.22b}$$

$$K_{\mu\nu} = \sum_{ijkl} c^*_{i\mu} c^*_{l\nu} c_{j\mu} c_{k\nu} \langle ik|lj\rangle. \tag{3.22c}$$

In order to introduce the molecular orbitals of diatomic systems we calculate in the next section the ground state of H_2^+ within the LCAO and assume hydrogen orbitals as a basis to construct molecular electronic states.

3.3 H_2^+ MOLECULE

The H_2^+ molecule is a one-electron system. We introduce this example because it is suitable to illustrate the LCAO method, the *Born-Oppenheimer potentials* and the symmetries of electronic molecular states. The electronic Hamiltonian for H_2^+ in atomic units reads

$$H_{\text{el}} = h_0 + \frac{1}{R} = \left(-\frac{\nabla^2_{\mathbf{r}}}{2} - \frac{1}{r_A} - \frac{1}{r_B}\right) + \frac{1}{R}, \tag{3.23}$$

where the coordinates are given in figure 3.1. The first term is the kinetic energy of the electron, the second and third terms are the attraction terms between the electron and the protons of atom A and of atom B whereas the last term describes the Coulomb repulsion between the protons. The Schrödinger equation for this system can be solved analytically in spheroidal coordinates [93]

$$\mu = \frac{r_A + r_B}{R}, \quad \nu = \frac{r_A - r_B}{R}, \quad \tan\varphi = \frac{y}{x}, \tag{3.24}$$

with x, y the components of $\mathbf{r}$. However, we do not follow this approach as it is not applicable to heavier molecules anymore. Instead, we solve the Schrödinger equation within the LCAO approximation which was introduced in the previous section.

3.3.1 *Potential energy curves*

In order to calculate the potential energy curves for the ground states of H_2^+ we assume that the molecular ground states can be approximated by a superposition of two ground state hydrogen orbitals $|1s_A\rangle$, $|1s_B\rangle$, centered on atom A and B, respectively. From equation (3.13) we then have

$$|\phi_\mu\rangle = c_{A\mu} |1s_A\rangle + c_{B\mu} |1s_B\rangle , \tag{3.25}$$

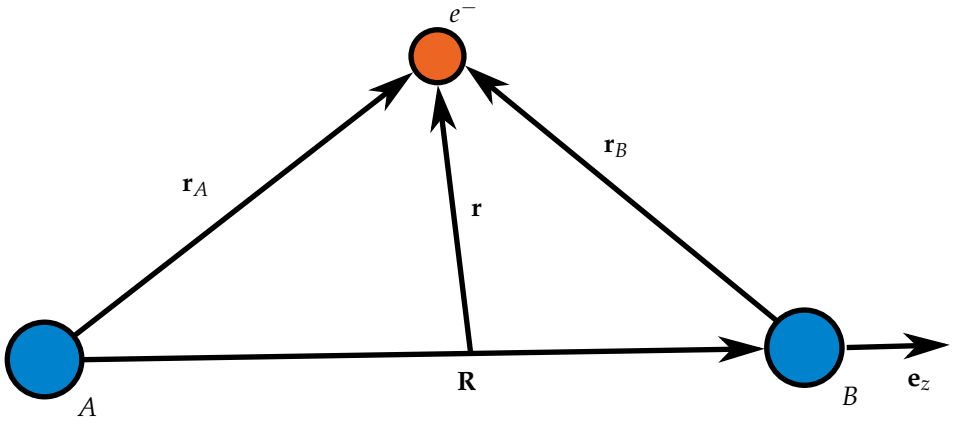

Figure 3.1: H_2^+ molecule and coordinate system. The internuclear axis is along z-direction.

with ϕ_μ the μth molecular orbital. The atomic orbitals $|1s_A\rangle$, $|1s_B\rangle$ are the hydrogen orbitals φ_{100} of table 2.1 with $Z = 1$, but displaced to the origin of the atoms A and B. If the atoms A and B are placed on the z-axis at $z = -R/2$ and $z = +R/2$, respectively, the radial distances r_A, r_B are given by

$$r_{A/B} = \sqrt{x^2 + y^2 + (z \mp R/2)^2}. \tag{3.26}$$

Inserting the LCAO ansatz (3.25) in the *Roothaan equations* (3.16) leads to nontrivial solutions for c_A, c_B only if

$$\begin{vmatrix} H_{11} - E_\mu & H_{12} - E_\mu S_{12} \\ E_{12} - E_\mu S_{12} & H_{22} - E_\mu \end{vmatrix} = 0, \tag{3.27}$$

holds. Here, H_{ij} is given by equation (3.18) where h_0 is defined in equation (3.23) and the indices i, j denote the hydrogen orbitals $|1s_A\rangle$, $|1s_B\rangle$. The atomic overlap integral S_{12} was given in equation (3.14) and the energy E_μ is the orbital energy. As H_2^+ is a one-electron system, E_μ corresponds also to the total electronic energy of the system. Solving equation (3.27) for E_μ we obtain the two solutions

$$E_1 = \frac{H_{11} + H_{12}}{1 + S_{12}}, \tag{3.28a}$$

$$E_2 = \frac{H_{11} - H_{12}}{1 - S_{12}}, \tag{3.28b}$$

where E_1, E_2 are the electronic ground state and first excited state energy of H_2^+, respectively. We have used that $H_{11} = H_{22}$. The coefficients c_{A1}, c_{B1} of solution 1 and c_{A2}, c_{B2} of solution 2 read

$$c_{A1} = c_{B1} = \frac{1}{\sqrt{2(1 + S_{AB})}}, \quad c_{A2} = -c_{B2} = \frac{1}{\sqrt{2(1 - S_{AB})}}, \tag{3.29}$$

respectively. In total we obtain a pair of solutions for the energy eigenvalues E_1, E_2 given by equation (3.28) and the molecular orbitals

$$|\phi_1\rangle = \frac{1}{\sqrt{2(1 + S_{AB})}} \left(|1s_A\rangle + |1s_B\rangle\right), \tag{3.30a}$$

$$|\phi_2\rangle = \frac{1}{\sqrt{2(1 - S_{AB})}} \left(|1s_A\rangle - |1s_B\rangle\right). \tag{3.30b}$$

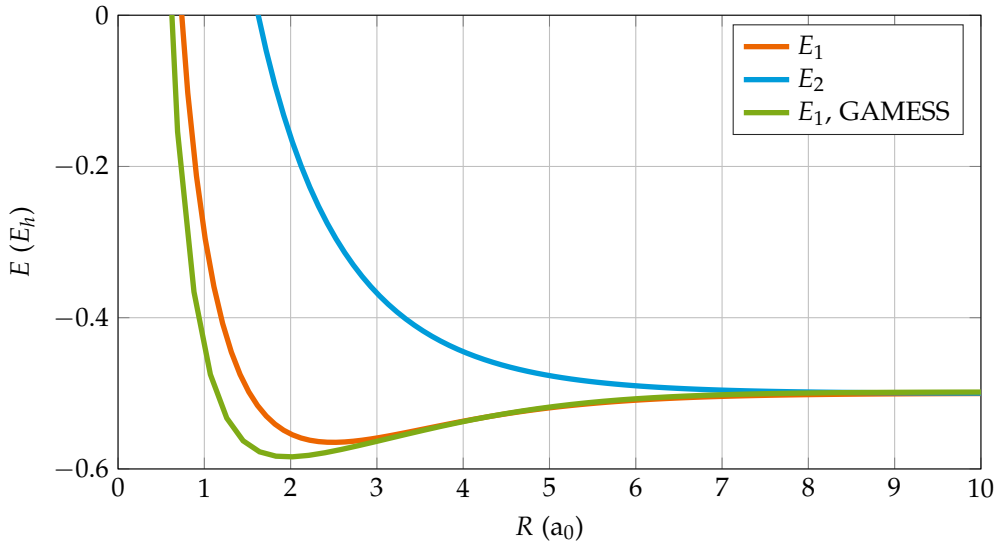

Figure 3.2: Potentials $E_1(R)$, $E_2(R)$ of H_2^+ in the LCAO approximation. The orange and blue lines are calculated by the equations (3.28). The green solid line for $E_1(R)$ was obtained by an electronic structure calculation using GAMESS with the $6-31G$ basis set.

With $|1s_A\rangle$, $|1s_B\rangle$ given by the displaced hydrogen atomic orbitals we can calculate the integrals H_{11}, H_{12} and S_{12} analytically. Using the spheroidal coordinates (3.24) we obtain [93–95]

$$H_{11}(R) = -\tfrac{1}{2} + e^{-2R}\left(\tfrac{1}{R}+1\right), \tag{3.31a}$$

$$H_{12}(R) = e^{-R}\left(\tfrac{1}{R} - \tfrac{1}{2} - \tfrac{7}{6}R - \tfrac{1}{6}R^2\right), \tag{3.31b}$$

$$S_{12}(R) = e^{-R}\left(1 + R + \tfrac{1}{3}R^2\right). \tag{3.31c}$$

Inserting these results in the equations (3.28) finally leads to the potential energy curves $E_1(R)$ and $E_2(R)$ of H_2^+. These are the *Born-Oppenheimer potentials* (3.4) of the electronic Hamiltonian H_{el} of H_2^+ (3.23). We have obtained these potential curves under the assumption that the molecular orbitals are given by the LCAO approximation (3.25).

Figure 3.2 shows $E_1(R)$ and $E_2(R)$. The potential curve $E_1(R)$ is attractive and leads to bonding solutions whereas $E_2(R)$ is repulsive and leads to anti-bonding solutions [78]. $E_1(R)$ and $E_2(R)$ are approximations to the energetically lowest-lying molecular states of H_2^+ with s character as they are constructed from hydrogen s-orbitals. To obtain higher-lying states one has to include more atomic basis functions in the LCAO ansatz (3.13) and also basis functions which are not only of s-type but also of p-type, d-type, etc. Figure 3.2 also shows the solution of an UHF calculation of $E_1(R)$ potential energy performed with GAMESS. The basis set chosen in GAMESS is a $6-31G$ basis which is larger than the set of basis states in equation (3.25). More details about this basis in GAMESS is given in section 6.5. Here we give the numerical GAMESS solution to demonstrate the variational principle. A larger basis has more free parameters and the energy eigenvalue becomes smaller. In order to verify that the $6-31G$ basis set is a good choice we depict the result in figure 3.2. The minimum of $E_1(R)$ (3.28a) is $E_{\text{min}} = -0.5648\,E_h$ while the numerical solution of GAMESS leads to $E_{\text{min}} = -0.5840\,E_h$. The exact solution is given by $E_{\text{min}} = -0.6025\,E_h$ [81] so that the solution with the minimal basis set differs by 6 % while the solution with the $6-31G$ basis set differs only by 3 %. Additionally, the equilibrium position R_{eq} or bond length of $E_1(R)$ which is the position of the minimum of $E_1(R)$ is closer to the exact solution for the $6-31G$ basis than for $E_1(R)$ in equation (3.28a). The exact value reads $R_{\text{eq}} = 2.00\ \text{a}_0$ [81]. The equilibrium distance obtained by the $6-31G$ basis set reads $R_{\text{eq}} = 2.02\ \text{a}_0$ differing by 1 % from the exact solution while the equilibrium distance obtained

by the minimal basis set (3.25) reads $R_{\text{eq}} = 2.49\,a_0$ differing by almost 25 % from the exact solution.

The molecular orbitals (3.30) of H_2^+ have certain symmetries. In the next subsection we discuss the symmetry aspects of the electronic molecular states from a group-theoretical point of view and introduce the notation for these molecular states.

3.3.2 *Symmetries of molecular states*

Symmetry operations on diatomic molecules are elements of the point symmetry group $D_{\infty h}$ [40], where the name $D_{\infty h}$ is due to the *Schoenflies notation* [78]. The elements of this group are given by

$$D_{\infty h} = \left\{E,\ 2C_\varphi,\ i,\ 2iC_\varphi = 2S_\varphi,\ \sigma_v,\ i\sigma_v = C_2\right\}, \tag{3.32}$$

where E is the identity transformation, $2C_\varphi$ are the rotations through the angle $\pm\varphi$ about the molecular axis (which is simply the internuclear axis of atom A and B for diatomic molecules), i is the inversion at the center of charge of the molecule, $2iC_\varphi$ is the rotation $2C_\varphi$ followed by the inversion i, σ_v is the reflection in a plane containing the molecular axis and $i\sigma_v$ is the reflection σ_v followed by the inversion i. We have introduced the symmetry operations i and σ_v already in the previous chapter for atoms. However, for molecules the reflection of electron coordinates is at the molecular center and the symmetry axis for σ_v is the internuclear axis.

In the previous section, we combined $|1s\rangle$ orbitals of atomic hydrogen centered on atom A and B and as a result of minimizing the energy we obtained two solutions to the Schrödinger equation for H_2^+ of the form

$$|\phi_1\rangle = |s_A\rangle + |s_B\rangle\,, \tag{3.33a}$$
$$|\phi_2\rangle = |s_A\rangle - |s_B\rangle\,, \tag{3.33b}$$

where $|s_A\rangle$ and $|s_B\rangle$ were the $1s$ orbitals of hydrogen, centered at atom A and atom B, respectively. Here, we neglected the normalization factor and also omitted the principal quantum number n as $|s_A\rangle$ and $|s_B\rangle$ are used in a more general sense denoting general atomic orbitals of s-type. It is also possible to combine other types of orbitals. Consider the hydrogen hybrid p_x, p_y and p_z orbitals of table 2.2. From these atomic orbitals we can construct molecular orbitals as

$$|\phi_3\rangle = |p_{zA}\rangle + |p_{zB}\rangle\,, \quad |\phi_4\rangle = |p_{zA}\rangle - |p_{zB}\rangle\,, \tag{3.34}$$

and as

$$|\phi_5\rangle = |p_{xA}\rangle + |p_{xB}\rangle\,, \quad |\phi_6\rangle = |p_{yA}\rangle + |p_{yB}\rangle\,, \tag{3.35a}$$
$$|\phi_7\rangle = |p_{xA}\rangle - |p_{xB}\rangle\,, \quad |\phi_8\rangle = |p_{yA}\rangle - |p_{yB}\rangle\,. \tag{3.35b}$$

Again the subscripts A, B denote the displaced atomic orbitals centered at atom A and B, respectively. As for s-type orbitals the discussion here is not restricted to hydrogen-like orbitals for given quantum number n but is general for all atomic orbitals of p_x, p_y or p_z type.

The electronic molecular states given in the equations (3.33), (3.34), (3.35) are basis functions of different representations Γ of the group $D_{\infty h}$. The symmetry operations of this group are given by the coordinate transformation

$$\mathbf{r}' = R\mathbf{r}, \tag{3.36}$$

where $\mathbf{r}$ are the electronic coordinates and R is the transformation which describes rotation or reflection of the coordinates. A function $f(\mathbf{r})$ transforms under this coordinate transformation as [40]

$$\mathcal{P}_R f(\mathbf{r}) = f(R^{-1}\mathbf{r}). \tag{3.37}$$

Applying the operator $\mathcal{P}_R$ to the basis functions $|\phi^{(j)}\rangle$ of the jth representation $\Gamma^{(j)}$ of $D_{\infty h}$ generates this particular representation $\Gamma^{(j)}$, i.e.

$$\mathcal{P}_R\,|\phi_k^{(j)}\rangle = \sum_{\lambda=1}^{n} |\phi_\lambda^{(j)}\rangle\,\Gamma_{\lambda k}^{(j)}(R). \tag{3.38}$$

The number n is the total number of basis functions for the jth representation of the group. As an example we apply $\mathcal{P}_R$ for all the elements of $D_{\infty h}$ to the molecular state $|\phi_1\rangle$ in (3.33a) which results in

$$\mathcal{P}_E |\phi_1\rangle = |\phi_1\rangle\,,\ \mathcal{P}_{C_\varphi} |\phi_1\rangle = |\phi_1\rangle\,,\ \mathcal{P}_{iC_2} |\phi_1\rangle = |\phi_1\rangle\,,$$
$$\mathcal{P}_i |\phi_1\rangle = |\phi_1\rangle\,,\ \mathcal{P}_{S\varphi} |\phi_1\rangle = |\phi_1\rangle\,,\ \mathcal{P}_{C_2} |\phi_1\rangle = |\phi_1\rangle\,. \tag{3.39}$$

This shows that the orbital $|\phi_1\rangle$ is a basis function for the *unit representation* where Γ is given by

$$\Gamma_E = 1,\ \Gamma_{C_\varphi} = 1,\ \Gamma_{iC_2} = 1,\ \Gamma_i = 1,\ \Gamma_{S\varphi} = 1,\ \Gamma_{C_2} = 1, \tag{3.40}$$

with $\Gamma(R) \equiv \Gamma_R$. Under a similarity transformation the trace of a matrix is invariant. In group theory, the trace $\xi_R^{(j)}$ of a representation matrix is called its character. The trace of $\Gamma_R^{(j)}$ is given by

$$\xi_R^{(j)} = \mathrm{Tr}\,\Gamma_R^{(j)} = \sum_\alpha \Gamma_{\alpha\alpha}^{(j)}(R). \tag{3.41}$$

For the *unit representation* we have $\xi_R = 1$ for all elements of the group. These characters characterize the symmetries of the basis functions $|\phi^{(j)}\rangle$ under the symmetry operations of the group. They are summarized in character tables. Table 3.1 displays the characters for the irreducible representations of the $D_{\infty h}$ group.

$D_{\infty h}$	E	$2C_\varphi$	σ_v	i	$2S_\varphi$	C_2
σ_g^+	1	1	1	1	1	1
σ_g^-	1	1	−1	1	1	−1
π_g	2	$2\cos\varphi$	0	2	$-2\cos\varphi$	0
δ_g	2	$2\cos 2\varphi$	0	2	$2\cos 2\varphi$	0
...	...	...	...	...	...	...
σ_u^+	1	1	1	−1	−1	−1
σ_u^-	1	1	−1	−1	−1	1
π_u	2	$2\cos\varphi$	0	−2	$2\cos\varphi$	0
δ_u	2	$2\cos 2\varphi$	0	−2	$-2\cos 2\varphi$	0
...	...	...	...	...	...	...

Table 3.1: Table of characters for the elements of the infinite point group $D_{\infty h}$. The states σ_g^+, σ_g^-, ... are the irreducible representations of $D_{\infty h}$ and E, $2C_\varphi$, ... are the elements of $D_{\infty h}$.

In the first row the characters of the unit representation is given and the irreducible representation is called σ_g^+. Thus, the molecular orbital $|\phi_1\rangle$ transforms according to the σ_g^+ irreducible representation of $D_{\infty h}$ and is therefore called a $|\sigma_g^+\rangle$ state. Here, the g symmetry reflects the symmetry of the molecular orbital under the inversion of the electronic coordinates at the molecular center given by the symmetry operation i. For $\mathcal{P}_i |\phi\rangle = |\phi\rangle$ the molecular state is denoted as a g state while for $\mathcal{P}_i |\phi\rangle = -|\phi\rangle$ the state has u symmetry. The g/u symmetry only occurs for homonuclear diatomic molecules. The $+$ symmetry reflects the symmetry of the molecular orbital under the symmetry operation σ_v. For $\mathcal{P}_{\sigma_v} |\phi\rangle = |\phi\rangle$ the state is denoted by $+$ while for $\mathcal{P}_{\sigma_v} |\phi\rangle = -|\phi\rangle$ it is denoted by $-$. The $+/-$ symmetry only occurs for σ molecular states. We can now apply the operators $\mathcal{P}_R$ to all the other orbitals in the equations (3.33), (3.34), (3.35). This generates different representations $\Gamma_R^{(j)}$ of $D_{\infty h}$ and from the characters of these representations we will find that the molecular state $|\phi_2\rangle$ transforms according to the σ_u^+ representation and is labeled as a $|\sigma_u^+\rangle$ state. The states $|\phi_3\rangle$, $|\phi_4\rangle$ transform accordingly to the σ_g^+ representation and are labeled as $|\sigma_g^+\rangle$ states. The states $|\phi_5\rangle$, $|\phi_6\rangle$ belong to the π_u representation and are labeled as $|\pi_u\rangle$ states while $|\phi_7\rangle$, $|\phi_8\rangle$ belong to the π_g representation and are correspondingly named as $|\pi_g\rangle$ states.

For more details regarding the group-theoretical aspects of the discussion in this subsection, we refer the interested reader to the literature [40]. Here we have discussed the symmetries of molecular states in terms of the one-electron states of H_2^+. However, as mentioned in the

introduction of this subsection, the results apply generally and also hold for many-electron molecular states constructed from the atomic orbitals.

3.4 COUPLING IN DIATOMIC MOLECULES

Here, we introduce different coupling schemes in molecular states which leads to the different molecular bases in which the interaction potentials of Ne* have been calculated. In figure 3.3 the angular momenta of diatomic molecules are shown. The angular momenta couple in different

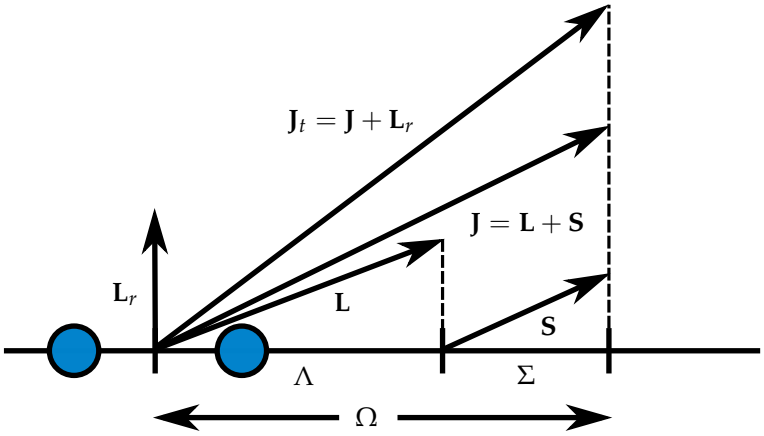

Figure 3.3: Diatomic molecule with total electronic orbital angular momentum $\mathbf{L}$ and total electronic spin $\mathbf{S}$ and the projections Λ, Σ on the internuclear axis. $\mathbf{L}$ and $\mathbf{S}$ couple to the total electronic angular momentum $\mathbf{J}$ with projection Ω on the internuclear axis. The total angular momentum operator, including rotation $\mathbf{L}_r$ of the molecule, is given by $\mathbf{J}_t = \mathbf{J} + \mathbf{L}_r$.

ways depending on the strengths of the different interaction types and the corresponding molecular states are classified due to the five *Hund's coupling cases* $(a) - (e)$ [47, 70, 71]. The molecular interaction potentials of Ne* have been calculated at short-range in the *Hund's case* (a) basis and at long-range in the *Hund's case* (c) basis.

The *Hund's case* (a) states are designated as $|L\Lambda S\Sigma\rangle$ states and the eigenvalue equations for total orbital angular momentum operator $\mathbf{L}$ and total electronic spin $\mathbf{S}$ read

$$\mathbf{L}^2 |L\Lambda S\Sigma\rangle = L(L+1) |L\Lambda S\Sigma\rangle , \qquad L_{\mathbf{R}} |L\Lambda S\Sigma\rangle = \Lambda |L\Lambda S\Sigma\rangle , \tag{3.42}$$

$$\mathbf{S}^2 |L\Lambda S\Sigma\rangle = S(S+1) |L\Lambda S\Sigma\rangle , \qquad S_{\mathbf{R}} |L\Lambda S\Sigma\rangle = \Sigma |L\Lambda S\Sigma\rangle . \tag{3.43}$$

Note that the eigenvalues L, S of the angular momentum operator and the spin operator are denoted by uppercase letters in order to not confuse them with the expectation values for atomic states. $L_{\mathbf{R}} = \mathbf{L}\mathbf{n}_R$, $S_{\mathbf{R}} = \mathbf{S}\mathbf{n}_R$ are the projections of orbital angular momentum and spin on the internuclear axis with $\mathbf{n}_R = \mathbf{R}/R$. In the *Hund's case* (a) the total spin $\mathbf{S}$ and the projection Λ of orbital angular momentum on the internuclear axis are the good quantum numbers. The projection Λ is given by

$$\Lambda \equiv |\Lambda_L|, \quad \Lambda_L = \sum_i \Lambda_{L,i}, \tag{3.44}$$

with $\Lambda_{L,i}$ the projection of the orbital angular momentum operator $\mathbf{L}_i$ of the ith electron on the internuclear axis. The electronic molecular states are classified due to different values of Λ. The reason is, that the electric field between the nuclei A and B generates at short internuclear distances preferred axis in the system so that the projection on the internuclear axis is a good quantum number. Similar to the *Stark effect* for atoms in a homogeneous electric field, the energy of the electronic states only depends on the absolute value of the projection $|\Lambda_L|$ [40]. For $\Lambda = 0, 1, 2, \ldots$ the molecular states are labeled as $\Sigma, \Pi, \Delta, \ldots$ states analogously to the

designation of atomic states as S, P, D states. Also analogously to atomic states the difference of a one-electron state and a many electron state in the notation is given by lowercase and upper case letters. Therefore, the states of H_2^+ discussed in the previous subsection were introduced as $\sigma, \pi, \delta, \ldots$ states. The spectroscopic notation of an n-electron molecular state in *Hund's case* (a) is given by [47]

$$^{(2S+1)}\Lambda_{g/u}^{+/-}, \tag{3.45}$$

and g/u and $+/-$ symmetries of the *Hund's case* (a) states are given by [46]

$$\mathcal{P}_i \left|L\Lambda S\Sigma\right\rangle = (-1)^{L+S} \left|L\Lambda S\Sigma\right\rangle, \quad \mathcal{P}_{\sigma_v} \left|L\Lambda S\Sigma\right\rangle = (-1)^{L-\Lambda} \left|L-\Lambda S\Sigma\right\rangle. \tag{3.46}$$

The *Hund's case* (c) states are designated as $|J\Omega\rangle$ states and the eigenvalue equations for the total electronic angular momentum $\mathbf{J}$ read

$$\mathbf{J}^2 \left|J\Omega\right\rangle = J(J+1) \left|J\Omega\right\rangle, \qquad J_{\mathbf{R}} \left|J\Omega\right\rangle = \Omega \left|J\Omega\right\rangle, \tag{3.47}$$

with $J_{\mathbf{R}} = \mathbf{J}\mathbf{n}_R$ the projection on the internuclear axis. Here, J and Ω are good quantum numbers instead of Λ and S. The spectroscopic notation for a *Hund's case* (c) state reads

$$J\Omega_{g/u}^{+/-}, \tag{3.48}$$

and the g/u symmetry of a *Hund's case* (c) state is given by [70]

$$\mathcal{P}_i \left|J\Omega\right\rangle = (-1)^J \left|J\Omega\right\rangle. \tag{3.49}$$

In chapter 6 we introduce the molecular potentials of Ne_2 in these two molecular bases. In order to illustrate the many-electron molecular orbitals we introduce in the next section the two-electron molecule H_2.

3.5 H_2 MOLECULE

Here, we discuss the two-electron molecular states of H_2 and introduce the *Heitler-London approximation* as a approximation method for molecular orbitals. The H_2 molecule consists of two electrons and two protons. The non-relativistic electronic Hamiltonian for the H_2 molecule in atomic units reads [40]

$$H_{\text{el}} = -\frac{1}{2}\left(\nabla_{\mathbf{r}_1}^2 + \nabla_{\mathbf{r}_2}^2\right) - \frac{1}{r_{A1}} - \frac{1}{r_{B1}} - \frac{1}{r_{A2}} - \frac{1}{r_{B2}} + \frac{1}{r_{12}} + \frac{1}{R} = h_0(1) + h_0(2) + \frac{1}{r_{12}} - \frac{1}{R}, \tag{3.50}$$

where $h_0(i)$ with $i \in \{1, 2\}$ is given by

$$h_0(i) = -\frac{1}{2}\nabla_{\mathbf{r}_i}^2 - \frac{1}{r_{Ai}} - \frac{1}{r_{Bi}} + \frac{1}{R}. \tag{3.51}$$

The terms $h_0(i)$ are identical to the Hamiltonian of H_2^+ (3.23) and describe the energy of the H_2^+ molecule ion so that the energy of H_2 is twice the energy of H_2^+ plus an additional term. This additional term describes the Coulomb repulsion between the two electrons in H_2 and the Coulomb repulsion between the two protons. Figure 3.4 shows a scheme of the H_2 molecule showing the positions of the two electrons and the two protons of the system and introduces the coordinates we are using.

3.5.1 *Two-electron molecular states*

For the spatial part of the electron wave function of the H_2 molecule we choose the LCAO ansatz (3.25) of H_2^+ where the molecular orbitals are constructed by hydrogen orbitals. This ansatz is natural as the H_2 molecule consists of two hydrogen atoms and for large internuclear

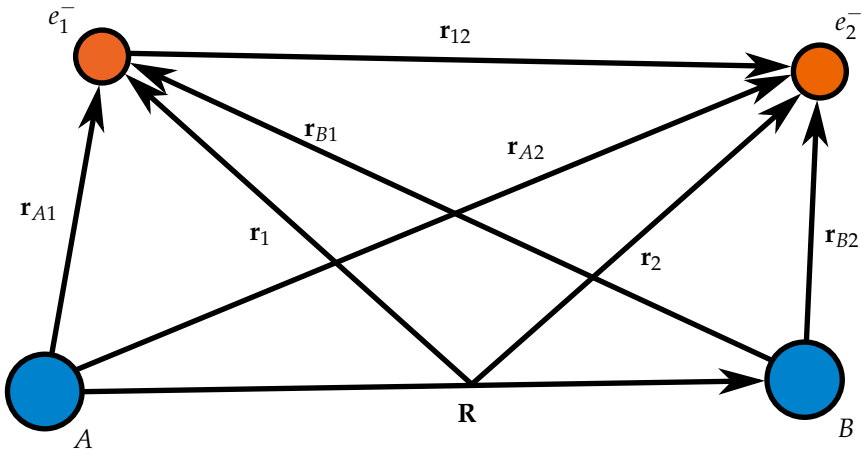

Figure 3.4: Coordinates in H_2 molecule.

separations dissociates into the atomic limit H–H. Within this ansatz we obtain the same molecular orbitals as for H_2^+ which read

$$|1\sigma_g\rangle = \frac{1}{\sqrt{2+2S_{12}}}\left(|1s_A\rangle + |1s_B\rangle\right), \quad |1\sigma_u\rangle = \frac{1}{\sqrt{2-2S_{12}}}\left(|1s_A\rangle - |1s_B\rangle\right). \tag{3.52}$$

Here, we have included the considerations on symmetries of molecular states of section 3.3.2 and labeled the one-electron molecular orbitals due to their symmetry properties. The overlap integral S_{12} is given by equation (3.14). In order to obtain the complete two-electron state of H_2 we have to introduce the electronic spin in the system. In full analogy to atomic systems we can represent the total two-electron state as a fully antisymmetric Slater determinant. Assume for example the ground state electronic configuration $1\sigma_g^2$ where both electrons of H_2 occupy the spatial orbital $|1\sigma_g\rangle$. The Slater determinant for this configuration reads

$$|1\sigma_g^2\ {}^1\Sigma_g^+\rangle \equiv |1\sigma_g\alpha\ 1\sigma_g\beta\rangle \equiv \frac{1}{\sqrt{2}}\begin{vmatrix} 1\sigma_g\alpha(1) & 1\sigma_g\beta(1) \\ 1\sigma_g\alpha(2) & 1\sigma_g\beta(2) \end{vmatrix}, \tag{3.53}$$

where α and β were introduced in chapter 2 as the spin projections of the electrons on the quantization axis. The designation of this state as ${}^1\Sigma_g^+$ state is due to the *Hund's case* (a). The symmetries arise from the properties under the symmetry transformations of $D_{\infty h}$ (see section 3.3.2). As the spins have to be anti-parallel because the electrons occupy the same spatial orbital, the ground state of H_2 is a singlet state.

Consider now the first excited state configuration $1\sigma_g 1\sigma_u$ of H_2. The possible ways for the electrons to occupy the orbitals $1\sigma_g$, $1\sigma_u$ are shown in the subfigures $(ii) - (v)$ of the figure 3.5. From the $1\sigma_g 1\sigma_u$ configuration one can construct singlet and triplet spin states. The singlet state reads

$$|1\sigma_g 1\sigma_u\ {}^1\Sigma_u^+\rangle = \frac{1}{\sqrt{2}}\left(|1\sigma_g\alpha\ 1\sigma_u\beta\rangle - |1\sigma_g\beta\ 1\sigma_u\alpha\rangle\right), \tag{3.54}$$

and the triplet state is given by

$$|1\sigma_g 1\sigma_u\ {}^3\Sigma_u^+\rangle = \begin{cases} |1\sigma_g\alpha\ 1\sigma_u\alpha\rangle, \\ \frac{1}{\sqrt{2}}\left(|1\sigma_g\alpha\ 1\sigma_u\beta\rangle + |1\sigma_g\beta\ 1\sigma_u\alpha\rangle\right), \\ |1\sigma_g\beta\ 1\sigma_u\beta\rangle. \end{cases} \tag{3.55}$$

These states transform according to the σ_u^+ irreducible representations of $D_{\infty h}$. If both electrons occupy the excited $1\sigma_u$ orbital the fully anti-symmetrized state for this configuration reads

$$|1\sigma_u^2\ {}^1\Sigma_g^+\rangle = |1\sigma_u\alpha\ 1\sigma_u\beta\rangle, \tag{3.56}$$

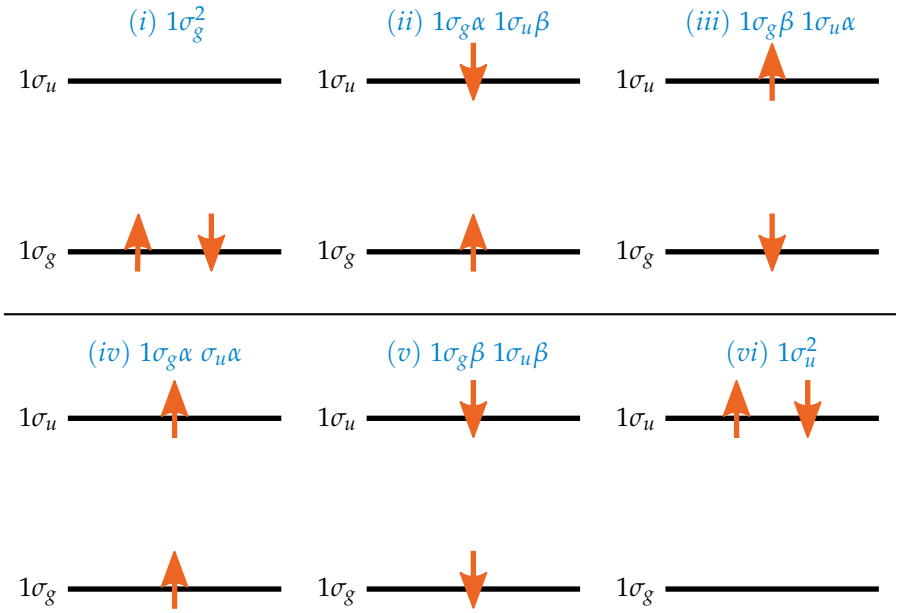

Figure 3.5: All six possibilities of the two electrons in H_2 to occupy the energetically lowest-lying spatial orbitals $1\sigma_g$, $1\sigma_u$. The orange arrows indicate the direction of the spin-projection of the electrons. The subfigure (i) shows the configuration $1\sigma_g^2$, the subfigures $(ii) - (v)$ show the configuration $1\sigma_g 1\sigma_u$ and the subfigure (vi) shows the configuration $1\sigma_u^2$.

which as the ground state is a Σ_g^+ state due to its symmetry properties and its singlet character. For the H_2 molecular orbitals $|1\sigma_g\rangle$, the one- and two-electron integrals I, J of molecular orbitals given in equation (3.22) read

$$I(1\sigma_g) = \langle 1\sigma_g | \, h_0 \, | 1\sigma_g \rangle \,, \quad J(1\sigma_g, 1\sigma_g) = \langle 1\sigma_g, 1\sigma_g | \, \frac{1}{|\mathbf{r}_1 - \mathbf{r}_2|} \, | 1\sigma_g, 1\sigma_g \rangle \,. \tag{3.57}$$

Together with the expression of the *Hartree-Fock* energy in LCAO form (3.21) we can write the total energy of the ground state of the H_2 molecule in the LCAO approximation as

$$E = \langle 1\sigma_g^2 \, {}^1\Sigma_g^+ | \, H_{\text{el}} \, | 1\sigma_g^2 \, {}^1\Sigma_g^+ \rangle = 2I(1\sigma_g) + J(1\sigma_g, 1\sigma_g). \tag{3.58}$$

For the energies of the excited states we remember the definition of the exchange integral K which reads

$$K(1\sigma_g, 1\sigma_u) = \langle 1\sigma_g, 1\sigma_u | \, \frac{1}{|\mathbf{r}_1 - \mathbf{r}_2|} \, | 1\sigma_u, 1\sigma_g \rangle \,, \tag{3.59}$$

and only exists for parallel spins of the electrons. With the equations (3.57), (3.59) we can calculate the energies of the excited states (3.54), (3.55), (3.56) of the H_2 molecule. In the LCAO we obtain from the *Hartree-Fock* energy (3.21) the following excited state energies

$$E = \langle 1\sigma_g 1\sigma_u \, {}^1\Sigma_u^+ | \, H_{\text{el}} \, | 1\sigma_g 1\sigma_u \, {}^1\Sigma_u^+ \rangle = I(1\sigma_g) + I(1\sigma_u) + J(1\sigma_g, 1\sigma_u) + K(1\sigma_g, 1\sigma_u), \tag{3.60}$$

$$E = \langle 1\sigma_g 1\sigma_u \, {}^3\Sigma_u^+ | \, H_{\text{el}} \, | 1\sigma_g 1\sigma_u \, {}^3\Sigma_u^+ \rangle = I(1\sigma_g) + I(1\sigma_u) + J(1\sigma_g, 1\sigma_u) - K(1\sigma_g, 1\sigma_u), \tag{3.61}$$

$$E = \langle 1\sigma_u^2 \, {}^1\Sigma_g^+ | \, H_{\text{el}} \, | 1\sigma_u^2 \, {}^1\Sigma_g^+ \rangle = 2I(1\sigma_u) + J(1\sigma_u, 1\sigma_u). \tag{3.62}$$

As stated above, these energies all result from the LCAO approximation for the molecular orbitals (3.52) and are valid within this approximation. There exist other ways of constructing molecular orbitals, for example, the *Heitler-London* (HL) method [77, 79]. In the next subsection we introduce this alternative approach and compare it to the LCAO method for the H_2 molecule. We calculate analytically the energy integrals within the HL approximation and compare the resulting energies to a numerical calculation for H_2 within the LCAO approximation.

3.5.2 *Heitler-London method*

Here, we introduce the *Heitler-London* (HL) method as an alternative approximation method to construct molecular orbitals. The spatial parts of the lowest two-electron states of H_2 in the HL method are given by [47]

$$|\phi(1,2)\rangle_{\mathrm{HL}} = |1s_A(1), 1s_B(2)\rangle \pm |1s_B(1), 1s_A(2)\rangle\,, \tag{3.63}$$

where $|1s_A\rangle$ and $|1s_B\rangle$ are again the atomic hydrogen orbitals and where we neglect the normalization factor. This ansatz differs from the spatial part of the two-electron states in the LCAO approximation, reading

$$\begin{aligned} |\phi(1,2)\rangle_{\mathrm{LCAO}} &= (|1s_A(1)\rangle \pm |1s_B(1)\rangle)\,(|1s_A(2)\rangle \pm |1s_B(2)\rangle) \\ &= |1s_A, 1s_A\rangle \mp |1s_A, 1s_B\rangle \mp |1s_B, 1s_A\rangle + |1s_B, 1s_B\rangle\,. \end{aligned} \tag{3.64}$$

In the second line we omitted the labeling of the electrons. By comparing this LCAO ansatz with the HL ansatz (3.63) we recover the HL terms in the LCAO state but also have two additional terms $|1s_A, 1s_A\rangle$, $|1s_B, 1s_B\rangle$. These terms are the ionic contributions to the molecular state where both electrons are centered at nucleus A or nucleus B, respectively. They are completely absent in the HL approach which is the major difference of LCAO method and HL method. It is considered that the ionic configurations are important at short internuclear distances and become less important for intermediate and large distances of the nuclei where the H_2 molecule dissociates in two hydrogen atoms. The dissociation limit of H_2 is given by two neutral hydrogen atoms where each electron is centered at one single proton. Therefore, the HL wave function describes the correct dissociation limit while the wave function of the LCAO method still contains the ionic contributions. Thus, the HL wave function is a better suited at long-range distances. At short distances, however, the ionic contributions are also important so that the wave function of the LCAO is a better approximation here [52]. Regarding slow atomic collisions, the short-range part of the potential is important as it determines the exact position of the bound state closest to the threshold energy which influences the low-energy collision properties as will be seen in chapter 7.

For H_2 we can calculate the ground state potential energy in the HL approach (3.63) analytically. We define the integrals

$$S_{12} = \langle 1s_A, 1s_B | 1s_A, 1s_B\rangle, \tag{3.65a}$$

$$H_{11} = \langle 1s_A, 1s_B |\, H_{\mathrm{el}}\, | 1s_A, 1s_B\rangle\,, \tag{3.65b}$$

$$H_{12} = \langle 1s_A, 1s_B |\, H_{\mathrm{el}}\, | 1s_B, 1s_A\rangle\,, \tag{3.65c}$$

where H_{el} in the second and third term is the electronic Hamiltonian of H_2 (3.50). These integrals (3.65) are non-trivial two-electron integrals but can be solved analytically by using spheroidal coordinates (3.24). The derivation is given in detail in [93, 94] and the results read

$$S_{12}(R) = e^{-2R}\left(1 + R + \frac{1}{3}R^2\right)^2, \tag{3.66a}$$

$$H_{11}(R) = -1 + \frac{1}{R} + \frac{-2 + e^{-2R}(2R+2)}{R} + I_{11}(R), \tag{3.66b}$$

$$H_{12}(R) = (-1 + \frac{1}{R})S_{AB} - \frac{2}{3}e^{-2R}(R+1)(R^2+3R+3) + K_{12}(R). \tag{3.66c}$$

These expressions are analytic functions of the internuclear distance R, where the Coulomb integral $I_{11}(R)$ is given by

$$I_{11}(R) = \frac{1}{R} - \left(\frac{1}{R} + \frac{11}{8} + \frac{3}{4}R + \frac{1}{6}R^2\right)e^{-2R}, \tag{3.67}$$

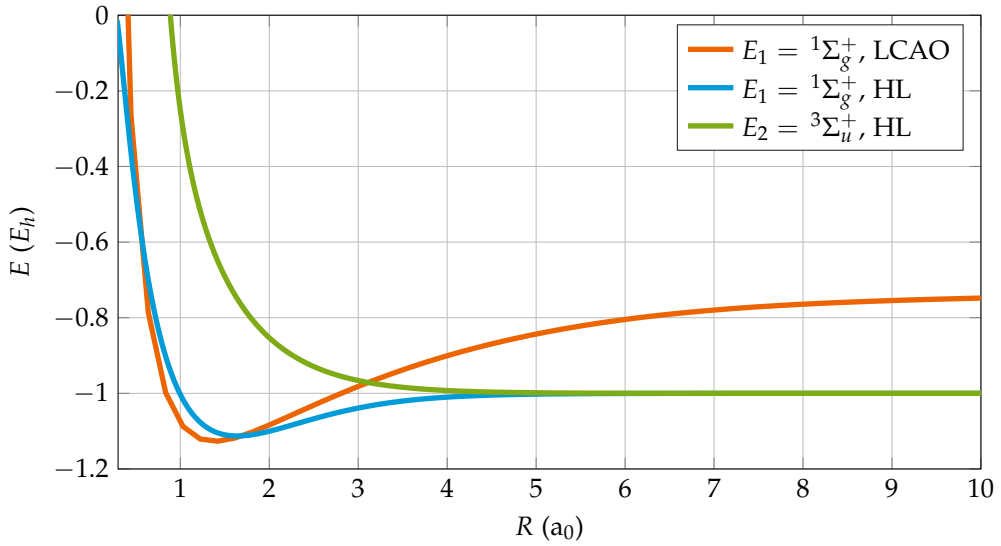

Figure 3.6: Potential energies of the lowest states of H_2 as functions of the internuclear distance R. The LCAO calculation was performed numerically by the GAMESS package in the $6-31G$ basis. The HL solutions are given by equation (3.69).

and the exchange integral $K_{12}(R)$ by

$$K_{12}(R) = \left(\frac{5}{8} - \frac{23}{20}R - \frac{3}{5}R^2 - \frac{1}{15}R^3\right)e^{-2R} + \frac{6}{5R}\left(1 + R + \frac{1}{3}R^2\right)^2 e^{-2R}\left(\gamma + \log(R)\right)$$
$$- 2(1 - \frac{1}{3}R^2 + \frac{1}{9}R^4)\mathrm{Ei}(-2R) + \left(1 - R + \frac{1}{3}R^2\right)^2 e^{-2R}\mathrm{Ei}(-4R). \tag{3.68}$$

The constant γ and the function $\mathrm{Ei}(x)$ are given in the appendix D.

With these results we can write the ground state energies of H_2 in the HL approximation (3.63) as

$$E_1 = \frac{H_{11} + H_{12}}{1 + S_{12}}, \qquad E_2 = \frac{H_{11} - H_{12}}{1 - S_{12}}. \tag{3.69}$$

The potential $E_1(R)$ describes the ground state potential ${}^1\Sigma_g^+(R)$ and the potential $E_2(R)$ the potential ${}^3\Sigma_u^+(R)$ of H_2. Both potential curves are shown in figure 3.6. Similarly to H_2^+, the ground state potential ${}^1\Sigma_g^+(R)$ is attractive while the excited state ${}^3\Sigma_u^+(R)$ is repulsive. For the ground state potential ${}^1\Sigma_g^+(R)$, a numerical solution is shown in the figure for the comparison of HL and LCAO approximation. The numerical solution is a RHF calculation in the LCAO approximation with a $6-31G$ basis set by the GAMESS package. The basis set $6-31G$ for the LCAO wave function is larger than the wave function of the HL approach (3.63). However, a comparison is conclusive. For large internuclear separations, the H_2 molecule dissociates in two neutral hydrogen atoms in their ground state. The ground state energy of a hydrogen atom was given by equation (2.14) as $E_H = 1/2\,E_h$. Thus, the correct energy dissociation limit is given by $E_{2H} = 1\,E_h$. It can be seen, that this dissociation limit is described accurately by the HL solution while for the LCAO solution the dissociation energy is overestimated. This overestimation is a result of the ionic contributions in the wave function which do not describe accurately the limit of two separate hydrogen atoms. This problem is known as the *RHF dissociation problem* [79].

For short-range distances the LCAO approximation is a better description than the HL approach, however. We calculated the potential minimum $E_{\min}$ and the equilibrium distance R_{eq} of the ground state of H_2 with the LCAO approximation as $E_{\min} = -1.1265\,E_h$ and $R_{eq} = 1.42\ a_0$ and with the HL approximation as $E_{\min} = -1.1128\,E_h$ and $R_{eq} = 1.6397\ a_0$. The accurate experimental values were determined as $E_{\min} = -1.1744\,E_h$ and $R_{eq} = 1.4003\ a_0$ [47]. Thus, the LCAO solution gives a good approximation with a difference of 4.08 % for $E_{\min}$ and 1.41 % for R_{eq} to the exact values while the HL approximation differs by 5.25 % for $E_{\min}$ and

17.1 % for R_{eq}. Particularly the equilibrium distance is not well described in the HL approach but also the minimum potential energy is not as close to the experimental value as the minimum potential energy calculated by the LCAO approximation. These results confirm the statements above that the HL approach is better suited at longer internuclear distances of the atoms and the LCAO approach at shorter distances.

CONCLUSION

The goal of this chapter was to illustrate the basic ideas of diatomic molecular physics in order to understand the molecular interaction potentials of Ne* and to introduce the different molecular basis states. For the derivation of the molecular potentials we introduced the *Born-Oppenheimer* approximation and the LCAO method. We compared the LCAO method to the *Heitler-London* approach and found that the LCAO method is better suited at short-range while the Heitler-London method describes the correct asymptotic limit. Furthermore, we illustrated for the H_2^+ and the H_2 molecule the notation for the molecular states in *Hund's case* (a) and *Hund's case* (c) notation as these are the bases in which the molecular potentials of Ne* were calculated and gave the symmetry properties of these states.

For larger distances of colliding atoms, different types of physics occur. The next chapter will be devoted to the long-range physics of two interacting atoms which gives rise to the *van der Waals* interaction and other multipole interactions.

4

LONG-RANGE INTERACTIONS

In cold collisions of Ne* the long-range physics is governed by the *van der Waals* interaction and the quadrupole–quadrupole interaction. In this chapter we show how these interaction terms arise from the multipole expansion of the electrostatic interaction energy between the atoms. The *van der Waals* interaction occurs for neutral atoms as a second-order energy correction to the dipole–dipole interaction. Therefore, we introduce briefly the time-independent perturbation theory. The matrix elements occurring in the *van der Waals* energy can be calculated with the *Wigner-Eckart theorem* which is introduced afterwards. As examples for the *van der Waals* interaction we calculate the *van der Waals* interaction energy in an atomic basis first of two hydrogen atoms in their ground state and second of two helium atoms in their ground state and introduce coefficient c_6. Furthermore, we show how the *van der Waals* interaction of two excited helium atoms in *P*-states can be calculated in principle. This example corresponds to the anisotropic *van der Waals* interaction between Ne* atoms and therefore it is introduced here.

4.1 MULTIPOLE EXPANSION

We start with the multipole expansion of the electrostatic interaction of the atoms. First we perform the multipole expansion of the electrostatic potential of a localized charge distribution in Cartesian coordinates. This introduces the dipole moment and quadrupole moment of a charge distribution. Then the multipole expansion of the interaction energy of two localized charge distributions in spherical coordinates is given from which the multipole interactions can be calculated.

4.1.1 *Electrostatic potential of a localized charge distribution*

We assume the electrostatic potential $V_{\mathrm{el}}(\mathbf{R})$ of a localized charge distribution of n point-like charged particles. This system corresponds to an n-electron atom. The electrostatic potential can be written as [96]

$$V_{\mathrm{el}}(\mathbf{R}) = \sum_{i=1}^{n} \frac{q_i(\mathbf{r}_i)}{|\mathbf{R} - \mathbf{r}_i|}, \tag{4.1}$$

where the coordinates are introduced in figure 4.1. The electrostatic potential is now evaluated at long-range $|\mathbf{R}| \gg |\mathbf{r}_1|, |\mathbf{r}_i|, |\mathbf{r}_N|$. For large distances $1/|\mathbf{R} - \mathbf{r}_i|$ can be expanded in a Taylor series

$$\frac{1}{|\mathbf{R} - \mathbf{r}|} = \frac{1}{R} - \mathbf{r} \cdot \nabla_{\mathbf{R}} \frac{1}{R} + \frac{1}{2}(\mathbf{r} \cdot \nabla_{\mathbf{R}})(\mathbf{r} \cdot \nabla_{\mathbf{R}}) \frac{1}{R} + \dots \tag{4.2}$$

Insertion of the expansion (4.2) into the electrostatic potential (4.1) leads to the multipole expansion of the electrostatic potential

$$V_{\mathrm{el}}(\mathbf{R}) = \frac{Q}{R} + \frac{\mathbf{R} \cdot \mathbf{d}}{R^3} + \frac{\mathbf{R}^T \tilde{Q} \mathbf{R}}{2R^5} + \dots, \tag{4.3}$$

where Q is the total charge or the *monopole moment* of the system

$$Q = \sum_{i=1}^{n} q_i, \tag{4.4}$$

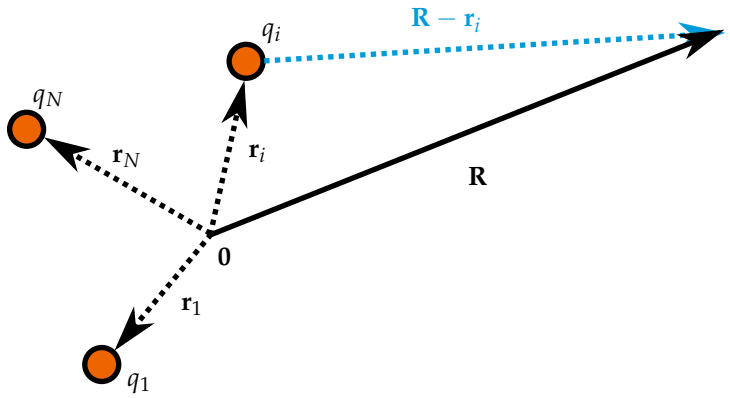

Figure 4.1: System of n point-like particles with charge q_i at positions $\mathbf{r}_i$. The electrostatic potential $V_{\text{el}}(\mathbf{R})$ is evaluated at large distances $\mathbf{R}$ where $|\mathbf{R}| \gg |\mathbf{r}_1|, |\mathbf{r}_i|, |\mathbf{r}_N|$, i.e. far away from the charge distribution.

and where we have introduced the *dipole moment*

$$\mathbf{d} = \sum_{i=1}^{n} q_i \mathbf{r}_i. \tag{4.5}$$

The *quadrupole moment tensor* reads

$$\tilde{Q} = \begin{pmatrix} \tilde{Q}_{11} & \tilde{Q}_{12} & \tilde{Q}_{13} \\ \tilde{Q}_{21} & \tilde{Q}_{22} & \tilde{Q}_{23} \\ \tilde{Q}_{31} & \tilde{Q}_{32} & \tilde{Q}_{33}. \end{pmatrix}, \tag{4.6}$$

and the elements are given by

$$\tilde{Q}_{ij} = \sum_{k=1}^{n} q_k \left(3 x_{ki} x_{kj} - r_k^2 \delta_{ij} \right). \tag{4.7}$$

Here, the coordinate x_{ki} is the ith Cartesian components of the position vector $\mathbf{r}_k$ of the ith particle.

For a neutral atom, the total charge is zero and the first term in the expansion (4.2) vanishes. The dipole term and the quadrupole term are important for Ne*, as in the interaction of Ne* atoms these terms give rise to the long-range interactions of Ne* atoms.

4.1.2 *Interaction energy of two localized non-overlapping charge distribution*

From the multipole expansion of one localized charge distributions we derive in this subsection the multipole expansion of the interaction energy of two localized charge distributions for the electrostatic interaction energy of two atoms. The interaction energy of the charge distributions reads [97]

$$W_{AB} = \sum_{i \in A} \sum_{j \in B} \frac{q_i q_j}{|\mathbf{r}_i - \mathbf{r}_j|}, \tag{4.8}$$

where the coordinates are introduced in figure 4.2. In equation (4.8) the first sum is over all charged particles centered at A and the second sum is over all charged particles centered at B. It can be easily seen from figure 4.2 that

$$\mathbf{R} + \mathbf{r}_{Bj} + \mathbf{r}_{ji} + \mathbf{r}_{iA} = 0 \quad \Leftrightarrow \quad \mathbf{r}_{ij} = \mathbf{R} - \mathbf{r}_{Ai} + \mathbf{r}_{Bj}. \tag{4.9}$$

The assumption that the two charge distributions are non-overlapping can be written in the form

$$|\mathbf{R}| > |r_{Bj} - r_{Ai}| \quad \text{for all } i, j. \tag{4.10}$$

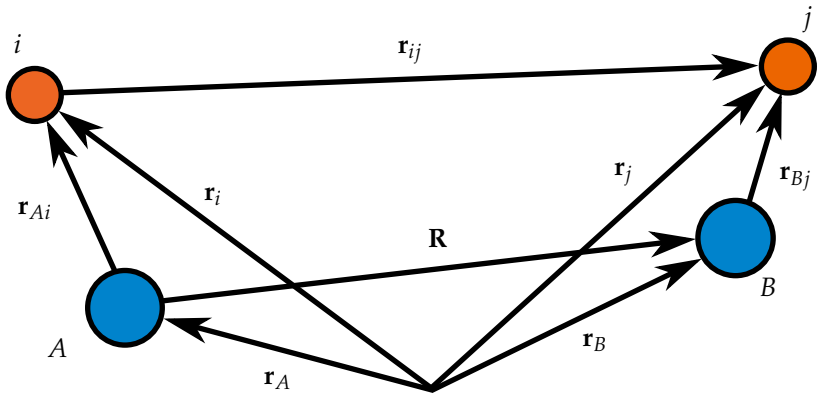

Figure 4.2: Coordinates of two atomic centers A, B with non-overlapping charge-distribution of particles $\{i\}$ with charges $\{q_i\}$ centered at atom A and particles $\{j\}$ with charge $\{q_j\}$ centered at atom B.

With the relations (4.9) and equation (4.10) one can perform the Laplace expansion of $1/|\mathbf{r}_j - \mathbf{r}_i|$ which reads

$$\frac{1}{|\mathbf{r}_j - \mathbf{r}_i|} = \frac{1}{|\mathbf{R} - (\mathbf{r}_{Ai} - \mathbf{r}_{Bj})|} = \sum_{L=0}^{\infty} \sum_{M=-L}^{L} (-1)^M I_{L,-M}(\mathbf{R}) R_{LM}(\mathbf{r}_{Ai} - \mathbf{r}_{Bj}), \tag{4.11}$$

where $I_{L,-M}(\mathbf{R})$ are the *irregular solid harmonics*, given by

$$I_{lm}(\mathbf{r}) \equiv \left[\frac{4\pi}{2l+1}\right]^{1/2} \frac{Y_{lm}(\mathbf{n}_r)}{R_{AB}^{l+1}}, \tag{4.12}$$

and $R_L^M(\mathbf{r}_{Ai} - \mathbf{r}_{Bj})$ denotes the *regular solid harmonics*, given by

$$R_{lm}(\mathbf{r}) = \sqrt{\frac{4\pi}{2l+1}} r^l Y_{lm}(\mathbf{n}_r), \tag{4.13}$$

with $\mathbf{n}_r = \mathbf{r}/r$. Furthermore, we introduce the *spherical multipole moments* [98]

$$Q_{lm} \equiv \sum_{i=1}^{N} q_i R_{lm}(\mathbf{r}_i). \tag{4.14}$$

For $l = 0$ this is the *monopole moment*, for $l = 1$ the *dipole moment* and for $l = 2$ the *quadrupole moment*. These moments were given in the equations (4.4), (4.5), (4.7) of the previous subsection, but in Cartesian coordinates rather than the *spherical multipole moments* introduced here. A shift of the *regular solid harmonics* is given by

$$\begin{aligned} R_{lm}(\mathbf{x} - \mathbf{y}) = \sum_{l_A=0}^{L} (-1)^{L-l_A} \binom{2L}{2l_A}^{1/2} \sum_{m_A=-l_A}^{l_A} R_{l_A,m_A}(\mathbf{x}) R_{L-l_A,M-m_A}(\mathbf{y}) \\ \langle l_A, m_A; L-l_A, M-m_A | LM \rangle, \end{aligned} \tag{4.15}$$

with the Clebsch-Gordan coefficient $\langle l_A, m_A; L-l_A, M-m_A|LM\rangle$. With the translation of the *regular solid harmonics* and the introduction of the *spherical multipole moments*, we can write the multipole expansion of two non-overlapping charge distributions with the Laplace expansion (4.11) as

$$\begin{aligned} W_{AB} = \sum_{l_A=0}^{\infty} \sum_{l_B=0}^{\infty} (-1)^{l_B} \binom{2l_A + 2l_B}{2l_A}^{1/2} \\ \times \sum_{m_A=-l_A}^{l_A} \sum_{m_B=-l_B}^{l_B} (-1)^{m_A+m_B} I_{l_A+l_B}^{-m_A-m_B}(\mathbf{R}) Q_{l_A}^{m_A} Q_{l_B}^{m_B} \langle l_A, m_A; l_B, m_B | l_A + l_B, m_A + m_B \rangle. \end{aligned} \tag{4.16}$$

This is the interaction potential of two atoms at long-range. The dependence of the interaction energy W_{AB} on the distance between the charge distributions R_{AB} (or the internuclear distance for atoms) is given by the *irregular solid harmonics* (4.12) as $1/R^{l_A+l_B+1}$. For dipole–dipole interactions, $l_A = l_B = 1$, we obtain a $1/R^3$ dependence and for quadrupole–quadrupole interactions we obtain a $1/R^5$ dependence. Both interaction types are present in Ne* collisions which will be discussed in chapter 6. The dipole–dipole interaction of Ne* occurs in second-order perturbation theory as the *van der Waals* interaction which will be introduced in the next section. A general discussion of quadrupole–quadrupole interaction of atoms can be found in [99, 100].

4.2 TIME-INDEPENDENT PERTURBATION THEORY

In order to calculate *van der Waals* interactions between atoms we discuss briefly the time-independent perturbation theory. Suppose that the Hamilton operator H of a diatomic system can be written as

$$H = H_0 + \lambda V, \tag{4.17}$$

where H_0 is the free Hamiltonian of two non-interacting atoms and V is the interaction potential of the atoms. We assume that the interaction is a small contribution to the total energy of the system so that the parameter $\lambda \ll 1$. Then we can treat the system in a perturbation approach. The unperturbed states $|\psi_i^{(0)}\rangle$ fulfill the eigenvalue equation

$$H_0 |\psi_i^{(0)}\rangle = E_i^{(0)} |\psi_i^{(0)}\rangle , \tag{4.18}$$

where $E_i^{(0)}$ are the corresponding unperturbed eigenenergies. At first we assume that the unperturbed states are non-degenerate so that only a single eigenenergy occurs for a single eigenstate. Following [101], we can expand the full energy and the full state of the system in a power series of λ as

$$E_i(\lambda) = \sum_{n=0}^{\infty} \lambda^n E_i^{(n)}, \quad |\psi_i(\lambda)\rangle = \sum_{n=0}^{\infty} \lambda^n |\psi_i^{(n)}\rangle , \tag{4.19}$$

where the first series is called the *Rayleigh-Schrödinger series*. Equating the coefficients leads to the first-order energy correction

$$E_i^{(1)} = \langle \psi_i^{(0)}| V |\psi_i^{(0)}\rangle , \tag{4.20}$$

and to

$$E_i^{(2)} = \langle \psi_i^{(0)}| V S_i V |\psi_i^{(0)}\rangle = \sum_{i\neq j} \frac{|\langle \psi_i^{(0)}| V |\psi_j^{(0)}\rangle|^2}{E_i^{(0)} - E_j^{(0)}}, \tag{4.21}$$

at second order, where we have introduced

$$S_i = \sum_{j\neq i} \frac{|\psi_j^{(0)}\rangle \langle \psi_j^{(0)}|}{E_i^{(0)} - E_j^{(0)}}. \tag{4.22}$$

The first-order energy correction is simply the expectation value of the interaction V in terms of the unperturbed states and the second-order correction is a sum over all unperturbed eigenstates, excluding the state $|\psi_i^{(0)}\rangle$. In the discussion of *van der Waals* interactions of atoms we will identify the interaction V with the multipole interaction W_{AB} (4.16), where only the dipole–dipole terms with $l_A = l_B = 1$ occur. The unperturbed states $|\psi_i^{(0)}\rangle$ are then diatomic product states. For atoms in non-degenerate levels, the energy $E_i^{(2)}$ is the *van der Waals* interaction energy, there are no first order corrections $E_i^{(1)}$. In Ne* interactions the ground state is degenerate. In order to calculate *van der Waals* interactions of degenerate levels we have to discuss degenerate perturbation theory.

Degenerate perturbation theory

For degenerate levels we investigate briefly *Kato's theory* [102]. This theory is based on the study of the resolvent $G(z) = 1/(z - H)$ [101]. Let the degeneracy of the ith eigenstate $|\psi_{i,\alpha}\rangle$ of the Hamiltonian be given by $g_i > 1$. Assume further, that the g_i-fold unperturbed degenerate energy of the ith eigenstate of H_0 is given by $E_i^{(0)}$ and the g_i-fold exact degenerate energy of the ith eigenstate of H by E_i. The unperturbed g_i-dimensional space $\mathscr{E}_i^{(0)}$ is spanned by the unperturbed eigenstates $|\psi_{i,\alpha}^{(0)}\rangle$, where $\alpha = 1, \ldots, g_i$, while the g_i-dimensional space $\mathscr{E}_i$ of the full solution is spanned by the eigenstates $|\psi_{i,\alpha}\rangle$ of the full Hamiltonian, where again $\alpha = 1, \ldots, g_i$. The eigenvalues of H approaching $E_i^{(0)}$ as $\lambda \to 0$ are given by the g_i roots of the equation

$$\det\left[\lambda \langle\psi_{i,\beta}^{(0)}| V |\psi_{i,\alpha}^{(0)}\rangle + \lambda^2 \langle\psi_{i,\beta}^{(0)}| VS_iV |\psi_{i,\alpha}^{(0)}\rangle - (E - E_i^{(0)})\delta_{\beta\alpha}\right] = 0, \tag{4.23}$$

where the operator S_i is given by equation (4.22) with $\psi_j^{(0)}$ replaced by $\psi_{j,g_j}^{(0)}$ and the summation is also over the g_j unperturbed degenerate states of the g_j-dimensional spaces $\mathscr{E}_j^{(0)}$. If there is no first-order correction to the energy, the correction to the energy of degenerate levels is solely given by the second-order expression

$$\langle\psi_{i,\beta}^{(0)}| VS_iV |\psi_{i,\alpha}^{(0)}\rangle = \sum_{j\neq i}\sum_{g_j} \frac{\langle\psi_{i,\beta}^{(0)}| V |\psi_{j,g_j}^{(0)}\rangle \langle\psi_{j,g_j}^{(0)}| V |\psi_{i,\alpha}^{(0)}\rangle}{E_i^{(0)} - E_j^{(0)}}. \tag{4.24}$$

The second-order energy correction is calculated by diagonalizing the $g_i \times g_i$ matrix whose elements are given by this equation. All matrix elements are infinite sums over all unperturbed degenerate states excluding the unperturbed ground state $|\psi_{i,\alpha}^{(0)}\rangle$ with $\alpha = 1, \ldots, g_i$. The diagonalized matrix can lead in principle to g_i distinct eigenenergies. If the interaction V is given by W_{AB} and the states $|\psi_{i,\beta}^{(0)}\rangle$ are g_i-fold degenerate product states of two atoms we retrieve the *van der Waals* interaction of atoms in degenerate states. We show this more explicitly for the *van der Waals* interaction of excited He atoms.

A useful tool for the evaluation of the matrix elements occurring in the calculation of the energy corrections (4.20), (4.21), (4.24) for the multipole interactions of atoms is the *Wigner-Eckart theorem*. We introduce this theorem in the next section.

4.3 WIGNER-ECKART THEOREM

The *Wigner-Eckart theorem* reads [103]

$$\langle\alpha jm| T_q^{(k)} |\alpha' j' m'\rangle = \frac{1}{\sqrt{2j+1}} \langle j' k m' q | j' k j m\rangle \langle\alpha j||\mathbf{T}^{(k)}||\alpha' j'\rangle, \tag{4.25}$$

where $\mathbf{T}^{(k)}$ is a tensor of rank k with $T_q^{(k)}$ is the qth component of this tensor with $q = -k, \ldots, +k$. The states $|\alpha' j' m'\rangle$ are total angular momentum states introduced in chapter 2 where $\langle\alpha j||\mathbf{T}^{(k)}||\alpha' j'\rangle$ is the *reduced matrix element*. The important statement of the *Wigner-Eckart theorem* is that the matrix elements of $T_q^{(k)}$ can be decomposed into two parts. One part of the decomposition depends only on the geometry of the system, i.e. solely on the quantum numbers j', j, m', m, while the second part is given by the *reduced matrix element* which is the radial integral depending solely on the quantum numbers α', α.

We are particularly interested in the evaluation of dipole moments and the dipole–dipole interaction of atoms in order to understand the *van der Waals* interaction of atoms. Dipole moments can be evaluated in a spherical basis or a Cartesian basis. If we write the position operator $\mathbf{r}$ in the spherical basis, we have

$$\mathbf{r} = \sqrt{\frac{4\pi}{3}} r \left(-Y_{11}\mathbf{e}_{-1} + Y_{10}\mathbf{e}_0 - Y_{1-1}\mathbf{e}_{+1}\right), \tag{4.26}$$

with the spherical basis vectors

$$\mathbf{e}_{+1} = -\frac{1}{\sqrt{2}}\left(\mathbf{e}_x + i\mathbf{e}_y\right), \quad \mathbf{e}_0 = \mathbf{e}_z, \quad \mathbf{e}_{-1} = \frac{1}{\sqrt{2}}\left(\mathbf{e}_x - i\mathbf{e}_y\right). \tag{4.27a}$$

We immediately conclude that the position operator is a tensor of rank 1 as the spherical harmonics Y_{1m} as well as the spherical basis vectors are tensors of rank 1. The transformation of the Cartesian components of $\mathbf{r}$ to the spherical basis is given by

$$x = \sqrt{\frac{2\pi}{3}} r \left(Y_{1-1} - Y_{11}\right), \quad y = i\sqrt{\frac{2\pi}{3}} r \left(Y_{1-1} + Y_{11}\right), \quad z = \sqrt{\frac{4\pi}{3}} Y_{10}. \tag{4.28}$$

In order to calculate matrix elements of these components we can immediately apply the *Wigner-Eckart theorem* (4.25) where $T_q^{(k)}$ are the spherical harmonics and $k = 1$. The Clebsch-Gordan coefficient in equation (4.25) leads to the dipole selection rules and reduced matrix elements for the dipole transitions is given in the literature [73] as

$$\langle \alpha j || r Y^{(1)} || \alpha' j' \rangle = \sqrt{2j+1} \left(\frac{3\varepsilon_0 \hbar \lambda^3 \Gamma}{8\pi^2 e^2} \right)^{1/2}, \tag{4.29}$$

where λ is the wavelength of the transition of the states $|\alpha j\rangle$ and $|\alpha' j'\rangle$ and Γ is the decay rate of the higher-lying state. (The numerical values of the physical constants e, ε_0, $\hbar$ are given in the appendix A, table A1.) Now we have all the ingredients in order to calculate the *van der Waals* interaction of atoms. This will be done in the next section.

4.4 VAN DER WAALS INTERACTION OF ATOMS

The dipole–dipole interaction of two atoms is given by the multipole expansion of the interaction energy (4.16) for $l_A = l_B = 1$ and reads

$$W_{dd} = \frac{1}{R^3}\left\{\mathbf{d}_A \cdot \mathbf{d}_B - 3\left(\mathbf{d}_A \cdot \mathbf{n}_R\right)\left(\mathbf{d}_B \cdot \mathbf{n}_R\right)\right\}, \tag{4.30}$$

with $\mathbf{n}_R = \mathbf{R}/R$. Figure 4.3 shows the scheme of two atoms at internuclear distance $\mathbf{R}$ with dipole moments $\mathbf{d}_A$, $\mathbf{d}_B$ [see equation (4.5)]. The subscripts A, B refer to coordinates with respect the atomic centers A and B, respectively. Note that even though the expectation values of the dipole moments may vanish, the matrix elements of the second-order energy in equation (4.21) do not necessarily. From W_{dd} can calculate the *van der Waals* interaction energy of two hydrogen atoms which is done in the following subsection.

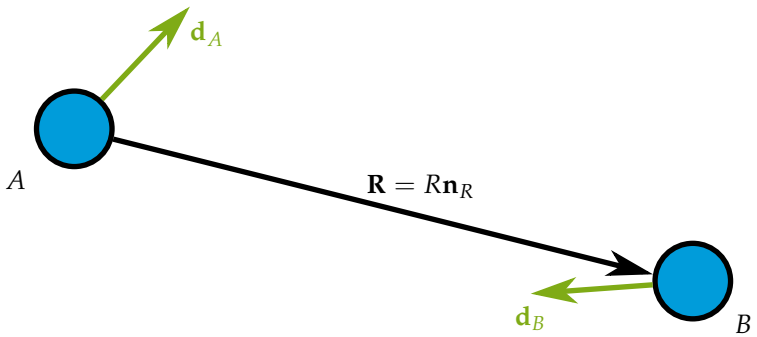

Figure 4.3: Two atoms A and B with dipole moments $\mathbf{d}_A$, $\mathbf{d}_B$. The position vector $\mathbf{R}$ points from atom A to atom B.

4.4.1 *Van der Waals interaction of hydrogen*

Assume that we are given two hydrogen atoms at fixed distance R. The dipole moments of the two hydrogen atoms read

$$\mathbf{d}_A = \mathbf{r}_A, \quad \mathbf{d}_B = \mathbf{r}_B, \tag{4.31}$$

where the coordinates are introduced in figure 4.4. We choose the coordinate system where

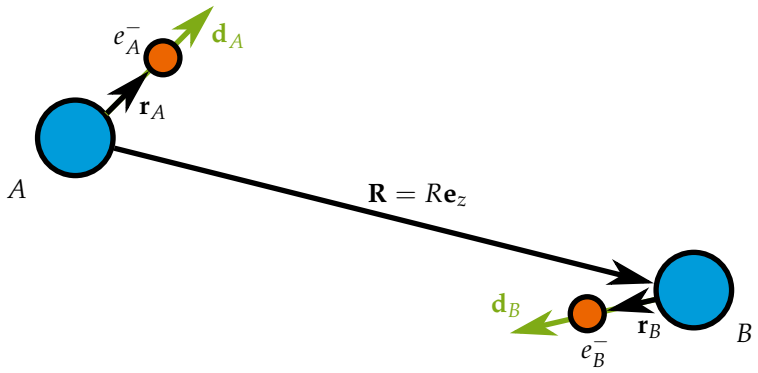

Figure 4.4: Scheme of induced dipole–dipole interaction for H. Electron e_A^- of atom A is at position $\mathbf{r}_A$ with respect to the center of atom A and $\mathbf{r}_B$ is the position of electron e_B^- with respect to the atomic center B. The electrons are distinguishable as the atoms are far apart. The vectors $\mathbf{d}_A$, $\mathbf{d}_B$ are the dipoles of atom A and B, respectively.

$\mathbf{R} = R\mathbf{e}_z$ as indicated in the figure. The dipole–dipole interaction term (4.30) then reads

$$W_{dd} = \frac{1}{R^3}\left(x_A x_B + y_A y_B - 2z_A z_B\right), \tag{4.32}$$

where x_A, y_A, z_A are the Cartesian components of $\mathbf{r}_A$ and x_B, y_B, z_B are those of $\mathbf{r}_B$. The Hamiltonian for this system reads

$$H = H_{0,A} + H_{0,B} + W_{dd}, \tag{4.33}$$

where $H_{0,A}$, $H_{0,B}$ are the free Hamiltonian operators of the atoms A and B. As we assume that the interaction term W_{dd} only gives a small contribution to the total energy we treat the system in a perturbation approach. The unperturbed eigenenergies and eigenstates of the system are given by

$$\left(H_{0,A} + H_{0,B}\right)|\psi_1^{(0)}\rangle = 2E_1^{(0)}\,|\psi_1^{(0)}\rangle\,, \tag{4.34}$$

where $E_1^{(0)} = 1/2\,E_h$ is the ground state energy of hydrogen and the unperturbed eigenstate $|\psi^{(0)}\rangle$ is the product state

$$|\psi_1^{(0)}\rangle = |1s_A, 1s_B\rangle\,. \tag{4.35}$$

The first order energy correction (4.20) for the system (4.33) is given by

$$E_1^{(1)} = \langle 1s_A, 1s_B|\, W_{dd}\,|1s_A, 1s_B\rangle\,. \tag{4.36}$$

The single-atom states $|1s_A\rangle$, $|1s_B\rangle$ only act on the coordinates of $\mathbf{r}_A$, $\mathbf{r}_B$, respectively. One can show with the *Wigner-Eckart theorem* (4.25) that all the terms in equation (4.36) vanish so that the first order correction of the dipole–dipole interaction of two ground state hydrogen atoms is zero.

The second-order energy correction (4.21) reads

$$E_1^{(2)} = -\sum_{nlm}{}' \sum_{n'l'm'}{}' \frac{|\,\langle 1s_A, 1s_B|\, W_{dd}\,|(nlm)_A, (n'l'm')_B\rangle\,|^2}{2E_1^{(0)} + E_n^{(0)} + E_{n'}^{(0)}}, \tag{4.37}$$

where the summation is over all excited states $|(nlm)_A, (n'l'm')_B\rangle$ with $n \neq 2$ and E_n, $E_{n'}$ are the excited state energies of hydrogen, given by equation (2.14). The energy $E_1^{(0)}$ is positive and the energies $E_n^{(0)}$, $E_{n'}^{(0)}$ are negative but smaller in magnitude than $2E_1^{(0)}$. Thus, the second-order energy $E_1^{(2)}$ is always attractive. The two sums in equation (4.37) are infinite sums not only including bound states but also continuum states. The latter make the sums problematic as it is not guaranteed that the matrix elements can be neglected even though the denominator becomes very small for larger energies. There exist *sum rules* such as the *Thomas-Reiche-Kuhn sum rule* [104] in order to simplify the infinite sum of equation (4.37) [73, 105, 106].

In the case of hydrogen–hydrogen interactions there exists another, elegant way of evaluating the second-order energy correction (4.37). This is shown in [81]. The energies of the H atom scale as $|E_n| \simeq 1/n^2$ [see equation (2.14)]. We therefore assume that $E_n = E_{n'} = 0$ for $n \geq 2$ which is called the Unsöld approximation [107]. If we use the Unsöld approximation and the completeness relation for the states of the H atom, which reads

$$\sum_{nlm}^{\prime} \sum_{n'l'm'}^{\prime} |(nlm)_A, (n'l'm')_B\rangle \langle (nlm)_A, (n'l'm')_B| = \mathbb{1} - |1s_A, 1s_B\rangle \langle 1s_A, 1s_B|, \tag{4.38}$$

the infinite sums in equation (4.37) reduce to two terms

$$E_1^{(2)} = -\frac{\langle 1s_A, 1s_B| W_{dd}^2 |1s_A, 1s_B\rangle}{2E_1^{(0)}} + \frac{(\langle 1s_A, 1s_B| W_{dd} |1s_A, 1s_B\rangle)^2}{2E_1^{(0)}}. \tag{4.39}$$

Note, that the second term in this equation is similar to the first-order correction (4.36) and therefore is equal to zero. The first term contains W_{dd}^2 and we have to evaluate matrix elements of the form

$$\langle 1s_A, 1s_B| W_{dd}^2 |1s_A, 1s_B\rangle \propto \langle 1s_A| x_A^2 |1s_A\rangle \langle 1s_B| x_B^2 |1s_B\rangle. \tag{4.40}$$

All the mixed terms with $x_A y_A x_B y_B$, etc. are zero as can be shown by the *Wigner-Eckart theorem* (4.25). We calculate one matrix element occurring in equation (4.40) explicitly which yields

$$\langle 1s| x^2 |1s\rangle = \int_0^\infty dr \int_0^\pi d\theta \int_0^{2\pi} d\phi \, r^2 \sin\theta \, |\varphi_{100}(\mathbf{r})|^2 \underbrace{(r \sin\theta \cos\phi)^2}_{=x^2} = 1. \tag{4.41}$$

It can be shown that the integrals for the other components y^2, z^2 lead to the same result so that in total the interaction energy for hydrogen–hydrogen ground state atoms in second-order (4.39) becomes

$$E_1^{(2)} = -\frac{c_6}{R^6}, \quad c_6 = 6\,\text{a.u.} \tag{4.42}$$

where we introduced the dispersion coefficient c_6. This is an important result which shows that the *van der Waals* or induced dipole–dipole interaction gives rise to an attraction between neutral atoms that depends on the internuclear distance R as $1/R^6$. The strength of the attraction is given by the c_6 coefficient and for hydrogen, we obtain in this simple calculation the result $c_6 = 6.000$ a.u. This value is very close to the literature value $c_6 = 6.499$ a.u. [108].

4.4.2 *Van der Waals interaction of helium*

In the following we establish an upper bound on the *van der Waals* interaction for two interacting He atoms in their ground states by calculating the first term in the second-order energy correction of the dipole–dipole interaction. This situation is more complicated than two interacting H atoms as He consists of two electrons. The atomic states need to be anti-symmetrized with respect to the exchange of the electrons.

In figure 4.5 the coordinates for a system consisting of two He atoms are given. The dipole moments $\mathbf{d}_A$, $\mathbf{d}_B$ introduced in the figure read

$$\mathbf{d}_A = \mathbf{r}_{A1} + \mathbf{r}_{A2}, \quad \mathbf{r}_B = \mathbf{r}_{B1} + \mathbf{r}_{B2}. \tag{4.43}$$

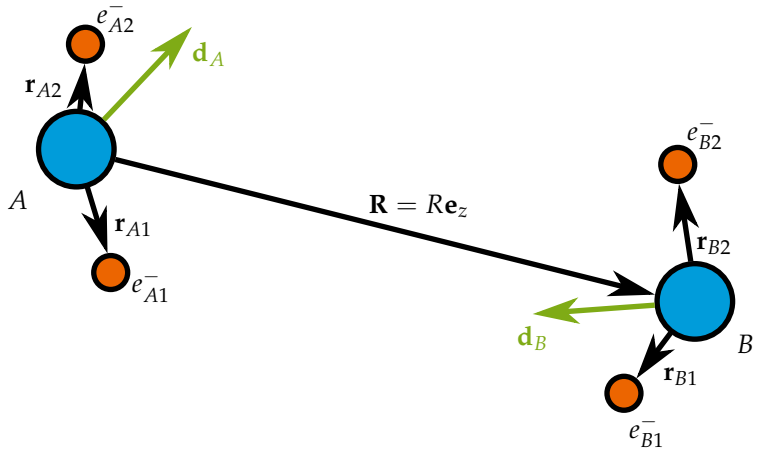

Figure 4.5: Induced dipole–dipole interaction for He. The electrons e^-_A of atom A are distinguishable from the electrons e^-_B of atom B but indistinguishable with respect to the exchange $e^-_{A1} \leftrightarrow e^-_{A2}$ and correspondingly for the electrons of atom B. $\mathbf{d}_A$ and $\mathbf{d}_B$ are the dipole moments of atom A and B, respectively.

Inserting the dipole moments (4.43) in the dipole-dipole interaction (4.30) leads to

$$W_{dd} = W_{d_{A1}d_{B1}} + W_{d_{A1}d_{B2}} + W_{d_{A2}d_{B1}} + W_{d_{A2}d_{B2}}, \tag{4.44}$$

where the individual terms $W_{d_{Ai}d_{Bj}}$ are given by equation (4.32) but with the coordinates x_A, y_B, ... replaced with x_{Ai}, y_{Bj}, ... As in the case of hydrogen interactions we treat the system in a perturbation approach. The unperturbed eigenstate of the system is the product state

$$|\psi_1^{(0)}\rangle = |(1^1S)_A, (1^1S)_B\rangle\,, \tag{4.45}$$

with the atomic states $|(1^1S)_A\rangle$, $|(1^1S)_B\rangle$ centered at atom A and B, respectively. The atomic ground state of helium is given by

$$|1s^2\ 1^1S\rangle = \frac{1}{\sqrt{2}} \begin{vmatrix} 1s\alpha(1) & 1s\beta(1) \\ 1s\alpha(2) & 1s\beta(2) \end{vmatrix}, \tag{4.46}$$

where $1s$ denotes the lowest spatial orbital of He. The term of this two-electron state is given by 1^1S, which is a singlet state where the electronic orbital angular momentum is zero (see section 2.2.1). With W_{dd} given by equation (4.44) we obtain as in the case of hydrogen, that the first-order energy correction (4.20) in terms of the unperturbed states (4.45) vanishes.

Due to the selection rules for dipole transitions mentioned in section 4.3 the first non-vanishing term in the second-order energy (4.21) is the overlap with the product state of atomic helium singlet P states, i.e.

$$|\psi_2^{(0)}\rangle = |(2^1P, m_l)_A, (2^1P, m_l)_B\rangle\,, \tag{4.47}$$

where the atomic P-state for He is given by

$$|1s2p\ 2^1P, m_l\rangle = \frac{1}{\sqrt{2}} \left\{ \begin{vmatrix} 1s\alpha(1) & 2p_{m_l}\beta(1) \\ 1s\alpha(2) & 2p_{m_l}\beta(2) \end{vmatrix} - \begin{vmatrix} 1s\beta(1) & 2p_{m_l}\alpha(1) \\ 1s\beta(2) & 2p_{m_l}\alpha(2) \end{vmatrix} \right\}, \tag{4.48}$$

with m_l the projection on a space-fixed axis of the single-electron p-orbital which also determines the projection of the total two-electron state, as the other electron occupying the $1s$ orbital has zero orbital angular momentum. With these states we can establish an upper bound on the *van der Waals* interaction of helium atoms

$$E_1^{(2)} \leq -\sum_{m_l=-1}^{1} \sum_{m_{l'}=-1}^{1} \frac{|\langle (2^1P, m_l)_A, (2^1P, m_{l'})_B | W_{dd} | (1^1S)_A, (1^1S)_B \rangle|^2}{2E_1^{(0)} - 2E_2^{(0)}}. \tag{4.49}$$

Here, the energy $E_1^{(0)} = 2.9006\,E_h$ is the ground state energy of He and $E_2^{(0)} = 2.1209\,E_h$ is the energy of the excited 1^1P state. The numerical values are given by the *NIST Atomic Spectra Database* [109]. The symbol $\leq$ results from the fact that all the other terms of the infinite sums in second-order perturbation theory are negative, as $E_I - E_n - E_{n'} > 0$, where E_n, $E_{n'}$ denote the energies of the excited states, so that the total sum becomes smaller with every summand. Due to the *Wigner-Eckart theorem*, the only non-vanishing matrix elements in equation (4.49) are for $m_l = m_{l'} = 0$ and $m_l = -m_{l'} = \pm 1$. Again, as in the case of hydrogen interactions, the atoms are far apart so that atomic states of atom A only act on the electronic coordinates of atom A and correspondingly for the electrons of atom B. We calculate explicitly the matrix elements occurring in equation (4.49) where we assume that the spatial orbitals are given by the hydrogen wave functions $\varphi_{100}(\mathbf{r})$ and $\varphi_{21m_l}(\mathbf{r})$ with $m_l = -1, 0, +1$ with $Z = 2$ (see table 2.1). This is an approximation where no electron correlation effects are included. For the purpose of establishing an upper bound on the *van der Waals* interaction of He this is a reasonable simplification. The matrix elements read

$$\langle 1^1P, \pm 1|\, x\, |1^1S\rangle = \frac{32\sqrt{2}}{243}, \quad \langle 1^1P, \pm 1|\, y\, |1^1S\rangle = \pm\frac{32i\sqrt{2}}{243}, \quad \langle 1^1P, 0|\, z\, |1^1S\rangle = \frac{64}{243}, \tag{4.50}$$

where we have omitted the labels A, B, since the results for both atomic centers are the same. Inserting the calculated matrix elements in equation (4.49) leads to an upper bound on the *van der Waals* interaction energy of

$$E_1^{(2)} \leq -\frac{c_6}{R^6}, \text{ with } c_6 \geq 0.2962\,\text{a.u.}. \tag{4.51}$$

The corresponding literature value is given by $c_6 = 1.4610$ a.u. [108] which is consistent with the bound established here. It is evident that our value is not close to this value, as hydrogen wave functions were used to calculate the matrix elements and only the first terms (4.49) of the infinite sums of second-order perturbation theory was calculated. It is assumed, however, that the other terms become smaller for higher states so that a significant contribution to the total sum is expected to be given by the first terms (4.49). Note, that the He dispersion coefficient $c_6 = 1.4610$ a.u. is much smaller than the H dispersion coefficient $c_6 = 6.499$ a.u. The reason for this is that He in its ground state configuration is a closed-shell system which is harder to perturb than the open-shell system H. Thus, the polarizability of He is lower than the polarizability of H and, as a consequence, the attraction of two He atoms due to the *van der Waals* interaction is smaller than that of two H atoms.

Excited state interactions

To close the discussion of helium we examine the *van der Waals* interaction of two helium atoms in triplet states 1^3P_2 of the $1s2p$ configuration. This case corresponds to the case of Ne* interactions as the lowest states of Ne* are states of the $^3P_2$ manifold. In a perturbation approach the unperturbed product state for this system is given by

$$|\psi_{i,\alpha}^{(0)}\rangle = |(1^3P_2, m_1)_A, (1^3P_2, m_2)_B\rangle\,, \tag{4.52}$$

where the atomic states $|1^3P_2, m\rangle$ are total angular momentum states of the $1s2p$ configuration. The label α of the state $|\psi_i^{(0)}\rangle$ denotes the set of projections (m_1, m_2). Without a magnetic field the unperturbed state $|\psi_{i,\alpha}^{(0)}\rangle$ is $g_i = (2j+1)(2j+1) = 25$-fold degenerate for all different magnetic sub levels. In order to calculate the *van der Waals* interaction of two helium atoms in the degenerate state $|\psi_{i,\alpha}^{(0)}\rangle$ we have to apply degenerate perturbation theory. The matrix elements of the second-order correction are given by equation (4.24) with $V = W_{dd}$. For all different internal levels (m_1, m_2) we obtain a $g_i \times g_i = 25 \times 25$ matrix which has to be diagonalized in order to obtain the *van der Waals* interaction of the two helium atoms in states of the $^3P_2$ manifold. For anisotropic systems this will result in a maximum of 25 different c_6 coefficients, depending on the magnetic internal states of the diatomic system. The anisotropy of the c_6 coefficients is present in Ne* interactions which we discuss in chapter 6. There, the c_6 coefficients for Ne* will

be given in the molecular *Hund's case* (c) basis instead of the atomic basis we used throughout this chapter.

In order to calculate polarizabilities of atoms and multipole dispersion forces between atoms, different approaches based on variational methods instead of the standard second-order perturbation method exist. These different approaches are discussed in [48, 110].

CONCLUSION

In this chapter we illustrated the long-range interactions which are important for Ne* collisions. The multipole expansion of the electrostatic interaction energy leads to the dipole–dipole interactions and the quadrupole–quadrupole interactions between two atoms. In second-order perturbation theory, the *van der Waals* interaction of atoms appears and the *Wigner-Eckart theorem* is an important tool to evaluate transition matrix elements between different states which need to be calculated. We calculated approximations to the c_6 coefficient for H(1s)-H(1s) interactions and for He (1^1S)-He (1^1S) interactions in an atomic basis. The He$(^3P_2)$-He$(^3P_2)$ interaction gives rise to 25 c_6 coefficients depending on the internal magnetic states of the atoms similar to Ne* interactions. However, the long-range interactions of Ne* have been calculated in the *Hund's case* (c) basis in the body-fixed frame instead of the diatomic basis in the space-fixed frame used in this chapter.

In the previous chapter we introduced the short-range interactions in atom–atom collisions. In this chapter, the topic was the long-range interactions. The question remains how the atoms interact dynamically. This is solved by quantum scattering theory which is introduced in the next chapter.

5

CONCEPTS OF QUANTUM SCATTERING THEORY

Cold atomic collisions are described in the framework of quantum scattering theory. Here we give an overview of the basic concepts of quantum scattering theory and follow mainly [37, 38]. More topics in scattering theory may be found in [36, 91, 103] and in the theory of atomic collisions in [39, 41, 42, 52]. A quick overview is also given in [111].

The following chapters are based on the insights of scattering theory, i.e. the *coupled-channel equations* resulting from an expansion of the scattering states in a molecular basis in chapter 6, the analysis of the S matrix in the complex k plane in chapter 7 and the calculation of cross sections and two-body loss rate coefficients of Ne* in chapter 8. Therefore, the study of quantum scattering theory is crucial for this work.

We start by the time-dependent formalism in order to introduce the basic operators of quantum scattering theory such as the Møller operators, the S operator and the K or *reactance* operator. From this time-dependent approach, we switch to the time-independent formalism and introduce the scattering cross section, two-particle scattering and the partial-wave expansion of the scattering states. In order to analyze the S matrix for complex wave numbers for the square-well model in chapter 7 we introduce the regular solution which in the asymptotic region yields the Jost function. From the analytic properties of the Jost function we establish the analytic properties of the S matrix and give the pole expansion of the S matrix in terms of the bound states, virtual states and resonant states of the scattering potential.

Cold reactive collisions of Ne* are described in the framework of multichannel scattering theory. We introduce the basic concepts and generalize the results of single-channel scattering for the S operator, cross section, etc. In order to calculate elastic and inelastic collision processes in Ne* collisions for the coupled two-channel model of this work we introduce the elastic and inelastic scattering cross sections of multichannel scattering theory. We introduce the complex energy-dependent scattering length and show how the cross sections are parametrized in terms of this complex scattering length. It is also shown in this chapter that the expansion of the multichannel scattering wave function in the basis of the target states leads to the *coupled-channel equations* when the infinite sum of the expansion is truncated at a finite value. For two-channels only we obtain the coupled two-channel equations which are of special importance as we introduce in the later chapters of this work the coupled two-channel model for cold Ne* collisions.

In the two-channel model with square-well potentials we investigate the S matrix in the complex k plane. In order to perform a pole expansion of the multichannel S matrix we first have to establish its analytic properties. This is done by studying the multichannel regular solution which, in the asymptotic region, yields the Jost matrices. From the analytic properties of the Jost matrices for complex energies we can establish the analytic properties of the multichannel S matrix.

The atomic states of Ne* are angular momentum states in different internal spin-states which will be shown in the next chapter. In order to describe ionizing collisions of Ne* we introduce the inelastic scattering of identical particles with spin. We derive the two-particle inelastic cross sections for this case and establish the relationship of the inelastic cross section of theory and the macroscopic two-body loss rate coefficients measured in the experiment.

5.1 TIME-DEPENDENT FORMAL SCATTERING THEORY

Here we describe the scattering process in time. By introducing the Green's operators we can define the asymptotically free in- and out-states and their relation to the full scattering state. In this context, the important Møller operators and the S and K operator are introduced.

5.1.1 *Time development of state vectors in the Schrödinger picture*

Let us suppose that we can split the Hamilton operator $H(t)$ as in [37]

$$H(t) = H_0(t) + V(t), \tag{5.1}$$

where $H_0(t)$ is the free Hamilton operator and where $V(t)$ describes the interactions of the particles. We define the free Green's operators $G_0^{\pm}(t)$ and the full Green's operators $G^{\pm}(t)$ by the equations [37]

$$\left(i\frac{\partial}{\partial t} - H_0(t)\right) G_0^{\pm}(t) = \delta(t), \text{ with } G_0^{\pm}(t) \text{ for } t \lesseqgtr 0, \tag{5.2a}$$

$$\left(i\frac{\partial}{\partial t} - H(t)\right) G^{\pm}(t) = \delta(t), \text{ with } G^{\pm}(t) = 0 \text{ for } t \lesseqgtr 0 \tag{5.2b}$$

where we use natural units ($\hbar = 1$) and where $G_0^+(t)$, $G^+(t)$ are the *retarded* Green's operators while $G_0^-(t)$, $G^-(t)$ are the *advanced* Green's operators $G_0^-(t)$, $G^-(t)$. The solutions are given in terms of the free time evolution operator $U_0(t,t')$ and the full time evolution operator $U(t,t')$

$$G^{\pm}(t,t') = \mp iU(t,t')\theta(t-t'), \tag{5.3}$$

$$G_0^{\pm}(t,t') = \mp iU_0(t,t')\theta(t-t'). \tag{5.4}$$

The time-dependent Schrödinger equations for the full Hamilton operator $H(t)$ and for the free Hamilton operator $H_0(t)$ read

$$i\frac{\partial}{\partial t}\left|\Psi(t)\right\rangle = H(t)\left|\Psi(t)\right\rangle, \quad i\frac{\partial}{\partial t}\left|\Psi_0(t)\right\rangle = H_0(t)\left|\Psi_0(t)\right\rangle, \tag{5.5}$$

respectively. With the help of the *retarded* Green's operators we can describe the time evolution of the full state $|\Psi(t)\rangle$ and the free state $|\Psi_0(t)\rangle$ after the collision $t' > t$ as

$$\left|\Psi(t')\right\rangle = iG^+(t',t)\left|\Psi(t)\right\rangle, \quad \left|\Psi_0(t')\right\rangle = iG_0^+(t',t)\left|\Psi_0(t)\right\rangle, \tag{5.6}$$

respectively. Before the collision $t' < t$, analogous expressions for the full solution and the free solution are obtained in terms of the *advanced* Green's operators

$$\left|\Psi(t')\right\rangle = -iG^-(t',t)\left|\Psi(t)\right\rangle, \quad \left|\Psi_0(t')\right\rangle = -iG_0^-(t',t)\left|\Psi_0(t)\right\rangle. \tag{5.7}$$

The free states $|\Psi_0(t)\rangle$ are defined as

$$\left|\Psi_0(t)\right\rangle \equiv iG_0^+(t,t')\left|\Psi(t')\right\rangle, \quad \left|\Psi_0(t)\right\rangle \equiv -iG_0^-(t,t')\left|\Psi(t')\right\rangle. \tag{5.8}$$

At times long before or long after the collision these states are equivalent to the full scattering state $|\Psi(t_0)\rangle$. The limits $t' \to \pm\infty$ define the in- and out-states as

$$\left|\Psi_{\text{in}}(t)\right\rangle \equiv \lim_{t'\to-\infty} iG_0^+(t,t')\left|\Psi(t')\right\rangle. \tag{5.9a}$$

$$\left|\Psi_{\text{out}}(t)\right\rangle \equiv \lim_{t'\to+\infty} -iG_0^-(t,t')\left|\Psi(t')\right\rangle. \tag{5.9b}$$

In the infinite past $t' \to -\infty$, the in-state $|\Psi_{\text{in}}(t)\rangle$ evolves with the free *retarded* Green's operator and in the infinite future $t' \to +\infty$, the out-state $|\Psi_{\text{out}}(t)\rangle$ evolves with the free *advanced* Green's operator. Figure 5.1 shows schematically, how $|\Psi_{\text{in}}(t)\rangle$, $|\Psi_{\text{out}}(t)\rangle$ and the full scattering state $|\Psi(t)\rangle$ are related.

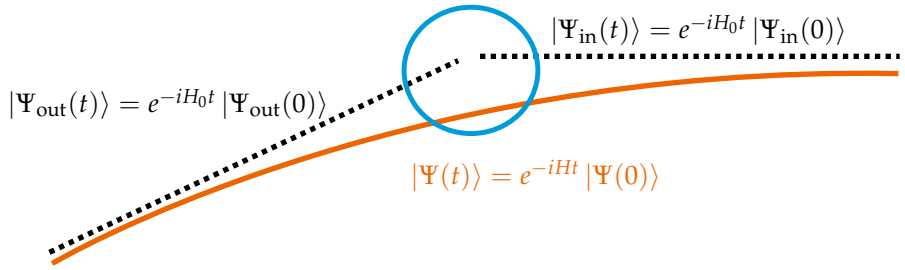

Figure 5.1: Full scattering state $|\Psi(t)\rangle$ evolving with the full Hamilton operator H and the in- and out-states $|\Psi_{\text{in}}(t)\rangle$, $|\Psi_{\text{out}}(t)\rangle$ evolving with the free Hamilton operator H_0. For $t \to \pm\infty$ the full state approaches the in- and out-state, respectively.

The full scattering state $|\Psi(t)\rangle$ can be written in integral form in terms of $|\Psi_{\text{in}}(t)\rangle$ and $|\Psi_{\text{out}}(t)\rangle$ as

$$|\Psi(t)\rangle = |\Psi_{\text{in}}(t)\rangle + \int_{-\infty}^{\infty} dt' G_0^+(t,t')V(t)\,|\Psi(t')\rangle\,, \tag{5.10a}$$

$$|\Psi(t)\rangle = |\Psi_{\text{out}}(t)\rangle + \int_{-\infty}^{\infty} dt' G_0^-(t,t')V(t)\,|\Psi(t')\rangle\,. \tag{5.10b}$$

We can also write the full scattering wave function in terms of the full Green's operators $G^{\pm}(t)$ as

$$|\Psi(t)\rangle = |\Psi_{\text{in}}(t)\rangle + \int_{-\infty}^{\infty} dt' G^+(t,t')V(t)\,|\Psi_{\text{in}}(t')\rangle\,, \tag{5.11a}$$

$$|\Psi(t)\rangle = |\Psi_{\text{out}}(t)\rangle + \int_{-\infty}^{\infty} dt' G^-(t,t')V(t)\,|\Psi_{\text{out}}(t')\rangle\,. \tag{5.11b}$$

The in-state $|\Psi_{\text{in}}(t)\rangle$ is controlled in the infinite past. In the time-dependent picture, it is considered to be a wave packet specified by a set of quantum numbers labeled by α which commute with H_0. A full scattering state determined by $|\Psi_{\text{in}}(t)\rangle$ and its quantum numbers α is then denoted by $|\Psi^{(+)}(\alpha,t)\rangle$. This state was identical to $|\Psi_{\text{in}}(\alpha,t)\rangle$ in the infinite past. It satisfies the integral equation

$$|\Psi^{(+)}(\alpha,t)\rangle = |\Psi_{\text{in}}(\alpha,t)\rangle + \int_{-\infty}^{\infty} dt' G_0^+(t,t')V(t)\,|\Psi^{(+)}(\alpha,t)\rangle\,. \tag{5.12}$$

The state $|\Psi^{(+)}(\alpha,t)\rangle$ in the infinite future will be given by $|\Psi_{\text{out}}\rangle$ and also satisfies the integral equations (5.10b), (5.11b) but these equations are of no practical use since $|\Psi_{\text{out}}\rangle$ is uncontrolled and unknown. The inverse situation occurs for the state $|\Psi^{(-)}(\beta,t)\rangle$ which is specified by the quantum numbers β which again commute with H_0 but are quantum numbers which are specified for the state $|\Psi_{\text{out}}(\beta,t)\rangle$. Here, the quantum numbers of the out-state are known but the in-state is uncontrolled. The state $|\Psi^{(-)}(\beta,t)\rangle$ satisfies

$$|\Psi^{(-)}(\beta,t)\rangle = |\Psi_{\text{out}}(\beta,t)\rangle + \int_{-\infty}^{\infty} dt' G_0^-(t,t')V(t)\,|\Psi^{(-)}(\beta,t)\rangle\,. \tag{5.13}$$

This state satisfies the equations (5.10a), (5.11a) but again this is of no practical use since $|\Psi_{\text{in}}\rangle$ is unknown. The state $|\Psi^{(-)}(\beta,t)\rangle$ is physically not meaningful as in the experiment typically a state is prepared and controlled before the collision process, then scattered and finally an outgoing amplitude is measured. As the states $|\Psi^{(+)}(\alpha,t)\rangle$, $|\Psi^{(-)}(\alpha,t)\rangle$ are constructed from an controlled in-state with quantum numbers α and from an out-state with specified quantum numbers β in (5.12), respectively, the quantum labels α, β of the full scattering states $|\Psi^{(\pm)}\rangle$ are conceptually quite different [37].

5.1.2 *Møller wave operators*

The Møller wave operators $\Omega^{(\pm)}(t)$ map the asymptotically free in- and out-states to the full scattering state $|\Psi(t)\rangle$

$$|\Psi(t)\rangle = \Omega^{(+)}(t)\,|\Psi_{\text{in}}(t)\rangle\,, \tag{5.14}$$

where $\Omega^{(+)}(t)$ is derived by inserting $|\Psi_0(t')\rangle$ of equation (5.7) in equation (5.11a) which leads to

$$\Omega^{(+)}(t) = \mathbb{1} - i\int_{-\infty}^{\infty} dt' G^{+}(t,t')VG_0^{-}(t',t), \tag{5.15}$$

with $\Omega^{(+)}(t)$ given in terms of the Green's operators. In terms of the Hamilton operator of the system the Møller operator $\Omega^{(+)}(t)$ reads

$$\Omega^{(+)}(t) = \lim_{t\to-\infty} e^{iHt}e^{-iH_0t} \coloneqq \lim_{\epsilon\to 0^+}\int_0^{-\infty} dt\;(-\epsilon)\cdot e^{-\epsilon|t|}e^{iHt}e^{-iH_0t}. \tag{5.16}$$

Similarly, the Møller operator $\Omega^{(-)}$ maps the out-state $|\Psi_{\text{out}}(t)\rangle$ to the full scattering state

$$|\Psi(t)\rangle = \Omega^{(-)}(t)\,|\Psi_{\text{out}}(t)\rangle\,, \tag{5.17}$$

where $\Omega^{(-)}(t)$ may be derived by inserting $|\Psi_0(t')\rangle$ of equation (5.6) in equation (5.11b) which reads

$$\Omega^{(-)}(t) = \mathbb{1} + i\int_{\infty}^{\infty} dt G^{-}(t,t')VG_0^{+}(t',t). \tag{5.18}$$

Again, $\Omega^{(-)}(t)$ can be given in terms of the Hamilton operator of the system

$$\Omega^{(-)}(t) = \lim_{t\to\infty} e^{iHt}e^{-iH_0t} \coloneqq \lim_{\epsilon\to 0^+}\int_0^{\infty} dt\;\epsilon\cdot e^{-\epsilon|t|}e^{iHt}e^{-iH_0t}. \tag{5.19}$$

The Møller operators $\Omega^{(+)}(t)$ and $\Omega^{(-)}(t)$ are *isometric* operators and fulfill

$$\Omega^{(\pm)\dagger}(t)\Omega^{(\pm)}(t) = \mathbb{1}, \tag{5.20}$$

but in general $\Omega^{(\pm)}(t)\Omega^{(\pm)\dagger}(t) \neq \mathbb{1}$. As *unitary* operators *isometric* operators are linear operators on the Hilbert space $\mathcal{H}$ preserving the norm but in contrast to *unitary* operators they are not a one-to-one injective map over $\mathcal{H}$ [38]. This is a consequence of the scattering states $|\Psi(t)\rangle$ not necessarily spanning the full Hilbert space $\mathcal{H}$ as $\mathcal{H}$ also includes the bound states of the system [37]. The relation

$$H(t)\Omega^{(\pm)}(t) = \Omega^{(\pm)}(t)H_0(t), \tag{5.21}$$

is called the *intertwining relation* for the Møller operators [38].

5.1.3 *S operator*

Having established how the Møller operators act on the asymptotic in- and out- states we can now derive the relation of in- and out- state with the equations (5.14), (5.17) and introduce the S operator as

$$|\Psi_{\text{out}}(t)\rangle = \Omega^{(-)\dagger}(t)\Omega^{(+)}(t)\,|\Psi_{\text{in}}(t)\rangle = S(t)\,|\Psi_{\text{in}}(t)\rangle\,. \tag{5.22}$$

The significance of the S operator is shown if one calculates the probability that the system is in the state $|\Psi_0(\beta,t)\rangle$ in the infinite future when it was controlled in the infinite past $|\Psi_{\text{in}}(\alpha,t)\rangle = |\Psi_0(\alpha,t)\rangle$ and the actual scattering state is given by $|\Psi^{(+)}(\alpha,t)\rangle$. This probability reads

$$\begin{aligned}\lim_{t\to\infty}\langle\Psi_0(\beta,t)|\Psi^{(+)}(\alpha,t)\rangle =& \langle\Psi_0(\beta,t)|\Psi_{\text{out}}(t)\rangle = \langle\Psi_0(\beta,t)|\,\Omega^{(-)\dagger}(t)\Omega^{(+)}(t)\,|\Psi_{\text{in}}(t)\rangle \\ &= \langle\Psi_0(\beta,t)|\,S(t)\,|\Psi_0(\alpha,t)\rangle\,.\end{aligned} \tag{5.23}$$

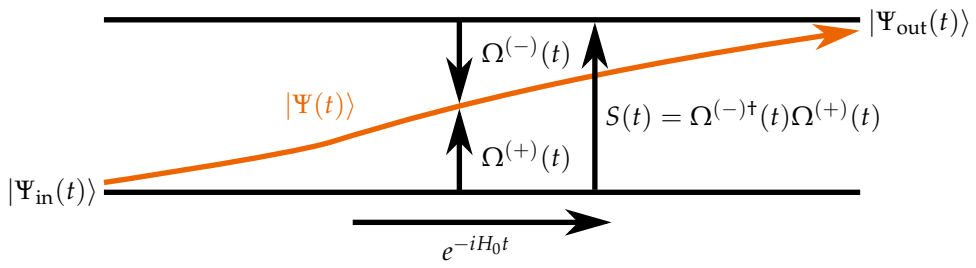

Figure 5.2: Schematically shown are the scattering state $|\Psi(t)\rangle$ and the asymptotically free states $|\Psi_{\text{in}}(t)\rangle$, $|\Psi_{\text{out}}(t)\rangle$. The S operator maps $|\Psi_{\text{in}}(t)\rangle$ to $|\Psi_{\text{out}}(t)\rangle$ while the Møller operators map $|\Psi_{\text{in}}(t)\rangle$ and $|\Psi_{\text{out}}(t)\rangle$ to the full scattering state $|\Psi(t)\rangle$.

From the *intertwining relation* (5.21) we conclude that the S operator commutes with H_0

$$[S(t), H_0(t)] = 0. \tag{5.24}$$

If the actual state is again given by $|\Psi^{(+)}(\alpha, t)\rangle$ the probability of finding the system in the state $|\Psi^{(-)}(\beta, t)\rangle$ evolving to the state $|\Psi_{\text{out}}(\beta, t)\rangle$ is given by

$$S_{\beta\alpha} = \langle\Psi^{(-)}(\beta, t)|\Psi^{(+)}(\alpha, t)\rangle = \langle\Psi_{\text{out}}(\beta, t)|\, S\, |\Psi_{\text{in}}(\alpha, t)\rangle = \langle\Psi_0(\beta, 0)|\, S\, |\Psi_0(\alpha, 0)\rangle\,, \tag{5.25}$$

which again is given in terms of the S operator. As seen from the equations (5.23), (5.25), all scattering properties of the system are known when the S operator is known. In contrast to the Møller operators which are *isometric* operators the S operator is a *unitary* operator with

$$S^\dagger S = SS^\dagger = \mathbb{1}. \tag{5.26}$$

In figure 5.2 the effect of the Møller operators and S operators acting on the asymptotic in- and out-states and the full scattering state are shown.

5.1.4 *Reactance operator*

The full information of the scattering process is also given by the reactance K operator. It is obtained from the *Caley transformation* of the S operator as [37]

$$K \equiv i(\mathbb{1} - S)(\mathbb{1} + S)^{-1}. \tag{5.27}$$

The inverse transformation reads

$$S = (\mathbb{1} + iK)(\mathbb{1} - iK)^{-1}. \tag{5.28}$$

From these definitions and from the fact that the S operator is *unitary* it may be easily verified that the K operator is Hermitian, $K = K^\dagger$. Rewriting equation (5.28) in another form leads to *Heitler's integral equation* [37]

$$S - \mathbb{1} = 2iK + iK(S - \mathbb{1}). \tag{5.29}$$

Equivalently to the S operator, full knowledge of the K operator leads to full knowledge of the scattering properties of the system.

5.2 TIME-INDEPENDENT FORMAL SCATTERING THEORY

For actual calculations we need the time-independent approach of scattering theory [38]. Here the Hamilton operator is not time-dependent $H \neq H(t)$. The time-independent picture of scattering can be deduced from the time-dependent picture by Fourier transformation of the operators and states introduced in the last section from the time domain to the energy domain. This Fourier transformation for an operator f reads

$$f(E) = \int_{-\infty}^{\infty} dt e^{iEt} f(t), \tag{5.30}$$

where E is the energy of the system. In this section we introduce the free momentum states and derive the decomposition of the S operator in terms of these states. This leads to a connection between the S matrix and the on-shell T matrix $t(\mathbf{k}, \mathbf{k}')$ and the scattering amplitude $f(\mathbf{k}, \mathbf{k}')$.

5.2.1 *Green's operators and state vectors*

In order to calculate the energy-dependent Green's operators we have to Fourier transform the time-dependent Green's operators defined together with the initial conditions in equation (5.2), reading

$$G^{\pm}(E) = \lim_{\epsilon \to 0^+} \int_{-\infty}^{\infty} dt e^{-\epsilon|t|} e^{iEt} G^{\pm}(t) = \lim_{\epsilon \to 0^+} G(E \pm i\epsilon), \tag{5.31}$$

where we have included a convergence factor $e^{-\epsilon|t|}$ and where $G(z)$ is the resolvent of the system, given by

$$G(z) = \frac{1}{z - H}. \tag{5.32}$$

We obtain the same result for the free energy-dependent Green's operators $G_0^{\pm}$ but with H replaced by H_0. The time-independent Green's operators fulfill the following equations

$$(E - H_0) G_0^{\pm}(E) = \mathbb{1}, \tag{5.33}$$

$$(E - H) G^{\pm}(E) = \mathbb{1}. \tag{5.34}$$

With the Fourier transform (5.30) we can also calculate the time-independent scattering states. The time-independent scattering states $|\Psi^{(\pm)}(E)\rangle$ are given by

$$|\Psi^{(\pm)}(E)\rangle = |\Psi_0(E)\rangle + G_0^{\pm}(E) V |\Psi^{(\pm)}(E)\rangle = |\Psi_0(E)\rangle + G^{\pm}(E) V |\Psi_0(E)\rangle . \tag{5.35}$$

These equations are referred to as the *Lippmann-Schwinger equations* [112]. The time-independent Schrödinger equations for the full scattering state $\Psi(E)$ and the free scattering state $\Psi_0(E)$ read

$$H_0 |\Psi_0(E)\rangle = E |\Psi_0(E)\rangle , \quad H |\Psi(E)\rangle = E |\Psi(E)\rangle . \tag{5.36}$$

As in the time-dependent picture, the Møller operators map the free states to the full scattering states

$$|\Psi^{(\pm)}(E)\rangle = \Omega^{(\pm)}(E) |\Psi_0(E)\rangle , \tag{5.37}$$

but now the Møller operators are energy-dependent. Again, we obtain the important result that the S operator maps the in amplitude $|\Psi_{\text{in}}(E)\rangle$ to the out amplitude $|\Psi_{\text{out}}(E)\rangle$

$$|\Psi_{\text{out}}(E)\rangle = \Omega^{(-)\dagger}(E) \Omega^{(+)}(E) |\Psi_{\text{in}}(E)\rangle \equiv S(E) |\Psi_{\text{in}}(E)\rangle , \tag{5.38}$$

and all the information about the scattering process is contained in the S operator. In the next subsection we derive the S operator in free momentum states and obtain the S matrix and its decomposition in terms of the T matrix.

5.2.2 *S matrix, T matrix and scattering amplitude*

From the formal scattering theory we now come to the specific representation in momentum space. As the S operator commutes with H_0 (see subsection 5.1.3), both operators have a common basis of eigenstates. The eigenstates of H_0 are the free momentum states $|\Psi_0(E)\rangle \equiv |\mathbf{k}\rangle$

$$H_0 |\mathbf{k}\rangle = \frac{\mathbf{k}^2}{2m} |\mathbf{k}\rangle \equiv E_k |\mathbf{k}\rangle , \tag{5.39}$$

where m is the mass of the particle. Here we highlight, that in natural units ($\hbar = 1$) momentum and wave number are identical, $\mathbf{p} = \mathbf{k}$, so that we call the eigenstates momentum states. The position representation of the free momentum states reads

$$\langle \mathbf{x} | \mathbf{k} \rangle = (2\pi)^{-3/2} e^{i\mathbf{k}\mathbf{x}}, \tag{5.40}$$

with normalization $\langle \mathbf{k}'|\mathbf{k}\rangle = \delta^{(3)}(\mathbf{k}' - \mathbf{k})$. The S operator in the momentum representation $\langle \mathbf{k}'| S |\mathbf{k}\rangle$ is often called the S matrix [38]. As the S matrix commutes with H_0 we obtain

$$\langle \mathbf{k}'| [S, H_0] |\mathbf{k}\rangle = (E_{k'} - E_k) \langle \mathbf{k}'| S |\mathbf{k}\rangle , \tag{5.41}$$

which is zero for $E_{k'} = E_k$. We conclude that the S matrix elements $\langle \mathbf{k}'| S |\mathbf{k}\rangle$ must have a form like $\langle \mathbf{k}'| S |\mathbf{k}\rangle = \delta(E_{k'} - E_k) \times \textit{remainder}$. The decomposition of the S matrix in the free momentum states reads [38]

$$\langle \mathbf{k}'| S |\mathbf{k}\rangle = \delta^{(3)}(\mathbf{k} - \mathbf{k}') - 2\pi i \delta(E_{k'} - E_k) T(\mathbf{k}, \mathbf{k}'), \tag{5.42}$$

where the factor $2\pi i$ is a conventional factor. The first term in equation (5.42) ensures we have unit transmission in the absence of a scatterer. The second term is only non-zero for $E_{k'} = E_k$ when the energy is conserved. The term $T(\mathbf{k}, \mathbf{k}')$ is therefore only defined on the energy-shell for $\mathbf{k}^2 = \mathbf{k}'^2$ and for this reason it is called the "on-shell" T matrix. Of course it is conceivable to define a T operator for momentum states, where the elements $\langle \mathbf{k}'| T |\mathbf{k}\rangle$ are not necessarily "on-shell", which is then consistently called the "off-shell" T matrix. The "on-shell" T matrix is closely related to the scattering amplitude $f(\mathbf{k}, \mathbf{k}')$

$$f(\mathbf{k}, \mathbf{k}') = -(2\pi)^2 m \cdot T(\mathbf{k}, \mathbf{k}'). \tag{5.43}$$

Before we introduce the concept of the scattering cross section and the relationship of scattering amplitude and differential cross section we discuss the topic of two-particle scattering in order to describe atomic collisions.

5.3 TWO-PARTICLE SCATTERING

So far we have only considered scattering of a single particle. In this section, we show that two-particle scattering is quite similar to this scenario if one separates the center-of-mass and the relative motion. The Hamiltonian for two particles interacting via V is given by

$$H = \frac{\mathbf{k}_1^2}{2m_1} + \frac{\mathbf{k}_2^2}{2m_2} + V \equiv H_0 + V, \tag{5.44}$$

where m_1, m_2 are the masses and $\mathbf{k}_1$, $\mathbf{k}_2$ the wave vectors of particle 1 and 2, respectively. The center-of-mass coordinates ($\bar{\mathbf{x}}$, $\bar{\mathbf{k}}$) and the relative coordinates ($\mathbf{x}$, $\mathbf{k}$) are given by

$$\bar{\mathbf{k}} = \mathbf{k}_1 + \mathbf{k}_2, \qquad \mathbf{k} = \frac{m_2\mathbf{k}_1 - m_1\mathbf{k}_2}{m_1 + m_2}, \tag{5.45a}$$

$$\bar{\mathbf{x}} = \frac{m_1\mathbf{x}_1 + m_2\mathbf{x}_2}{m_1 + m_2}, \qquad \mathbf{x} = \mathbf{x}_1 - \mathbf{x}_2. \tag{5.45b}$$

Inserting equation (5.45) in equation (5.44) leads to a separation of the Hamiltonian into center-of-mass and a relative parts

$$H = H_{\text{com}} + H_{\text{rel}} = H_{\text{com}} + H_{\text{rel}}^0 + V = \frac{\bar{\mathbf{k}}^2}{2M} + \left[\frac{\mathbf{k}^2}{2\mu} + V(\mathbf{x})\right], \tag{5.46}$$

with the total mass M and the reduced mass μ given by

$$M = m_1 + m_2, \qquad \mu = \frac{m_1 m_2}{m_1 + m_2}. \tag{5.47}$$

The relative Hamiltonian H_{rel} is an effective one-particle operator for the potential scattering of a particle with reduced mass μ and relative wave vector $\mathbf{k}$ and a potential $V(\mathbf{x})$.

If we insert the Hamiltonian of the two-particle system (5.46) in the equations (5.16), (5.19) we obtain the two-particle Møller operators

$$\mathbf{\Omega}^{(\pm)}(E) = \mathbb{1}_{\text{com}} \otimes \Omega^{(\pm)}(E), \quad \Omega^{(\pm)}(E) = \lim_{t \to \mp\infty} e^{iH_{\text{rel}}t} e^{-iH_{\text{rel}}^0 t}, \tag{5.48}$$

with a center-of-mass part and the Møller operators $\Omega^{(\pm)}(E)$ of the relative motion and where the last term is a shorthand notation for the integrals defined in the equations (5.16), (5.19). The center-of-mass part is simply given by the unit operator $\mathbb{1}_{\text{com}}$. With equation (5.48) we obtain the two-particle S operator as

$$\boldsymbol{S}(E) = \mathbb{1}_{\text{com}} \otimes S(E), \quad S(E) = \Omega^{(-)\dagger}(E)\Omega^{(+)}(E), \tag{5.49}$$

where S is the S operator for the relative motion of the two particles. We observe, that the center-of-mass part does not affect the scattering process, as it is given by the unit operator $\mathbb{1}_{\text{com}}$. For two interacting particles, the total wave vector $\bar{\mathbf{k}}$ is conserved and the center-of-mass $\bar{\mathbf{x}}$ of the system moves uniformly in space. The decomposition of the S matrix for the one-particle case in equation (5.42) in free momentum states translates in the two-particle case to [38]

$$\langle \mathbf{k}_1', \mathbf{k}_2' | \, \boldsymbol{S} \, | \mathbf{k}_1, \mathbf{k}_2 \rangle = \delta^{(3)}(\mathbf{k}_1' - \mathbf{k}_1)\delta^{(3)}(\mathbf{k}_2' - \mathbf{k}_2) - 2\pi i \delta \left(\sum_i E_i' - E_i \right) \delta(\bar{\mathbf{k}}' - \bar{\mathbf{k}}) T(\mathbf{k}, \mathbf{k}'), \tag{5.50}$$

where the first term describes no scattering, neither of particle 1 nor of particle 2 and the second term conserves total energy and total momentum of the system. The two-particle "on-shell" T matrix $T(\mathbf{k}, \mathbf{k}')$ is related to the two-particle scattering amplitude by an expression similar to equation (5.43)

$$f(\mathbf{k}', \mathbf{k}) = -(2\pi)^2 \mu \cdot T(\mathbf{k}, \mathbf{k}'), \tag{5.51}$$

where only the mass m is replaced by the reduced mass μ.

In conclusion, two-particle scattering is equivalent to the scattering of one particle with reduced mass μ and relative wave vector $\mathbf{k}$ off a potential, so it is sufficient to constrain our attention to the case of single-particle potential scattering.

5.4 SCATTERING STATES AND SCATTERING CROSS SECTION

In this section, we introduce the scattering wave function in $3D$ by solving the *Lippmann-Schwinger equations* (5.35). We then assume an isotropic potential and give the scattering states in a spherical basis. The resulting partial-wave expansion of the scattering states leads to a decomposition of the cross section σ in partial-wave contributions σ_l. This is of particular use in low-energy collisions as here only a few partial waves contribute to the actual scattering properties.

We start with the *Lippmann-Schwinger equations* (5.35) where we identify the states $|\Psi(E)\rangle$ with the momentum states $|\mathbf{k}\pm\rangle$, $|\mathbf{k}\rangle$ so that we write

$$|\mathbf{k}\pm\rangle = |\mathbf{k}\rangle + G_0^{\pm}(E) V \, |\mathbf{k}\pm\rangle \, . \tag{5.52}$$

In order to obtain the position representation of this state we have to calculate the free Green's function $G_{0,k}^{\pm}(\mathbf{x}, \mathbf{x}') \equiv \langle \mathbf{x} | \, G_0^{\pm}(E) \, | \mathbf{x}' \rangle$. The result is given in [111]

$$G_{0,k}^{\pm}(\mathbf{x}, \mathbf{x}') = -\frac{m}{2\pi} \frac{e^{\pm ik|\mathbf{x}-\mathbf{x}'|}}{|\mathbf{x}-\mathbf{x}'|}, \tag{5.53}$$

Under the assumption that the interaction potential is local, i.e. $\langle \mathbf{x} | \, V \, | \mathbf{x}' \rangle = V(\mathbf{x})\delta^{(3)}(\mathbf{x}-\mathbf{x}')$, we obtain for the *Lippmann-Schwinger equation* in position representation

$$\psi_k^{\pm}(\mathbf{x}) = \langle \mathbf{x} | \mathbf{k}\pm \rangle = \langle \mathbf{x} | \mathbf{k} \rangle - \frac{m}{2\pi} \int d^3x' \frac{e^{\pm ik|\mathbf{x}-\mathbf{x}'|}}{|\mathbf{x}-\mathbf{x}'|} V(\mathbf{x}') \psi_k^{\pm}(\mathbf{x}). \tag{5.54}$$

Usually the detector is placed far away from the scattering center to fulfill the requirement that the particles freely evolve after the scattering process and that there is no interaction between the particles anymore. Therefore, we evaluate the scattering wave function in the asymptotic region $|\mathbf{x}| \gg |\mathbf{x}'|$. With the coordinates $|\mathbf{x}| \equiv r$, $|\mathbf{x}'| \equiv r'$, $|\mathbf{x} - \mathbf{x}'| \simeq r - \hat{\mathbf{r}}\mathbf{x}'$ and $\mathbf{k}' \equiv k\hat{\mathbf{r}}$ we obtain

$$\psi_k^{\pm}(\mathbf{x}) \underset{r\to\infty}{\to} (2\pi)^{-3/2} \left[e^{i\mathbf{k}\mathbf{x}} - (2\pi)^2 m \, \langle \mp \mathbf{k}' | \, V \, | \mathbf{k}\pm \rangle \, \frac{e^{\pm ikr}}{r} \right]. \tag{5.55}$$

For the physically more meaningful wave function $\psi_k^+(\mathbf{x})$ we write

$$\psi_k^+(\mathbf{x}) \underset{r\to\infty}{\to} \psi_{\text{in}}(\mathbf{x}) + \psi_{\text{out}}(\mathbf{x}) = (2\pi)^{-3/2}\left[e^{i\mathbf{kx}} + f(\mathbf{k},\mathbf{k}')\frac{e^{ikr}}{r}\right], \tag{5.56}$$

with the scattering amplitude, given by

$$f(\mathbf{k},\mathbf{k}') = -(2\pi)^2 m \langle \mathbf{k}'| V |\mathbf{k}\pm\rangle = -(2\pi)^2 m \cdot T(\mathbf{k},\mathbf{k}'). \tag{5.57}$$

Thus, from equation (5.56) we conclude that the asymptotic scattering state is given by an incoming plane wave and a scattered outgoing spherical wave with the scattering amplitude $f(\mathbf{k},\mathbf{k}')$.

Scattering cross section

With the asymptotic form of the scattering wave function $\psi_k^+(\mathbf{x})$ (5.56) we now can calculate the scattering cross section. The scattering cross section is measured in experiment. Therefore, it is important to understand the concept of the cross section. The differential scattering cross section is defined as the scattered flux of particles in the surface element $d\mathbf{F}$ over the incoming flux particles, reading

$$d\sigma = \frac{\mathbf{j}_{\text{out}} \cdot d\mathbf{F}}{|\mathbf{j}_{\text{in}}|}. \tag{5.58}$$

The scattering process is depicted in figure 5.3.

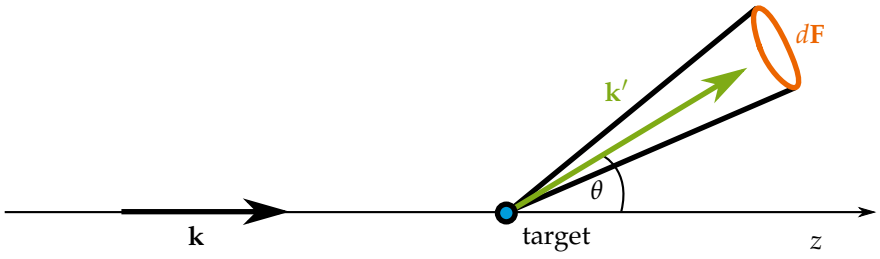

Figure 5.3: Incoming wave with wave vector $\mathbf{k}$ and scattered wave with wave vector $\mathbf{k}'$ through the surface element $d\mathbf{F}$. In elastic scattering the energy is conserved $k = k'$. The z-axis is chosen along $\mathbf{k}$.

The flux of particles or the particle current density is given by

$$\mathbf{j}(\mathbf{x}) = \frac{n_0}{2mi}\left(\psi_k^*(\mathbf{x})\nabla_{\mathbf{x}}\psi_k(\mathbf{x}) - \psi_k(\mathbf{x})\nabla_{\mathbf{x}}\psi_k^*(\mathbf{x})\right), \tag{5.59}$$

where n_0 is the particle density of the incoming wave. The incoming particle current density is calculated from the incoming wave $\psi_{\text{in}}(\mathbf{x})$ of equation (5.56) and the outgoing particle current density from the outgoing wave $\psi_{\text{out}}(\mathbf{x})$. With the surface element given by $d\mathbf{F} = r^2 d\Omega\, \mathbf{n}_r$ (with $\mathbf{n}_r = \mathbf{x}/r$ and for elastic scattering ($k = k'$) we find the important result

$$\frac{d\sigma}{d\Omega}(\mathbf{k},\mathbf{k}') = |f(\mathbf{k},\mathbf{k}')|^2. \tag{5.60}$$

Thus, the differential scattering cross section is simply given the absolute square of the scattering amplitude $f(\mathbf{k},\mathbf{k}')$. From the differential cross section one obtains the total scattering cross section as

$$\sigma(\mathbf{k},\mathbf{k}') = \int d\Omega \frac{d\sigma}{d\Omega}(\mathbf{k},\mathbf{k}'). \tag{5.61}$$

In the next section we decompose the scattering wave function and the scattering cross section in partial waves.

5.5 PARTIAL-WAVE EXPANSION

In the preceding discussion, we have assumed that the potential $V(\mathbf{x})$ is local. We further assume now, that $V(\mathbf{x}) = V(r)$, which means that the potential is isotropic. Thus, the potential is spherically symmetric the system rotationally invariant so that $[S, R] = 0$ and $S = R^\dagger S R$, where R is the rotation operator [38]. Rotational invariance also implies that the S operator commutes with the total angular momentum operator $\mathbf{J}$ which, for a single spinless particle, is equivalent to the orbital angular momentum operator $\mathbf{L}$. In this situation, $\left\{H_0, \mathbf{L}^2, L_z\right\}$ form a complete set of commuting observables with eigenvalues E, $l(l+1)$ and m, respectively. As consequence, the basis states are labeled $|E, l, m\rangle$ and the S operator is diagonal in this representation

$$\langle E', l', m'| S |E, l, m\rangle = \delta(E' - E)\delta_{ll'}\delta_{mm'} \times s_l(E) = \delta(E' - E)\delta_{ll'}\delta_{mm'} \times e^{2i\eta_l(E)}, \tag{5.62}$$

with the S matrix elements s_l and the scattering phase $\eta_l(E) \equiv \log(s_l)/2i$ which is real for real energies. Here the factor 2 is a conventional factor. The parametrization of s_l in terms of a scattering phase η_l follows from the unitarity of the S matrix, which means that its entries s_l are unimodular. The position representation of the basis states $|E, l, m\rangle$ is given by

$$\langle \mathbf{x}|E, l, m\rangle = i^l \left(\frac{2m}{\pi k}\right)^{1/2} \frac{1}{r} \hat{\jmath}_l(kr) Y_{lm}(\mathbf{n}_r), \tag{5.63}$$

where $\hat{\jmath}_l$ are the Riccati-Bessel functions (see appendix C.3) and $Y_{lm}(\mathbf{n}_r)$ are the spherical harmonics with $\mathbf{n}_r = \mathbf{x}/r$. The spherical basis in the momentum representation reads

$$\langle \mathbf{k}|E, l, m\rangle = (mk)^{-1/2} \delta(E_k - E) Y_{lm}(\mathbf{n}_k), \tag{5.64}$$

with $\mathbf{n}_k = \mathbf{k}/k$. Using this representation for the spherical basis together with the decomposition of the S matrix (5.42) we obtain the partial-wave expansion of the scattering amplitude [38]

$$f(\mathbf{k}', \mathbf{k}) = f(k, \cos\theta) = \sum_{l=0}^{\infty} (2l+1) f_l(k) P_l(\cos\theta), \tag{5.65}$$

where θ is the angle between the wave vectors $\mathbf{k}$, $\mathbf{k}'$ and $f_l(k)$ is the partial-wave scattering amplitude. We can also construct full scattering states in the $|E, l, m\rangle$ basis by applying the Møller operators $\Omega^{(\pm)}$ to the free states $|E, l, m\rangle$

$$|E, l, m\pm\rangle = \Omega^{(\pm)}(E) |E, l, m\rangle . \tag{5.66}$$

The full scattering states $|E, l, m\pm\rangle$ fulfill the Lippmann-Schwinger equation

$$|E, l, m\pm\rangle = |E, l, m\rangle + G_0^{\pm}(E) V |E, l, m\pm\rangle . \tag{5.67}$$

Reduced radial Schrödinger equation

The position representation of the full scattering state in the spherical basis is similar to the free scattering state in equation (5.63) but with $\hat{\jmath}_l$ replaced by $\psi^{\pm}_{l,k}$, reading [38]

$$\langle \mathbf{x}|E, l, m\pm\rangle = i^l \left(\frac{2m}{\pi k}\right)^{1/2} \frac{1}{r} \psi^{\pm}_{l,k}(r) Y_{lm}(\mathbf{n}_r), \tag{5.68}$$

where the partial scattering wave function $\psi^{\pm}_{l,k}(r)$ fulfills the reduced radial Schrödinger equation

$$\left[\frac{d^2}{dr^2} - \frac{l(l+1)}{r^2} - V(r) + k^2\right] \psi^{\pm}_{l,k}(r) = 0, \tag{5.69}$$

together with the boundary condition at the origin, $\psi^{\pm}_{l,k}(0) = 0$, and the asymptotic boundary condition at $r \to \infty$ for

$$\psi^{+}_{l,k}(r) \underset{r\to\infty}{\longrightarrow} \left[\hat{\jmath}_l(kr) + k f_l(k) \hat{h}^+_l(kr)\right] = \frac{i}{2}\left[\hat{h}^-_l(kr) - s_l(k)\hat{h}^+_l(kr)\right], \tag{5.70}$$

and correspondingly for $\psi^-_{l,k}$ which is given by $\psi^-_{l,k} = [\psi^+_{l,k}]^*$ [38]. In the equation (5.70) we introduced the Riccati-Hankel functions $\hat{h}^\pm_l$ (see appendix C.3) and we used the relation $\hat{\jmath}_l = (\hat{h}^+_l - \hat{h}^-_l)/2i$ (see appendix C.3). From the equation (5.70) we find the important relationship of S matrix and partial scattering amplitude as $s_l(k) = 1 + 2ikf_l(k)$. With the parametrization of the S matrix in terms of the scattering phase η_l we find that the partial scattering amplitude can also be written as

$$f_l(k) = \frac{s_l(k) - 1}{2ik} = \frac{e^{2i\eta_l(k)} - 1}{2ik} = \frac{e^{i\eta_l(k)} \sin \eta_l(k)}{k}. \tag{5.71}$$

In section 5.4 we established the relation of the scattering cross section σ and the scattering amplitude $f(\mathbf{k}, \mathbf{k}')$. Inserting the partial-wave expansion (5.65) in equation (5.61) and integrating over the solid angle $d\Omega$ by using the orthogonality of the Legendre polynomials [13] leads to the partial-wave expansion of the scattering cross section in terms of the scattering phase η_l or the S matrix s_l

$$\sigma = \sum_l \sigma_l = \frac{4\pi}{k^2} \sum_l (2l+1) \sin^2 \eta_l = \frac{2\pi}{k^2} \sum_l (2l+1)(1 - \operatorname{Re} s_l). \tag{5.72}$$

In the next section, we study a solution to the reduced radial Schrödinger equation (5.69) with different boundary conditions which leads to the *regular solution* and to the Jost function.

5.6 REGULAR SOLUTION

Here we introduce the regular solution as from the analytic properties of the regular solution one can establish the analytic properties of the S matrix. The regular solution is defined by the boundary condition

$$\phi_{l,k}(r) \underset{r\to 0}{\longrightarrow} \hat{\jmath}_l(kr), \tag{5.73}$$

which is a second boundary condition at the origin besides the condition $\phi_{l,k}(0) = 0$. The boundary condition (5.73) fixes the normalization of the regular solution. This solution is real since the boundary conditions and the radial Schrödinger equation (5.69) are real. We can also write the radial Schrödinger equation (5.69) together with the boundary conditions for the regular solution in an integral equation of the type

$$\phi_{l,k}(r) = \hat{\jmath}_l(kr) + \int_0^r dr' g_{l,k}(r, r') V(r') \phi_{l,k}(r'), \tag{5.74}$$

with the radial Green's function $g_{l,k}(r, r')$. The radial Green's function reads

$$g_{l,k}(r, r') = \frac{1}{k} \left[\hat{\jmath}_l(kr) \hat{n}_l(kr') - \hat{n}_l(kr) \hat{\jmath}(kr') \right], \tag{5.75}$$

with $\hat{n}_l(kr)$ the Riccati-Neumann function (see appendix C.3). The integral (5.74) is zero for $r' > r$. Integrals of the type (5.74) are called *Volterra integral equations* [37]. The advantage of *Volterra type* equations is that they can be solved by iteration. Thus, the regular solution can be found by iteration, independently of the strength of the interaction potential [37].

5.7 JOST FUNCTION

Here we introduce the Jost function and study its properties for complex wave numbers. The Jost function is given by the asymptotic behavior of the regular solution. For large r the regular solution reads

$$\phi_{l,k}(r) \underset{r\to\infty}{\longrightarrow} \frac{i}{2} \left[\mathfrak{f}_l(k) \hat{h}^-_l(kr) - \mathfrak{f}^*_l(k) \hat{h}^+_l(kr) \right], \tag{5.76}$$

where $\mathfrak{f}_l(k)$ is the Jost function [37]. Comparing the asymptotic behavior of the regular solution (5.76) with the asymptotic behavior of the scattering wave function (5.70) we obtain

$$\phi_{l,k}(r) = \psi^+_{l,k}(r) \mathfrak{f}_l(k) = \psi^-_{l,k}(r) \mathfrak{f}^*_l(k), \tag{5.77}$$

and the important connection between the S matrix s_l and the Jost function

$$s_l(k) = \mathfrak{f}_l(k)^*/\mathfrak{f}_l(k). \tag{5.78}$$

One can see from this relation that wherever the Jost function is zero, the S matrix has a pole.

Complex wave numbers

So far the discussion was restricted to real k. We now give up this restriction and study the analyticity of the regular solution, the Jost function and the S matrix in the complex k plane. Starting from the integral equation for the regular solution (5.74), one can show that the regular solution is an *entire* function of k which means that it is *analytic* everywhere in the complex k plane [38]. If we compare the integral equation for the regular solution (5.74) with the asymptotic form (5.76) we obtain an integral equation for the Jost function

$$\mathfrak{f}_l(k) = 1 + \frac{1}{k}\int_0^\infty dr \hat{h}_l^+(kr) V(r) \phi_{l,k}(r). \tag{5.79}$$

As this integral runs from zero to infinity it needs to be checked if it converges. Due to the properties of the Riccati-Hankel function $\hat{h}_l^+(kr)$ this integral converges for all k in the upper half plane. For finite-range potentials with range r_0, the integral (5.79) runs from 0 to r_0. In this case, the Jost function is *analytic* for all k in the complex k plane. Note that the assumption of finite-range potentials is sufficient for the discussion in this work. For more general potentials, however, the investigation of the analyticity of the Jost function in the complex k plane has to be done with great care. From the analyticity of $\mathfrak{f}_l(k)$ we cannot directly make conclusions about the analyticity of $s_l(k)$. This is due to the fact, that in general, if some function $f(z)$ is analytic on a region R this is not true for $f^*(z)$. Therefore, we have to think about the analyticity of $\mathfrak{f}_l^*(k)$. Consider a change if the real wave number k to the negative real wave number $-k$. Due to the properties of the Riccati-Hankel functions (see appendix C.3) we find for the Jost function the relation

$$\mathfrak{f}_l(-k) = \mathfrak{f}_l(k)^*. \tag{5.80}$$

Knowing that the Jost function is real on the imaginary axis one can generalize the relation (5.80) with the help of the *Schwarz reflection principle* [113] to complex k values and finds that

$$\mathfrak{f}_l(k) = \mathfrak{f}_l(-k^*)^*, \tag{5.81}$$

for all k in the complex plane. Therefore, we can rewrite the S matrix in terms of the Jost function as

$$s_l(k) = \frac{\mathfrak{f}_l(k)^*}{\mathfrak{f}_l(k)} = \frac{\mathfrak{f}_l(-k^*)}{\mathfrak{f}_l(k)}, \tag{5.82}$$

which holds for all k in the complex plane. Since $\mathfrak{f}_l(k)$ is *analytic* everywhere for finite-range potentials we conclude that the S matrix is a *meromorphic* function of k which means that it is *analytic* for all k except at the points where $\mathfrak{f}_l(k) = 0$ and $s_l(k)$ has a pole. These zeros of the Jost function or the poles of the S matrix have an important physical interpretation.

Weierstrass expansion

The poles of the S matrix or correspondingly the zeros of the Jost matrix in the complex k plane correspond to bound states, virtual states and resonance states of the scattering potential. We saw in the previous subsection that the Jost function is an entire function of k for finite-range potentials. Due to the *Weierstrass factorization theorem* [113, 114] an *entire* function can be represented as a product of the zeros of the function. In [37] the Weierstrass factorization of the Jost function has been given for potentials of finite range r_0 and $l = 0$ as

$$\begin{aligned}\mathfrak{f}_0(k) =& \mathfrak{f}_0(0) e^{ikr_0} \prod_{n=1}^{\infty} \left(1 - \frac{k}{k_n}\right) \\ =& \mathfrak{f}_0(0) e^{ikr_0} \prod_{n=1}^{N'} \left(1 - i\frac{k}{\varkappa_n}\right) \prod_{n=1}^{N} \left(1 + i\frac{k}{\mathcal{K}_n}\right) \prod_{n=1}^{\infty} \left(1 - \frac{k}{k_n}\right)\left(1 + \frac{k}{k_n^*}\right),\end{aligned} \tag{5.83}$$

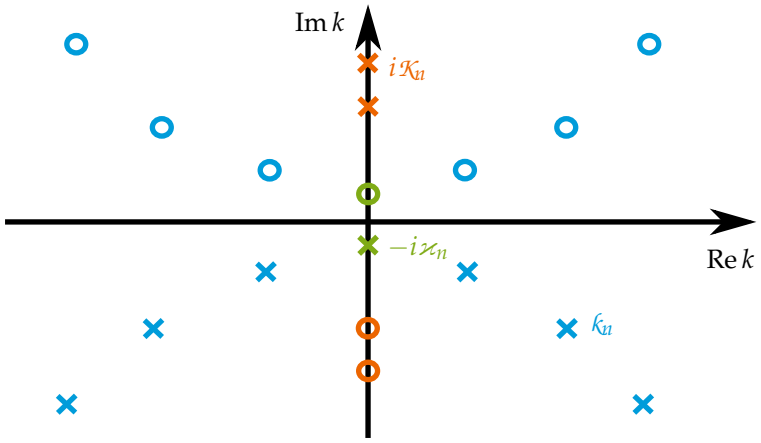

Figure 5.4: Poles and zeros of the S matrix in the complex k plane. The poles $i\mathcal{K}_n$ due to bound states are given as orange crosses, the pole $-i\varkappa_n$ due to a virtual state as a green cross and the poles k_n due to resonant states as blue crosses. Each pole corresponds to a zero of the S matrix in the lower/upper half plane which are shown as circles.

with $\mathfrak{f}_0(0) \neq 0$ and with k_n the positions of the zeros of the Jost-function. There are infinitely many zeros of the Jost function so that the product in equation (5.83) is an infinite product. The zeros of the Jost function in the complex k plane are due to bound, virtual and resonant states of the potential [37]. There can be zero or finitely many bound and virtual states in the potential but infinitely many resonant states [37]. If there are N bound and N' virtual states in the scattering potential then there are N zeros of the Jost function on the positive imaginary axis $k_n = i\mathcal{K}_n$, with $\mathcal{K}_n > 0$ and N' zeros on the negative imaginary axis $k_n = -i\varkappa_n$. The resonant states occur as two symmetric zeros of the Jost function at k_n, $-k_n^*$. Inserting the Weierstrass expansion of the Jost function in equation (5.82) we obtain the pole expansion of the S matrix

$$s_0(k) = e^{-2ikr_0} \prod_{n=1}^{N'} \frac{\varkappa_n + ik}{\varkappa_n - ik} \prod_{n=1}^{N} \frac{\mathcal{K}_n - ik}{\mathcal{K}_n + ik} \prod_{n=1}^{\infty} \frac{|k_n|^2 - k^2 - 2ik\,\mathrm{Im}\,k_n}{|k_n|^2 - k^2 + 2ik\,\mathrm{Im}\,k_n}, \tag{5.84}$$

in terms of the bound, virtual and resonant states of the potential. The of poles of the S matrix are depicted in figure 5.4.
In chapter 7 we show that for the poles due to bound, virtual or a resonant states close to the real axis, the pole expansion of the S matrix (5.84) is dominated by these poles and the infinite product over the other poles can be included in a background scattering phase. As the scattering phase η is related to the S matrix with $s_0 \equiv \exp(2i\eta_0)$, we can immediately give an expansion for the scattering phase in terms of the poles of the S matrix

$$\eta_0(k) = -kr_0 - \sum_{n=1}^{N} \tan^{-1} \frac{k}{\mathcal{K}_n} + \sum_{n=1}^{N'} \tan^{-1} \frac{k}{\varkappa_n} + \sum_{n=1}^{\infty} \tan^{-1} \frac{2k\,\mathrm{Im}\,k_n}{|k_n|^2 - k^2}. \tag{5.85}$$

We return to the discussion of analytic scattering theory in section 5.8.4 in terms multichannel scattering which we now introduce.

5.8 MULTICHANNEL SCATTERING

The results so far in this chapter have been derived for elastic scattering. In order to describe ionizing collisions of Ne* we have to generalize the results to multichannel scattering. The scattering processes in metastable neon collisions read

$$\begin{aligned} &\mathrm{Ne}^* + \mathrm{Ne}^* \longrightarrow \mathrm{Ne}^* + \mathrm{Ne}^*, \\ &\mathrm{Ne}^* + \mathrm{Ne}^* \longrightarrow \mathrm{Ne} + \mathrm{Ne}^+ + e^- \quad \text{(PI)}, \\ &\mathrm{Ne}^* + \mathrm{Ne}^* \longrightarrow \mathrm{Ne}_2^+ + e^- \quad \text{(AI)}, \end{aligned} \tag{5.86}$$

with the first line denoting elastic scattering of Ne* and the second and third line describe the PI and AI processes. Each reaction equation describes a different scattering process. Reactants and products define different *scattering channels*. There are different processes possible in multichannel scattering such as elastic collisions, excitations, rearrangement collisions and breakup collisions. In Ne* collisions all different types of processes are present. This is depicted in figure 5.5 for PI.

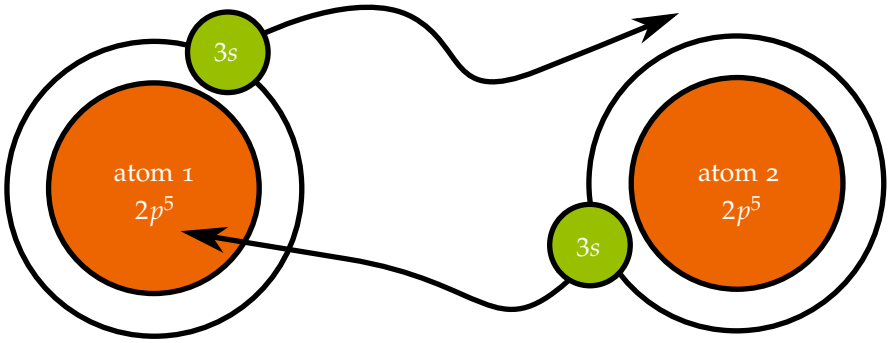

Figure 5.5: Penning Ionization in Ne* collisions. The black arrows indicate the exchange process of the valence electron of atom 2 and the ejection of the valence electron of atom 1.

The labeling of the atomic orbitals of Ne* in the figure will be explained in more detail in the next chapter 6. For the discussion of this section it is important to note, that PI is a rearrangement collision, a breakup collision and a deexcitation process at the same time. The $3s$ electron of atom 2 is transferred to atom 1 and the $3s$ electron of Ne* is ejected. Atom 1 is then in the atomic ground state and a Ne^+ ion and an electron are *produced*. The channel $Ne + Ne^+ + e^-$ is a *scattering channel* which is different from the $Ne^* + Ne^*$ *scattering channel*. For single-channel scattering we have defined the in- and out-states in equation (5.9) which evolved in time with the free Hamiltonian H_0. In the inelastic processes depicted here it is clear that the time evolution of the asymptotic states of *scattering channel* $Ne^* + Ne^*$ must be given in terms of a *free* Hamiltonian different from the one for the asymptotic states of $Ne + Ne^+ + e^-$ as different particles are considered as free particles. This defines different *channel Hamilton operators*.

In order to illustrate the concept of *channel Hamilton operators* we assume a system of three particles a, b, c and follow the discussion in [38]. We choose this system as the ionization processes of Ne* are not intuitive and the concepts of multichannel scattering can be better understood in terms of a simpler system.The three particles a, b, c can form bound states in different arrangements. Assume the scattering processes

$$a + (bc) \longrightarrow \begin{cases} a + (bc) & \text{elastic scattering,} \\ a + (bc)^* & \text{excitation,} \\ b + (ac) & \text{rearrangement,} \\ a + b + c & \text{breakup.} \end{cases} \tag{5.87}$$

Depending on the collision energy, some of the *scattering channels* might be energetically forbidden and are then called *closed channels*. Energetically accessible *scattering channels* are called *open channels*. If the particle a collides with the compound system (bc), the collision energy might be high enough to excite the bound system (bc) to the excited state $(bc)^*$ but could not be high enough to break up the bound system to end up in the *scattering channel* $a + b + c$. The total Hamiltonian for the three-particle system reads

$$H = \frac{\mathbf{k}_a^2}{2m_a} + \frac{\mathbf{k}_b^2}{2m_b} + \frac{\mathbf{k}_c^2}{2m_c} + V_{ab}(\mathbf{x}_{ab}) + V_{ac}(\mathbf{x}_{ac}) + V_{bc}(\mathbf{x}_{bc}), \tag{5.88}$$

where the first three terms are the kinetic energy terms with the masses m_a, m_b, m_c of the particles a, b, c, respectively and where $V_{ab}(\mathbf{x}_{ab})$, $V_{ac}(\mathbf{x}_{ac})$, $V_{bc}(\mathbf{x}_{bc})$ are the interaction potentials between the particles a, b and c. The *channel Hamiltonian* of the *scattering channel* $a + (bc)$, which we denote by α, reads

$$H_\alpha = \frac{\mathbf{k}_a^2}{2m_a} + \frac{\mathbf{k}_b^2}{2m_b} + \frac{\mathbf{k}_c^2}{2m_c} + V_{bc}(\mathbf{x}_{bc}) = \frac{\mathbf{k}_a^2}{2m_a} + \frac{\bar{\mathbf{k}}_{bc}^2}{2M_{bc}} + \left(\frac{\mathbf{k}_{bc}^2}{2\mu_{bc}} + V_{bc}, \right) \tag{5.89}$$

where in the second line we introduce the center-of-mass wave vector $\bar{\mathbf{k}}_{bc}$, the relative wave vector $\mathbf{k}_{bc}$, total mass M_{bc} and reduced mass μ_{bc} of the particles b and c. The expressions for $\bar{\mathbf{k}}_{bc}$, $\mathbf{k}_{bc}$, M_{bc} and μ_{bc} are given by the equations (5.45), (5.47) with the labels 1, 2 replaced by b, c, respectively. We define the channel Møller operators $\Omega_\alpha^{(\pm)}$ acting on the channel states $|\psi_{\text{in}}^\alpha\rangle$

$$|\psi\rangle = \Omega_\alpha^{(+)} |\psi_{\text{in}}\rangle = \lim_{t \to -\infty} e^{iHt} e^{-iH_\alpha t} |\psi_{\text{in}}^\alpha\rangle , \tag{5.90}$$

$$|\psi\rangle = \Omega_\alpha^{(-)} |\psi_{\text{out}}\rangle = \lim_{t \to +\infty} e^{iHt} e^{-iH_\alpha t} |\psi_{\text{out}}^\alpha\rangle , \tag{5.91}$$

where $|\psi\rangle$ is the full scattering state and $|\psi_{\text{in/out}}^\alpha\rangle$ are the asymptotically free scattering states in the *scattering channel* α. Consider the coordinates of the three particles in the notation

$$\underline{\underline{x}} \equiv (\mathbf{x}_a, \mathbf{x}_b, \mathbf{x}_c) , \tag{5.92}$$

where $\underline{\underline{x}}$ includes the coordinates of all the three particles. We then can write the asymptotic in-state in position representation as

$$\langle \underline{\underline{x}} | \psi_{\text{in}} \rangle = \chi(\mathbf{x}_a, \bar{\mathbf{x}}_{bc}) \phi_{(bc)}(\mathbf{x}_{bc}), \tag{5.93}$$

where the first term $\chi(\mathbf{x}_a, \bar{\mathbf{x}}_{bc})$ describes the motion of the incident particles a and (bc) and $\phi_{(bc)}(\mathbf{x}_{bc})$ describes the internal motion of the bound state (bc).

The most general scattering state is a superposition of all the *channel states* and is constructed by the channel Møller operators as

$$|\psi\rangle = \Omega_0^{(+)} |\psi_{\text{in}}^0\rangle + \cdots + \Omega_\alpha^{(+)} |\psi_{\text{in}}^\alpha\rangle + \cdots + \Omega_n^{(+)} |\psi_{\text{in}}^n\rangle , \tag{5.94}$$

$$|\psi\rangle = \Omega_0^{(-)} |\psi_{\text{out}}^0\rangle + \cdots + \Omega_\alpha^{(-)} |\psi_{\text{out}}^\alpha\rangle + \cdots + \Omega_n^{(-)} |\psi_{\text{out}}^n\rangle , \tag{5.95}$$

where we have assumed n different *scattering channels*. The most general asymptotic states include all the asymptotic *channel states* and may be written as

$$|\Psi_{\text{in}}\rangle = \left\{ |\psi_{\text{in}}^1\rangle , \ldots , |\psi_{\text{in}}^\alpha\rangle , \ldots , |\psi_{\text{in}}^n\rangle \right\} , \tag{5.96}$$

$$|\Psi_{\text{out}}\rangle = \left\{ |\psi_{\text{out}}^1\rangle , \ldots , |\psi_{\text{out}}^\alpha\rangle , \ldots , |\psi_{\text{out}}^n\rangle \right\} . \tag{5.97}$$

We define the multichannel Møller operators $\mathbf{\Omega}^{(\pm)}$ as those operators which act on the general multichannel states $|\Psi_{\text{in}}\rangle$, $|\Psi_{\text{out}}\rangle$ as

$$|\psi\rangle = \mathbf{\Omega}^{(+)} |\Psi_{\text{in}}\rangle = \Omega_0^{(+)} |\psi_{\text{in}}^0\rangle + \cdots + \Omega_\alpha^{(+)} |\psi_{\text{in}}^\alpha\rangle + \cdots + \Omega_n^{(+)} |\psi_{\text{in}}^n\rangle , \tag{5.98}$$

$$|\psi\rangle = \mathbf{\Omega}^{(-)\dagger} |\Psi_{\text{out}}\rangle = \Omega_0^{(-)\dagger} |\psi_{\text{out}}^0\rangle + \cdots + \Omega_\alpha^{(-)\dagger} |\psi_{\text{out}}^\alpha\rangle + \cdots + \Omega_n^{(-)\dagger} |\psi_{\text{out}}^n\rangle , \tag{5.99}$$

where $\Omega_\alpha^{(+)}$, $\Omega_\alpha^{(-)}$ are the channel Møller operators (5.90), (5.91). As in the equations (5.22), (5.38) we establish a relation between the asymptotic in- and out-states as

$$|\Psi_{\text{out}}\rangle = \mathbf{\Omega}^{(-)\dagger} \mathbf{\Omega}^{(+)} |\Psi_{\text{in}}\rangle , \tag{5.100}$$

and obtain the multichannel S operator

$$\boldsymbol{S} \equiv \mathbf{\Omega}^{(-)\dagger} \mathbf{\Omega}^{(+)} . \tag{5.101}$$

The probability of finding a system in the *scattering channel* α' in the state ϕ' when the system was initially prepared in channel α in the state $|\phi\rangle$ is given by

$$w(\phi', \alpha' \leftarrow \phi, \alpha) = |\langle \phi' | \Omega_{\alpha'}^{(-)\dagger} \Omega_{\alpha}^{(+)} |\phi\rangle|^2. \tag{5.102}$$

From the probabilities w one can calculate the cross sections in multichannel scattering. Transitions of different channels introduce the inelastic cross sections which are measured in the experiment as two-body loss rate coefficients. The multichannel scattering cross section is introduced in the next subsection.

5.8.1 *Cross sections in multichannel scattering*

We derive the scattering cross section in multichannel scattering in terms of the momentum eigenstates. Therefore, we first introduce the free momentum eigenstates for the three-particle system with particles a, b, c. These states are given by

$$|\mathbf{k}_a, \mathbf{k}_b, \mathbf{k}_c; 0\rangle \equiv |\underline{\underline{k}}, 0\rangle\,, \tag{5.103}$$

and the zero indicates the channel 0 where all particles are free. The momentum eigenstates are normalized

$$\langle \underline{\underline{k}}', 0 | \underline{\underline{k}}, 0\rangle = \delta^{(3)}(\mathbf{k}_a' - \mathbf{k}_a)\delta^{(3)}(\mathbf{k}_b' - \mathbf{k}_b)\delta^{(3)}(\mathbf{k}_c' - \mathbf{k}_c), \tag{5.104}$$

and are eigenstates of the channel Hamiltonian H_0

$$H_0 |\underline{\underline{k}}, 0\rangle = \left(\frac{\mathbf{k}_a^2}{2m_a} + \frac{\mathbf{k}_b^2}{2m_b} + \frac{\mathbf{k}_c^2}{2m_c} \right) |\underline{\underline{k}}, 0\rangle = E_0 |\underline{\underline{k}}, 0\rangle\,, \tag{5.105}$$

Consider again the channel $a + (bc)$. Equation (5.93) shows that the in-state of the channel $a + (bc)$ can be separated in a term depending on $\mathbf{x}_a$, $\bar{\mathbf{x}}_{bc}$ and a term solely depending on the internal coordinates $\mathbf{x}_{bc}$ of the compound system (bc). We can write the in-state of channel α as the momentum state

$$|\psi_{\text{in}}\rangle = |\mathbf{k}_a, \bar{\mathbf{k}}_{bc}, \alpha\rangle = |\underline{\underline{k}}, \alpha\rangle\,, \tag{5.106}$$

where $\underline{\underline{k}}$ includes $\mathbf{k}_a$ and the center-of-mass $\bar{\mathbf{k}}_{bc}$ of the bound state (bc). These states are normalized

$$\langle \underline{\underline{k}}', \alpha | \underline{\underline{k}}, \alpha\rangle = \delta^{(3)}(\mathbf{k}_a' - \mathbf{k}_a)\delta^{(3)}(\bar{\mathbf{k}}_{bc}' - \bar{\mathbf{k}}_{bc}), \tag{5.107}$$

and eigenstates of the channel Hamiltonian

$$H_\alpha |\underline{\underline{k}}, \alpha\rangle = \left(\frac{\mathbf{k}_a^2}{2m_a} + \frac{\bar{\mathbf{k}}_{bc}^2}{2M_{bc}} + E_{(bc)} \right) |\underline{\underline{k}}, \alpha\rangle = E_\alpha |\underline{\underline{k}}, \alpha\rangle\,, \tag{5.108}$$

where E_{bc} is the internal energy of the bound state (bc). The position representation of the momentum states is given by

$$\langle \underline{\underline{x}} | \mathbf{k}_a, \bar{\mathbf{k}}_{bc}, \alpha\rangle \equiv \langle \underline{\underline{x}} | \underline{\underline{k}}, \alpha\rangle = (2\pi)^{-3} \exp\left[i(\mathbf{k}_a \cdot \mathbf{x}_a + \bar{\mathbf{k}}_{bc} \cdot \bar{\mathbf{x}}_{bc}) \right] \phi_{(bc)}(\mathbf{x}_{bc}). \tag{5.109}$$

As for the two-particle system described in section 5.3, the motion of the multichannel system factors in relative and center-of-mass motion with $\bar{\mathbf{k}}^2/2M$ so that the S operator can again be written as

$$\boldsymbol{S} = \mathbb{1}_{\text{com}} \otimes S. \tag{5.110}$$

Similar to the decomposition of the S matrix in terms of the free momentum states in the equations (5.42), (5.50) for single-channel scattering, we obtain in multichannel scattering

$$\langle \underline{\underline{\mathbf{k}}}', \alpha' | S | \underline{\underline{\mathbf{k}}}, \alpha\rangle = \delta_{\alpha'\alpha}\delta(\underline{\underline{k}}' - \underline{\underline{k}}) - 2\pi i \delta(E' - E)\delta(\bar{\mathbf{k}}' - \bar{\mathbf{k}}) t(\underline{k}', \alpha'; \underline{k}, \alpha), \tag{5.111}$$

where $\underline{k}$, $\underline{k}'$ denote the sets of relative momenta of the $n_\alpha - 1$ and $n_{\alpha'} - 1$ fragments of the channels α, α', respectively. The first term ensures unit transmission in the absence of a scatterer

and the second term defines the "on-shell" T matrix $t(\underline{k}', \alpha'; \mathbf{k}, \alpha)$ which is only defined if energy and total momentum of the system are conserved. With this expression for the S matrix in momentum eigenstates, one finally can derive the scattering cross section in terms of the T matrix. The multichannel scattering from channel α to channel α' can be calculated from the probability $w(\phi', \alpha' \leftarrow \phi, \alpha)$ (5.102) and the decomposition of the S matrix (5.111). It is given by

$$\sigma(\Delta', \alpha' \leftarrow \mathbf{k}, \alpha) = (2\pi)^4 \frac{\mu}{k} \int_{\Delta'} d\underline{k}' \cdot \delta(E' - E) |t(\underline{k}', \alpha'; \mathbf{k}, \alpha)|^2, \tag{5.112}$$

where Δ' is an arbitrary volume in the space of final momenta and μ is the reduced mass of the initial two particles in the in-channel α with initial momentum $\mathbf{k}$. The detailed calculation is given in [38]. If one assumes that the initial and final states are only two-body states, as for example in AI collisions $\mathrm{Ne}^* + \mathrm{Ne}^* \rightarrow \mathrm{Ne}_2^+ + e^-$, the expression for the differential cross section becomes very similar to the single-channel differential cross section in equation (5.60) and reads

$$\frac{d\sigma}{d\Omega}(\mathbf{k}', \alpha'; \mathbf{k}, \alpha) = \frac{k'}{k} |f(\mathbf{k}', \alpha'; \mathbf{k}, \alpha)|^2, \tag{5.113}$$

with the multichannel scattering amplitude $f(\mathbf{k}', \alpha'; \mathbf{k}, \alpha)$ defined by

$$f(\mathbf{k}', \alpha'; \mathbf{k}, \alpha) = -(2\pi)^2 (\mu' \mu)^{1/2} t(\mathbf{k}', \alpha'; \mathbf{k}, \alpha). \tag{5.114}$$

Here, μ and μ' are the reduced masses of channel α and α', respectively. Our goal is to derive a partial-wave series for the total scattering cross section in multichannel scattering. Therefore, we introduce in the next subsection the stationary scattering states.

5.8.2 *Scattering states*

In order to derive the scattering states in multichannel scattering we start with the multichannel *Lippmann-Schwinger equation*

$$|\underline{k}, \alpha\pm\rangle = |\underline{k}, \alpha\rangle + G_\alpha(E \pm i\epsilon) V_\alpha \, |\underline{k}, \alpha\pm\rangle \,, \tag{5.115}$$

where $\underline{k}$, $\underline{k}'$ denote the $n_\alpha - 1$ relative wave numbers for the n_α fragments of channel α and of the $n'_\alpha - 1$ relative wave numbers for the $n_{\alpha'}$ fragments of channel α', respectively. The potential V_α is the channel potential given by

$$V_\alpha \equiv H - H_\alpha, \tag{5.116}$$

and the free Green's operator G_α of channel α is given by

$$G_\alpha(z) = (z - H_\alpha)^{-1}, \tag{5.117}$$

with the channel Hamiltonian H_α. The multichannel *Lippmann-Schwinger equation* is much harder to solve than the single-channel *Lippmann-Schwinger equation*. Different asymptotic limits cover different *scattering channels* and one has to take great care to distinguish between collisions with no rearrangements and rearrangement collisions [38].

We consider an example where a single incident particle scatters off an arbitrary target in order to show how the expansion of the scattering wave function in terms of the target states leads to an infinite series of *coupled-channel equations*. If one truncates this infinite series at a finite number n one obtains the *coupled-channel approximation* or *close-coupling approximation*. In order to describe Ne* collisions we will work in the framework of the *coupled-channel approximation*. We start with the channel Hamiltonian

$$H_1 = \frac{\mathbf{k}^2}{2m} + H_{\mathrm{tar}}, \tag{5.118}$$

where $\mathbf{x}$ and m denote the position and mass of the incident particle and H_{tar} is the Hamiltonian of the kinetic energies and internal interactions of the target. We introduce $\underline{x}_{\mathrm{tar}}$ as the set of

coordinates of all the target particles. The asymptotic wave function for this system, derived from the Lippmann-Schwinger equation (5.115) reads [38]

$$\langle \mathbf{x}, \underline{x}_{\text{tar}} | \mathbf{k}, 1+ \rangle \underset{x\to\infty}{\longrightarrow} (2\pi)^{-3/2} \left[e^{i\mathbf{k}\mathbf{x}} \phi_1(\underline{x}_{\text{tar}}) + \sum\!\!\!\!\!\!\int_\alpha f(\mathbf{k}', \alpha; \mathbf{k}, 1) \frac{e^{ik_\alpha r}}{r} \phi_\alpha(\underline{x}_{\text{tar}}) \right], \tag{5.119}$$

where $\phi_\alpha(\underline{x}_{\text{tar}})$ are the eigenstates of H_{tar} which are partly discrete eigenstates but also continuum states with the eigenenergies Δ_α. The full scattering state in position representation $\langle \mathbf{x}, \underline{x}_{\text{tar}} | \mathbf{k}, 1+ \rangle$ can also be expanded in target eigenstates

$$\langle \mathbf{x}, \underline{x}_{\text{tar}} | \mathbf{k}, 1+ \rangle = \sum\!\!\!\!\!\!\int_\alpha \eta_\alpha(\mathbf{x}) \phi_\alpha(\underline{x}_{\text{tar}}), \tag{5.120}$$

where as before the target eigenstates depend only on the internal set of coordinates $\underline{x}_{\text{tar}}$ and the expansion coefficients η_α depend only on the position $\mathbf{x}$ of the incident particle. Comparing equation (5.120) and the asymptotic form of the wave function in (5.119) leads to the asymptotic form of η_α

$$\eta_\alpha(\mathbf{x}) \underset{x\to\infty}{\longrightarrow} (2\pi)^{-3/2} \left[e^{i\mathbf{k}\mathbf{x}} \delta_{\alpha 1} + f(\mathbf{k}', \alpha; \mathbf{k}, 1) \frac{e^{ik_\alpha r}}{r} \right], \tag{5.121}$$

which for $\alpha = 1$ is simply the single-channel solution of the asymptotic scattering wave function. The difference for $\alpha \neq 1$ is that there is no incoming wave in channel α. One could view the expansion (5.120) as a decomposition of the full scattering state into the channel scattering states, however, the channel states do not include the rearrangement channels which are present in the full scattering wave function. Therefore, the effect of these rearrangement channels is hidden in the infinite sum in (5.120). The full scattering state $|\mathbf{k}, 1+\rangle$ is an eigenstate of the Hamiltonian, given by

$$H |\mathbf{k}, 1+\rangle = (H_1 + V_1) |\mathbf{k}, 1+\rangle = \left(\frac{\mathbf{k}^2}{2m} + H_{\text{tar}} + V_1 \right) |\mathbf{k}, 1+\rangle, \tag{5.122}$$

where in V_1 all interactions of the incident particle with the target particles are included. Inserting the expansion (5.120) in the Schrödinger equation for the Hamiltonian (5.122) and projecting on $\phi_\alpha(\underline{x}_{\text{tar}})$ leads to a Schrödinger equation for the "channel wave functions" η_α, given by

$$-\nabla^2_{\mathbf{x}} \eta_\alpha(\mathbf{x}) + \sum\!\!\!\!\!\!\int_{\alpha'} \bar{V}_{\alpha\alpha'}(\mathbf{x}) \eta_{\alpha'}(\mathbf{x}) = (E - \Delta_\alpha) \eta_\alpha(\mathbf{x}), \tag{5.123}$$

where Δ_α are the eigenenergies of the target Hamiltonian H_{tar} which define the channel thresholds Δ_α. Furthermore, we have introduced the interaction potential

$$\bar{V}_{\alpha\alpha'}(\mathbf{x}) = \int d\underline{x}_{\text{tar}} \phi_\alpha(\underline{x}_{\text{tar}})^* V^1(\mathbf{x}, \underline{x}_{\text{tar}}) \phi_{\alpha'}(\underline{x}_{\text{tar}}). \tag{5.124}$$

Equation (5.123) shows, that the expansion of the full scattering wave function in terms of the target states (5.120) results in a set of infinite coupled equations for $\eta_\alpha(\mathbf{x})$. The truncation at a finite number of channels n is called the *coupled-channel approximation*, *close-coupling approximation* or the *n-state approximation* [38]. For the two-channel model we work within this approximation for $n = 2$. In cold collisions only a few partial waves contribute to the scattering rates. We introduce the decomposition of the scattering solutions in multichannel scattering in terms of the partial-waves by investigating rotationally invariant systems.

5.8.3 *Partial-wave expansion*

As in single-channel scattering we assume now a system which is rotationally invariant and introduce the spherical multichannel basis states $|E, l, m; \alpha\rangle$ of channel α, where again the operators $\{H_0, \mathbf{L}^2, L_z\}$ form a complete set of commuting observables. In the basis $|E, l, m; \alpha\rangle$ the S operator becomes diagonal

$$\langle E', l', m'; \alpha' | S | E, l, m; \alpha \rangle = \delta(E' - E) \delta_{l'l} \delta_{m'm} \times s_{l,\alpha'\alpha}(E). \tag{5.125}$$

The diagonal elements of the S matrix with $\alpha = \alpha'$ no longer fulfill the condition that they are unimodular as outgoing flux in other channels is possible. For real energies the diagonal elements can be parametrized in terms of a complex scattering phase $\eta_{l,\alpha}(E)$ or a real scattering phase $\delta_{l,\alpha}(E)$ but then including an additional inelasticity factor $0 \leq \epsilon_l(E) \leq 1$

$$s_{l,\alpha\alpha}(E) \equiv e^{2i\eta_{l,\alpha}(E)} \equiv \epsilon_l(E) e^{2i\delta_{l,\alpha}(E)}. \tag{5.126}$$

Within the *n-state approximation* the S matrix S_l is a $n \times n$ matrix, given by

$$S_l = \begin{pmatrix} s_{l,11} & s_{l,12} & \cdots & s_{l,1n} \\ \vdots & \ddots & \ddots & \vdots \\ s_{l,n1} & s_{l,n2} & \cdots & s_{l,nn} \end{pmatrix}, \tag{5.127}$$

and is *unitary*

$$S_l(E)^\dagger S_l(E) = S_l(E) S_l(E)^\dagger = \mathbb{1}. \tag{5.128}$$

n-channel coupled radial Schrödinger equation

From the spherical basis states $|E, l, m, \alpha\rangle$ we obtain in position representation the n-channel reduced coupled radial Schrödinger equation in matrix form

$$\left[\frac{d^2}{dr^2} - \frac{l(l+1)}{r^2} - V(r) + K^2\right] \Psi^{\pm}_{l,k}(r) = 0, \tag{5.129}$$

where K is a $n \times n$ matrix with the matrix elements $K_{\alpha\alpha'} = k_\alpha \delta_{\alpha\alpha'}$. The channel wave numbers k_α are given by

$$k_\alpha = \left[2\mu_\alpha (k^2 - \Delta_\alpha)\right]^{1/2}, \tag{5.130}$$

where Δ_α is the threshold energy of channel α and μ_α is the reduced mass of the two colliding particles in channel α. For $E > \Delta_\alpha$, k_α is real and the channel is *open*. For $E < \Delta_\alpha$, k_α is purely imaginary and the channel is *closed*. The scattering wave function $\Psi^\pm$ is a $n \times n$ matrix where the αth column gives the solution of the Schrödinger equation with the initial condition of an incident wave in channel α [38]. In principle, the incident wave can lie in any of the channels so that n distinct solutions are obtained and arranged in matrix form. The scattering wave function Ψ^+ has the asymptotic form

$$\Psi^+_{l,k}(r) \underset{r\to\infty}{\longrightarrow} \left[\hat{\jmath}_l(Kr) + \hat{h}^+_l(Kr) F_l K\right] = \frac{i}{2}\left[\hat{h}^-_l(Kr) - \hat{h}^+_l(Kr) K^{-1/2} S_l K^{1/2}\right], \tag{5.131}$$

where the matrices $\hat{\jmath}_l(Kr)$ and $\hat{h}^+_l(Kr)$ are diagonal $n \times n$ matrices with the matrix elements $[\hat{\jmath}_l(Kr)]_{\alpha'\alpha} = \hat{\jmath}_l(k_{\alpha'} r)\delta_{\alpha'\alpha}$ and $[\hat{h}^\pm_l(Kr)]_{\alpha'\alpha} = \hat{h}^\pm_l(k_{\alpha'} r)\delta_{\alpha'\alpha}$. The corresponding asymptotic form of the solution Ψ^- is given by the relation $\Psi^- = [\Psi^+]^\dagger$.

The $n \times n$ matrix S_l is the S matrix given by equation (5.127) and the $n \times n$ matrix F_l is the scattering amplitude matrix with the matrix elements $f_{l,\alpha'\alpha}$. Rewriting the scattering wave function (5.131) in terms of S_l instead of F_l leads to the relation of S matrix elements and scattering amplitude matrix elements

$$f_{l,\alpha'\alpha}(E) = \frac{s_{l,\alpha'\alpha}(E) - \delta_{\alpha'\alpha}}{2i(k_{\alpha'} k_\alpha)^{1/2}}. \tag{5.132}$$

In a partial-wave series, the total multichannel scattering amplitude matrix elements are given by

$$f(\mathbf{k}', \alpha'; \mathbf{k}, \alpha) = \sum_l (2l+1) f_{l,\alpha'\alpha} P_l(\cos\theta), \tag{5.133}$$

where θ is the angle of $\mathbf{k}$ and $\mathbf{k}'$. Note, that we restrict the discussion to two-body initial states and final states only. Inserting the partial-wave expansion of the scattering amplitude (5.133) in equation (5.113) and integrating over the solid angle $d\Omega$ leads to the partial cross section

$$\sigma_{l,\alpha'\leftarrow\alpha}(E) = \frac{\pi}{k^2_\alpha} \sum_l (2l+1)\left(|s_{l,\alpha'\alpha}(E)|^2 - 2\delta_{\alpha'\alpha} \operatorname{Re} s_{l,\alpha'\alpha}(E) + (\delta_{\alpha'\alpha})^2\right), \tag{5.134}$$

from channel α to channel α'. For elastic scattering ($\alpha' = \alpha$) the elastic partial cross section of channel α reads

$$\sigma^{\mathrm{el}}_{l,\alpha}(E) = \sigma_{l,\alpha\leftarrow\alpha}(E) = \frac{\pi}{k^2_\alpha}(2l+1)|1 - s_{l,\alpha\alpha}(E)|^2. \tag{5.135}$$

The inelastic partial cross section of channel α is defined as the sum of the partial cross section of channel α to all other channels $\alpha' \neq \alpha$ and is then given by

$$\sigma^{\mathrm{inel}}_{l,\alpha}(E) = \sum_{\alpha'}{}' \sigma_{l,\alpha'\leftarrow\alpha}(E) = \frac{\pi}{k^2_\alpha}(2l+1)\left(1 - |s_{l,\alpha\alpha}(E)|^2\right), \tag{5.136}$$

where the prime in the summation denotes a sum excluding the summation over channel α. The overall partial cross section of channel α is given by a sum of the cross section of channel α to all channels α' including α or simply by the sum of elastic cross section (5.135) and inelastic cross section (5.136) and reads

$$\sigma^{\mathrm{tot}}_{l,\alpha}(E) = \sum_{\alpha'}\sigma_{l,\alpha'\leftarrow\alpha}(E) = \frac{2\pi}{k^2_\alpha}(2l+1)\left(1 - \mathrm{Re}\, s_{l,\alpha\alpha}(E)\right). \tag{5.137}$$

The total elastic cross section, inelastic cross section and overall total cross sections are given by a sum over all partial waves l as

$$\sigma^{\mathrm{el}}_{\alpha}(E) = \sum_l \sigma^{\mathrm{el}}_{l,\alpha}(E), \quad \sigma^{\mathrm{inel}}_{\alpha}(E) = \sum_l \sigma^{\mathrm{inel}}_{l,\alpha}(E), \quad \sigma^{\mathrm{tot}}_{\alpha}(E) = \sum_l \sigma^{\mathrm{tot}}_{l,\alpha}(E). \tag{5.138}$$

Note that neither in single-channel nor in multichannel scattering we have addressed the issue of the scattering of identical particles. In section 5.8.5 we discuss this issue and show, that the sums in the equations (5.72) for single-channel scattering and in the equations (5.138) need to be modified for properly (anti-)symmetrized scattering wave functions. In the equations (5.135), (5.136) and (5.137) the diagonal S matrix elements $s_{l,\alpha\alpha}(E)$ appear in the partial cross sections. In equation (5.126) we parametrized these elements in terms of a complex scattering phase $\eta_{l,\alpha}$. Another parametrization is given by introducing an energy-dependent complex scattering length in terms of the complex scattering phase $\eta_{l,\alpha}$ [60, 115–117]

$$\tilde{a}_{l,\alpha}(E) = \tilde{\alpha}_{l,\alpha}(E) - i\tilde{\beta}_{l,\alpha}(E) \equiv -\frac{\tan\eta_{l,\alpha}(E)}{k_\alpha} = \frac{1}{ik_\alpha}\frac{1 - s_{l,\alpha\alpha}(E)}{1 + s_{l,\alpha\alpha}(E)}, \tag{5.139}$$

with real part $\tilde{\alpha}_{l,\alpha}(E)$ and imaginary part $-\tilde{\beta}_{l,\alpha}(E)$. The elastic cross sections and inelastic cross sections of channel α in terms of the complex scattering length read

$$\sigma^{\mathrm{el}}_{l,\alpha}(E) = \frac{4\pi|\tilde{a}_{l,\alpha}(E)|^2}{1 + k^2_\alpha|\tilde{a}_{l,\alpha}(E)|^2 + 2k_\alpha\tilde{\beta}_{l,\alpha}(E)}(2l+1), \tag{5.140}$$

$$\sigma^{\mathrm{inel}}_{l,\alpha}(E) = \frac{4\pi\tilde{\beta}_{l,\alpha}(E)}{k_\alpha\left(1 + k^2_\alpha|\tilde{a}_{l,\alpha}(E)|^2 + 2k_\alpha\tilde{\beta}_{l,\alpha}(E)\right)}(2l+1). \tag{5.141}$$

The complex scattering length is used in chapter 8 to analyze cold collision properties of Ne*. Similar to the discussion of single-channel scattering we introduce in the next subsection the multichannel regular solution to the Schrödinger equation (5.129). The asymptotic form leads to the Jost matrix. From the analytic properties of the regular solution and the Jost matrix for complex energies we establish the analytic properties of the multichannel S matrix in the complex k plane. These properties will be used in chapter 7 to analyze the coupled two-channel model with square-well potentials.

5.8.4 *Analytic properties of the regular solution and of the Jost matrices*

The regular solution is a solution to the n-channel coupled radial Schrödinger equation (5.129) with the boundary condition [38]

$$\Phi_{l,k}(r) \underset{r\to 0}{\longrightarrow} \hat{\jmath}_l(Kr). \tag{5.142}$$

At $r = 0$, the αth column of the regular solution behaves as the free solution of channel α. The multichannel regular solution of the n-channel Schrödinger equation together with the boundary conditions (5.142) and $\Phi_l(0) = 0$ can be written in integral form, reading

$$\Phi_{l,k}(r) = \hat{j}_l(Kr) + \int_0^r dr' \cdot G_{l,k}(r,r')V(r')\Phi_{l,k}(r'), \tag{5.143}$$

where $G_{l,k}(r,r')$ is a diagonal matrix with the single-channel Green's functions $g_{l,k_\alpha}(r,r')$, given by equation (5.75) on the diagonal. This is multichannel matrix *Volterra integral equation* for the regular solution.

Jost matrix

The asymptotic form of the regular solution $\Phi_{l,k}(r)$ is given by [38]

$$\Phi_{l,k}(r) \underset{r\to\infty}{\longrightarrow} \frac{i}{2}\left\{\hat{h}_l^-(Kr)\mathfrak{F}_l(K) - \hat{h}_l^+(Kr)\mathfrak{F}_l(-K)\right\}, \tag{5.144}$$

which introduces the $n \times n$ Jost matrix $\mathfrak{F}_l$. Comparison of the asymptotic form of the scattering solution (5.131) and the regular solution (5.144) leads to the important relations of regular and scattering solution

$$\Phi_{l,k}(r) = \Psi_{l,k}^+(r)\mathfrak{F}_l(K), \tag{5.145}$$

and of the Jost matrix and the S matrix

$$S_l = K^{1/2}\mathfrak{F}_l(-K)\mathfrak{F}_l^{-1}(K)K^{-1/2}. \tag{5.146}$$

As in single-channel scattering, the study of the multichannel regular solution and the Jost matrix for complex energies leads to the analytic properties of the S matrix. This is done in the next subsection.

Complex energies

We now investigate the analyticity of the multichannel regular solution $\Phi_{l,k}$ for complex energies [38]. The channel wave numbers k_α are related by the conservation of energy so that we have

$$\frac{k_1^2}{2m} + \Delta_1 = \ldots = \frac{k_n^2}{2m} + \Delta_n = E. \tag{5.147}$$

However, in the integral equation (5.143) the channel wave numbers are not restricted to the conservation of energy and one can treat $\Phi_l(r)$ as a function of n independent variables $k_1, \ldots, k_n$. If a function $\Phi(k_1, \ldots, k_n)$ is an analytic function of the independent variables $k_1, \ldots, k_n$, the function $\Phi(k_1(E), \ldots, k_n(E))$ is an analytic function of E except at the channel thresholds $E = \Delta_1, \ldots, \Delta_n$. Comparing the integral equation (5.143) with the asymptotic form (5.144) of the multichannel regular solution $\Phi_{l,k}$, one can write the Jost matrix in integral form [38]

$$\mathfrak{F}_l(k_1, \cdots, k_N) = \mathfrak{F}_l(K) = 1 + K^{-1}\int_0^\infty dr\hat{h}_l^+(Kr)V(r)\Phi_l(r). \tag{5.148}$$

Here, the Jost matrix is seen as a function of the independent variables $k_1, \ldots, k_n$. The integral in equation (5.148) can be studied for complex channel wave numbers $k_1, \ldots, k_n$ and is in general not convergent for arbitrary potentials. However, if we assume finite-range potentials which are identically zero for distances r larger than some finite distance r_0, then the integral in equation (5.148) is convergent for arbitrary channel wave numbers and an entire function of $k_1, \ldots, k_n$ [38].

We can then rewrite the S matrix (5.146) in terms of the Jost matrices as

$$S_l = K^{1/2}\mathfrak{F}_l(-K)\mathfrak{F}_l(K)^{-1}K^{-1/2} = \frac{K^{1/2}\mathfrak{F}_l(-K)\operatorname{cof}\mathfrak{F}_l(K)K^{-1/2}}{\det\mathfrak{F}_l(K)}, \tag{5.149}$$

where $\det \mathfrak{F}_l$ is the determinant of the Jost matrix and $\operatorname{cof} \mathfrak{F}_l$ the $n \times n$ matrix made up of the co-factors of $\mathfrak{F}_l^T$. Both $\operatorname{cof} \mathfrak{F}_l(K)$ and $\det \mathfrak{F}_l(K)$ are analytic wherever $\mathfrak{F}_l(K)$ is analytic. Replacing the channel wave numbers $k_\alpha \to 2\mu_\alpha(E - \Delta_\alpha)^{1/2}$, we obtain the important analytic properties of the S matrix as a function of the energy E for finite range potentials; $S_l(E)$ is an analytic function of E for all E, except for branch points at the thresholds $\Delta_1, \ldots, \Delta_n$ and for the poles at those points where $\det \mathfrak{F}_l(K) = 0$ [38]. In the complex E plane the poles on the negative real axis correspond to bound states in the scattering potential and the poles in the lower half plane, $\operatorname{Im} E < 0$, correspond to the resonant states of the multichannel system [38]. In the complex k plane of the channel wave number k_α the poles occur for bound states, virtual states and resonant states in a similar way as in the complex k plane of single-channel scattering (given in section 5.6). This will be studied explicitly in chapter 7.

5.8.5 *Inelastic cross sections of identical particles with spin*

In the coupled two-channel model of this work, ionizing collisions of Ne* are described by the transitions of the scattering channel to the loss channel. In the last two subsections of this chapter, we introduce the inelastic cross sections and two-body loss rate coefficients for this process for homo- and heteronuclear collisions of Ne*. Therefore, we assume in the general discussion that the elastic channel is given by the scattering of two particles in the total angular momentum states $|j_1 m_1\rangle$, $|j_2 m_2\rangle$ and denote the loss channel with α'. We discuss the transition from elastic to loss channel for identical fermions/bosons as well as for distinguishable particles which corresponds to homonuclear and heteronuclear collisions of Ne*. In the elastic channel, we denote different particles by F and G and the internal spin states as m_1, m_2. The inelastic process in this model is given by the transition $\alpha = (FGm_1m_2) \to \alpha'$ where we introduce α as the shorthand notation for the elastic channel, specified by the quantum numbers m_1, m_2 for the isotopes F, G. As in Ne* collisions the atoms have the same angular momentum, we assume that $j_1 = j_2$ holds. The asymptotic scattering part of the scattering wave function $\psi^{\mathrm{sc}}_{\alpha' \leftarrow FGm_1m_2}$ for the transition $\alpha \to \alpha'$ reads

$$\psi^{\mathrm{sc}\pm}_{\alpha' \leftarrow FGm_1m_2}(\mathbf{r}) \underset{r\to\infty}{\longrightarrow} \left(f_{\alpha' \leftarrow FGm_1m_2}(\theta) \, |j_1 j_1 m_1 m_2\rangle \pm f_{\alpha' \leftarrow FGm_1m_2}(\pi - \theta) \, |j_1 j_1 m_2 m_1\rangle \right) \frac{e^{ik_{\alpha'} r}}{r}, \tag{5.150}$$

where the $\pm$ sign refers to whether the particles are bosons or fermions and where $f_{\alpha' \leftarrow FGm_1m_2}(\theta)$ is the scattering amplitude for the process $FGm_1m_2 \to \alpha'$. The incoming scattering wave vector $\mathbf{k}$ is assumed to be in z direction so that the angle θ is the azimuthal angle in spherical coordinates. In a coupled angular momentum representation, equation (5.150) becomes

$$\begin{aligned} \psi^{\mathrm{sc}\pm}_{\alpha' \leftarrow FGm_1m_2}(\mathbf{r}) \underset{r\to\infty}{\longrightarrow} \sum_{jm} \Big\{ & f_{\alpha' \leftarrow FGm_1m_2}(\theta) \langle jm | j_1 j_1 m_1 m_2 \rangle \\ & \pm f_{\alpha' \leftarrow FGm_1m_2}(\pi - \theta) \langle jm | j_1 j_1 m_2 m_1 \rangle \Big\} \, |jm\rangle \, \frac{e^{ik_{\alpha'} r}}{r}, \end{aligned} \tag{5.151}$$

where j is the total angular momentum eigenvalue of the coupled state which may take the values $j = 0, \ldots, 2j_1$ while m is the projection on the space-fixed axis and $m = -j, \ldots, +j$. Using the symmetry properties of the Clebsch-Gordan coefficients (B.6) we obtain for the asymptotic wave function

$$\begin{aligned} \psi^{\mathrm{sc}\pm}_{\alpha' \leftarrow FGm_1m_2}(\mathbf{r}) \underset{r\to\infty}{\longrightarrow} \Bigg[& \sum_{j \text{ even}, m} f^{\pm}_{\alpha' \leftarrow FGm_1m_2}(\theta) \langle jm | j_1 j_1 m_1 m_2 \rangle \, |jm\rangle \\ & + \sum_{j \text{ odd}, m} f^{\mp}_{\alpha' \leftarrow FGm_1m_2}(\theta) \langle jm | j_1 j_1 m_1 m_2 \rangle \, |jm\rangle \Bigg] \frac{e^{ik_{\alpha'} r}}{r}, \end{aligned} \tag{5.152}$$

where we have introduced the abbreviation

$$f^{\pm}_{\alpha' \leftarrow FGm_1m_2}(\theta) \equiv f_{\alpha' \leftarrow FGm_1m_2}(\theta) \pm f_{\alpha' \leftarrow FGm_1m_2}(\pi - \theta). \tag{5.153}$$

If we use the partial-wave expansion of the scattering amplitude (5.133) together with the relation of partial scattering amplitude $f_{l,\alpha'\alpha}$ and S matrix element $s_{l,\alpha'\alpha}$ (5.132) for $\alpha \neq \alpha'$, with $\alpha = (m_1 m_2)$, we obtain the scattering amplitudes decomposed in partial waves as

$$f^{\pm}_{\alpha' \leftarrow FGm_1m_2} = \frac{1}{2i(k_\alpha k_{\alpha'})^{1/2}} \sum_l (2l+1) s_{l,\alpha'\alpha} \left[1 \pm (-1)^l\right] P_l(\cos\theta). \tag{5.154}$$

Here, we have used the symmetry properties of the Legendre polynomials [13]. The total inelastic cross section of the process $\alpha \to \alpha'$ can be calculated as the particle current density generated by the wave function (5.152) in the surface element $d\mathbf{F}$ over the absolute value of the incoming particle current density. For identical isotopes it reads

$${}^{FF}\sigma^{\text{inel}}_{\alpha' \leftarrow m_1m_2} = 2\Bigg(\sum_{j \text{ even},m} |\langle j_1 j_1 m_1 m_2 | jm\rangle|^2 \, {}^{FF}\sigma^{\text{inel}\pm}_{\alpha' \leftarrow m_1m_2} + \sum_{j \text{ odd},m} |\langle j_1 j_1 m_1 m_2 | jm\rangle|^2 \, {}^{FF}\sigma^{\text{inel}\pm}_{\alpha' \leftarrow m_1m_2} \Bigg), \tag{5.155}$$

where we have assumed an incoming plane wave in channel α and where we have introduced

$${}^{FF}\sigma^{\text{inel}\pm}_{\alpha' \leftarrow m_1m_2} = \frac{k_{\alpha'}}{k_\alpha} \int d\Omega |f^{\pm}_{\alpha' \leftarrow FFm_1m_2}|^2 = \sum_{l \text{ even/odd}} {}^{FF}\sigma^{\text{inel}}_{l,\alpha' \leftarrow m_1m_2}. \tag{5.156}$$

with ${}^{FF}\sigma^{\text{inel}}_{l,\alpha' \leftarrow m_1m_2}$ given by equation (5.134) for $\alpha \neq \alpha'$. The $+$ sign corresponds to a summation over even partial waves only and holds for identical bosons while the $-$ sign corresponds to a summation over odd partial waves and holds for identical fermions. The inelastic cross section (5.155) holds generally for identical bosons/fermions. For identical bosons/fermions in the same state ($m_1 = m_2$) we evaluate the inelastic cross section (5.155) and obtain

$${}^{FF}\sigma^{\text{inel}}_{\alpha' \leftarrow m_1m_1} = \begin{cases} \dfrac{2\pi}{k_\alpha^2} \displaystyle\sum_{l \text{ even}} (2l+1) |s_{l,\alpha'\alpha}(E)|^2 & \text{bosons,} \\ \dfrac{2\pi}{k_\alpha^2} \displaystyle\sum_{l \text{ odd}} (2l+1) |s_{l,\alpha'\alpha}(E)|^2 & \text{fermions.} \end{cases} \tag{5.157}$$

For identical bosons/fermions in different internal states ($m_1 \neq m_2$) we calculate from equation (5.155) the expression

$${}^{FF}\sigma^{\text{inel}}_{\alpha' \leftarrow m_1 \neq m_2} = \frac{\pi}{k_\alpha^2} \sum_l (2l+1) |s_{l,\alpha'\alpha}(E)|^2. \tag{5.158}$$

In the case of non-identical particles, the inelastic cross section reads

$${}^{F\neq G}\sigma^{\text{inel}}_{\alpha' \leftarrow m_1m_2} = \sum_l {}^{F\neq G}\sigma^{\text{inel}}_{l,\alpha' \leftarrow m_1m_2}, \tag{5.159}$$

for $m_1 = m_2$ and $m_1 \neq m_2$. From the inelastic cross sections for the process $(FGm_1m_2) \to \alpha'$ given in this subsection we can calculate the two-body loss rate coefficients.

5.8.6 *Boltzmann equation and two-body loss rate coefficients*

In the experiment, Ne* atoms are trapped and laser-cooled and from the decreasing number of the atoms in the trap or from the counting of produced ions due to PI and AI processes, two-body loss rate coefficients $\beta(T)$ are extracted. These two-body loss rate coefficients are dependent of the temperature T of the thermal gas and of the different isotope and internal spin states. We introduce these parameters by starting with the Boltzmann equation. The discussion here is analogous to the discussion of the Boltzmann equation for elastic processes given in [118].

We assume a thermal gas in an atom trap, where, as in the previous subsection, the different isotopes are denoted by F and G with internal states m_1, m_2. The number $N_F(t)$ of atoms F in

the trap decreases as a function of time due to inelastic two-body collisions to the loss channel α' and the Boltzmann equation for these inelastic collisions reads [118]

$$\frac{dN_F(t)}{dt} = -\sum_{Gm_1m_2}\left(\frac{1}{2\pi\hbar}\right)^6 \int d^3r d^3p_F d^3p_G \; h_{Fm_1}(\mathbf{r},\mathbf{p}_F,t)\cdot h_{Gm_2}(\mathbf{r},\mathbf{p}_G,t) \times {}^{FG}\sigma^{\text{inel}}_{\alpha'\leftarrow m_1m_2}(v_{FG})\cdot v_{FG}, \tag{5.160}$$

where v_{FG} is the relative velocity of isotope F and G and ${}^{FG}\sigma^{\text{inel}}_{\alpha'\leftarrow m_1m_2}$ is the inelastic cross section for the scattering process $\alpha = (FGm_1m_2) \rightarrow \alpha'$. The scattering channel α is specified by the internal states (m_1, m_2) of the atoms and by the different isotopes (F, G). The distribution function $h_{Fm_1}(\mathbf{r},\mathbf{p}_F,t)$ for isotope F in the state m_1 is given by

$$h_{Fm_1}(\mathbf{r},\mathbf{p}_F,t) = n_{Fm_1}(t)e^{-H_{Fm_1}(\mathbf{r},\mathbf{p}_F)/k_BT}\Lambda_F^3, \tag{5.161}$$

where Λ_F is the *de Broglie wavelength* given by

$$\Lambda_F = \left(\frac{2\pi\hbar^2}{m_Fk_BT}\right)^{1/2}, \tag{5.162}$$

and m_F is the mass of isotope F. The Hamiltonian H_{Fm_1} of isotope F reads

$$H_{Fm_1}(\mathbf{r},\mathbf{p}_F) = \frac{\mathbf{p}_F^2}{2m_F} + V_{Fm_1}(\mathbf{r}), \tag{5.163}$$

where $V_{Fm_1}(\mathbf{r})$ is the trapping potential. The central density $n_{Fm_1}(t)$ of the cloud consisting of N_{Fm_1} atoms is given by

$$n_{Fm_1}(t) = \frac{N_{Fm_1}(t)}{\int d^3r\; e^{-V_{Fm_1}(\mathbf{r})/k_BT}}, \tag{5.164}$$

and the particle density distribution trapped in the potential V_{Fm_1} reads

$$n_{Fm_1}(\mathbf{r},t) = n_{Fm_1}(t)e^{-V_{Fm_1}(\mathbf{r})/k_BT}. \tag{5.165}$$

The corresponding expressions are obtained for the isotope G in the internal state m_2 by simply replacing (Fm_1) with (Gm_2) in the above expressions (5.161), (5.162), (5.163), (5.164), (5.165). Inserting the distribution functions $h(\mathbf{r},\mathbf{p}_F,t)$ for (Fm_1) and (Gm_2) in the Boltzmann equation (5.160) leads to the rate equation for the number of atoms N_F

$$\frac{dN_F(t)}{dt} = -\sum_{Gm_1m_2} {}^{FG}\beta_{m_1m_2}(T)\int d^3r\; n_{Fm_1}(\mathbf{r})\cdot n_{Gm_2}(\mathbf{r}) = -\sum_{Gm_1m_2} {}^{FG}\beta_{m_1m_2}(T)\frac{N_{Fm_1}(t)\cdot N_{Gm_2}(t)}{V_{\text{eff},FGm_1m_2}}, \tag{5.166}$$

where we have introduced the effective volume V_{eff,FGm_1m_2} as

$$V_{\text{eff},FGm_1m_2} = \frac{\int d^3r\; e^{-\left(V_{Fm_1}(\mathbf{r})-V_{Gm_2}(\mathbf{r})\right)/k_BT}}{\int d^3r\; e^{-V_{Fm_1}(\mathbf{r})/k_BT}\cdot\int d^3r\; e^{-V_{Gm_2}(\mathbf{r})/k_BT}}. \tag{5.167}$$

Furthermore, we have introduced the important two-body loss rate coefficient

$${}^{FG}\beta_{m_1m_2}(T) = \langle\, {}^{FG}\sigma^{\text{inel}}_{\alpha'\leftarrow m_1m_2}(v_{FG})\cdot v_{FG}\rangle = \int_0^\infty dv\; P(v_{FG},T)\cdot\; {}^{FG}\sigma^{\text{inel}}_{\alpha'\leftarrow m_1m_2}(v_{FG})\cdot v_{FG}, \tag{5.168}$$

which is the thermal average over the relative velocities of the colliding particles in the thermal ensemble. The Maxwell-Boltzmann distribution $P(v,T)$ for the relative velocities is given by

$$P(v,T) = \sqrt{\frac{2}{\pi}\left(\frac{\mu}{k_BT}\right)^3}\cdot v^2\cdot\exp\left(-\frac{\mu v^2}{2k_BT}\right), \tag{5.169}$$

where μ is the reduced mass of isotope F and G. The two-body loss rate coefficient was obtained from the transformation in relative and center-of-mass coordinates $(\mathbf{p}_F, \mathbf{p}_G) \rightarrow (\mathbf{P}, \mathbf{p})$. The integration over the total momentum coordinate $\mathbf{P}$ is already performed in equation (5.168).

The two-body loss rate coefficients can be decomposed in partial waves. From the discussion of the previous subsection, which incorporated the case of identical particle scattering, we find from equation (5.157) the partial-wave series of the two-body loss rate coefficients for homonuclear collisions in identical states as

$$ {}^{FF}\beta_{m_1 m_1} = \begin{cases} 2 \sum\limits_{l \text{ even}} \langle {}^{FF}\sigma^{\text{inel}}_{l,\alpha' \leftarrow m_1 m_1}(v_{FF}) \cdot v_{FF} \rangle = \sum\limits_{l \text{ even}} {}^{FF}\beta_{l,m_1 m_1}(T) & \text{bosons,} \\ 2 \sum\limits_{l \text{ odd}} \langle {}^{FF}\sigma^{\text{inel}}_{l,\alpha' \leftarrow m_1 m_1}(v_{FF}) \cdot v_{FF} \rangle = \sum\limits_{l \text{ odd}} {}^{FF}\beta_{l,m_1 m_1}(T), & \text{fermions,} \end{cases} \tag{5.170} $$

where we introduced the partial two-body loss rate coefficients as

$$ {}^{FG}\beta_{l,m_1 m_2}(T) = 2 \cdot \langle \sigma^{\text{inel}}_{l,\alpha' \leftarrow FG m_1 m_2}(v) \cdot v \rangle = 2 \cdot \int_0^\infty dv \cdot P_T(v) \sigma^{\text{inel}}_{l,\alpha' \leftarrow FG m_1 m_2}(v) \cdot v. \tag{5.171} $$

For homonuclear collisions in different internal states we find from equation (5.158)

$$ {}^{FF}\beta_{m_1 \neq m_2} = \sum_l \langle {}^{FF}\sigma^{\text{inel}}_{l,\alpha' \leftarrow m_1 \neq m_2}(v_{FF}) \cdot v_{FF} \rangle = \frac{1}{2} \sum_l {}^{FF}\beta_{l,m_1 \neq m_2}(T), \tag{5.172} $$

and for heteronuclear collisions we find from equation (5.159)

$$ {}^{F \neq G}\beta_{m_1 m_2} = \sum_l \langle {}^{F \neq G}\sigma^{\text{inel}}_{l,\alpha' \leftarrow m_1 m_2}(v_{FG}) \cdot v_{FG} \rangle = \frac{1}{2} \sum_l {}^{F \neq G}\beta_{l,m_1 m_2}(T). \tag{5.173} $$

Unpolarized two-body loss rate coefficients in homonuclear ensembles

An important study case in Ne* experiments is the measurement of unpolarized two-body loss rate coefficients of homonuclear ensembles where the internal spin states are all equally populated. Therefore, we specify the rate equation (5.166) for this case. We assume atoms with total angular momentum $\mathbf{J}$ with $2j+1$ different internal states m_1. If the atoms equally populate m_1, one has to sum over all internal states and the number of atoms are given by

$$ N_{F m_1}(t) = N_{G m_2}(t) = \frac{1}{2j+1} N_F(t). \tag{5.174} $$

The rate equation (5.166) then becomes

$$ \frac{dN_F(t)}{dt} = -{}^{FF}\beta_{\text{unp}}(T) \frac{N_F^2(t)}{V_{\text{eff}}}, \tag{5.175} $$

where the unpolarized two-body loss rate coefficient is given by

$$ {}^{FF}\beta_{\text{unp}}(T) = \left(\frac{1}{2j+1} \right)^2 \sum_{m_1 m_2} {}^{FF}\beta_{m_1 m_2}(T). \tag{5.176} $$

CONCLUSION

In this chapter we introduced the basic concepts of scattering theory which are important for describing Ne* collisions. We started with the formal description of scattering theory in order to introduce the S matrix and studied its analytic properties in the complex k plane in order to given the pole expansion which we use in 7 to derive a parametrization of two-body loss rate coefficients in the two-channel model. We generalized the results to the case of multichannel scattering as ionization collisions of Ne* are described in this work in terms of two channels. The Jost matrix was studied in the multichannel case and we showed that it is an analytic function of the channel wave numbers for finite-range potentials. For the model with an elastic scattering channel specified by different isotopes and internal spin states and a loss channel denoted by α' we found at the end of this chapter the two-body loss rate coefficients for homonuclear and heteronuclear collisions of particles with spin. We will employ these results in chapter 8 for the coupled two-channel model of Ne* collisions.

6

INTERACTION POTENTIALS OF METASTABLE NEON ATOMS

The major goal of this chapter is to introduce the molecular potentials of Ne_2 at short-range and at long-range, which were calculated in the *Hund's case* (a) and *Hund's case* (c) molecular basis in order to show how they are introduced in the scattering or *coupled-channel* equations for Ne*. In analogy to the general discussion of the previous sections we first start with the atomic properties of Ne* where we introduce the metastable configuration and the fine-structure states in different coupling schemes. We then introduce the diatomic molecular system Ne_2 by a numerical calculation of the ground state molecular potential and discuss the resulting molecular orbitals for Ne_2. Then we introduce the short-range molecular potentials which were calculated in [6] in the *Hund's case* (a) basis. The long-range potentials were given in [9] in the *Hund's case* (c) basis and are introduced afterwards. We set up the scattering equations for Ne* by expanding the scattering state in an atomic basis and transforming this basis to the molecular basis states of *Hund's case* (a) and *Hund's case* (c). This introduces the molecular interaction potentials of Ne* in the scattering equations. In order to account for ionizing collisions we give at the end of this chapter the two-body loss rate coefficients in the molecular basis of *Hund's case* (a).

6.1 ATOMIC HAMILTONIAN

We start with the discussion of the single Ne atom. The three stable isotopes of Ne ^{20}Ne, ^{21}Ne, ^{22}Ne occur with relative abundancies of 90.48 % of the ^{20}Ne isotope, 0.27 % of the ^{21}Ne isotope and 9.25 % of the ^{22}Ne isotope [119]. The isotopes ^{20}Ne and ^{22}Ne are bosons and the isotope ^{21}Ne is a fermion.

In this section, we give the non-relativistic Hamiltonian for Ne as well as the Hamiltonian including spin-orbit coupling. Figure 6.1 depicts a scheme of the Ne atom and introduces the coordinates used throughout this section. The Hamiltonian for Ne in space-fixed electron $\mathbf{r}_i'$ and nuclear $\mathbf{R}'$ coordinates in atomic units is given by [44, 46]

$$H = -\frac{1}{2m_{\mathrm{Ne}}}\nabla^2_{\mathbf{R}'} + \sum_i \left\{ -\frac{1}{2}\nabla^2_{\mathbf{r}_i'} - \frac{Z}{|\mathbf{R}' - \mathbf{r}_i'|} + V_{LS}(|\mathbf{R}' - \mathbf{r}_i'|) \right\} + \sum_{i<j} \frac{1}{|\mathbf{r}_i' - \mathbf{r}_j'|}, \tag{6.1}$$

with summation over the 10 electrons. The term $V_{LS}(|\mathbf{R}' - \mathbf{r}_i'|)$ describes the spin-orbit coupling arising from the interaction of the spin of the electron in its rest frame with the magnetic field created by the moving nucleus. The spin-orbit coupling only depends on the distances between the nucleus and the electrons. The mass m_{Ne} is the mass of the nucleus of Ne which is different for the different isotopes ^{20}Ne, ^{21}Ne, ^{22}Ne. For the Ne atom, the nuclear charge is $Z = 10$.

We want to write the Hamiltonian (6.1) in the center-of-mass frame of the atom. Therefore, we introduce the center-of-mass coordinates $\mathbf{R}$ and the relative electron coordinates $\mathbf{r}_i$ by the transformation

$$\mathbf{R} = \frac{m_{\mathrm{Ne}}\mathbf{R}' + \sum_i \mathbf{r}_i'}{M_{\mathrm{Ne}}}, \quad \mathbf{r}_i = \mathbf{r}_i' - \frac{m_{\mathrm{Ne}}\mathbf{R}' + \sum_i \mathbf{r}_i'}{M_{\mathrm{Ne}}}. \tag{6.2}$$

The total mass $M_{\mathrm{Ne}} = m_{\mathrm{Ne}} + 10$ of Ne includes the masses of the 10 electrons. Considering the proton-to-electron mass ratio $m_p/m_e \approx 1836$, the electron masses give only a small contribution to the total mass of the atom.

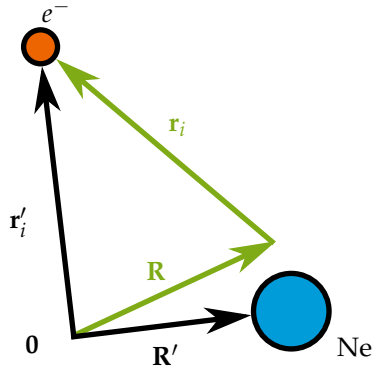

Figure 6.1: Internal and external coordinates of the Ne atom. In a space-fixed laboratory frame with origin **0** the vector $\mathbf{R}'$ points to the nucleus center-of-mass which consists of 10 protons and $10-12$ neutrons for the respective isotopes. The vectors $\{\mathbf{r}'_i\}$ indicate the positions of the 10 electrons in the space-fixed frame. $\mathbf{R}$ is the center-of-mass of the full Ne atom and $\mathbf{r}_i$ are the relative coordinates of the electrons in the center-of-mass frame.

Under the transformation of coordinates (6.2), the Coulomb interaction terms read

$$-\frac{Z}{|\mathbf{R}'-\mathbf{r}'_i|} = -\frac{Z}{|\mathbf{r}_i|} + \mathcal{O}\left(\frac{1}{m_{\mathrm{Ne}}}\right), \tag{6.3}$$

$$\frac{1}{|\mathbf{r}'_i-\mathbf{r}'_j|} = \frac{1}{|\mathbf{r}_i-\mathbf{r}_j|}. \tag{6.4}$$

The spin-orbit interaction in the new coordinates can be written as [44]

$$V_{LS}(|\mathbf{R}'-\mathbf{r}'_i|) \simeq \xi(r_i)\mathbf{l}_i\cdot\mathbf{s}_i + \mathcal{O}\left(\frac{1}{m_{\mathrm{Ne}}}\right), \tag{6.5}$$

with $\mathbf{l}_i$ the orbital angular momentum and $\mathbf{s}_i$ the spin of the ith electron and $\xi(r_i)$ is a function only dependent on the distance between electron and nucleus. This function depends on the details of the electrostatic potentials (see discussion in section 2.1.3). For hydrogen-like atoms $\xi(r)$ was given by equation (2.30).

In order to transform the Hamiltonian (6.1) from the space-fixed coordinate system into the center-of-mass frame of the atom, one also has to transform the kinetic energy terms which leads to

$$-\frac{1}{2m_{\mathrm{Ne}}}\nabla^2_{\mathbf{R}'} - \frac{1}{2}\sum_i \nabla^2_{\mathbf{r}'_i} = -\frac{1}{2M_{\mathrm{Ne}}}\nabla^2_{\mathbf{R}} - \frac{1}{2}\sum_i \nabla^2_{\mathbf{r}_i} - \frac{1}{2M_{\mathrm{Ne}}}\left(\sum_i \nabla_{\mathbf{r}_i}\right)^2. \tag{6.6}$$

The last term on the right-hand side of this equation is called the *mass polarization term* [120]. Now we have rewritten all the terms of the Hamiltonian (6.1) in the new coordinates. If we insert these terms (6.3), (6.4), (6.5), in the Hamiltonian (6.1), we obtain the atomic Hamiltonian for Ne in the center-of-mass frame

$$\begin{aligned} H =& T_{\mathrm{nuc}} + H_{\mathrm{Ne}} + \sum_i V_{LS}(r_i) + \mathcal{O}\left(\frac{1}{M_{\mathrm{Ne}}}\right) \\ =& -\frac{1}{2M_{\mathrm{Ne}}}\nabla^2_{\mathbf{R}} - \sum_i\left(\frac{1}{2}\nabla^2_{\mathbf{r}_i} + \frac{Z}{|\mathbf{r}_i|}\right) + \sum_{i<j}\frac{1}{|\mathbf{r}_i-\mathbf{r}_j|} + \sum_i V_{LS}(r_i) + \mathcal{O}\left(\frac{1}{M_{\mathrm{Ne}}}\right). \end{aligned} \tag{6.7}$$

Here, we have neglected the *mass polarization term*, as it is assumed to be a small correction to the kinetic energies.

The non-relativistic electronic Hamiltonian H_{Ne} forms a complete set of commuting observables with the total electron orbital angular momentum $\mathbf{L}^2$, its z component L_z and with the total electron spin operator $\mathbf{S}^2$ and S_z. Therefore, the atomic states $|(n)lsm_l m_s\rangle$ are simultaneous eigenfunctions of these five operators with the eigenvalues $\{E_{nls}, l(l+1), m_l, s(s+1), m_s\}$, where n is the principal quantum number of the state. The energy eigenvalue equation reads

$$H_{\mathrm{Ne}} |(n)lsm_l, m_s\rangle = E_{nls} |(n)lsm_l m_s\rangle , \tag{6.8}$$

with E_{nls} the total electronic energy of the atom. If we construct the total angular momentum states (see section 2.1.2), we obtain for the relativistic Hamiltonian, including the spin-orbit coupling the eigenvalue equation

$$(H_{\mathrm{Ne}} + V_{LS}) |(n)lsjm\rangle = E_{njls} |(n)lsjm\rangle . \tag{6.9}$$

E_{njls} is the total electronic energy of the atom, including the spin-orbit energy. We further specify the electronic states of Ne in the next sections.

6.2 ELECTRONIC CONFIGURATION AND FINE-STRUCTURE OF NEON

As for all rare gases in their ground states, the neon atom has a closed outer shell and therefore it is highly non-reactive. According to the shell-model one can fill up the atomic orbitals with electrons by respecting the Pauli exclusion principle [74] and the ground state configuration of Ne is given by

$$1s^2 2s^2 2p^6.$$

In this notation, two electrons with opposite spin directions occupy the inner $1s$-shell, two electrons the $2s$-shell and three times two electrons occupy the three p-orbitals with $m_l = -1, 0, 1$. In Ne* one electron is raised from one of the $2p$-shells to the $3s$-shell so that the metastable configuration reads

$$1s^2 2s^2 2p^5 3s,$$

The metastable configuration has an excitation energy of 16.619 eV [1] and a lifetime of 14.73(14) s [121, 122]. As a shorthand notation for the metastable configuration we simply write $2p^5 3s$ as the interactions of Ne* atoms are rarely influenced by the properties of the inner s-shell electrons. The $2p^5 3s$ configuration has four fine-structure states which are shown in figure 6.2 together with their fine-structure splittings. In addition, figure 6.3 shows all the

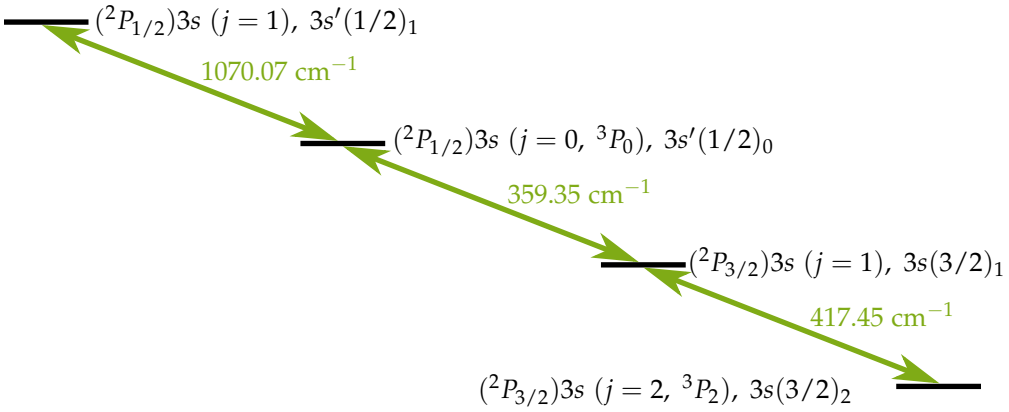

Figure 6.2: Fine-structure states of the $2p^5 3s$ configuration of Ne. The notation is given by (6.10) and (6.14). If applicable, also the notation for LS coupled terms is indicated.

electronic terms arising from the $2p^5 3p$ configuration, where the excited electron occupies the $3p$-shell. The four states arising from the $2p^5 3s$ configuration and the ten states arising from

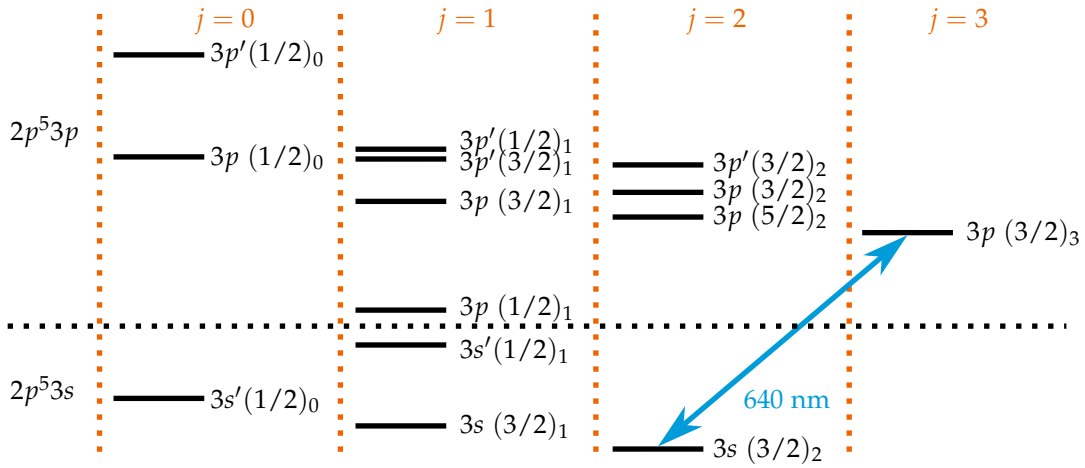

Figure 6.3: Spectroscopic notation for $2p^5 3s$ and $2p^5 3p$ configuration of Ne. The states are ordered according to increasing excitation energies ranging from $E = 16.62$ eV for the $3s(3/2)_2$ state up to $E = 18.97$ eV for the $3p'(1/2)_0$ state. The laser-cooling transition is indicated as blue arrow with the wavelength of $\lambda = 640$ nm [1].

the $2p^5 3p$ configuration are given in three different spectroscopic notations which we discuss now. Assume first the notation

$$nl_v(K)_j, \quad nl'_v(K)_j, \tag{6.10}$$

which is used to label all the 14 states in figure 6.2 and figure 6.3. Here, n is the principal quantum number and l_v the orbital angular momentum quantum number of the single excited electron occupying the $3s$-shell or the $3p$-shell of the metastable state. This electron is referred to as the valence electron. The spin of the valence electron is denoted as s_v. The angular momentum $\mathbf{K}$ in the notation (6.10) is given by

$$\mathbf{K} = \mathbf{J}_c + \mathbf{L}_v, \tag{6.11}$$

where $\mathbf{J}_c$ is the total angular momentum of the core of the atom. The core designates the inner electrons $1s^2 2s^2 2p^5$ of the metastable configuration. The inner s-shells are closed shells with zero spin and zero angular momentum, so that $\mathbf{J}_c$ is given by the $2p^5$ configuration solely. It can be shown that the terms arising from the $2p^5$ configuration are equivalent to the terms arising from a single electron in a p-shell [40, 73]. Therefore, the $2p^5$ configuration can be treated as a electron hole with spin $\mathbf{S}_c$ and orbital angular momentum $\mathbf{L}_c$ and the total angular momentum

$$\mathbf{J}_c = \mathbf{L}_c + \mathbf{S}_c. \tag{6.12}$$

For the electron hole of the $2p^5$ shell we have $s_c = 1/2$, $l_c = 1$ and $j_c = 1/2, 3/2$. For the $2p^5 3s$ configuration, we have $l_v = 0$ and $K = j_c = 1/2, 3/2$ and for the $2p^5 3p$ configuration $l_v = 1$ and $K = 1/2, 3/2, 5/2$. The total angular momentum $\mathbf{J}$ of the atom is given by the coupling of $\mathbf{K}$ and the spin s_v of the valence electron, reading

$$\mathbf{J} = \mathbf{K} + \mathbf{S}_v. \tag{6.13}$$

For the $2p^5 3s$ configuration we have $j = 0, 1, 2$ and for the $2p^5 3p$ configuration $j = 0, 1, 2, 3$. The quantum number j_c is either given by $j_c = 1/2$ or by $j_c = 3/2$. The former case corresponds to the unprimed notation l_v in (6.10) and the latter case corresponds to the primed notation with l'_v. The coupling scheme described here and in (6.10) holds generally for all the rare gases in metastable states [1, 7, 8].

A second, similar notation is used in figure 6.2 for the terms arising from the $2p^5 3s$ configuration. It is given by

$$\left({}^{2s_c+1}(l_c)_{j_c}\right) nl_v\, j, \tag{6.14}$$

with j_c, l_c, s_c the quantum numbers of the core, n, l_v the quantum numbers of the valence electron and j the total angular momentum number of the atom. The spectroscopic notations (6.14) and (6.10) describe the same coupling scheme and both are used in the literature [5].

In figure 6.2 the states $3s(3/2)_2$ and $3s'(1/2)_0$ are also given in the *Russel-Saunders* (LS) notation. We want to show that for the $2p^5 3s$ configuration, the LS coupling scheme is only valid for the two fine-structure levels $3s(3/2)_2$, $3s'(1/2)_0$. Therefore, we perform a basis transformation for the states arising from the different coupling schemes. A state of the intermediate coupling scheme for the $2p^5 3s$ configuration of Ne is given by

$$\begin{aligned}|(s_v(s_c l_c)j_c)jm\rangle &= \sum_{m_{j_c},m_{s_v}} \langle s_v j_c m_{s_v} m_{j_c}|jm\rangle \, |j_c m_{j_c}\rangle \otimes |s_v m_{s_v}\rangle \\ &= \sum_{m_{j_c},m_{s_v},m_{l_c},m_{s_c}} \langle s_v j_c m_{s_v} m_{j_c}|jm\rangle \langle s_c l_c m_{s_c} m_{l_c}|j_c m_{j_c}\rangle \, |l_c m_{l_c}\rangle \otimes |s_c m_{s_c}\rangle \otimes |s_v m_{s_v}\rangle \,,\end{aligned} \tag{6.15}$$

where we have used that $l_v = 0$. A state in LS coupling for the $2p^5 3s$ configuration reads

$$\begin{aligned}|(l_c(s_c s_v)s)jm\rangle &= \sum_{m_{l_c},m_s} \langle l_c s m_{l_c} m_s|jm\rangle \, |l_c m_{l_c}\rangle \otimes |(s_c s_v)s m_s\rangle \\ &= \sum_{m_{l_c},m_s,m_{s_c},m_{s_v}} \langle l_c s m_{l_c} m_s|jm\rangle \langle s_c s_v m_{s_c} m_{s_v}|s m_s\rangle \, |l_c m_{l_c}\rangle \otimes |s_c m_{s_c}\rangle \otimes |s_v m_{s_v}\rangle \,.\end{aligned} \tag{6.16}$$

The unitary basis transformation between these states is given by [40]

$$\begin{aligned}|(s_v(s_c l_c)j_c)jm\rangle &= \sum_s \langle (l_c(s_c s_v)s)j|(s_v(s_c l_c)j_c)j\rangle \, |((s_c s_v)s l_c)jm\rangle \\ &= \sum_s (-1)^{s_c+s_v+l_c+j} \left[(2s+1)(2j_c+1)\right]^{1/2} \begin{Bmatrix} s_c & s_v & s \\ l_c & j & j_c \end{Bmatrix} |((s_c s_v)s l_c)jm\rangle \,,\end{aligned} \tag{6.17}$$

where the expression in the curly brackets is a Wigner $6j$ symbol (see appendix B). With $l_c = 1$, $s_c = 1/2$, $l_v = 0$ and $s_v = 1/2$ we evaluate equation (6.17) for the four fine-structure levels of the $2p^5 3s$ configuration and obtain

$$|(s_v(s_c l_c)j_c = \tfrac{1}{2})j = 0, m\rangle = \underbrace{|(l_c(s_c s_v)s = 1)j = 0, m\rangle}_{|^3P_0\rangle}, \tag{6.18a}$$

$$|(s_v(s_c l_c)j_c = \tfrac{1}{2})j = 1, m\rangle = \sqrt{\tfrac{2}{3}} \underbrace{|(l_c(s_c s_v)s = 1)j = 1, m\rangle}_{|^3P_1\rangle} - \sqrt{\tfrac{1}{3}} \underbrace{|(l_c(s_c s_v)s = 0)j = 1, m\rangle}_{|^1P_0\rangle}, \tag{6.18b}$$

$$|(s_v(s_c l_c)j_c = \tfrac{3}{2})j = 1, m\rangle = \sqrt{\tfrac{1}{3}} \underbrace{|(l_c(s_c s_v)s = 1)j = 1, m\rangle}_{|^3P_1\rangle} + \sqrt{\tfrac{2}{3}} \underbrace{|(l_c(s_c s_v)s = 0)j = 1, m\rangle}_{|^1P_0\rangle}, \tag{6.18c}$$

$$|(s_v(s_c l_c)j_c = \tfrac{3}{2})j = 2, m\rangle = \underbrace{|(l_c(s_c s_v)s = 1)j = 2, m\rangle}_{|^3P_2\rangle}. \tag{6.18d}$$

The $3s(3/2)_2$ states in the standard spectroscopic notation for metastable rare gases are equivalent to the $^3P_2$ states in the Russel-Saunders (or LS) coupling scheme and are pure triplet states. This is also true for the single $j = 0$ state. Here, the $3s'(1/2)_0$ state is equivalent to the $^3P_0$ state and has also pure triplet character. In contrast, the states with $j = 1$ of the $2p^5 3s$ manifold cannot be written in terms of a single LS coupled state. The total electronic spin s of the atom is not a good quantum number for these states, the $j = 1$ states are rather given by a superposition of singlet and triplet LS states.

The $3s(3/2)_2$ states (or equivalently the $^3P_2$ states) of the $2p^5 3s$ configuration are of particular importance for this work, as in the experiment Ne* collisions are investigated for atoms in these states [2]. Therefore, it is important to look more closely at these states. This is done in the next section.

6.3 CONSTRUCTION OF SLATER DETERMINANTS FOR THE $^3P_2$ STATE MANIFOLD

The states of the previous section were characterized by their quantum numbers and not further specified. In this section, we construct explicitly the states of the $^3P_2$ manifold which are fully antisymmetric 10-electron states. In order to illustrate the LS coupling for these states, starting from the single-electron orbitals, we choose one specific state

$$|\Psi\rangle = |1s\alpha\ 1s\beta\ 2s\alpha\ 2s\beta\ 2p_{+1}\alpha\ 2p_{+1}\beta\ 2p_0\alpha\ 2p_0\beta\ 2p_{-1}\alpha\ 3s\alpha\rangle\,. \tag{6.19}$$

Here, α and β designate the spin projections with $m_s = \pm 1/2$ of the individual electron spins. For example, $1s\alpha$ designates a spin-orbital, where one electron occupies the spatial $1s$-orbital of Ne with spin projection $m_s = +1/2$. The subscripts of the p-orbitals designate the projections m_l of the single-electron orbital angular momenta $\mathbf{L}_i$ with $l = 1$ and $m_l = -1, 0, +1$. As the quantum numbers of the complete state are specified by the outer electrons only we introduce as shorthand notation

$$|\Psi\rangle \equiv |2p_{-1}\alpha\ 3s\alpha\rangle\,. \tag{6.20}$$

The total electron state of n electrons can be written as Slater determinant

$$|\Psi\rangle = \frac{1}{\sqrt{10!}} \begin{vmatrix} 1s\alpha(1) & 1s\beta(1) & \dots & 2p_0\alpha(1) & 2p_0\beta(1) & 2p_{-1}\alpha(1) & 3s\alpha(1) \\ 1s\alpha(2) & 1s\beta(2) & \dots & \dots & \dots & \dots & 3s\alpha(2) \\ \vdots & \ddots & \dots & \dots & \dots & \ddots & \vdots \\ 1s\alpha(10) & 1s\beta(10) & \dots & 2p_0\alpha(10) & 2p_0\beta(10) & 2p_{-1}\alpha(10) & 3s\alpha(10) \end{vmatrix}, \tag{6.21}$$

where the omitted single-electron orbitals are given in (6.19). The state $|\Psi\rangle$ is a simultaneous eigenstate of $\mathbf{L}^2$, $\mathbf{S}^2$, L_z and S_z, with the total orbital angular momentum $\mathbf{L}$ and the total electronic spin $\mathbf{S}$ given by equation (2.37). With the Slater-Condon rules for one-electron operators [see section 2.2.3, equation (2.53)] one can show that for the Slater determinant (6.21) the quantum numbers m_l, m_s are given by

$$m_l = \sum_i m_{l,i}, \quad m_s = \sum_i m_{s,i}, \tag{6.22}$$

with $m_{l,i}$, $m_{s,i}$ the projections of the orbital angular momentum $\mathbf{L}_i$ and the electron spin $\mathbf{S}_i$ of the electron in the ith spin-orbital, respectively. In order to obtain the total orbital angular momentum $\mathbf{L}$ and the total electron spin quantum number $\mathbf{S}$ of $|\Psi\rangle$ we need to recall, that all closed shells simply give a ^1S term with $l = 0$ and $s = 0$ for the respective shell. Furthermore, we stated in the previous section that a p^5-shell can be treated as a single electron-hole with $l_c = 1$ and $s_c = 1/2$. As the other electrons, which do not occupy the p^5 shell, have zero orbital angular momentum, the overall angular momentum of the Ne* atom is given solely by the orbital angular momentum of the p^5 shell, $l = 1$. Therefore, $|\Psi\rangle$ is a P state. With $m_s = 1$, $|\Psi\rangle$ must be a triplet state, $s = 1$ as the total spin is determined by $s_c = s_v = 1/2$. From this discussion we find that $|\Psi\rangle$ is an eigenstate of the operators $\mathbf{L}^2$, $\mathbf{S}^2$, L_z, S_z and can be written as

$$|\Psi\rangle = |l = 1, s = 1, m_l = 1, m_s = 1\rangle\,. \tag{6.23}$$

The uncoupled $|lsm_lm_s\rangle$ states are in general not eigenstates of the total angular momentum operator $\mathbf{J}$ and J_z. The coupling to a total angular momentum state was given in equation (2.24). From the couplings to total angular momentum states (2.24) we conclude that the $|\Psi\rangle$ is also a total angular momentum state and we write

$$|\Psi\rangle = |^3P_2, m = +2\rangle = |(l = 1, s = 1)j = 2, m = 2\rangle = |l = 1, s = 1, m_l = 1, m_s = 1\rangle\,, \tag{6.24}$$

Thus, the state (6.21) is a simultaneous eigenstate of $\mathbf{L}^2$, $\mathbf{S}^2$, $\mathbf{J}^2$, L_z, S_z, J_z and furthermore one of the states of the $^3P_2$ manifold we wanted to construct. Specifically, it is the state $|^3P_2, m = +2\rangle$. It is of special importance in the experiment and in this work, as it is a spin-stretched state. For collisions of two Ne* atoms in these states, PI reactions are suppressed. In total, there are $2j + 1 = 5$ states of the $^3P_2$ manifold and we construct these states now. Using the basis transformation (2.24) we obtain

$$|^3P_2, m = +1\rangle = \tfrac{1}{\sqrt{2}}\left(|ls, m_l = 1, m_s = 0\rangle + |ls, m_l = 0, m_s = 1\rangle\right). \tag{6.25}$$

In contrast to the $^3P_2$ state with $m = 2$, this state is not given only by a single term, but by a superposition of two angular momentum states. Remember the shorthand notation we have introduced in equation (6.20), where we omit all the electrons in the closed shells of the system. In this notation we can write the angular momentum states in terms of Slater determinants as

$$|ls, m_l = 1, m_s = 0\rangle = \tfrac{1}{\sqrt{2}} \left(|2p_{-1}\alpha\ 3s\beta\rangle + |2p_{-1}\beta\ 3s\alpha\rangle\right), \tag{6.26a}$$

$$|ls, m_l = 0, m_s = 1\rangle = |2p_0\alpha\ 3s\alpha\rangle\,,. \tag{6.26b}$$

The states $|2p_{-1}\alpha\ 3s\beta\rangle, \ldots$ are characterized with the quantum numbers s_c, s_v, l_c, l_v, m_{s_c}, m_{s_v}, m_{l_c}, m_{l_v} and related to $|lsm_lm_s\rangle$ by

$$|lsm_lm_s\rangle = \sum_{m_{s_c}, m_{s_v}} \sum_{m_{l_c}, m_{l_v}} \langle l_c l_v m_{l_c} m_{l_v} | lm_l\rangle \langle s_c s_v m_{s_c} m_{s_v} | sm_s\rangle \, |l_c l_v m_{l_c} m_{l_v}\rangle \, |s_c s_v m_{s_c} m_{s_v}\rangle\,, \tag{6.27}$$

with $l_v = m_{l_v} = 0$ for the $2p^5 3s$ configuration. Inserting (6.26a), (6.26b) in (6.25) we obtain

$$|^3P_2, m = +1\rangle = \tfrac{1}{\sqrt{2}} \left(\tfrac{1}{\sqrt{2}} \left(|2p_{-1}\alpha\ 3s\beta\rangle + |2p_{-1}\beta\ 3s\alpha\rangle\right) + |2p_0\alpha\ 3s\alpha\rangle \right). \tag{6.28}$$

Similarly, by using the transformation (6.27) we obtain the other states of the $^3P_2$ manifold as

$$|^3P_2, m = 0\rangle = \sqrt{\tfrac{2}{6}} \left[|2p_0\alpha\ 3s\beta\rangle + |2p_0\beta\ 3s\alpha\rangle\right] + \tfrac{1}{\sqrt{6}} \left[|2p_{-1}\beta\ 3s\beta\rangle + |2p_{+1}\alpha\ 3s\alpha\rangle\right], \tag{6.29}$$

$$|^3P_2, m = -1\rangle = \tfrac{1}{\sqrt{2}} \left(\tfrac{1}{\sqrt{2}} \left(|2p_{+1}\alpha\ 3s\beta\rangle + |2p_{+1}\beta\ 3s\alpha\rangle\right) + |2p_0\beta\ 3s\beta\rangle \right), \tag{6.30}$$

$$|^3P_2, m = -2\rangle = |2p_{+1}\beta\ 3s\beta\rangle\,. \tag{6.31}$$

With the discussion of the fine-structure of we close the topic of single-atom physics of Ne* and continue with diatomic system Ne_2 and the interaction properties.

6.4 DIATOMIC HAMILTONIAN

In order to derive the molecular Hamiltonian for Ne_2 we use similar notation as in [46]. In figure 6.4 the coordinates for the diatomic system are shown.

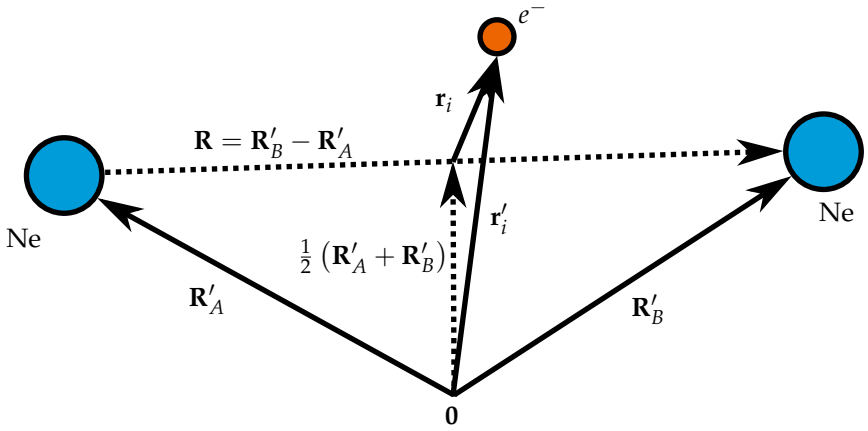

Figure 6.4: Internal and external coordinates of Ne_2. In a space-fixed laboratory frame with origin $\mathbf{0}$ the vector $\mathbf{R}'_A$ points to the nucleus of atom A and $\mathbf{R}'_B$ to the nucleus of atom B. The vectors $\{\mathbf{r}'_i\}$ indicate the position of the ith electron out of the 20 electrons of the Ne_2 system. The vector $\mathbf{R}$ is the center-of-mass of the two nuclei and $\mathbf{r}_i$ is the relative coordinate of the ith electron with respect to $\mathbf{R}$.

The non-relativistic Hamiltonian for Ne_2 in these coordinates in the space-fixed frame in atomic units reads

$$H = -\frac{1}{2m_{\mathrm{Ne}}}\nabla^2_{\mathbf{R}'_A} - \frac{1}{2m_{\mathrm{Ne}}}\nabla^2_{\mathbf{R}'_B} - \frac{1}{2}\sum_i \nabla^2_{\mathbf{r}'_i} - \sum_i \left\{ \frac{Z}{|\mathbf{R}'_A - \mathbf{r}'_i|} + \frac{Z}{|\mathbf{R}'_B - \mathbf{r}'_i|} \right\} + \sum_{i<j} \frac{1}{|\mathbf{r}'_i - \mathbf{r}'_j|} + \frac{Z^2}{|\mathbf{R}'_B - \mathbf{R}'_A|}, \tag{6.32}$$

with a summation over all electrons. The first three terms describe the kinetic energies of nucleus A, B and of all the electrons, respectively. The last two terms of the first line describe the Coulomb attraction between the electrons and the nuclei. The two terms in the second line describe the Coulomb repulsion of all the electrons and the Coulomb repulsion of the nuclei.

We define the center-of-mass vector $\mathbf{R}_{\mathrm{com}}$, the relative vector $\mathbf{R}$ and the new electron coordinates $\mathbf{r}_i$ as follows [46]

$$\mathbf{R}_{\mathrm{com}} = \frac{m_{\mathrm{Ne}}\left(\mathbf{R}^{A'}_{\mathrm{Ne}} + \mathbf{R}^{B'}_{\mathrm{Ne}}\right) + \sum_i \mathbf{r}'_i}{2m_{\mathrm{Ne}} + 20}, \tag{6.33a}$$

$$\mathbf{R} = \mathbf{R}'_B - \mathbf{R}'_A, \tag{6.33b}$$

$$\mathbf{r}_i = \mathbf{r}'_i - \frac{1}{2}\left(\mathbf{R}'_A + \mathbf{R}'_B\right). \tag{6.33c}$$

Under this transformation of coordinates, the kinetic energy terms of the Hamiltonian in equation (6.32) transform as

$$-\frac{1}{2m_{\mathrm{Ne}}}\left(\nabla^2_{\mathbf{R}'_A} + \nabla^2_{\mathbf{R}'_B}\right) - \frac{1}{2}\sum_i \nabla^2_{\mathbf{r}'_i} = -\frac{1}{2M_{\mathrm{Ne}}}\nabla^2_{\mathbf{R}_{\mathrm{com}}} - \frac{1}{m_{\mathrm{Ne}}}\nabla^2_{\mathbf{R}} - \frac{1}{2}\sum_i \nabla^2_{\mathbf{r}_i} - \frac{1}{4m_{\mathrm{Ne}}}\left(\sum_i \nabla_{\mathbf{r}_i}\right)^2, \tag{6.34}$$

where the last term of the second line is the *mass polarization term*.

Now, we derive the diatomic Hamiltonian (6.32) in the new coordinates (6.33). We separate the center-of-mass motion, insert the transformed kinetic energy terms (6.34) in the Hamiltonian (6.32), neglect again the *mass polarization term* and obtain for the Hamiltonian of the relative motion of the nuclei and electrons

$$H = T_{\mathrm{nuc}} + H_{\mathrm{el}} = -\frac{1}{m_{\mathrm{Ne}}}\nabla^2_{\mathbf{R}} - \frac{1}{2}\sum_i \nabla^2_{\mathbf{r}'_i} - \sum_i \left\{ \frac{Z}{|\mathbf{r}_i + \frac{1}{2}\mathbf{R}|} + \frac{Z}{|\mathbf{r}_i - \frac{1}{2}\mathbf{R}|} \right\} + \sum_{i<j} \frac{1}{|\mathbf{r}_i - \mathbf{r}_j|} + \frac{Z^2}{R}. \tag{6.35}$$

The "electronic" Hamiltonian H_{el} also includes the Coulomb repulsion of the nuclei.

Separating nuclear motion and electronic motion (see section 3.1), we write the total state $|\Psi(\mathbf{r},\mathbf{R})\rangle$ of the system as

$$|\Psi(\mathbf{r},\mathbf{R})\rangle = \sum_n F_n(\mathbf{R})\,|\phi_n(\mathbf{r},\mathbf{R})\rangle, \tag{6.36}$$

where the electronic wave functions $|\phi_n(\mathbf{r},\mathbf{R})\rangle$ are eigenfunctions of the electronic Hamiltonian

$$H_{\mathrm{el}}\,|\phi_n(\mathbf{r},\mathbf{R})\rangle = V_n(R)\,|\phi_n(\mathbf{r},\mathbf{R})\rangle, \tag{6.37}$$

with $V_n(R)$ the *Born-Oppenheimer potentials*. The subscript n refers to the good quantum numbers of the molecular system, given by $n = \{\Lambda, S, \Sigma, \Gamma\}$ [46]. The meaning of the quantum numbers Λ, S, Σ was discussed in section 3.4, Γ refers to any additional quantum number necessary to specify the electronic state. The *Born-Oppenheimer potentials* V_n have been calculated for the Ne*–Ne* system in the *Hund's case* (a) basis and are presented in section 6.6.

Note, that so far, no spin-orbit coupling has been included. As in the case of atomic Ne, the electronic states $|\phi_n(\mathbf{r},\mathbf{R})\rangle$ are no eigenstates of the spin-orbit operator and one needs to construct molecular states which are eigenstates to the total electron angular momentum operator $\mathbf{J}^2$ and the projection on the internuclear axis $J_{\mathbf{R}}$. These *Hund's case* (c) states are the

eigenstates of the molecular Hamiltonian H_{el} plus the spin-orbit operator V_{LS} of the diatomic molecule

$$(H_{\mathrm{el}} + V_{LS}) \, |J\Omega\rangle = V_{J\Omega} \, |J\Omega\rangle \, . \tag{6.38}$$

Here, we do not further specify the spin-orbit coupling term V_{LS} of the diatomic system. The molecular potentials $V_{J\Omega}$ describe the molecular electronic energy of *Hund's case* (c) states. These potentials have been calculated at long-range for the Ne*–Ne* system and the dispersion coefficients c_5, c_6 are tabulated in section 6.7.

In the next section, we introduce the molecular potentials of Ne_2 by calculating the ground state potential and the corresponding molecular orbitals before introducing the excited state potentials in the following sections.

6.5 CALCULATION OF MOLECULAR ORBITALS

In order to understand the molecular potentials of Ne* which result from electronic structure calculations, we discuss briefly atomic and molecular basis sets which are employed in these calculations, for example in the GAMESS package. We discuss explicitly basis sets for Ne and calculate electronic energies for Ne_2 in a RHF calculation. We then illustrate the building-up principle for molecules which is an alternative way to introduce the designation and symmetries of the molecular states.

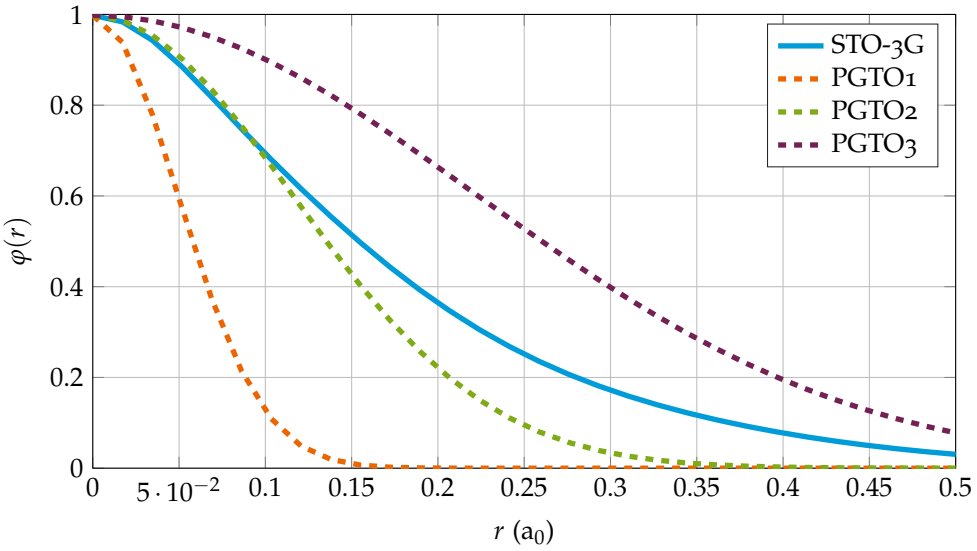

Figure 6.5: Radial part $\varphi(r)$ of atomic wave function for an s-type orbital as a function of radial distance r. The blue solid line shows the 1s orbital of Ne in the STO-3G basis for Ne which is composed of three *primitive Gaussian-type orbitals* PGTOs of different widths, shown as dashed lines.

In figure 6.5 the radial wave function of an s-type orbital for Ne in the STO-3G basis is shown. Here, STO stands for *Slater-type orbital* which is given by a sum of 3G (Gaussian-type orbitals), or more specifically, 3 *primitive Gaussian-type orbitals* (PGTOs) [79]. The radial wave function can be written as

$$\varphi(r) = \sum_{i=1}^{3} \varphi_i(r) = \sum_{i=1}^{3} a_i e^{-\zeta_i r^2}, \tag{6.39}$$

with real coefficients a_i and exponents ζ_i. The radial function $\varphi_i(r)$ is a PGTO and $\varphi(r)$ is given by the contraction of three Gaussian functions. The coefficients a_i and ζ_i of the STO-3G basis

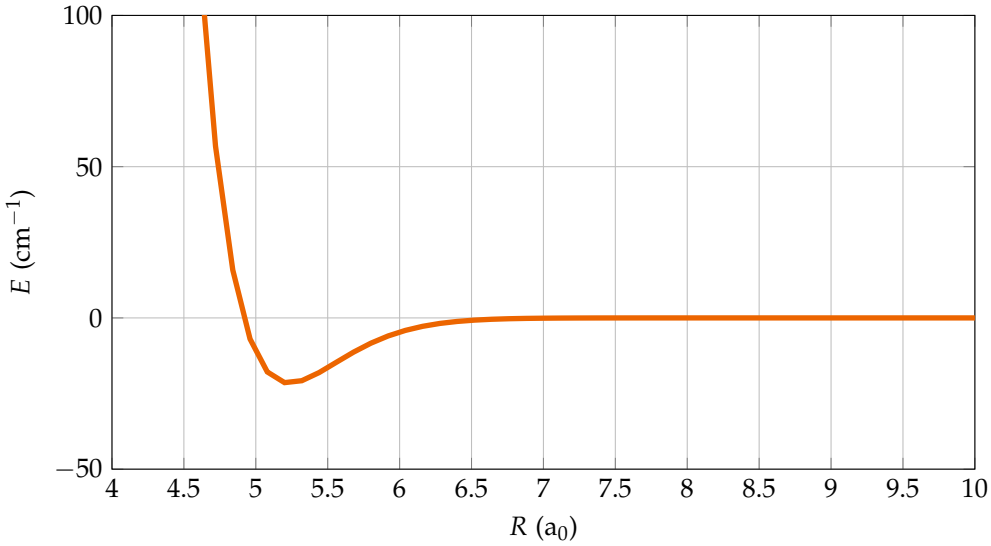

Figure 6.6: Lowest potential energy curve of Ne_2 as a function of the internuclear distance R where the energy of the atomic limit Ne–Ne has been shifted to the zero energy. The potential has a minimum at $R = 5.2\,a_0$ with $E_{min} = -21.39\ cm^{-1}$. The potential curve is the result of a RHF calculation with a 6-31G basis set for Ne.

have been found from fitting to the STO [79] and are tabulated in the EMSL database [1]. For the 1s-orbital of Ne, these coefficients read [79]

$$a_1 = 0.15432897, \quad a_2 = 0.53532814, \quad a_3 = 0.44463454, \tag{6.40a}$$
$$\zeta_1 = 207.0156100, \quad \zeta_2 = 37.7081510, \quad \zeta_3 = 10.2052970. \tag{6.40b}$$

All three PGTOs φ_i are shown in figure 6.5 and the total radial wave function as the sum of the PGTOs. Here, the PGTOs and the total wave functions are normalized to $\varphi(0) = 1$. In general, the *Gaussian-type orbitals* in Cartesian coordinates may be written in the form

$$\varphi_{\zeta,l_x,l_y,l_z}(x,y,z) = N x^{l_x} y^{l_y} z^{l_z} e^{-\zeta r^2}, \tag{6.41}$$

where N is a normalization constant and l_x, l_y, l_z are integer numbers ≥ 0 determining the type of the orbital by the value $l = l_x + l_y + l_z$. Note, that the basis functions (6.39), (6.41) are real. This is similar to the real orbitals which we have constructed for the hydrogen-like atoms in section 2.1.1. However, these orbitals (2.15) were *Slater-type orbitals* instead of *Gaussian-type orbitals* (6.39), (6.41).

We have performed a RHF calculation for the lowest state of Ne_2 in a 6-31G basis set. This basis set was also employed in the calculations of potential curves for H_2^+ and H_2 in chapter 2. It is a *Pople style basis set* and a *split valence basis* where the core orbitals of the atoms are contractions of six PGTOs instead of the three PGTOs while the inner part of the atomic valence orbitals is a contraction of three PGTOs. The outer part of the valence orbitals is given by a single PGTO [79]. The coefficients for Ne of this basis set can be found in the EMSL database. Figure 6.6 shows the resulting potential energy curve for Ne_2. Even though the potential is attractive for some internuclear distances R, it does not support a bound state. Strictly speaking, there is no stable bonding ground state Ne_2 molecule.

We have performed a further RHF calculation of the ground state energy of Ne_2, but in the smaller STO-3G basis set, in order to illustrate the LCAO again and the molecular orbitals for Ne_2. In this calculation, two s-type orbitals and three p-type orbitals are centered at each atom A and B. Atom A and B were placed at an internuclear distance of $R = 5.2\,a_0$, which is the

1 https://bse.pnl.gov/bse/portal

equilibrium distance of the ground state Ne_2 potential. Within the LCAO approximation, the molecular orbitals are given by

$$|\phi_\mu\rangle = \sum_j c_{\mu j} |\varphi_j\rangle \,. \tag{6.42}$$

In the STO-3G basis, the atomic orbitals are $\{1s, 2s, 2p_x, 2p_y, 2p_z\}$-orbitals centered at each atom. The results for the LCAO coefficients $c_{j\mu}$ for the occupied orbitals and the respective orbital energies ε_i of the calculation are shown in table 6.1.

				σ_g	σ_u	σ_g	σ_u	σ_g
				-32.2125	-32.2125	-1.7065	-1.7057	-0.5450
1	Ne	A	$1s$	$+0.704$	-0.704	-0.190	$+0.191$	
2	Ne	A	$2s$	$+0.014$	-0.014	$+0.729$	-0.729	
3	Ne	A	$2p_x$					
4	Ne	A	$2p_y$					
5	Ne	A	$2p_z$					-0.707
6	Ne	B	$1s$	$+0.704$	$+0.704$	-0.190	-0.191	
7	Ne	B	$2s$	$+0.014$	$+0.014$	$+0.729$	$+0.729$	
8	Ne	B	$2p_x$					
9	Ne	B	$2p_y$					
10	Ne	B	$2p_z$					$+0.707$

				π_{uy}	π_{ux}	π_{gx}	π_{gy}	σ_u
				-0.5432	-0.5432	-0.5429	-0.5429	-0.5411
1	Ne	A	$1s$					
2	Ne	A	$2s$					
3	Ne	A	$2p_x$	$+0.389$	$+0.590$	$+0.612$	$+0.354$	
4	Ne	A	$2p_y$	$+0.590$	-0.389	-0.354	$+0.612$	
5	Ne	A	$2p_z$					$+0.707$
6	Ne	B	$1s$					
7	Ne	B	$2s$					
8	Ne	B	$2p_x$	$+0.389$	$+0.590$	-0.612	-0.354	
9	Ne	B	$2p_y$	$+0.590$	-0.389	$+0.354$	-0.612	
10	Ne	B	$2p_z$					$+0.707$

Table 6.1: Molecular orbitals resulting from a RHF calculation in the STO-3G basis for Ne_2 with internuclear distance $R = 5.2\,a_0$. The orbitals are ordered from the left top to the right bottom by their orbital energies, starting from $\varepsilon_1 = -32.2125$ for σ_g up to $\varepsilon_{10} = -0.5411$ for σ_u. The LCAO coefficients $c_{j\mu}$ display from which atomic orbitals $1s$, $2s$,... the molecular orbitals are constructed. For example, the lowest σ_g orbital reads $\sigma_g = 0.704 \cdot 1s_A + 0.014 \cdot 2s_A + 0.704 \cdot 1s_B + 0.014 \cdot 2s_B$, with s_A, s_B are the atomic orbitals of the atoms A, B. The labeling of the π orbitals as x, y orbitals was chosen to indicate, from which p-type atomic orbitals they originate. The main atomic orbital contribution for π_{uy} for example is from the atomic p_y-orbitals.

Figure 6.7 and figure 6.8 illustrate the resulting orbitals as isosurface plots. The g/u symmetry of these states is evident from the illustration in the figures as well as from the LCAO coefficients in table 6.1. All the σ-type molecular orbitals are rotationally invariant around the internuclear axis. Figure 6.8 shows the resulting molecular π orbitals. As for the σ-type molecular orbitals, the g/u symmetry of these states is evident from the illustration and the LCAO coefficients.

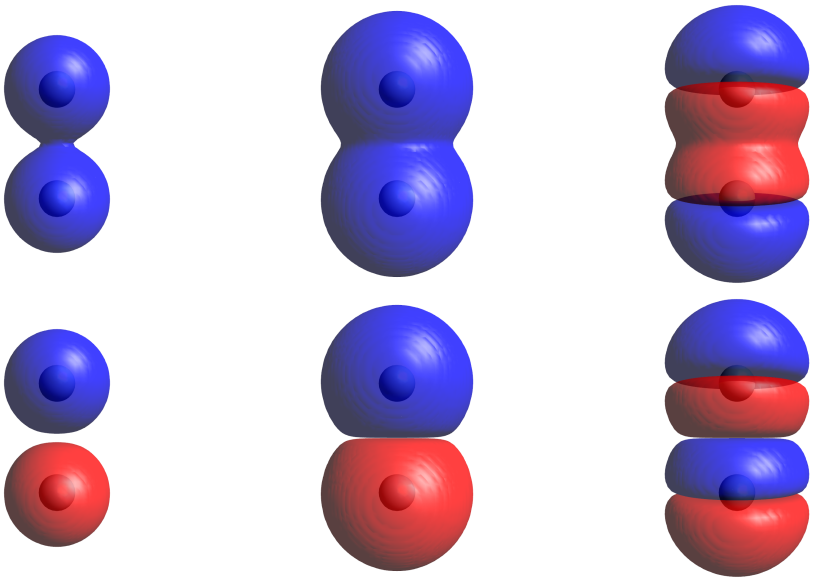

(a) $1\sigma_g$ (upper), $1\sigma_u$ (lower) (b) $2\sigma_g$ (upper), $2\sigma_u$ (lower) (c) $3\sigma_g$ (top), $3\sigma_u$ (bottom)

Figure 6.7: Isosurface plot of σ-type molecular orbitals of Ne_2 resulting from a RHF calculation in the STO-3G basis for the internuclear distance $R = 5.2\,a_0$. The subfigures (a), (b) show the σ-type molecular orbitals constructed from s-type atomic orbitals and subfigure (c) show the σ-type molecular orbitals constructed from p_z-type atomic orbitals. Shown in the top figures are the molecular orbitals with g symmetry and in the bottom figures the molecular orbitals with u symmetry. Blue surfaces indicate an isosurface value of the electronic wave function of $\phi(r) = +0.0001$ and red surfaces of $\phi(r) = -0.0001$.

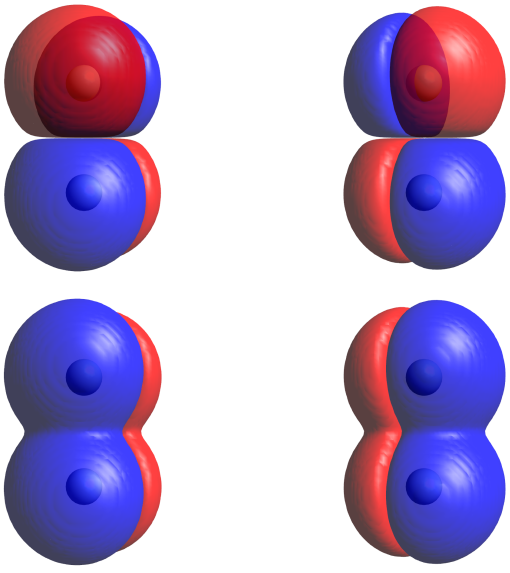

(a) $1\pi_{gx}$ (top), $1\pi_{ux}$ (bottom) (b) $1\pi_{gy}$ (top), $1\pi_{uy}$ (bottom)

Figure 6.8: Isosurface plot of π-type molecular orbitals of Ne_2 resulting from a RHF calculation in the STO-3G basis for the internuclear distance $R = 5.2\,a_0$. Subfigure (a) shows the π_x-type orbitals which are mainly given and subfigure (b) shows the π_y-type orbitals. Shown in the top figures are the molecular orbitals with g symmetry and in the bottom figures the molecular orbitals with u symmetry. Blue surfaces indicate an isosurface value of the electronic wave function of $\phi(r) = +0.0001$ and red surfaces of $\phi(r) = -0.0001$.

Building-up principle

The calculations of this section have been performed for ground state Ne and for the "ground state" diatomic molecule Ne_2. In section 6.6 potential energy surfaces are given for the excited Ne_2 molecule which dissociates in the Ne*–Ne* atomic limit with the atomic metastable configuration $2p^5 3s$. In order to illustrate these excited states of Ne_2 we show in figure 6.9 an example for an excited molecular state of Ne_2. One can see how the molecular orbitals and the

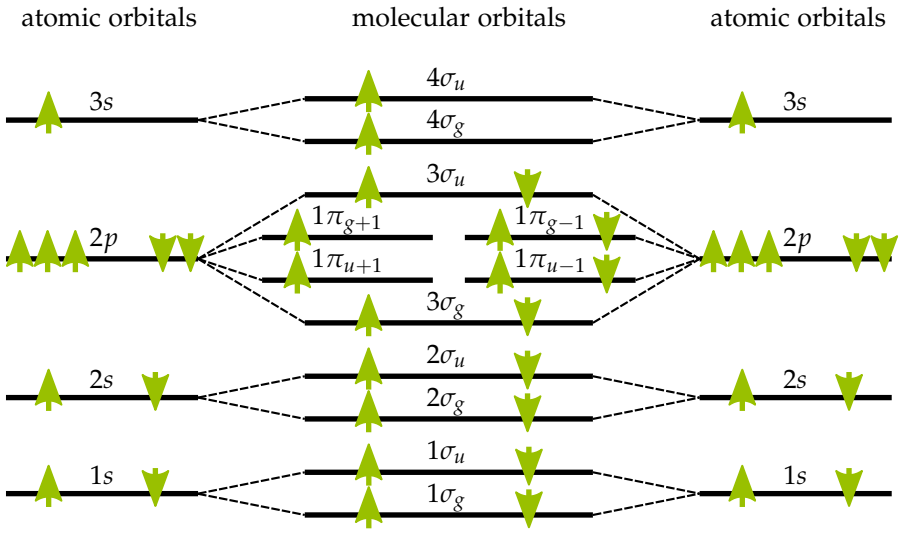

Figure 6.9: Excited electronic configuration of Ne_2. The green arrows indicate the electrons and their spin projections. The particular configuration of Ne_2 shown here reads $1\sigma_g^2\ 1\sigma_u^2\ 2\sigma_g^2\ 2\sigma_u^2\ 3\sigma_g^2\ 1\pi_{g-1}^2\ 1\pi_{u-1}^2\ 3\sigma_u^2\ 1\pi_{g+1}\ 1\pi_{u+1}\ 4\sigma_g\ 4\sigma_u$ which in total is a ${}^5\Delta_g$ state. The atomic limit of this molecular state are two Ne* atoms in the metastable $2p^5 3s$ configuration in an atomic triplet state.

atomic orbitals are connected and how the electronic configuration of the molecular state is built up from single electrons filling the molecular orbitals respecting the Pauli exclusion principle. One particular configuration is shown, where two electrons are excited from the $\pi_{g/u+1}$ orbitals to the $4\sigma_g$ and $4\sigma_u$ orbitals. The $\pi_{g/u\pm1}$-orbitals are the complex π-type molecular orbitals instead of the $\pi_{x/y}$ real molecular orbitals which were used in the RHF calculation. The advantage of the complex molecular orbitals is the well-defined projection of angular momentum $\Lambda_L = \pm 1$. The 4σ atomic orbitals are constructed from $3s$ atomic orbitals of Ne. Thus, the dissociation limit of the specific configuration is given by Ne*–Ne*, where both atoms are in the metastable $2p^5 3s$ configuration. The quantum numbers of the total molecular state are determined solely by the quantum numbers of the open-shell orbitals as all closed shells result in ${}^1\Sigma_g^+$ states. Four of the ten electrons in figure 6.9 occupy open shells and their spin projections point in the same direction so that the total electronic spin of this state is given by $S = 2$ and its multiplicity by $2S + 1 = 5$ [40]. The product state of the open-shell orbitals has symmetry $g \times g \times u \times u = g$ and the projection of the total electronic orbital angular momentum is given by $\Lambda = 2$ as the only two electrons occupying open π-type orbitals have projections $\Lambda_L = +1$. In total, the state arising from the configuration shown in figure 6.9 is one of the ${}^5\Delta_g$ states in *Hund's case* (a) notation. Similarly, one can construct the other molecular states of Ne_2 from building up the molecular orbitals.

Having illustrated the spatial molecular orbitals and the designation of the molecular states of Ne_2 we present next the calculated excited state potentials of Ne_2 which are the interaction potentials for Ne* at short-range.

6.6 SHORT-RANGE INTERACTION POTENTIALS

The short-range interaction potentials of Ne* are given in the *Hund's case* (a) basis dissociating in the atomic limit Ne*$(2p^5 3s)$–Ne*$(2p^5 3s)$, and more specifically in Ne(^3P)–Ne(^3P), Ne(^3P)–Ne(^1P) and Ne(^1P)–Ne(^1P). These potentials have been given in [6] and were thankfully provided to us by *S. Kotochigova*. They were calculated by using an adapted version of the *Generalized Valence Bond* (GVB) method described in [123]. The GVB method is a special type of the *valence bond methods* which are based on the *Heitler-London method*, discussed in section 3.5.2. The potentials are the eigenvalues $V_n(R)$ of the non-relativistic electronic Hamiltonian H_{el} (6.35) of Ne_2. We are particularly interested in the atomic limit ^3P–^3P as in experiments with Ne* the atoms are prepared in these states. The possible molecular states which dissociate to the ^3P–^3P atomic limit are tabulated in [70]. In the atomic limit of Ne*, both atoms are in triplet states so that the total spin S of the molecular state may take the values $S = 0, 1, 2$ and the molecular state is either a singlet, a triplet or a quintet state. Furthermore, in the ^3P–^3P atomic limit, both atoms are in P states. Therefore, by simple angular momentum algebra we conclude that the projection of orbital angular momentum on the internuclear axis may take the values $\Lambda = 0, 1, 2$. Thus, Σ, Π and Δ potentials occur. We have ordered these potentials according to their multiplicity.

In figure 6.10 the singlet Ne_2 potentials of of [6] are shown. It is also included the $^1\Delta_g$ potential which connects to the (^1P)Ne–(^1P)Ne asymptotic limit. Note, that the potential depth with $\sim 4500\ \text{cm}^{-1}$ of the singlet potential dissociating to the ^3P–^3P limit is very large compared to the potential depths $\sim 20\ \text{cm}^{-1}$ we have calculated in section 6.5 for the ground state Ne_2. In contrast to the ground state Ne_2, the singlet potentials shown here support many bound states. A potential depth of $4500\ \text{cm}^{-1}$ corresponds to a temperature of $T \sim 6500$ K with $T = E/k_B$. This temperature is very large compared to the relative collision energy of cold Ne* collisions which is on the order of ~ 1 mK.

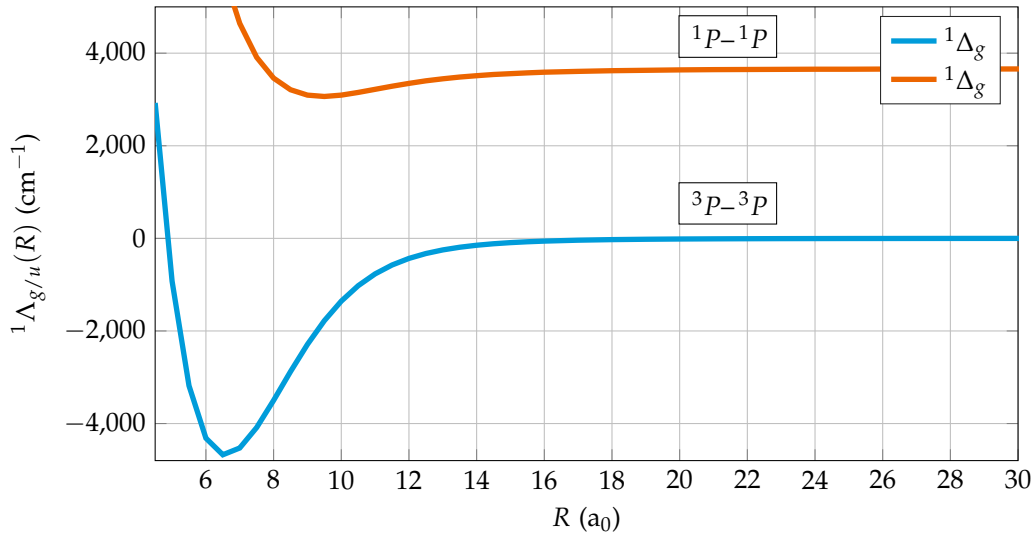

Figure 6.10: Singlet ($S = 0$) *Born-Oppenheimer potentials* of Ne_2 as functions of the internuclear distance R connecting to the atomic metastable limit Ne*$(2p^5 3s)$–Ne*$(2p^5 3s)$.

In figure 6.11 the triplet potentials of Ne_2 of [6] dissociating to the ^3P–^3P and the ^3P–^1P atomic limits are depicted. Again, the potentials which connect to the ^3P–^3P atomic limit are very deep with a potential depth on the order of $\sim 3300\ \text{cm}^{-1}$ which corresponds to $T \sim 4700$ K. As the singlet potentials, these potentials contain many bound states.

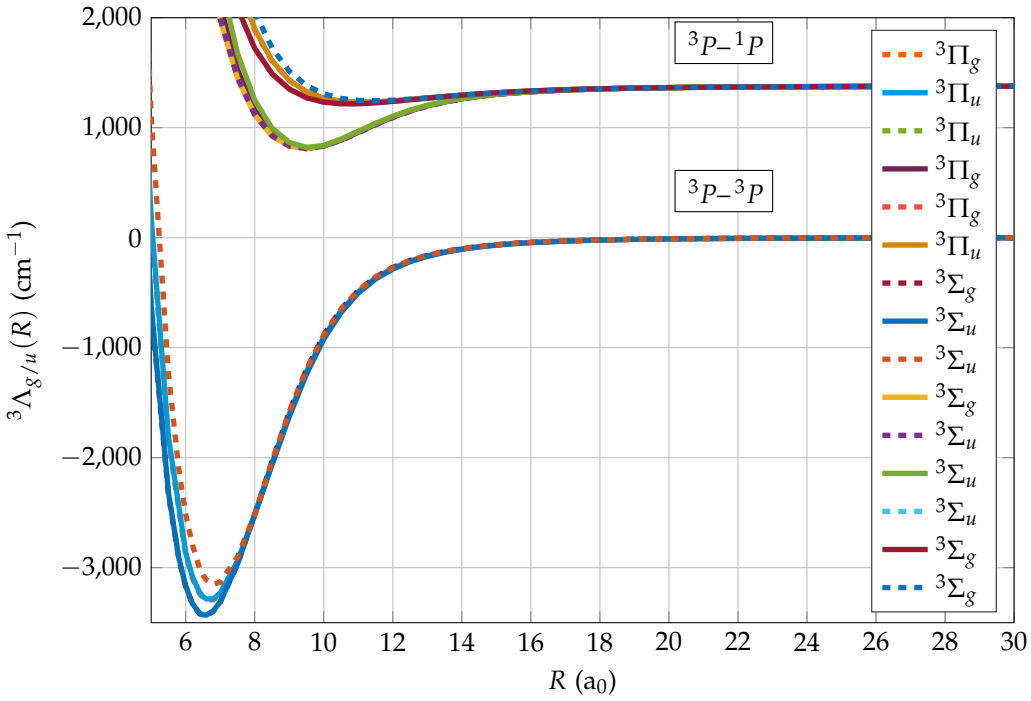

Figure 6.11: Triplet ($S = 1$) *Born-Oppenheimer potentials* of Ne_2 as functions of the internuclear distance R connecting to the atomic metastable limit Ne*($2p^5 3s$)–Ne*($2p^5 3s$).

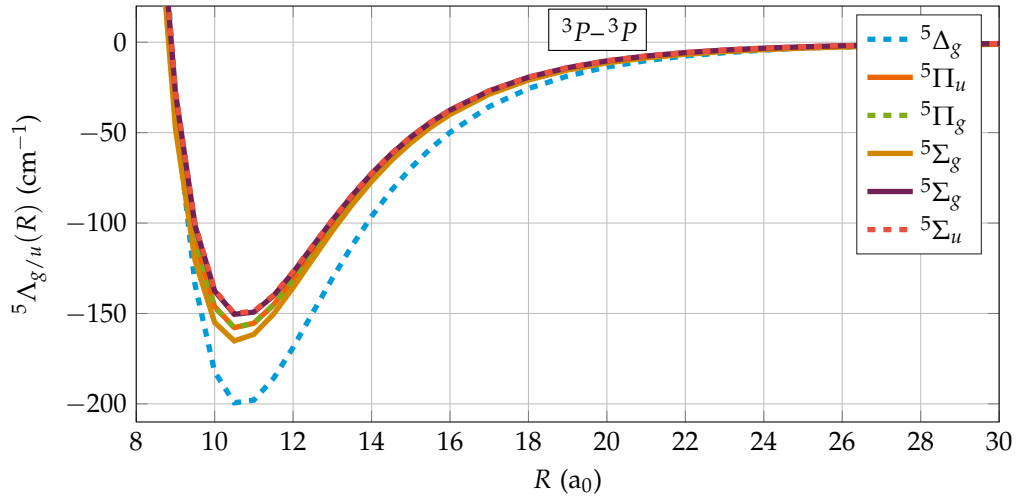

Figure 6.12: Quintet ($S = 2$) *Born-Oppenheimer potentials* of Ne_2 as functions of the internuclear distance R connecting to the atomic metastable limit Ne*($2p^5 3s$)–Ne*($2p^5 3s$).

In figure 6.12 the quintet potentials of Ne_2 of [6] are shown. It is striking, that these six quintet potentials are much shallower than the triplet and singlet potentials connecting to the ^3P–^3P limit. The potential depths are on the order of $\sim 155\ \mathrm{cm}^{-1}$ which corresponds to $T \sim 240$ K. This is still a large energy compared to the typical relative collision energies in the experiment, but an order of magnitude smaller than for the singlet and triplet potentials. Another difference of the quintet potentials compared to the singlet and triplet potentials are the positions of the minima of the potential curves. The singlet and triplet potentials connecting to the ^3P–^3P atomic limit have potential minima at internuclear distance $R \sim 6.5\ a_0$ while the potential minima of the quintet potentials are at $R \sim 10.5\ a_0$. The quintet potentials are particularly interesting as they describe the case of spin-aligned atoms. It is expected that the ionization rates drop for spin-polarized samples of atoms, as the PI processes are forbidden for spin-polarized collisions. Without considering the $^5\Delta_g$ potential, which is a bit deeper than the other potentials, all the quintet potentials have energy splittings of $\sim 10\ \mathrm{cm}^{-1}$ at $R \sim 10.5\ a_0$. It is pronounced that these splittings affect the inelastic collision rates [6].

The molecular potentials discussed here are supposed to describe the Ne* collisions at short-range [6]. The long-range interactions will be given in the next section.

6.7 LONG-RANGE INTERACTIONS

We have studied the long-range interactions of hydrogen and helium in chapter 4 in an atomic basis. The long-range interactions of Ne* were calculated in the *Hund's case* (c) molecular basis $|J\Omega\rangle$. In *Hund's case* (c) basis of Ne*, the total angular momentum $\mathbf{J}$ is given by $\mathbf{J} = \mathbf{J}_A + \mathbf{J}_B$, where $\mathbf{J}_A$ and $\mathbf{J}_B$ are the total angular momenta of the atoms A and B, respectively. The molecular states dissociating to the atomic limit Ne*($^3P_2$)–Ne*($^3P_2$) have total angular momentum $J = 0, 1, \ldots, 4$ as $j_A = j_B = 2$. With $\Omega = 0, \ldots, J$ and the states with $\Omega \neq 0$ being doubly degenerate, we have in total 25 molecular states dissociating to the atomic limit Ne*($^3P_2$)–Ne*($^3P_2$). Therefore, 25 dispersion coefficients are given.

The Ne atom in its metastable configuration $2p^5 3s$ has a non-vanishing quadrupole moment due to the spherical asymmetry of the $2p^5$ core. This leads to the quadrupole–quadrupole interaction of Ne* atoms which is given by a c_5/R^5 interaction potential. The 25 dispersion coefficients c_5 are tabulated in 6.2. They have been calculated in [8].

Term	c_5 (a.u.)	c_6 (a.u.)
4_g	0.2467	1877
3_g	−0.3700	1919
3_u	0.1233	1922
2_g	0.1233	1967
2_g	−0.2673	1935
2_u	−0.2878	1934
1_u	0.1730	1983
1_g	0.1617	1982
1_g	−0.2028	1920
1_u	−0.1318	1920
0_g^+	0.2173	1999
0_g^+	−0.0679	1968
0_u^-	−0.1525	1966
0_u^-	0.3992	1877
0_g^+	0.4673	1877

Table 6.2: Dispersion coefficients c_5, c_6 of the molecular states $|J\Omega\rangle$ of Ne in *Hund's case* (c), dissociating to the atomic limit Ne*($^3P_2$)–Ne*($^3P_2$). The c_5 coefficients are from [8] and the c_6 coefficients from [9].

As discussed in chapter 4 for the cases of H–H and He–He, the interaction of two neutral atoms at long-range is governed by the *van der Waals* interaction which is of the form $-c_6/R^6$.

This interaction is negative and leads to an attractive force between two neutral atoms. The c_6 coefficients for Ne_2 dissociating to the limit $Ne^*(^3P_2)$–$Ne^*(^3P_2)$ have also been calculated in the *Hund's case* (c) basis and the results are given in [9]. The error of the results is estimated to be 4 %. We have listed these c_6 coefficients in table 6.2. Note the difference in magnitude of the c_5 and the c_6 coefficients. All the c_5 coefficients are on the order of ~ 0.5 a.u. while the c_6 coefficients are on the order of ~ 2000 a.u. so that the strength of the quadrupole–quadrupole term c_5/R^5 only becomes comparable to the strength of the induced dipole–dipole term c_6/R^6 at internuclear distances on the order of $R \sim 4000\ a_0$. Thus, the scattering properties of Ne* at long-range will be mainly determined by the *van der Waals* interaction. For ionizing collisions of spin-polarized atoms, however, the quadrupole–quadrupole interaction is expected to have an influence, as the anisotropy of the c_5 coefficients, which is on the same order as the c_5 coefficients themselves, leads to depolarizing collisions [8].

Given the c_6 coefficients of table 6.2 we can calculate the *van der Waals parameters*. These parameters are used in the *non-universal model* to analyze cold collisions and read [60]

$$R_6 = \frac{1}{2}\left(\frac{2\mu c_6}{\hbar^2}\right)^{1/4}, \quad \bar{a} = \frac{4\pi R_6}{\Gamma(\frac{1}{4})^2}, \tag{6.43}$$

with the characteristic *van der Waals* length R_6 and the mean scattering length $\bar{a}$. $\Gamma(x)$ is the Gamma function [13]. The *van der Waals parameters* solely depend on the c_6 coefficient and the reduced mass μ. Table 6.3 lists the *van der Waals parameters* R_6 and $\bar{a}$ for the minimal c_6 coefficient $c_6^{\min} = 1877$ a.u. and the maximal c_6 coefficient $c_6^{\max} = 1999$ a.u. of Ne* interactions and for all isotope combinations of Ne which are explored in the experiment.

		$c_6 = 1877$ a.u.		$c_6 = 1999$ a.u.	
	μ	R_6 (a_0)	$\bar{a}$ (a_0)	R_6 (a_0)	$\bar{a}$ (a_0)
^{20}Ne–^{20}Ne	18222	45.47	43.47	46.19	44.16
^{21}Ne–^{20}Ne	18667	45.75	43.73	46.47	44.43
^{22}Ne–^{20}Ne	19090	46.00	43.98	46.73	44.68
^{21}Ne–^{22}Ne	19579	46.30	44.26	47.03	44.96
^{22}Ne–^{22}Ne	20044	46.57	44.52	47.31	45.22

Table 6.3: *Van der Waals parameters* R_6 and $\bar{a}$ for Ne* for different isotope combinations. The reduced masses μ are taken from [124].

Having discussed the short-range and long-range interaction potentials of Ne* we continue with the full scattering equations and the two-body loss rate coefficients of Ne* collisions in terms of these potentials.

6.8 SCATTERING EQUATIONS IN A MOLECULAR BASIS

Here, we show how the *coupled-channel equations* and the molecular potentials of Ne* emerge from an expansion of the scattering states of Ne* in a molecular basis [44, 46, 52, 125]. The scattering state reads

$$|\Psi(J_t, M_t, E)\rangle = \sum_{J',l'} \underbrace{F^{J_t M_t E}_{J'l',Jl}(R)}_{\substack{\text{radial}\\ \text{part}}} \times \underbrace{|J_t, M_t, J', l'\rangle}_{\substack{\text{rotational \&}\\ \text{electronic part}}}, \tag{6.44}$$

where $\mathbf{J}_t$ is the total angular momentum of the diatomic state given by the total electronic angular momentum $\mathbf{J}$ and the rotational angular momentum $\mathbf{L}_r$ of the diatomic system so that $\mathbf{J}_t = \mathbf{J} + \mathbf{L}_r$. The quantum number M_t is the projection of $\mathbf{J}_t$ on the space-fixed quantization axis and E is the relative collision energy of the relative motion of the two atoms. For particles with spin, electronic degrees of freedom and rotational degrees of freedom can change, but J_t and M_t are conserved quantum numbers if no external electric and magnetic field is applied.

The scattering state (6.44) is given by a separation ansatz, where the radial part $F^{J_t M_t E}_{J'l',Jl}(R)$ is separated from the molecular *channel states* $|J_t, M_t, j', l'\rangle$. The *channel states* consist of a rotational part and an electronic part for the electronic states of the diatomic system. They read

$$|J_t, M_t, j, l\rangle = \sum_{m_J, m_l} C(JlJ_t; m_J m_l M_t) \underbrace{|Jm_J\rangle}_{\substack{\text{electronic}\\ \text{part}}} \times \underbrace{|lm_l\rangle}_{\substack{\text{rotational}\\ \text{part}}}, \tag{6.45}$$

with the Clebsch-Gordan coefficient $C(JlJ_t; m_J m_l M_t)$. The rotational part $|lm_l\rangle$ is characterized by the rotational quantum number l and its projection m_l on a space-fixed quantization axis. The electronic part $|Jm_J\rangle$ describes the state in a diatomic basis with total electronic angular momentum number J and projection m_J on the space-fixed quantization axis. This state itself is given in a LS coupled representation of atomic states $|jm\rangle$ with quantum numbers (l_1, s_1, j_1) and (l_2, s_2, j_2), with (l_1, l_2) the orbital angular momentum numbers, (s_1, s_2) the total electronic spins and (j_1, j_2) the total electronic angular momentum numbers of the atom $(1, 2)$, respectively. We saw in section 6.2 that the LS coupling scheme is valid for the $3s(3/2)_2$ states of Ne in the $2p^5 3s$ configuration and the corresponding states in LS coupling are arising from the $^3P_2$ manifold, so that $s_1 = s_2 = 1$, $l_1 = l_2 = 1$ and $j_1 = j_2 = 2$.

The diatomic electronic state $|Jm_J\rangle = |((l_1 s_1) j_1 (l_2 s_2) j_2) J m_J\rangle$ can be transformed to a molecular basis, where the atomic orbital angular momenta $\mathbf{L}_1$, $\mathbf{L}_2$ couple to a total orbital angular momentum $\mathbf{L} = \mathbf{L}_1 + \mathbf{L}_2$ and where the total electron spins of the atoms $\mathbf{S}_1$, $\mathbf{S}_2$ couple to a total electronic spin $\mathbf{S} = \mathbf{S}_1 + \mathbf{S}_2$. The transformation reads

$$\begin{aligned} |Jm_J\rangle &= |((l_1 s_1) j_1 (l_2 s_2) j_2) J m_J\rangle \\ &= \sum_{LS} \sqrt{(2j_1+1)(2j_2+1)(2S+1)(2L+1)} \begin{Bmatrix} s_1 & s_2 & S \\ l_1 & l_2 & L \\ j_1 & j_2 & J \end{Bmatrix} |((l_1 l_2) L (s_1 s_2) S) J m_J\rangle , \end{aligned} \tag{6.46}$$

where $\{\cdot\}$ is a Wigner $9j$ symbol (see appendix B.1). The state $|Jm_J\rangle$ is characterized by the quantum number m_J, which is the projection on the space-fixed quantization axis while the molecular states of section 6.6 and 6.7 are given in a basis, where the projection axis is the internuclear axis $\mathbf{R}$. In order to connect the diatomic states (6.46) to these molecular states we have to rotate the state $|Jm_J\rangle$ to this quantization axis. The transformation of the state $|((l_1 l_2) L (s_1 s_2) S) J m_J\rangle$ in the space-fixed frame to the state $|((l_1 l_2) L (s_1 s_2) S) J\Omega\rangle$ in the body-fixed frame reads

$$|((l_1 l_2) L (s_1 s_2) S) J m_J\rangle = \sum_{\Omega} D^{J*}_{m_J \Omega}(\phi, \theta, 0) \, |((l_1 l_2) L (s_1 s_2) S) J\Omega\rangle , \tag{6.47}$$

where $D^{J*}_{m_J\Omega}(\phi, \theta, 0)$ is the Wigner D matrix (see appendix B) and (ϕ, θ) are the polar and azimuthal angles of the internuclear axis $\mathbf{R}$ (see appendix B.2). The transformed states $|J\Omega\rangle$ are the molecular basis states of Ne_2. The long-range properties of these states were given in section 6.7. We can furthermore transform the molecular basis $|J\Omega\rangle$ of *Hund's case* (c) to the molecular *Hund's case* (a) basis $|L\Lambda S\Sigma\rangle$. The transformation reads

$$|((l_1 l_2) L (s_1 s_2) S) J\Omega\rangle = \sum_{\Lambda\Sigma} C(LSJ; \Lambda\Sigma\Omega), |(l_1 l_2) L\Lambda (s_1 s_2) S\Sigma\rangle , \tag{6.48}$$

with the Clebsch-Gordan coefficient $C(LSJ; \Lambda\Sigma\Omega)$. Note, that so far in the discussion of the scattering states we have not referred to the issue of identical particle scattering. For homonuclear collisions, the *channel states* (6.45) have to be symmetric or antisymmetric under the exchange of the nuclei. We address this issue in the next section and show how electronic and rotational part of the scattering wave function are modified for identical particle scattering.

The states $|L\Lambda S\Sigma\rangle$ in equation (6.48) are the eigenstates of the electronic Hamiltonian of Ne*. We write the eigenvalue equation (6.37) more explicitly, in terms of the quantum numbers L, S, Λ, Σ, as

$$H_{\text{el}} \, |L\Lambda S\Sigma\rangle = V_{L\Lambda S\Sigma}(R) \, |L\Lambda S\Sigma\rangle , \tag{6.49}$$

with $V_{L\Lambda S\Sigma}(R)$ the molecular potentials in *Hund's case* (a) notation.

With the expansion of the scattering state (6.44) in a molecular basis (see equation (6.47) for the basis $|J\Omega\rangle$ and equation (6.48) for the basis $|L\Lambda S\Sigma\rangle$) it is evident, how the molecular potentials of section 6.6 and of section 6.7 enter the scattering equations for Ne* collisions. The Schrödinger equation for the scattering state (6.44) reads

$$(H + V_{LS})\,|\Psi(J_t, M_t, E)\rangle = E\,|\Psi(J_t, M_t, E)\rangle\,, \tag{6.50}$$

where H is the diatomic Hamiltonian given in equation (6.35) and V_{LS} describes the spin-orbit coupling for diatomic Ne. The *coupled-channel equations* for the Schrödinger equation (6.50) are generated by constructing the matrix elements

$$\langle J_t, M_t, J'', l''|\,(H + V_{LS})\,|\Psi(J_t, M_t, E)\rangle = E\langle J_t, M_t, J'', l''|\Psi(J_t, M_t, E)\rangle. \tag{6.51}$$

The resulting equations are solved for the radial functions $F^{J_t M_t E}_{J'l',Jl}(R)$ for which the asymptotic form is given by [44]

$$F^{J_t M_t E}_{J'l',Jl}(R) \underset{R\to\infty}{\longrightarrow} \left(k_J/v_J^{1/2}\right)^{1/2} j_l(k_J R)\delta_{JJ'}\delta_{ll'} - \frac{1}{2}T^{J}_{J'l',Jl}\left(k_{J'}/v_{J'}^{1/2}\right)^{1/2} h_{l'}(k_{J'}R), \tag{6.52}$$

with $j_l(k_J R)$ is the spherical Bessel function and $h_{l'}(k_{J'}R)$ the spherical Hankel function of first kind (see appendix C.2). The channel wave numbers are given by $k_J^2 = E - \Delta_J$, with Δ_J the asymptotic channel energies. The relative velocities v_J are defined with respect to the scattering channel J. The elements $T^{J_t}_{J'l',Jl}$ are the on-shell T matrix elements. The connection of S matrix and T matrix was given in equation (5.42) for single-channel scattering and in equation (5.111) for multichannel scattering. All the scattering properties can be extracted from either the S matrix or the T matrix.

The *coupled-channel equations* (6.51) describe the full interaction of Ne* atoms. In the derivation it was important to construct *channel states* (6.45), which dissociate into the correct asymptotic limit of two Ne* atoms in states of the $^3P_2$ manifolds, in a space-fixed frame and express them in the molecular basis $|J\Omega\rangle$ or $|LS\Lambda\Sigma\rangle$ in the body-fixed frame. This introduces the *Born-Oppenheimer potentials* $V_{L\Lambda S\Sigma}(R)$ or the long-range potentials in the scattering equations. At low energies, the colliding Ne* atoms follow these potential curves adiabatically and one solves the *coupled-channel equations* for the radial wave functions $F^{J_t M_t E}_{J'l',Jl}(R)$.

The *coupled-channel equations* of this section do not account for the ionization channels of PI in Ne* scattering. In the next section we show, how the two-body loss rate coefficients for an unpolarized sample of Ne* atoms can be calculated from the contributions of the individual molecular *Hund's case* (a) states .

6.9 UNPOLARIZED TWO-BODY LOSS RATE COEFFICIENTS IN A MOLECULAR BASIS

In this section, we assume an unpolarized ensemble of trapped Ne* atoms, prepared in the $^3P_2$ states where the magnetic sublevels m are equally populated. We follow the discussion in [58, 59]. Consider, that $N_F(t)$ is the number of trapped atoms of the isotope F and that the ensemble consists either of this single isotope species F or of two different isotopes F, G. The rate equation (5.166) for $N_F(t)$ can then be written as

$$\frac{dN_F(t)}{dt} = -^{FF}\beta_{\mathrm{unp}} \int d^3r\; n_F^2(\mathbf{r}, t) - \;^{FG}\beta_{\mathrm{unp}} \int d^3r\; n_F(\mathbf{r}, t) n_G(\mathbf{r}, t), \tag{6.53}$$

with $n_F(\mathbf{r}, t)$, $n_G(\mathbf{r}, t)$ the particle densities of the species F, G. The two-body loss rate coefficients $^{FG}\beta_{\mathrm{unp}}$ for an unpolarized ensemble of atoms was given in section 5.8.6 in terms of an atomic product basis $|j_1 m_1\rangle \otimes |j_2 m_2\rangle$. Our goal in this section is, to decompose the two-body loss rate coefficients in terms of the contributions of the molecular basis states $|L\Lambda S\Sigma\rangle$. In an unpolarized ensemble these molecular states are all equally populated and $^{FG}\beta_{\mathrm{unp}}$ is given by the individual molecular state contributions.

Heteronuclear two-body loss rate coefficients

We first consider the case of heteronuclear Ne* collisions including the cases of ^{20}Ne–^{22}Ne, ^{20}Ne–^{21}Ne and ^{21}Ne–^{22}Ne collisions. Heteronuclear collisions are the simplest case as the particles are distinguishable. When the molecular states are equally populated, we can write the unpolarized two-body loss rate coefficient as

$$ {}^{FG}\beta_{\text{unp}} = \left(\frac{1}{2j_1+1}\right)^2 \sum_{J=0}^{3} \sum_{\Omega=-J}^{+J} {}^{FG}\beta_{J\Omega}, \tag{6.54} $$

where $j_1 = 2$ is the total angular momentum of the atomic states, which are states of the $^3P_2$ manifold and ${}^{FG}\beta_{J\Omega}$ is the two-body loss rate contribution from the molecular state $|J\Omega\rangle$ in the *Hund's case* (c) basis. Note, that the sum in equation (6.54) only extends up to $J = 3$. The molecular states with $J = 4$ correspond to the spin-polarized case where the PI channels are forbidden. Thus, there are no two-body loss rate contributions from these states. The loss rate contributions ${}^{FG}\beta_{J\Omega}$ are given in terms of the molecular *Hund's case* (c) states $|J\Omega\rangle$. We want to further decompose the loss rates in terms of the *Hund's case* (a) states $|L\Lambda S\Sigma\rangle$. The basis transformation between these states, including the rotational part of the atoms, reads [46]

$$ |((s_1 l_1) j_1, (s_2 l_2) j_2) J\Omega\rangle \, |l m_l\rangle = \sum_{LS} \sum_{\Lambda\Sigma} a_{LS\Lambda\Sigma} \, |(l_1 l_2) L\Lambda (s_1 s_2) S\Sigma\rangle \, |l m_l\rangle \,, \tag{6.55} $$

with the coefficients

$$ a_{LS\Lambda\Sigma} = \sqrt{(2S+1)(2L+1)(2j_1+1)(2j_2+1)} \begin{Bmatrix} s_A & s_B & S \\ l_A & l_B & L \\ j_A & j_B & J \end{Bmatrix} C(LSJ; \Lambda\Sigma\Omega). \tag{6.56} $$

The quantum numbers $(l_1 = 1, s_1 = 1, j_1 = 2)$ and $(l_2 = 1, s_2 = 1, j_2 = 2)$ are given by the atomic limit of Ne*($^3P_2$)–Ne*($^3P_2$). With the transformation of the *channel states* (6.55) we find for the unpolarized two-body loss rate coefficient in a partial-wave series in l as

$$ {}^{FG}\beta_{\text{unp}} = \left(\frac{1}{2j_1+1}\right)^2 \sum_{l} \sum_{LS} \sum_{\Lambda\Sigma} |a_{LS\Lambda\Sigma}|^2 \, {}^{FG}\beta_{l,LS\Lambda\Sigma}. \tag{6.57} $$

Here, ${}^{FG}\beta_{l,LS\Lambda\Sigma}$ are the partial two-body loss rate contributions from the molecular states $|L\Lambda S\Sigma\rangle$. The sum (6.57) does not include the sum over $S = 2$. These are the quintet state loss rate contributions which are zero as PI reactions from these states are forbidden. Keeping this in mind, the evaluation of the sum (6.57) leads to

$$ \begin{aligned} {}^{FG}\beta_{\text{unp}} = \frac{1}{25} \Bigg\{ & \sum_l \frac{7}{18} \left({}^{FG}\beta_l \left({}^1\Delta_g\right) + {}^{FG}\beta_l \left({}^1\Pi_g\right) \right) \\ & + \frac{7}{36} \, {}^{FG}\beta_l \underbrace{\left({}^1\Sigma_g^+\right)}_{L=2} + \frac{5}{9} \, {}^{FG}\beta_l \underbrace{\left({}^1\Sigma_g^+\right)}_{L=0} + \frac{10}{9} \, {}^{FG}\beta_l \left({}^3\Sigma_g^-\right) + \frac{20}{9} \, {}^{FG}\beta_l \left({}^3\Pi_g\right) \\ & + \frac{3}{2} \left({}^{FG}\beta_l \left({}^3\Delta_u\right) + {}^{FG}\beta_l \left({}^3\Pi_u\right) \right) + \frac{3}{4} \, {}^{FG}\beta_l \underbrace{\left({}^3\Sigma_u^+\right)}_{L=2} + \frac{5}{4} \underbrace{{}^{FG}\beta_l \left({}^3\Sigma_u^+\right)}_{L=0} \\ & + \frac{5}{6} \, {}^{FG}\beta_l \left({}^1\Pi_u\right) + \frac{5}{12} \, {}^{FG}\beta_l \left({}^1\Sigma_u^-\right) \Bigg\}. \end{aligned} \tag{6.58} $$

We used the symmetry properties (3.46) of the states $|L\Lambda S\Sigma\rangle$ to determine the g/u and $+/-$ symmetries of the states. In the sum (6.58), the notation ${}^{FG}\beta_l({}^1\Delta_g)$ designates for example the lth partial two-body loss rate contribution from the molecular $^1\Delta_g$ state.

Homonuclear two-body loss rate coefficients

For homonuclear collisions of ^{20}Ne and ^{22}Ne, the *channel states* need to by symmetric under the exchange of the nuclei. The properly symmetrized states in *Hund's case* (a) basis, including the rotational part of the atoms, read [58]

$$\begin{aligned}|(l_1l_2)L\Lambda(s_1s_2)S\Sigma\rangle\,|lm_l\rangle =&\frac{1}{\sqrt{2}}\left\{|(l_1s_1)_A(l_2s_2)_B)L\Lambda S\Sigma\rangle + |(l_1s_1)_B(l_2s_2)_A)L\Lambda S\Sigma\rangle\right\}|lm_l\rangle\\ =&\frac{1}{\sqrt{2}}\left(1+(-1)^{l+L+S}\right)|(l_1s_1)_A(l_2s_2)_B)L\Lambda S\Sigma\rangle\,|lm_l\rangle\,,\end{aligned} \tag{6.59}$$

where the unsymmetrized electronic state $|(l_1s_1)_A(l_2s_2)_B)L\Lambda S\Sigma\rangle$ is a coupled diatomic state which reads

$$\begin{aligned}|((l_1s_1)_A(l_2s_2)_B)LS)J\Omega\rangle =&\sum_{\Lambda\Sigma}\langle L\Lambda S\Sigma|J\Omega\rangle\,|L\Lambda S\Sigma\rangle\\ =&\sum_{\Lambda\Sigma}\sum_{\lambda_1\lambda_2}\sum_{\sigma_1\sigma_2}\langle L\Lambda S\Sigma|J\Omega\rangle\langle l_1l_2\lambda_1\lambda_2|L\Lambda\rangle\langle s_1s_2\sigma_1\sigma_2|S\Sigma\rangle\\ &\times|l_1l_2\lambda_1\lambda_2\rangle\,|s_1s_2\sigma_1\sigma_2\rangle\,.\end{aligned} \tag{6.60}$$

Here, $(l_1,\lambda_1,s_1,\sigma_1)$ are the quantum numbers of atom A while $(l_2,\lambda_2,s_2,\sigma_2)$ are the quantum numbers of atom B. The quantum numbers (λ_1,λ_2) are the projections of the atomic orbital angular momenta (l_1,l_2) on the internuclear axis and (σ_1,σ_2) are the projections of the atomic electronic spins (s_1,s_2) on the internuclear axis. An exchange of the nuclei in the state (6.60) leads to an exchange of the quantum numbers $(l_1\lambda_1s_1\sigma_1 \leftrightarrow l_2\lambda_2s_2\sigma_2)$. Exchanging $A \leftrightarrow B$ in (6.60) leads to the factor $(-1)^{L+S}$. Furthermore, the factor $(-1)^l$ in (6.59) results from the effect of the exchange $A \leftrightarrow B$ on $|lm_l\rangle$. In total we find indeed, that the state (6.59) is the properly symmetrized state for bosons. It is evident that this state vanishes if $L+S$ is an even number and l is odd or if $L+S$ is an odd number and l is even.Thus, we conclude that for identical bosons in *gerade* molecular states only even partial waves contribute while in *ungerade* states only odd partial waves contribute. If we insert the symmetrized state in (6.55) we find for the unpolarized loss rate in equation (6.57)

$${}^{FF}\beta_{\text{unp}} = \begin{cases}\displaystyle\sum_{l\text{ even}}\sum_{LS\Lambda\Sigma}|a_{LS\Lambda\Sigma}|^2\;{}^{FF}\beta_{l,LS\Lambda\Sigma} & L+S\text{ even},\\ \displaystyle\sum_{l\text{ odd}}\sum_{LS\Lambda\Sigma}|a_{LS\Lambda\Sigma}|^2\;{}^{FF}\beta_{l,LS\Lambda\Sigma} & L+S\text{ odd},\end{cases} \tag{6.61}$$

which holds for homonuclear collisions of bosons. The summation is again excluding the $S=2$ states, as there is no two-body loss from the quintet states. Evaluation of the sum (6.61) leads to

$$\begin{aligned}{}^{FF}\beta_{\text{unp}} = \frac{1}{25}\Bigg\{&\sum_{l\text{ even}}\Bigg[\frac{7}{18}\left({}^{FF}\beta_l\left({}^1\Delta_g\right)+{}^{FF}\beta_l\left({}^1\Pi_g\right)\right)\\ &+\frac{7}{36}\,{}^{FF}\beta_l\underbrace{\left({}^1\Sigma_g^+\right)}_{L=2}+\frac{5}{9}\,{}^{FF}\beta_l\underbrace{\left({}^1\Sigma_g^+\right)}_{L=0}+\frac{10}{9}\,{}^{FF}\beta_l\left({}^3\Sigma_g^-\right)+\frac{20}{9}\,{}^{FF}\beta_l\left({}^3\Pi_g\right)\Bigg]\\ &+\sum_{l\text{ odd}}\Bigg[\frac{3}{2}\left({}^{FF}\beta_l\left({}^3\Delta_u\right)+{}^{FF}\beta_l\left({}^3\Pi_u\right)\right)+\frac{3}{4}\,{}^{FF}\beta_l\underbrace{\left({}^3\Sigma_u^+\right)}_{L=2}+\frac{5}{4}\,{}^{FF}\beta_l\underbrace{\left({}^3\Sigma_u^+\right)}_{L=0}\\ &+\frac{5}{6}\,{}^{FF}\beta_l\left({}^1\Pi_u\right)+\frac{5}{12}\,{}^{FF}\beta_l\left({}^1\Sigma_u^-\right)\Bigg]\Bigg\},\end{aligned} \tag{6.62}$$

where again the g/u and $+/-$ symmetries are determined from the symmetries (3.46) of the molecular states $|L\Lambda S\Sigma\rangle$.

The two-body loss rate coefficients of unpolarized samples of Ne* in the equations (6.58), (6.62), decomposed in the contributions of the molecular potentials, of course, are only of use, if

the inelastic cross sections to the ionization channels are known. The considerations of this section are however of importance as it is shown how the suppression of PI reactions for spin-polarized states can be included explicitly in the calculation. Furthermore, in this section the basis transformation of *Hund's case* (a) to *Hund's case* (c) basis states is given. It is also shown how the symmetrization of the *channel states* for identical atoms together with the inversion symmetries of the molecular states affects the two-body scattering rates.

CONCLUSION

In this chapter, we gave an overview of the atomic and diatomic properties of Ne* and showed how these properties relate to the full interaction properties of Ne*. We started with the Hamiltonian of Ne and discussed the fine-structure of the metastable Ne configuration. It was shown that the fine-structure notation of the lowest metastable $3s(3/2)_2$ state is equivalent to the $^3P_2$ state of LS coupling.

In order to introduce the molecular potentials of Ne* we calculated the potential energy of the ground state of Ne_2 and investigated the resulting molecular orbitals. In section 6.6 the excited potential energies were given and in section 6.7 the dispersion coefficients c_5, c_6 of the long-range interactions in the different molecular basis states. In order to account for the loss processes in Ne* collisions we briefly discussed PI afterwards. In the last two sections of this chapter we introduced the short-range and long-range interaction potentials of Ne* in the scattering equations. We expanded the scattering state in an atomic basis and transformed this stete to the molecular basis in order to introduce the molecular potentials in the scattering equations. Finally, we demonstrated how the two-body loss rate coefficients for an unpolarized sample of Ne* atoms can be calculated from the individual contributions from the molecular.

The scattering equations for Ne* collisions contain a large amount of molecular potentials as was seen in this chapter. We find however, that the collision physics of Ne* at low collision energies can be described by the coupled two-channel model which we introduce in the next chapter in the version, where elastic channel and loss channel is given by square-well potentials.

7

TWO-CHANNEL MODEL WITH SQUARE-WELL POTENTIALS

From the description of collisions physics of Ne* in terms of the full interactions we introduce in this chapter a model for cold reactive collisions of Ne*. This model is given by two coupled channels where the channels are given by square-well potentials. From the pole expansion of the S matrix in terms of a single term we obtain simple expressions for inelastic cross sections and two-body loss rate coefficients. In the next chapter we then show that this parametrization of the two-body loss rate coefficients agrees with the experimental measurements on ionizing collisions of Ne* and the numerical results of the two-channel model with a realistic interaction potential of Ne* which then is introduced.

The scattering rates of different isotopes of Ne* are not universal [2]. This suggests that the *quantum reflection model* which was briefly discussed in the introduction is not valid and the atoms do not ionize with 100 % probability at short-range. Therefore, we assume that the coupling of elastic channel to inelastic channel in the coupled two-channel model is weak. In this case, the matrix elements for the S matrix for the two-channel model are given in terms of the uncoupled solutions of the single-channel square-well potential. Therefore we start this chapter by studying these single-channel solutions. As in cold collisions only a few partial waves contribute to the scattering cross section, we solely investigate the lowest partial waves $l = 0, 1, 2$.

7.1 SINGLE-CHANNEL SOLUTIONS

The single-channel square-well potential introduces many features of scattering physics such as the scattering phase, the scattering length and scattering resonances. Since the Schrödinger equation for this potential is analytically solvable all these concepts of scattering theory can be studied analytically. The single-channel Schrödinger equation in dimensionless units reads

$$\left[\frac{d^2}{dr^2} - V_l(r) + k^2\right] \psi_{l,k}(r) = 0, \tag{7.1}$$

where $\psi_{l,k}$ is the "+" solution and we omit this label throughout this chapter. Furthermore, we have introduced the effective potential

$$V_l(r) = \begin{cases} -\kappa^2 + \dfrac{l(l+1)}{r^2} & r \leq 1, \\ \dfrac{l(l+1)}{r^2} & r > 1, \end{cases} \tag{7.2}$$

with $\kappa > 0$. Figure 7.1 shows the square-well potential for $l = 0$ which contains a single bound state. The effective potential is piecewise constant and the scattering solutions $k > 0$ for the two regions $r \leq 1$ and $r > 1$ are given by (see appendix C.3)

$$\psi_{l,k}(r) = \begin{cases} \psi^{\mathrm{I}}_{l,k}(r) = (k/K_0)^{l+1} \mathfrak{f}_l^{-1}(k) \hat{\jmath}_l(K_0 r) & r \leq 1, \\ \psi^{\mathrm{II}}_{l,k}(r) = \dfrac{i}{2}\left\{\hat{h}_l^-(kr) - s_l(k)\hat{h}_l^+(kr)\right\} & r > 1, \end{cases} \tag{7.3}$$

with $K_0^2 \equiv k^2 + \kappa^2$. The ansatz in the inner region is given in terms of the Jost function $\mathfrak{f}_l(k)$ which results from the relation of regular solution and scattering wave function [see

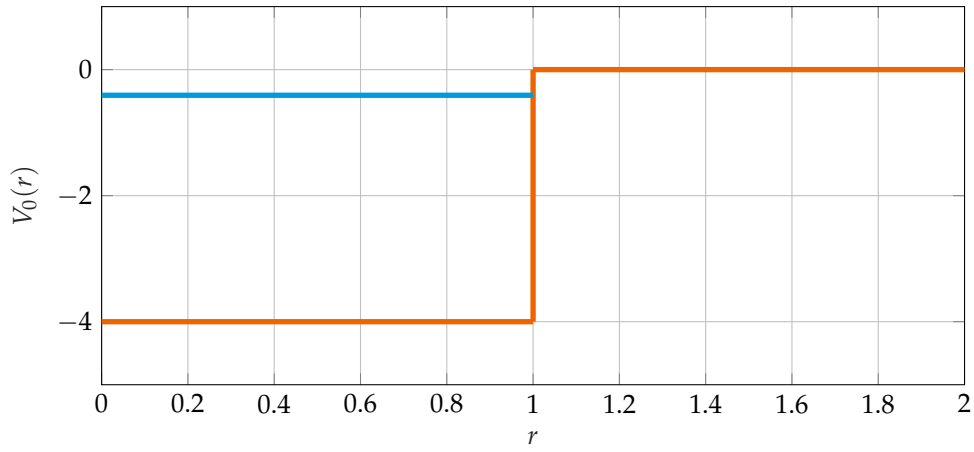

Figure 7.1: Square-well potential as a function of r. The potential depth is $\kappa = 2$ and the potential contains one single bound state at $E_{\mathrm{bs}} = -\mathcal{K}_1^2$, indicated as blue solid line.

equation (5.77)]. The factor $(k/K_0)^{l+1}$ is given by the boundary condition (5.73) of the regular solution at the origin and the behavior of the Riccati-Bessel function for small arguments [see equation (C.15)].

The wave functions $\psi_{l,k}(r)$ and $\psi'_{l,k}(r)$, where the prime indicates the derivative with respect to the radial coordinate r, are continuous at $r = 1$. Therefore, the Jost function $\mathfrak{f}_l$ and the S matrix s_l can be determined from the continuity conditions

$$\psi^{\mathrm{I}}_{l,k}(1) = \psi^{\mathrm{II}}_{l,k}(1), \quad \psi^{\mathrm{I}\prime}_{l,k}(1) = \psi^{\mathrm{II}\prime}_{l,k}(1). \tag{7.4}$$

as

$$s_l(k) = \frac{\hat{\jmath}'_l(K_0)\hat{h}^-_l(k) - \hat{h}^{-\prime}_l(k)\hat{\jmath}_l(K_0)}{\hat{\jmath}'_l(K_0)\hat{h}^+_l(k) - \hat{h}^{+\prime}_l(k)\hat{\jmath}_l(K_0)}, \tag{7.5}$$

$$\mathfrak{f}_l(k) = 2i\left(\frac{k}{K_0}\right)^{l+1} \frac{\hat{\jmath}'_l(K_0)\ \hat{h}^+_l(k) - \hat{h}^{+\prime}_l(k)\ \hat{\jmath}_l(K_0)}{\hat{h}^{+\prime}_l(k)\hat{h}^-_l(k) - \hat{h}^{-\prime}_l(k)\hat{h}^+_l(k)}. \tag{7.6}$$

From these solutions it can be easily checked with the properties of the Riccati-Hankel functions [see equation (C.21)] that the relation (5.78) of S matrix and Jost functions holds for the square-well potential.

7.1.1 *s-wave scattering*

From the general solution we can study the particular partial-wave solutions. The s-wave Jost function reads

$$\mathfrak{f}_0(k) = e^{ik}\frac{K_0\cos K_0 - ik\sin K_0}{K_0}, \tag{7.7}$$

and the single-channel S matrix is given by

$$s_0(k) = e^{2i\eta_0(k)} = s_0^{\mathrm{bg}}(k)\cdot s_0^{\mathrm{res}}(k) = e^{-2ik}\cdot\frac{K_0\cot K_0 + ik}{K_0\cot K_0 - ik}. \tag{7.8}$$

The S matrix factorizes and there is a slowly varying background part and a resonant part which has poles wherever $\mathfrak{f}_0(k) = 0$. The scattering phase $\eta_0(k)$ reads

$$\eta_0(k) = \eta_0^{\mathrm{bg}}(k) + \eta_0^{\mathrm{res}}(k) = -k + \tan^{-1}\frac{k}{K_0\cot K_0}, \tag{7.9}$$

which can be calculated from $s_0(k)$ by simple trigonometric identities. The scattering phase is given by the slowly varying background scattering phase η_0^{bg} and the "resonant" part η_0^{res} which gives rise to resonance phenomena in the cross sections.

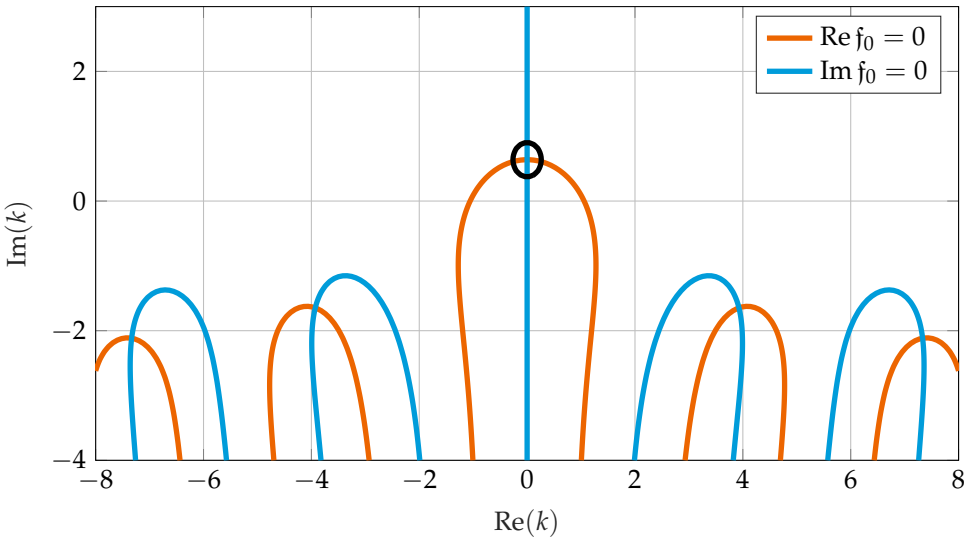

Figure 7.2: Real and imaginary zero contour lines of the Jost function $\mathfrak{f}_0$ for $l = 0$. The intersections of blue line and orange line indicate the positions of the zeros $\mathfrak{f}_0$. The black circle indicates the position $\varkappa_1$ of the zero of $\mathfrak{f}_0$ due to the bound state of the potential for the potential depth $\kappa = 2$.

7.1.1.1 *Pole expansion of the s-wave S matrix*

From the exact analytic solution we derive now the pole expansion of the S matrix. In figure 7.1 the square-well potential for a potential depth $\kappa = 2$ is shown. It is indicated that this potential contains a single bound state at the energy $E_{\text{bs}} = -\varkappa_1^2$. In section 5.7 we have discussed that bound states in the scattering potential occur as poles of the S matrix or correspondingly as zeros of the Jost function on the positive imaginary axis in the complex k plane. We study this now explicitly and investigate the Jost function in the complex k plane. The Jost function is a complex function with real part and imaginary part, reading

$$\mathfrak{f}_0(k) = \operatorname{Re}\mathfrak{f}_0(k) + i \operatorname{Im}\mathfrak{f}_0(k). \tag{7.10}$$

This function has a zero for $\operatorname{Re}\mathfrak{f}_0(k) = \operatorname{Im}\mathfrak{f}_0(k) = 0$. Figure 7.2 shows the zero contour lines of real part and imaginary part of $\mathfrak{f}_0(k)$ in the complex k plane for $\kappa = 2$.
Whenever the zero contour lines of real part and imaginary part intersect we obtain a zero of the Jost function in the complex k plane. It is seen that there is a single zero on the positive imaginary axis at $k_1 = i\varkappa_1$ indicated by the black circle. This zero is due to the bound state in the scattering potential. Figure 7.2 also shows other zeros in the lower half k plane which move away from the real axis as the absolute value of k becomes larger. One can either determine the positions of the zeros numerically or by an approximate analytic expression. In order to obtain an approximation we introduce the substitutions

$$k \equiv z\kappa_1, \quad z \equiv -i\cos w. \tag{7.11}$$

Inserting these substitutions in the Jost function (7.7), setting the Jost function to zero, $\mathfrak{f}_0(k) = 0$ we obtain the equation

$$\kappa \sin w = w + n\pi, \quad n \in \mathbb{N}_0^+. \tag{7.12}$$

Solving this equation for w and for all n we obtain the zeros of the Jost function. A further approximation is made for the zeros close to the origin of the complex k plane so that $|k|/\kappa_1 \ll 1$ and $w \approx \pi/2$. We can Taylor expand equation (7.12) at the point $w = \pi/2$ up to quadratic order and obtain

$$w_\pm = \frac{-1 + \pi\kappa_1 \pm \sqrt{1 - \pi\kappa_1 - 2n\pi\kappa_1 + 2\kappa_1^2}}{\kappa_1}. \tag{7.13}$$

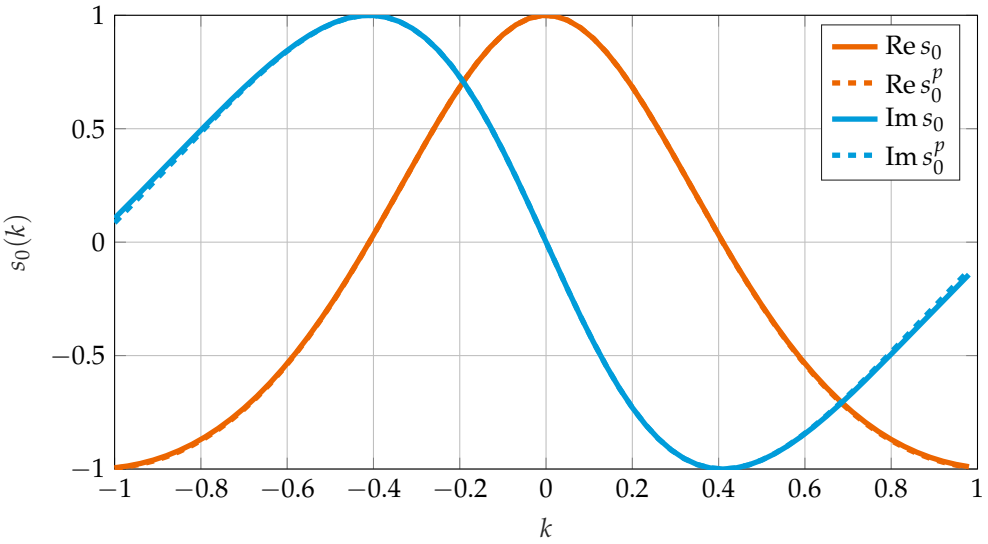

Figure 7.3: Real and imaginary part of the S matrix for $l = 0$. Shown are the exact solution $s_0(k)$ and the pole expansion $s_0^p(k)$. The potential depth is $\kappa = 2$.

The zero of the Jost function due to the first bound state of the potential is given by w_+ and $n = 0$, the zero of the Jost function due to the second bound state by w_+ and $n = 1$ and so forth. If there are N bound states and N' virtual states present in the scattering potential, the zero of the Jost function of the first virtual state is given by w_+ for $n = N$, for the second virtual state by w_+ for $n = N + 1$ and so forth up to $n = N + N' - 1$. The zeros of the Jost function due to scattering resonances of the potential are symmetric with respect to the imaginary axis and given by the two solutions $w_\pm$ for $n > N + N' - 1$.

For the potential depth $\kappa = 2$ we obtain with $n = 0$ for the zero of the Jost function due to the single bound state in the scattering potential $w_+ = 1.895$ which leads to a zero of the Jost function at $k_1 = i\mathcal{K}_1 = 0.637i$ with $\mathcal{K}_1 = 0.637$. Determining the position of this zero numerically leads to the result $\mathcal{K}_1 = 0.638$. Therefore, equation (7.13) gives a good approximation of the position of the zeros of the Jost function.

It was shown in section 5.7 that due to *Weierstrass factorization theorem* the Jost function can be represented as an infinite product in terms of its zeros and equivalently the S matrix as an infinite product in terms of its poles. We see in figure 7.2 that the single zero indicated by the black circle is close to the real axis and the others are far away. We make now the important assumption that the *Weierstrass expansion* of the Jost function given by (5.83) is dominated by this single zero close to the real axis. This corresponds to a single pole of the S matrix and therefore we assume that the pole expansion of the S matrix in (5.84) is given in terms of this single pole. The infinitely other zeros of the Jost function in the *Weierstrass expansion* correspond to infinitely many other poles in the pole expansion of the S matrix but we assume that the effect of all these other poles are given in terms of a background scattering phase $\eta_0^{p,\mathrm{bg}}$. The pole expansion (5.84) of the S matrix then reads

$$s_0^p(k) = s_0^{p,\mathrm{bg}}(k) \cdot s_0^{p,\mathrm{res}}(k) = e^{2i\eta_0^{p,\mathrm{bg}}(k)} \cdot \frac{\mathcal{K}_1 - ik}{\mathcal{K}_1 + ik}. \tag{7.14}$$

The background scattering phase $\eta_0^{p,\mathrm{bg}}$ is assumed to be a slowly varying function of k. We obtain this scattering phase by the assumption that s_0^p is a good approximation to the exact solution s_0. Therefore, we write $s_0^p \simeq s_0$, with s_0 given by (7.8), solve this equation for $\eta_0^{p,\mathrm{bg}}$ and do a series up to linear order in k, reading

$$\eta_0^{p,\mathrm{bg}}(k) = -\frac{i}{2}\left[s_0(0) + k\left(s(k')\frac{\mathcal{K}_1 + ik'}{\mathcal{K}_1 - ik'}\right)'\Big|_{k'=0} + \ldots\right] = (-a_{sc}\mathcal{K}_1 + 1)\,\frac{k_1}{\mathcal{K}_1} + \ldots, \tag{7.15}$$

where in the first equation the prime around the curly brackets indicates the derivative with respect to k' and in the second equation we have introduced the s-wave scattering length a_{sc} which we discuss in the next subsection.

In figure 7.3 the exact solution $s_0(k)$ is compared to the single-pole expansion $s_0^p(k)$. It can be seen that the real part and the imaginary part are almost identical. Therefore, the single-pole expansion (7.14) together with the assumption of a slowly varying background scattering phase (7.15), which is linear in k, is a very good approximation to the exact solution.

7.1.1.2 *Scattering length*

The s-wave scattering length is an important concept of scattering theory. It parametrizes the s-wave cross section and is a crucial parameter for the stability of a BEC [12]. We discuss the s-wave scattering length briefly in terms of the square-well potential. The scattering length is defined in the limit $k \to 0$. Therefore, we have to study the scattering wave function in this limit. For $l = 0$ the scattering wave function reads

$$\psi_{0,k}(r) = \begin{cases} (k/K_0)\mathfrak{f}_0^{-1}(k)\sin(K_0 r) & r \leq 1, \\ e^{i\eta_0(k)}\sin(kr + \eta_0(k)) & r > 1. \end{cases} \tag{7.16}$$

Comparing this solution in the outer region to the free solution for $V(r) = 0$, which is simply given by $\psi_{0,k}^{\text{free}}\sin(kr)$ illuminates the parametrization of the S matrix in terms of a scattering phase. The scattering due to the potential simply leads to a phase shift η_0 in the asymptotic region of the wave function.

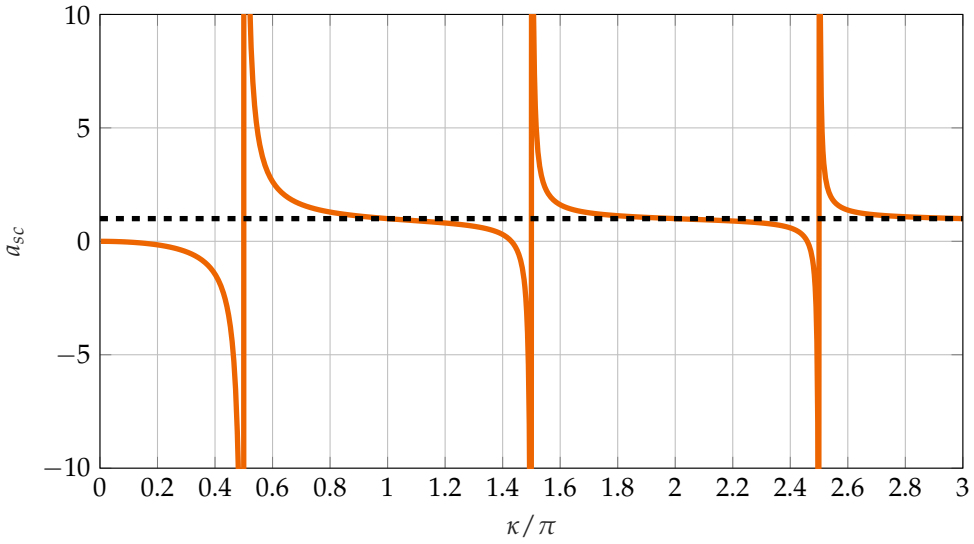

Figure 7.4: Scattering length a_{sc} for the square-well potential as a function of the potential depth κ. The black dashed line indicates the potential range $r_0 = 1$.

This phase shift contains all information about the scattering process. We now define the energy-independent s-wave scattering length a_{sc} by the equation

$$\eta_0(k) \equiv -ka_{sc}. \tag{7.17}$$

By this definition, the scattering phase is parametrized in terms of the scattering length a_{sc}. Note, that this parametrization is not unique and other ways of defining the scattering length are possible [118]. Now take a look at the continuity condition (7.4) of $\psi_{0,k}$, which in log-derivative form reads

$$K_0 \cot K_0 = k\cot(k + \eta_0(k)). \tag{7.18}$$

If we insert the parametrization of the scattering phase (7.17) in this continuity condition and evaluate it in the limit $k \to 0$ we obtain the s-wave scattering length a_{sc} for the square-well potential

$$a_{sc} = \left(1 - \frac{\tan\kappa}{\kappa}\right). \tag{7.19}$$

From this definition we see that a_{sc} may take positive and negative values and can also diverge at certain points. This is shown in figure 7.4 which shows a_{sc} as a function of the potential depth. The scattering length diverges for $\kappa = (n + 1/2)\pi$ with $n \in \mathbb{N}_0^+$. For these particular potential strengths, a bound state occurs at the potential at $E = 0$. For $l = 0$ these bound states at $E = 0$ are called *half-bound states* [37]. If the potential is slightly too shallow to support bound states we have a virtual state with $E_{\mathrm{vs}} > 0$ and in the presence of virtual states, the scattering length is largely negative. For a slightly deeper potential with a *weakly bound state* the scattering length jumps to a largely positive value while it diverges for a *half-bound state*. For the square-well potential the scattering length a_{sc} is typically on the order of the potential range.

As mentioned above, the scattering length a_{sc} parametrizes the s-wave scattering cross section in the limit $k \to 0$ and the cross section reads

$$\sigma_0(k) \underset{k\to 0}{\longrightarrow} 4\pi a_{sc}^2. \tag{7.20}$$

From the statements above it becomes clear that for potential strengths with a weakly bound state or a virtual state, the s-wave cross section becomes very large.

7.1.2 *Pole expansion of the p-wave S matrix*

After this excursion to the scattering length we return to the discussion of the pole expansion of the S matrix for the single-channel square-well potential for low partial waves, in particular in this subsection for p-wave scattering. For $l = 1$ the Jost function reads

$$\mathfrak{f}_1(k) = \frac{e^{ik}\left(k^2 K_0 \cos K_0 + (\kappa^2 - ikK_0^2)\sin K_0\right)}{K_0^3}. \tag{7.21}$$

and the S matrix is given by

$$s_1(k) = e^{2i\eta_1(k)} = s_1^{\mathrm{bg}}(k)\cdot s_1^{\mathrm{res}}(k) = e^{-2ik}\cdot\frac{\kappa^2 + k^2 K_0\cot K_0 + ikK_0^2}{\kappa^2 + k^2 K_0\cot K_0 - ikK_0^2}. \tag{7.22}$$

Again, the S matrix factorizes in a background term and a resonant term and the scattering phase η_1 is given by

$$\eta_1(k) = \eta_1^{\mathrm{bg}}(k) + \eta_1^{\mathrm{res}}(k) = -k + \tan^{-1}\frac{kK_0^2}{\kappa^2 + k^2 K_0\cot K_0}, \tag{7.23}$$

where η_1^{bg} is the background scattering phase η_1^{res} is the resonant scattering phase.

Here we study a particular example where the effective potential contains a single resonant state which is called a quasi-bound state. Figure 7.5 shows this situation for a potential depth $\kappa = 3$. The position of the quasi-bound state is given by $E_{\mathrm{qbs}} = \mathrm{Re}^2\, k_1 - \mathrm{Im}^2\, k_1$.

Due to the discussion of section 5.7 we know that the quasi-bound state occurs as two poles of the S matrix in the complex k plane at k_1 and $-k_1^*$ which are the zeros of the Jost function. In figure 7.6 we show the zero contour lines of the Jost function for $\kappa = 3$, $\mathrm{Re}\,\mathfrak{f}_1(k) = 0$, $\mathrm{Im}\,\mathfrak{f}_1(k) = 0$ and the zeros of the Jost function are given by the intersections these zero contour lines. Indeed, there are two zeros close to the real axis which are due to the quasi-bound state of the scattering potential. These zeros are indicated by the black circles. We determine the position of the zeros numerically and obtain $k_1 = 0.539 - 0.100i$. The other zeros of the Jost function move away from the real axis for larger values of the absolute value $|k|$. All these zeros correspond to poles of the S matrix and we assume that the pole expansion of the S

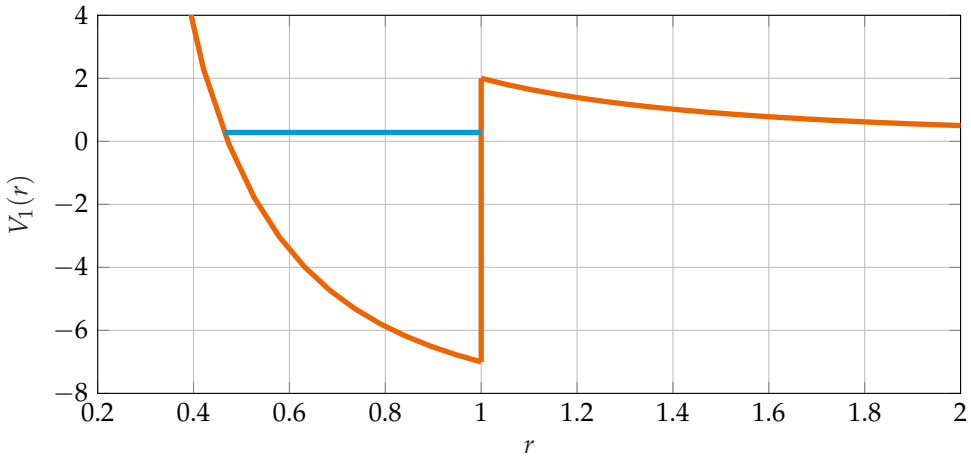

Figure 7.5: Effective single channel square-well potential for $l = 1$. The potential depth is $\kappa = 3$ and the potential contains one single resonant state close to threshold (also called quasi-bound state) at $E_1 = \mathrm{Re}^2\, k_1 - \mathrm{Im}^2\, k_1$, indicated as blue solid line.

matrix (5.84) is given in terms of a single term due to the poles at k_1 and $-k_1^*$. Again we assume that the effect of all the other poles can be written in a background scattering phase $\eta_1^{p,\mathrm{bg}}$ and the pole expansion of the S matrix reads

$$s_1^p(k) = s_1^{p,\mathrm{bg}}(k) \cdot s_1^{p,\mathrm{res}}(k) = e^{2i\eta^{p,\mathrm{bg}}(k)} \cdot \frac{|k_1|^2 - k^2 - 2ik\,\mathrm{Im}\,k_1}{|k_1|^2 - k^2 + 2ik\,\mathrm{Im}\,k_1}, \tag{7.24}$$

where the S matrix factorizes in a background part $s_1^{p,\mathrm{bg}}$ and a resonant part $s_1^{p,\mathrm{res}}$. We assume again, that the background scattering phase $\eta_1^{p,\mathrm{bg}}$ is slowly varying function of k which can be obtained from $s_1^p(k) \simeq s_1(k)$, with $s_1(k)$ given by equation (7.22), and a linear approximation, valid for small k, reading

$$\eta_1^{p,\mathrm{bg}}(k) = -\frac{i}{2}\left[s_1(0) + k \cdot \left(s_1(k')\frac{|k_1|^2 - k'^2 + 2ik'\,\mathrm{Im}\,k_1}{|k_1|^2 - k'^2 - 2ik'\,\mathrm{Im}\,k_1}\right)'\Bigg|_{k'=0} + \ldots\right]. \tag{7.25}$$

In figure 7.7 the exact solution $s_1(k)$ is compared to the pole expansion $s_1^p(k)$. Both, real part and imaginary part of the S matrix are almost identical. Again the pole expansion (7.14) together with the assumption of a slowly varying background scattering phase (7.15) which is linear in k is a very good approximation to the exact solution. In contrast to the single-pole expansion of the s-wave S matrix, the pole expansion shown in this subsection is now given in terms of two poles of the S matrix due to the quasi-bound state in the scattering potential. However, with s_1^p given by equation (7.24), these two poles can be written in a single term.

Breit-Wigner formula

The form of $s_1^p(k)$ has an interesting consequence for the scattering cross section. In equation (5.72) of chapter 5 the relation between partial cross section and S matrix was established. If we only assume the resonant part $s_1^{p,\mathrm{res}}$ of the pole expansion s_1^p, we obtain the *Breit-Wigner form* [37] of the resonant part of the partial cross section as

$$\sigma_1^{\mathrm{res}} = \frac{6\pi}{k^2}\left(1 - \mathrm{Re}\, s_1^{p,\mathrm{res}}\right) = \frac{12\pi}{\mathrm{Re}^2\, k_1}\frac{(\Gamma/2)^2}{(E_1 - E)^2 + (\Gamma/2)^2}, \tag{7.26}$$

where we have introduced the resonance width $\Gamma/2 \equiv 2\,\mathrm{Re}\,k_1\,\mathrm{Im}\,k_1$ and the resonance position $E_1 \equiv \mathrm{Re}^2\, k_1 - \mathrm{Im}^2\, k_1$. This resonance position was indicated in the beginning of this subsection in figure 7.5 as the energy position of the quasi-bound state or equivalently, as seen in equation (7.26), as the resonance position in the scattering cross section.

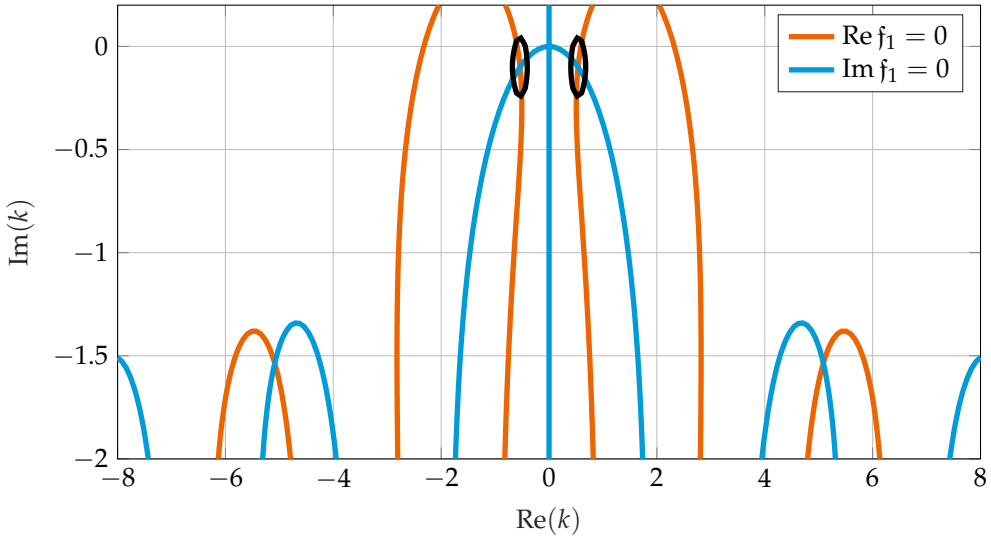

Figure 7.6: Real and imaginary zero contour lines of the Jost function $\mathfrak{f}_1$ for $l = 1$. The intersections of blue line and orange line indicate the positions of the zeros $\mathfrak{f}_1$. The black circles indicate the positions κ_1, $-\kappa_1^*$ of the zero of $\mathfrak{f}_1$ due to the quasi-bound state of the potential for the potential depth $\kappa = 3$.

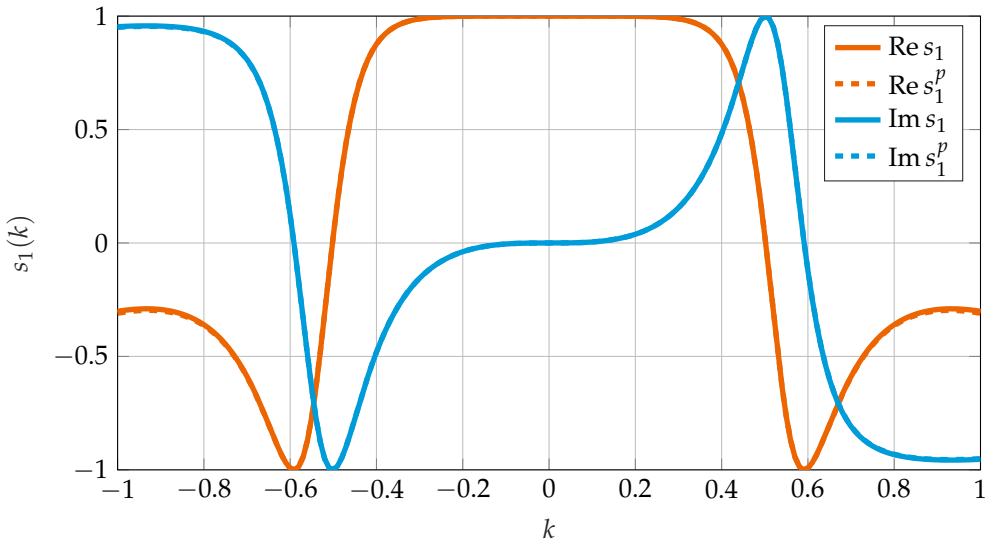

Figure 7.7: Real and imaginary part of the S matrix for $l = 1$. Shown are the exact solution $s_1(k)$ and the pole expansion $s_1^p(k)$. The potential depth is $\kappa = 3$.

7.1.3 *Pole expansion of the d-wave S matrix*

Having discussed the pole expansion of the S matrix for $l = 1$ in terms of a quasi-bound state we repeat this discussion in this subsection for $l = 2$. There is no fundamental difference to the case of $l = 1$ but we want to point out some subtleties which occur for higher partial waves. In addition, in cold Ne* collisions, there are also d-wave contributions present and therefore we discuss this particular case explicitly. For $l = 2$ the Jost function is given by

$$\mathfrak{f}_2(k) = \frac{e^{ik}}{K_0^5}\left[\left(k^4 - 3\kappa^2 + 3ik\kappa^2 + k^2\kappa^2\right) K_0 \cos K_0 - i\left(k^5 + 3i\kappa^2 + 3k\kappa^2 + k^3\kappa^2\right)\sin K_0\right], \quad (7.27)$$

and the S matrix by

$$\begin{aligned} s_2(k) =& e^{2i\eta_2(k)} = s_2^{\mathrm{bg}}(k)\cdot s_2^{\mathrm{res}}(k) \\ =& e^{-2ik}\frac{\left(k^4 - 3\kappa^2 + k^2\kappa^2\right) K_0 \cot K_0 + 3\kappa^2 + i\left(k^5 + 3k\kappa^2 + k^3\kappa^2 - 3k\kappa^2 K_0 \cot K_0\right)}{\left(k^4 - 3\kappa^2 + k^2\kappa^2\right) K_0 \cot K_0 + 3\kappa^2 - i\left(k^5 + 3k\kappa^2 + k^3\kappa^2 - 3k\kappa^2 K_0 \cot K_0\right)}. \end{aligned} \quad (7.28)$$

The scattering phase $\eta_2(k)$ reads

$$\eta_2(k) = \eta_2^{\mathrm{bg}}(k) + \eta_2^{\mathrm{res}}(k) = -k + \tan^{-1}\frac{k^5 + 3k\kappa^2 + k^3\kappa^2 - 3k\kappa^2 K_0 \cot K_0}{\left(k^4 - 3\kappa^2 + k^2\kappa^2\right) K_0 \cot K_0 + 3\kappa^2}. \quad (7.29)$$

containing the background part η_2^{bg} and the resonant part η_2^{res}.

We choose the potential depth $\kappa = \sqrt{19.5}$. This potential depth contains a single quasi-bound state at $E_2 = \mathrm{Re}^2\, k_2 - \mathrm{Im}^2\, k_2^2$, with k_2 the zero of the Jost function in the complex k plane due to this quasi-bound state. In figure 7.8 the zero contour lines $\mathrm{Re}\,\mathfrak{f}_2(k) = 0$, $\mathrm{Im}\,\mathfrak{f}_2(k) = 0$ are shown in the complex k plane for $\kappa = \sqrt{19.5}$.

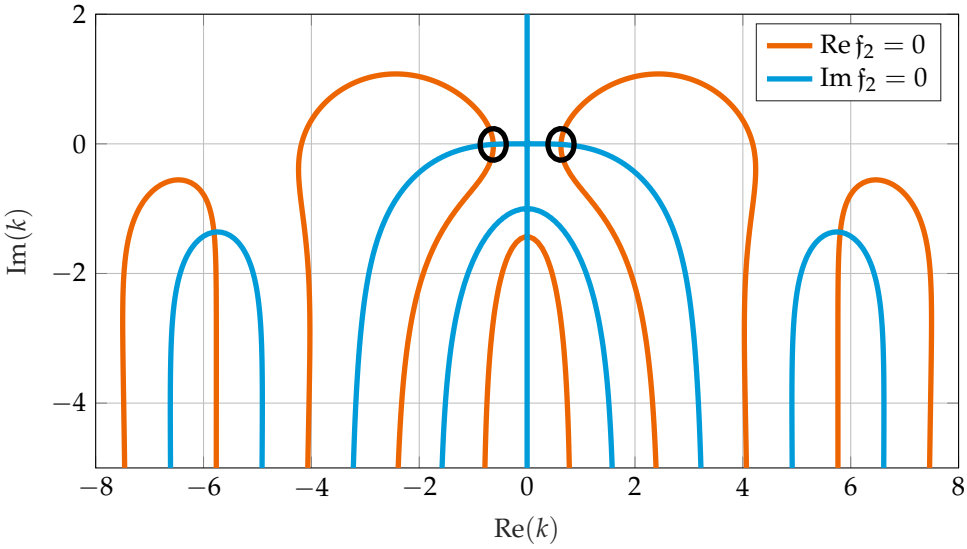

Figure 7.8: Real and imaginary zero contour lines of the Jost function $\mathfrak{f}_2$ for $l = 2$. The intersections of blue line and orange line indicate the positions of the zeros $\mathfrak{f}_2$. The black circles indicate the positions k_2, $-k_2^*$ of the zero of $\mathfrak{f}_2$ due to the quasi-bound state of the potential for the potential depth $\kappa = \sqrt{19.5}$.

The intersections of these contour lines indicate the zeros of $\mathfrak{f}_2(k)$. The two zeros due to the quasi-bound state are indicated by the black circles. Again, different zeros can be observed which move away from the real axis. We determine the position of the zeros due to the quasi-bound state numerically and obtain $k_2 = 0.628 - 0.009i$. The zeros of the Jost function correspond to the poles of the S matrix and again assume that the pole expansion of the S matrix in (5.84) is dominated by a single term due to the poles at k_2 and $-k_2^*$. The effect of all

the other zeros of the Jost function, or equivalently of the poles of the S matrix, is assumed to be small and can be summarized in a background scattering phase $\eta_2^{p,\mathrm{bg}}$. We obtain

$$s_2^p(k) = s_2^{p,\mathrm{bg}}(k) \cdot s_2^{p,\mathrm{res}}(k) = e^{2i\eta_2^{p,\mathrm{bg}}(k)} \cdot \frac{|k_2|^2 - k^2 - 2ik \operatorname{Im} k_2}{|k_2|^2 - k^2 + 2ik \operatorname{Im} k_2}, \tag{7.30}$$

where $\eta_2^{p,\mathrm{bg}}(k)$ is found from $s_2^p(k) \simeq s_2(k)$, with $s_2(k)$ given by equation (7.28), and a linear expansion in k, reading

$$\eta_2^{p,\mathrm{bg}}(k) = -\frac{i}{2}\left[s_2(0) + k \cdot \left(s_2(k') \frac{|k_2|^2 - k'^2 + 2ik' \operatorname{Im} k_2}{|k_2|^2 - k'^2 - 2ik' \operatorname{Im} k_2}\right)' \Bigg|_{k'=0} + \ldots\right]. \tag{7.31}$$

In figure 7.9 we compare the real and imaginary part of the exact solution $s_2(k)$ and the pole expansion $s_2^p(k)$. Again, the exact solution and the pole expansion again agree very well. However, for larger values of k we see a deviation of the pole expansion from the exact solution which is more prominent than in the case of p-wave scattering. One can correct for these deviations by taking into account also higher order terms in the expansion of the background scattering phase $\eta_2^{p,\mathrm{bg}}$. However, for higher partial waves, the potential barriers become higher and the scattering resonances become narrower. Therefore, it becomes more challenging to describe the correct behavior of $s_l(k)$ for small values of k as well as the correct shape of the resonances. In this case, one might has to take into account further poles in the pole expansion.

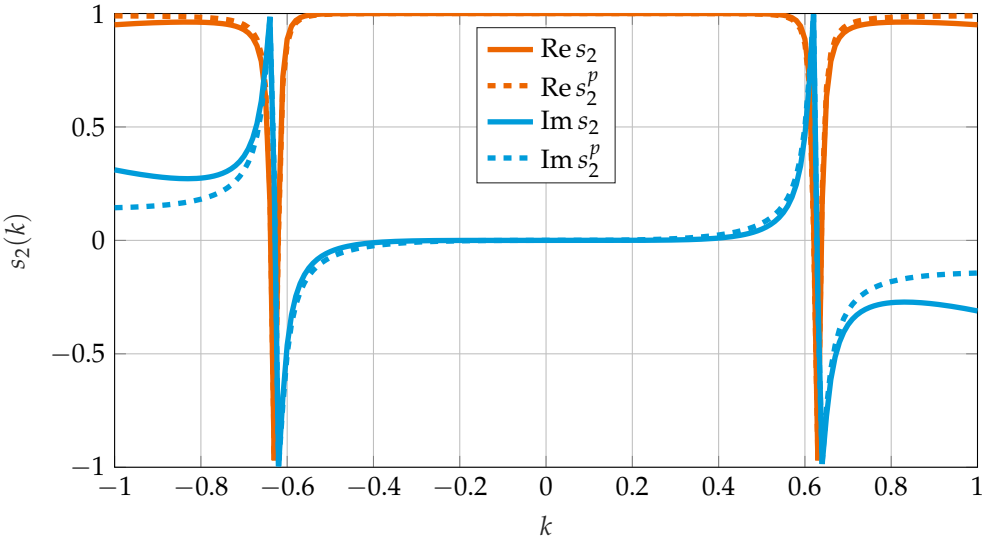

Figure 7.9: Real and imaginary part of the S matrix for $l = 2$. Shown are the exact solution $s_2(k)$ and the pole expansion $s_2^p(k)$. The potential depth is $\kappa = \sqrt{19.5}$.

7.2 COUPLED TWO-CHANNEL SOLUTIONS

From the study of the analytic solutions of the single-channel square well potential we now introduce the coupled two-channel square-well potential which is a model for reactive collisions of Ne*. Figure 7.10 shows a scheme of the two-channel model with an incoming wave $\mathbf{k}_1$ in channel 1 where a fraction scatters elastically and stays in channel 1 and the other fraction scatters inelastically and couples in channel 2 with wave vector $\mathbf{k}_2$. This transition models the ionization process in Ne* collisions.

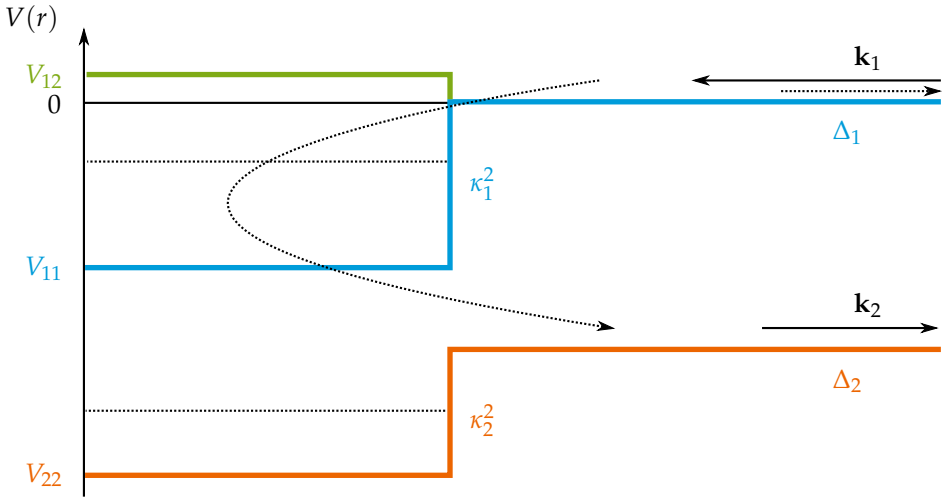

Figure 7.10: Coupled two channel square-well potential and notation. The curved dashed arrow indicates the inelastic process from the upper channel to the lower channel.

The reduced radial Schrödinger equation for this system in dimensionless units reads

$$\left[\frac{d^2}{dr^2} - V(r) - \frac{l(l+1)}{r^2} + k^2\right] \Psi^{\pm}_{l,k}(r) = 0, \tag{7.32}$$

where again we omit the $+$ superscript for the $+$ solution. The potential matrix reads

$$V(r) = \begin{pmatrix} V_{11} & V_{12} \\ V_{12} & V_{22} \end{pmatrix} = \begin{pmatrix} \Delta_1 - \kappa_1^2 & V_{12} \\ V_{12} & \Delta_2 - \kappa_2^2 \end{pmatrix}, \; r \leq 1, \quad V(r) = \begin{pmatrix} \Delta_1 & 0 \\ 0 & \Delta_2 \end{pmatrix}, \; r > 1, \tag{7.33}$$

with $V_{ii} = \Delta_i - \kappa_i^2 > 0$. This potential is piecewise constant and we can solve the radial Schrödinger equation analytically, obtaining

$$\Psi_{l,k}(r) = \begin{cases} \Psi^{\mathrm{I}}_{l,k}(r) = R \cdot \hat{\jmath}_l(K_{\pm} r) \cdot \phi_{\mathrm{coeff}} & r \leq 1, \\ \Psi^{\mathrm{II}}_{l,k}(r) = \dfrac{i}{2}\left\{\hat{h}^-_l(Kr) - \hat{h}^+_l(Kr) K^{-1/2} S_l(k) K^{1/2}\right\} & r > 1, \end{cases} \tag{7.34}$$

with $S_l(k)$ the S matrix and K the diagonal matrix with the matrix elements $[K]_{ij} = k_i \delta_{ij}$ and $k_i = \sqrt{k^2 - \Delta_i}$. The matrix R is given by

$$R = \begin{pmatrix} \cos\alpha & -\sin\alpha \\ \sin\alpha & \cos\alpha \end{pmatrix}, \tag{7.35}$$

where the angle α is defined as

$$\sin\alpha \equiv \frac{V_{12}}{\left(2V_{12}^2 + \frac{1}{2}J\left(J + \sqrt{J^2 + 4V_{12}^2}\right)\right)^{1/2}}, \tag{7.36}$$

with $J = V_{11} - V_{22}$. This matrix performes a rotation into a system where the potential matrix is diagonal with the eigenvalues

$$\lambda_{\pm}(r) = \frac{1}{2}\left(V_{11} + V_{22} \pm \sqrt{J^2 + 4V_{12}^2}\right). \tag{7.37}$$

The matrix $\hat{\jmath}_l(K_\pm r)$ in the inner region is given by

$$\hat{\jmath}_l(K_\pm r) = \begin{pmatrix} \hat{\jmath}_l(K_+ r) & 0 \\ 0 & \hat{\jmath}_l(K_- r) \end{pmatrix}, \tag{7.38}$$

where we have $K_+ \equiv \sqrt{k^2 - \lambda_+}$, $\quad K_- \equiv \sqrt{k^2 - \lambda_-}$. The coefficient matrix is given in terms of the Jost matrix $\mathfrak{F}_l(k)$ and reads

$$\phi_{\text{coeff}} = \begin{pmatrix} (k_1/K_+)^{l+1} \cos\alpha & (k_2/K_+)^{l+1} \sin\alpha \\ -(k_1/K_-)^{l+1} \sin\alpha & (k_2/K_-)^{l+1} \cos\alpha \end{pmatrix} \mathfrak{F}_l^{-1}(k), \tag{7.39}$$

This ansatz is obtained from the relation of the regular solution and the scattering wave function (5.145) together with the boundary condition of the regular solution at the origin (5.142) and the behavior of the Riccati-Bessel functions at the origin [see equation (C.15)]. The solutions for $S_l(k)$ and $\mathfrak{F}_l(k)$ are obtained from the boundary conditions

$$\Psi^{\text{I}}_{l,k}(1) = \Psi^{\text{II}}_{l,k}(1), \quad \Psi^{\text{I}\prime}_{l,k}(1) = \Psi^{\text{II}\prime}_{l,k}(1). \tag{7.40}$$

If we define the function

$$g_l(k, K_0) \equiv 2i \left(\frac{k}{K_0}\right)^{l+1} \frac{\hat{\jmath}_l'(K_0)\hat{h}_l^+(k) - \hat{h}_l^{+\prime}(k)\hat{\jmath}_l(K_0)}{\hat{h}_l^{+\prime}(k)\hat{h}_l^-(k) - \hat{h}_l^{-\prime}(k)\hat{h}_l^+(k)}, \tag{7.41}$$

we can write the diagonal matrix elements $\mathfrak{f}_{l,ii}$ for the full solution of the Jost matrix $\mathfrak{F}_l$ as

$$\mathfrak{f}_{l,11} = g_l(k_1, K_+)\cos^2\alpha + g_l(k_1, K_-)\sin^2\alpha, \tag{7.42}$$

$$\mathfrak{f}_{l,22} = g_l(k_2, K_-)\cos^2\alpha + g_l(k_2, K_+)\sin^2\alpha, \tag{7.43}$$

and the off-diagonal elements $\mathfrak{f}_{l,i\neq j}$ as

$$\mathfrak{f}_{l,12} = \frac{1}{2}\sin 2\alpha\,(k_2/k_1)^{l+1}\,[g_l(k_1, K_+) - g_l(k_1, K_-)] \tag{7.44}$$

$$\mathfrak{f}_{l,21} = \frac{1}{2}\sin 2\alpha\,(k_1/k_2)^{l+1}\,[g_l(k_2, K_+) - g_l(k_2, K_-)] \tag{7.45}$$

The S matrix can be calculated from equation (5.149). We are interested in parametrizing the two-body loss rate coefficients which are given in this square-well model by the inelastic scattering of channel 1 to channel 2. This transition is given by the off-diagonal S matrix element $s_{l,12}$ which, in terms of the Jost functions, reads

$$s_{l,12}(k) = \frac{\mathfrak{f}^*_{l,12}(k)\mathfrak{f}_{l,11}(k) - \mathfrak{f}^*_{l,11}(k)\mathfrak{f}_{l,12}(k)}{\det \mathfrak{F}_l(k)} \sqrt{\frac{k_1}{k_2}}. \tag{7.46}$$

The results so far in this section are exact solutions. We assume next, that the coupling matrix element V_{12} between the two channels is small. Therefore, we perform a series in terms of the coupling strength V_{12} in lowest order and obtain the solutions in the Distorted-Wave Born Approximation.

7.2.1 *Low coupling expansion of the S matrix*

A Taylor series of the diagonal Jost matrix elements for small V_{12} up to quadratic order gives the result

$$\mathfrak{f}_{l,ii} = \mathfrak{f}^{(0)}_{l,ii} + \mathcal{O}\left(V_{12}^2\right), \tag{7.47}$$

where $\mathfrak{f}^{(0)}_{l,ii}$ is simply the single-channel Jost function given by equation (7.6) with (k, K) replaced with (k_1, K_1) for $\mathfrak{f}^{(0)}_{l,11}$ and with (k, K) replaced with (k_2, K_2) for $\mathfrak{f}^{(0)}_{l,22}$. Here K_1 and K_2 are given by

$$K_1^2 \equiv k^2 - V_{11} = k_1^2 + \kappa_1^2, \quad K_2^2 \equiv k^2 - V_{22} = k_2^2 + \kappa_2^2. \tag{7.48}$$

The (0) in (7.47) indicates that this term is of 0th order in V_{12}. The off-diagonal Jost matrix elements are of first order in V_{12} and read

$$\mathfrak{f}_{l,12}^{(1)} = \frac{V_{12}}{K_2^2 - K_1^2} \left(k_2/k_1\right)^{l+1} \left[g_l(k_1, K_1) - g_l(k_1, K_2)\right] + \mathcal{O}\left(V_{12}^2\right), \tag{7.49}$$

$$\mathfrak{f}_{l,21}^{(1)} = \frac{V_{12}}{K_2^2 - K_1^2} \left(k_2/k_1\right)^{l+1} \left[g_l(k_2, K_1) - g_l(k_2, K_2)\right] + \mathcal{O}\left(V_{12}^2\right). \tag{7.50}$$

In this order, we obtain the transition S matrix element $s_{l,12}$ from equation (7.46) as

$$s_{l,12}^{(1)}(k) = \frac{\mathfrak{f}_{l,12}^{(1)*}(k)\mathfrak{f}_{l,11}^{(0)}(k) - \mathfrak{f}_{l,11}^{(0)*}(k)\mathfrak{f}_{l,12}^{(1)}(k)}{\mathfrak{f}_{l,11}^{(0)}(k)\mathfrak{f}_{l,22}^{(0)}(k)} \sqrt{\frac{k_1}{k_2}} + \mathcal{O}\left(V_{12}^2\right). \tag{7.51}$$

This result is of special importance because it shows that the denominator is simply given by the single-channel Jost functions (7.6) for the two uncoupled channels. In order to study the poles of the coupled channel $s_{l,12}^{(1)}$ matrix element one has to study the zeros of the single-channel Jost function which has already been done in the previous subsections for s-wave, p-wave and d-wave scattering respectively. In order to perform a single-pole expansion of $s_{l,12}^{(1)}$ in channel 1 one simply has to check that the dominant pole of the S matrix is given by the zero of the uncoupled solution $\mathfrak{f}_{l,11}^{(0)}$ in channel 1 and that there are no other zeros of $\mathfrak{f}_{l,22}^{(0)}$ of the second channel close to threshold. This will be studied in the next subsection. Beforehand we give the explicit expressions of $s_{l,12}^{(1)}$ for s-wave and p-wave scattering which read for s-wave scattering

$$s_{0,12}^{(1)} = 2i\sqrt{k_1 k_2} e^{-i(k_1+k_2)} \frac{V_{12}}{K_2^2 - K_1^2} \frac{K_2 \cot K_2 - K_1 \cot K_1}{(K_2 \cot K_2 - ik_2)(K_1 \cot K_1 - ik_1)}, \tag{7.52}$$

and for p-wave scattering

$$s_{1,12}^{(1)} = 2i \left(k_1 k_2\right)^{3/2} e^{-i(k_1+k_2)} \frac{V_{12}}{K_2^2 - K_1^2} \frac{K_1^2 K_2 \cot K_2 - K_1 K_2^2 \cot K_1 + K_2^2 - K_1^2}{(\kappa_1^2 + k_1^2 K_1 \cot K_1 - ik_1 K_1^2)(\kappa_2^2 + k_2^2 K_2 \cot K_2 - ik_2 K_2^2)}. \tag{7.53}$$

Here one can see explicitly that the denominators are given by the single-channel Jost functions (7.7), (7.21) of the two uncoupled channels. We have also performed a pole expansion of d-wave scattering but do not give an explicit expression for $s_{2,12}^{(1)}$ as it is too lengthy. However, as for $l = 0$ and $l = 1$ the denominator is given by the product of the single-channel Jost functions (7.27) of the uncoupled channels 1, 2 for $l = 2$.

The results of this subsection can also be obtained from the Distorted-Wave Born Approximation (DWBA) [38] where the potential is split in two parts

$$V = V_{\mathrm{I}} + V_{\mathrm{II}} = \begin{pmatrix} V_{11} & 0 \\ 0 & V_{22} \end{pmatrix} + \begin{pmatrix} 0 & V_{12} \\ V_{12} & 0 \end{pmatrix}. \tag{7.54}$$

Solving the reduced radial Schrödinger equation (7.32) with potential V_{I} simply leads to the uncoupled single-channel solutions discussed in the previous section. The solutions for $V(r)$ in lowest order are then given by the matrix elements of V_{II} in terms of the uncoupled solutions. We obtain for the transition S matrix element

$$s_{l,12}^{(1)} = -\frac{2i}{\sqrt{k_1 k_2}} V_{12} \int_0^1 dr\ \psi_{l,11}^{+(0)}(r) \cdot \psi_{l,22}^{+(0)}(r), \tag{7.55}$$

where $\psi_{l,11}^{+(0)}(r)$, $\psi_{l,22}^{+(0)}(r)$ are the uncoupled solutions of channel 1 and 2, given by (7.3) with (k, K) replaced by (k_1, K_1) for channel 1 and with (k, K) replaced by (k_2, K_2) for channel 2.

In order to parametrize the two-body loss rate coefficients we therefore apply the results of the pole expansion of the uncoupled solutions to the matrix element $s_{l,12}^{(1)}$.

7.2.2 *Parametrization of two-body loss rate coefficients*

Here we introduce the pole expansion of $s^{(1)}_{l,12}$ for s-wave, p-wave and d-wave scattering in order to obtain the pole expansion for the two-body loss rate coefficients. For the coupled two-channel square-wells we choose the potential depths

$$l = 0: \ \kappa_1^2 = \kappa_2^2 = 4, \qquad l = 1: \ \kappa_1^2 = \kappa_2^2 = 9, \qquad l = 2: \ \kappa_1^2 = \kappa_2^2 = 19.5, \tag{7.56}$$

and for all three cases $\Delta_1 = 0$, $\Delta_2 = -3$ and the coupling strength $V_{12} = 0.1$. Note, that the potential depths correspond to the potential depths of the single-channel scattering case. From equation (7.53) we conclude that the poles of $s^{(1)}_{l,12}$ are given by the zeros of the uncoupled Jost functions $f^{(0)}_{l,ii}$ and we can adopt the results of single-channel scattering.

In order to check for the zeros of the uncoupled Jost functions $f^{(0)}_{l,ii}$ as functions of the upper channel wave number k_1 we show in figure 7.11a and in figure 7.11b the zero contour lines of real part and imaginary part of the Jost functions of the uncoupled scattering channels $\mathfrak{f}^{(0)}_{11}$, $\mathfrak{f}^{(0)}_{22}$ for $l = 0$ and $l = 1$.

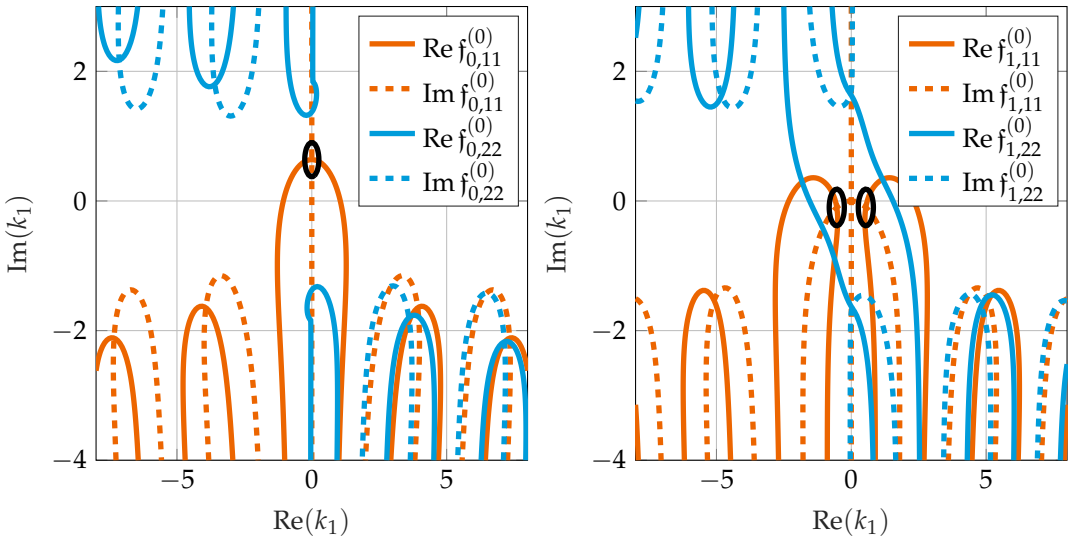

(a) $l = 0$ (b) $l = 1$

Figure 7.11: Zero contour lines of the uncoupled Jost functions of scattering channel 1 and 2 as functions of the channel wave number k_1 of channel 1 for $l = 0, 1$. The black circle in figure (a) indicates the position $\mathcal{K}_1$ of the zero of $f^{(0)}_{0,11}$. The black circles in figure (b) indicate the positions $\mathcal{k}_1$, $-\mathcal{k}_1^*$ of the zeros of $f^{(0)}_{1,11}$.

It is shown that the uncoupled Jost function of the upper channel corresponds to the Jost function of single-channel scattering which was displayed in figure 7.2 for $l = 0$ and in figure 7.6 for $l = 1$. The zeros of the Jost functions of the lower channel are far away from the real k axis and threshold. As in the single-channel case, we can expect that the pole expansion of the $s_{l,12}$ matrix elements is dominated by the zeros of the Jost function closest to the real axis. As a function of k_1 the positions of these zeros were already determined as $\mathcal{K}_1$, $\mathcal{k}_1$, $-\mathcal{k}_1^*$, $\mathcal{k}_2$ and $-\mathcal{k}_2$. We assume that the pole expansion is given by

$$s^p_{0,12}(k_1) = \frac{\exp[2i\eta_0^{\mathrm{bg}}(k_1)]}{\mathcal{K}_1 - ik_1}, \tag{7.57a}$$

$$s^p_{l,12}(k_1) = \frac{\exp[2i\eta_l^{\mathrm{bg}}(k_1)]}{|\mathcal{k}_l|^2 - k_1^2 + 2ik_1 \operatorname{Im} \mathcal{k}_l}, \tag{7.57b}$$

where the second line holds for $l = 1, 2$. In this pole expansion it is assumed again that η_0^{bg}, η_1^{bg}, η_2^{bg} are slowly varying background scattering phases. We assume that the pole expansion

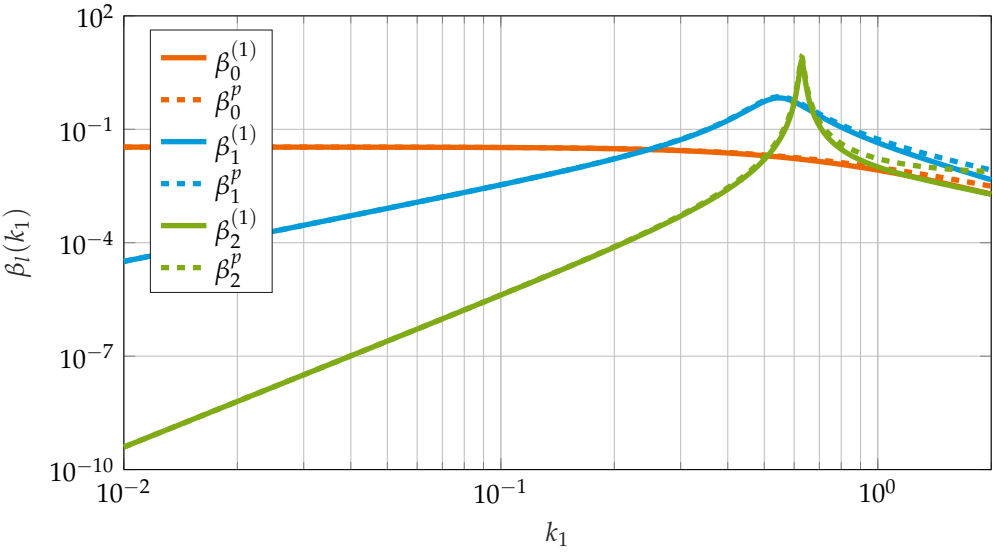

Figure 7.12: Partial two-body loss rate coefficients β_l. Compared are the DWBA two-body loss parameters $\beta_l^{(1)}$ to the two-body loss parameters β_l^p obtained from the pole expansion of the S matrix. The *Wigner-Threshold behavior* can be observed for the different partial wave contributions.

is a good approximation to the DWBA solution so that $s_{0,12}^p \simeq s_{0,12}^{(0)}$ and $s_{l,12}^p \simeq s_{l,12}^{(0)}$. Similarly to the single-channel scattering case we then obtain the background scattering phases from a series of k in zero. The background scattering lengths then read

$$\eta_0^{\mathrm{bg}}(k_1) = -\frac{i}{2}\left[\left(s_{0,12}^{(1)}(k_1)\cdot(\mathcal{K}_1 - ik_1)\right)|_{k_1=0} + k_1\left(s_{0,12}^{(1)}(k_1)\cdot(\mathcal{K}_1 - ik_1)\right)'|_{k_1=0} + \ldots\right] \tag{7.58a}$$

$$= \log a_0 + k_1 b_0 + \ldots, \tag{7.58b}$$

$$\eta_l^{\mathrm{bg}}(k_1) = -\frac{i}{2}\left[\left(s_{l,12}^{(1)}(k_1)\cdot(|\mathcal{k}_l|^2 - k_1^2 + 2ik_1\,\mathrm{Im}\,\mathcal{k}_l)\right)|_{k_1=0}\right.$$
$$\left. + k_1\left(s_{l,12}^{(1)}(k_1)\cdot(|\mathcal{k}_l|^2 - k_1^2 + 2ik_1\,\mathrm{Im}\,\mathcal{k}_l)\right)'|_{k_1=0} + \ldots\right] \tag{7.58c}$$

$$= \log a_l + k_1 b_l + \ldots, \tag{7.58d}$$

where the second line holds again for $l = 1, 2$ and where we have introduced the coefficients a_l, b_l which are the expansion coefficients in given in terms of the potential parameters. In this approximation the series of η^{bg} in $k = 0$ is crucial in order to obtain the correct behavior of the two-body loss rate coefficients for small k_1 as will be shown next. We define the unaveraged two-body loss rate coefficients as

$$\beta_l^{(1)}(k_1) \equiv 2\cdot\sigma_{l,12}^{\mathrm{inel}}(k_1)\cdot k_1 = \frac{2\pi}{k_1}(2l+1)|s_{l,12}^{(1)}|^2, \tag{7.59a}$$

$$\beta_l^p(k_1) \equiv 2\cdot\sigma_{l,12}^{\mathrm{inel}}(k_1)\cdot k_1 = \frac{2\pi}{k_1}(2l+1)|s_{l,12}^p|^2, \tag{7.59b}$$

where the first line is the two-body loss rate parameter obtained from the DWBA and the second line is the two-body loss parameter obtained from the pole expansion. With the pole expansion (7.57) together with the background scattering phases (7.58) we obtain for β_l^p the explicit results

$$\beta_0^p(k_1) = \frac{2\pi|a_0|^2}{k_1^2 + \mathcal{K}_1^2}, \tag{7.60a}$$

$$\beta_l^p(k_1) = \frac{2(2l+1)\pi|a_l|^2}{\left(k_1^2 - \varkappa_l^2\right)^2 + 4\,\mathrm{Re}^2\,\mathcal{k}_l\,\mathrm{Im}^2\,\mathcal{k}_l}\cdot k_1^{2l}, \tag{7.60b}$$

where $\varkappa_l^2 \equiv \mathrm{Re}^2\, k_l - \mathrm{Im}^2\, k_l$. The coefficients b_l of (7.58) vanished as they are purely imaginary. The factors k_1^{2l} show the familiar *Wigner-threshold behavior* [50, 54, 55] in the partial two-body loss rate coefficients β_l which are known to behave in the limit $k_1 \to 0$ as $\beta_l \to k_1^{2l}$. Therefore the linear approximation in (7.58) in $k = 0$ gives the correct threshold behavior of the two-body loss rate coefficients. This is an important result.

In figure 7.12 we compare β_l^p and $\beta_l^{(1)}$. It is seen that not only in the threshold regime ($k_1 \to 0$) the behavior of β_l is displayed correctly by the pole expansion β_l^p but also for higher wave numbers, where resonant behavior occurs, the pole expansion is an accurate approximation of the loss rates. Thus, the single-pole expansion (7.58) with the linear background scattering phase (7.58) is a very good approximation to the solutions of the DWBA and for low coupling strengths V_{12} to the full solution.

CONCLUSION

In this chapter we derived a parametrization of the two-body loss rate coefficients for the coupled two-channel model with square-well potentials for the lowest partial waves. In the course of the derivation of these rate coefficients we expanded the S matrix in terms of its poles in the complex k plane. We solved the Schrödinger equation for the single-channel square-well potential and the coupled two-channel case. We demonstrated that the pole expansion of the S matrix in terms of a single term due to the poles of the dominant bound, virtual or resonant state agrees very well with the analytic solutions. We showed this for the pole expansion in single-channel scattering as well as for two-channel scattering in the DWBA for $l = 0, 1, 2$. In the next chapter we show that the parametrized two-body loss rate coefficients describe ionizing collisions of Ne*.

8

TWO-CHANNEL MODEL WITH A REALISTIC INTERACTION POTENTIAL

Here, we present a coupled two-channel model with a realistic molecular interaction potential and a model ionization potential as a model for elastic and ionizing collisions of Ne*. It will be shown in this chapter, that this two-channel model incorporates the main features of Ne* scattering such as suppression of PI due to spin-polarization of the atoms, the *non-universal behavior* of the scattering rates and agrees with most of the experimental measurements for all different isotope mixtures.

The experimental data [2, 4, 5, 126, 127] on cold Ne* collisions suggests that different isotopes of Ne* show different scattering properties. Previously, the *quantum reflection model* has been applied successfully to cold reactive collisions of metastable rare gases [56–59]. It predicts *universal* behavior of scattering for different isotopes. We present in this chapter the basic ideas of the *quantum reflection model* and demonstrate that it does not describe cold collisions of Ne*. Instead, the two-channel model presented in this chapter replicates the scattering data of Ne* for different isotopes.

A generalization of the *quantum reflection model* is the *non-universal model* [60, 61]. We also give an overview of this model and compare its predictions for the two-body loss rate coefficients with these from the coupled two-channel model. We will see that the two-body loss rate coefficients of the *non-universal model* are a good parametrization of the two-body loss rate coefficients of the coupled two-channel model in the ultracold limit $T \to 0$ and the resulting parameters are consistent with the experimental observations. However, at finite temperatures, where most scattering rates were determined experimentally, we have to apply the coupled two-channel model.

Furthermore, we show that the two-channel model with square-well potentials, which was investigated in the previous chapter, gives a good description of the two-body loss rate coefficients in cold Ne* collisions. We fit the two-body loss rate coefficients of the coupled square-well potentials to the two-body loss rate coefficients of the coupled two-channel model and find good agreement of these results and also agreement with the experimental measurement.

8.1 POTENTIALS AND COUPLINGS

We present the coupled two-channel model for cold collisions of Ne* and introduce the potentials and couplings. The reduced radial two-channel Schrödinger equation for the relative motion of Ne* collisions in natural units reads

$$\left[\partial_r^2 + k^2 - \frac{l(l+1)}{r^2} - 2\mu V(r)\right] \psi_{l,k}(r) = 0, \tag{8.1}$$

with the reduced mass μ of the colliding atoms. We introduce the potential matrix

$$V(r) = \begin{pmatrix} V_{\text{int}}(r) & V_{12}(r) \\ V_{12}(r) & V_{\text{ion}}(r) \end{pmatrix}, \tag{8.2}$$

with the interaction potential V_{int}, the ionization potential V_{ion} and the coupling matrix element V_{12}. As discussed for the coupled two-channel square-well model in the previous chapter, one can calculate two-body loss rate coefficients in the two-channel model by calculating the

inelastic cross section from the interaction channel to the ionization channel. The interaction potential is given by

$$V_{\text{int}}(r) = \begin{cases} V_{\text{int,sr}}(r) & r \leq 20\ \text{a}_0, \\ V_{\text{int,lr}}(r) & r > 20\ \text{a}_0, \end{cases} \tag{8.3}$$

with a short-range part $V_{\text{int,sr}}$ and a long-range part $V_{\text{int,lr}}$. We choose the short-range part as the ${}^5\Pi_g$ molecular interaction potential of Ne* which is given in section 6.6. This quintet potential describes Ne* interactions with aligned internal spins and suppressed PI. The long-range part of the interaction potential reads

$$V_{\text{int,lr}}(r) = c_5/r^5 + c_6/r^6 + c_8/r^8 + c_{10}/r^{10}, \tag{8.4}$$

with the dispersion coefficients c_5 and c_6 as the physical parameters, describing the quadrupole–quadrupole interaction and the *van der Waals* interaction of Ne*, respectively. These coefficients are found from an optimization of the calculated scattering properties to experimental data points within the anisotropy given in table 6.2. The detailed description of the optimization routine will be given in section 8.5. The coefficients c_8 and c_{10} in equation (8.4) are also dispersion coefficients [108, 128] but here they serve as matching parameters to connect the short-range potential $V_{\text{int,sr}}$ to the long-range potential $V_{\text{int,lr}}$. In order to determine c_8 and c_{10} and connect short-range and long-range part, we choose the matching distances $r_1 = 20\ \text{a}_0$, $r_2 = 22\ \text{a}_0$, because at distances $r \gtrsim 20\ \text{a}_0$ the short-range exchange interactions vanish [58, 129].

In the literature, there is little information available on the ionization potentials of Ne* [8]. In the discussion of the previous chapter we found that the exact details of the loss channel only weakly influence the scattering rates of the scattering channel. Therefore, the particular shape of ionization potential is not crucial in the calculation. For numerical reasons we choose the model ionization potential

$$V_{\text{ion}}(r) = \begin{cases} V_{\text{ion,sr}}(r) & r \leq 20\ \text{a}_0, \\ V_{\text{ion,lr}}(r) & r > 20\ \text{a}_0, \end{cases} \tag{8.5}$$

with the short-range part $V_{\text{ion,sr}}$ and the long-range part $V_{\text{ion,lr}}$. The short-range part is given by

$$V_{\text{ion,sr}}(r) = V_{\text{int,sr}}(r) + \Delta, \tag{8.6}$$

which is simply the short-range interaction potential shifted by $\Delta < 0$. The long-range part of the model ionization potential is given by

$$V_{\text{ion,r}}(r) = c_5^{\text{ion}}/r^5 + c_6^{\text{ion}}/r^6 + c_8^{\text{ion}}/r^8 + c_{10}^{\text{ion}}/r^{10} + \Delta, \tag{8.7}$$

where c_5^{ion} and c_6^{ion} are found from optimization (see section 8.5) and c_8^{ion}, c_{10}^{ion} are the matching parameters to connect short-range and long-range potential. Again, the matching distances are given by $r_1 = 20\ \text{a}_0$ and $r_2 = 22\ \text{a}_0$.

A crucial part of the two-channel model of this chapter is the choice of the coupling matrix element

$$V_{12}(r) = \frac{V_{12}}{\exp\left[(r - r_\Omega)/r_\Delta\right] + 1}. \tag{8.8}$$

This is a Fermi-Dirac distribution with the coupling strength V_{12}, the coupling range r_Ω and the coupling width r_Δ. It describes PI of Ne*. The particular choice of a Fermi-Dirac distribution is due to a number of reasons. First, it was assumed that for small distances r the coupling becomes a constant in order account for the fact that atoms should not ionize with 100 % probability at short-range as for example in the *quantum reflection model*. This will be discussed in more detail in subsection 8.6.1. Secondly, with r_Δ one can make the coupling "smooth". A discontinuity in a step-like matrix element for example would lead to numerical instabilities. Furthermore, in (8.8) one can easily control the coupling range with the parameter r_Ω. PI occurs for internuclear distances at which the electron orbitals of the colliding atoms overlap which typically is around the minimum of the interaction potential $r = 10.7\ \text{a}_0$.

It was mentioned that PI is suppressed for collisions in spin-aligned states. In the experiment, suppression of PI due to spin-polarization of the atoms for Ne* collisions in the ${}^3P_2$ manifold

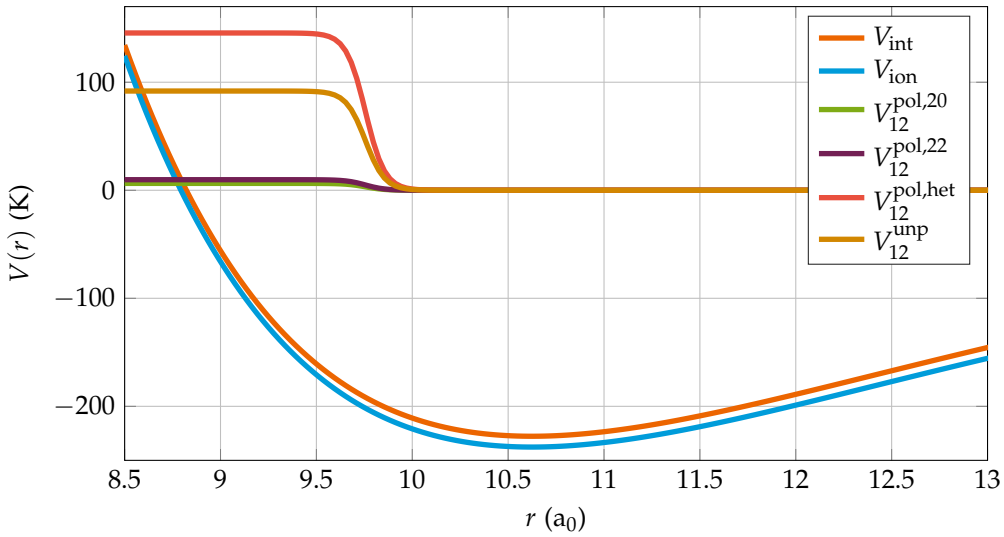

Figure 8.1: Matrix element of the potential matrix $V(r)$ of the two-channel model. The numerical values for the potential parameters are given in table 8.1 and were found from an optimization. The loss channel is shifted downwards by an amount of 10 K in order to make it visible in the graph.

was demonstrated [2]. Furthermore, it was shown that the suppression of PI is stronger in homonuclear collisions of ^{20}Ne than of ^{22}Ne. In order to account for these experimentally observed phenomena we assume different strengths of coupling

$$V_{12} = \left\{ V_{12}^{\text{pol,20}},\ V_{12}^{\text{pol,22}},\ V_{12}^{\text{pol,het}},\ V_{12}^{\text{unp}} \right\}. \tag{8.9}$$

The Schrödinger equation (8.1) is solved for homonuclear collisions of ^{20}Ne and ^{22}Ne and for heteronuclear collisions of ^{21}Ne–^{20}Ne, ^{22}Ne–^{20}Ne and ^{21}Ne–^{22}Ne. For homonuclear collisions of ^{20}Ne we solve the Schrödinger equation two times, first with the coupling strength $V_{12}^{\text{pol,20}}$ for collisions in the spin-aligned case and second with the coupling strength V_{12}^{unp} for collisions in all other states arising from the $^3P_2$ manifold of Ne*. For homonuclear collisions, we follow the same procedure but use the coupling strength $V_{12}^{\text{pol,22}}$ instead of $V_{12}^{\text{pol,20}}$. The introduction of different coupling strengths includes suppression of PI due to spin-polarization in the two-channel model. Without this assumption, the scattering of particles with spin leads to enhancement of low energy scattering rates of polarized collisions compared to unpolarized collisions [57] which is not observed in Ne* collisions. In our model, the different coupling strengths are free parameters, however. We do not presume *a priori*, that ionization in spin-polarized collisions are suppressed. We show in section 8.5 that this will be the result of an optimization in order to find good agreement with the experiment. For heteronuclear collisions, there is no information available on suppression of PI due to spin-polarization of the atoms. Therefore, we assume a single coupling strength $V_{12}^{\text{pol,het}}$. All the parameters of the coupling matrix element (8.8) are found from a fit to the experimental data. In figure 8.1 the potentials and different types of coupling matrix elements of our two-channel model are shown.

We solve the Schrödinger equation (8.1) for the different isotope combinations and different coupling strengths and for the partial waves $l = 0, 1, 2$. As we are interested in the cold collision properties of Ne* with relative collision energies of $E_{\text{rel}} \sim 1$ mK we do not need to take into account higher partial waves due to the Wigner-threshold behavior of the scattering rates (see previous chapter). The numerical methods we use to solve the Schrödinger equation will be presented in the next section.

8.2 NUMEROV METHOD

The numerical methods we describe shortly in this section have been reviewed and developed in detail in [111]. They are based on the method of Numerov [130, 131]. This method is particularly suited for differential equations of second order and is employed in scattering calculations or for the calculations of bound states [132–136].

The Schrödinger equation is an ordinary differential equation of second order which can be written in the form

$$y''(x) = f(x, y), \tag{8.10}$$

where $y : [a, b] \to \mathbb{R}^n$ and $f(x, y)$ are nonlinear functions in the variables x, y. Consider a Taylor expansion of y around x in forward direction and backward direction by stepsize h, reading

$$y(x+h) = y(x) + hy'(x) + \frac{h^2}{2}y''(x) + \frac{h^3}{6}y'''(x) + \frac{h^4}{24}y^{(4)}(x) + \frac{h^5}{120}y^{(5)}(x) + \mathcal{O}(h^6), \tag{8.11}$$

$$y(x-h) = y(x) - hy'(x) + \frac{h^2}{2}y''(x) - \frac{h^3}{6}y'''(x) + \frac{h^4}{24}y^{(4)}(x) - \frac{h^5}{120}y^{(5)}(x) + \mathcal{O}(h^6), \tag{8.12}$$

Addition of these two equations leads to

$$y(x+h) - 2y(x) + y(x-h) = h^2y''(x) + \frac{h^4}{12}y^{(4)}(x) + \mathcal{O}(h^6). \tag{8.13}$$

We can discretize the integration interval in $[a, b]$ with fixed step size h as

$$a = x_0 < x_1 < ... < x_n < x_{n+1} = b, \qquad x_j = a + jh, \quad h \equiv \frac{b-a}{n+1}, \tag{8.14}$$

and write equation (8.13) as

$$y_{i+1} - 2y_i + y_{i-1} = \frac{h^2}{12}\left(f_{i+1} + 10f_i + f_{i-1}\right) + \mathcal{O}(h^6), \tag{8.15}$$

where we have introduced the notation $y_i \equiv y(x_i)$ and $f_i \equiv f(x_i, y_i)$ and we have used the threepoint formula for $y^{(4)}$, reading

$$y_i^{(4)} = \frac{y''_{i+1} - 2y''_i + y''_{i-1}}{h^2} + \mathcal{O}(h^2). \tag{8.16}$$

Equation (8.15) is known as the *Numerov method*. It is an iterative equation for equidistant step size with an error on the order $\mathcal{O}(h^6)$ per step and a global accuracy of $\mathcal{O}(h^4)$ [132, 133].

Variable grid size

The fixed grid size of the *Numerov method* is not very practical for solving the Schrödinger equation at low collision energies. In order to illustrate this we show in figure 8.2 the numerical solution for two components of the scattering wave function of the two-channel model obtained by the *Numerov method*. The wave functions show the typical separation of length scales at short-range and long-range in cold collisions. For $r \leq 20$ a_0 the wave function oscillates heavily with a local wavelength of $\lambda \sim 1$ a_0, in the asymptotic region the local wavelength is given by $\lambda \sim 300$ a_0. For good numerical accuracy, we need to resolve the wave function with ~ 10 grid points per wavelength. In order to resolve the short-range oscillations of the wave function one wastes a lot of computation time in the asymptotic region since the wavelength here is much larger. The method of Numerov allows to halve and double the step size. However, in this work we use a different approach. Assume again a Taylor expansion of y around x, this time with step size h_2 in forward direction and step size h_1 in backward direction

$$y(x+h_2) = y(x) + h_2y'(x) + \frac{h_2^2}{2}y''(x) + \frac{h_2^3}{3!}y'''(x) + \frac{h_2^4}{4!}y^{(4)}(x) + \mathcal{O}(h_2^5), \tag{8.17}$$

$$y(x-h_1) = y(x) - h_1y'(x) + \frac{h_1^2}{2}y''(x) - \frac{h_1^3}{3!}y'''(x) + \frac{h_1^4}{4!}y^{(4)}(x) + \mathcal{O}(h_1^5). \tag{8.18}$$

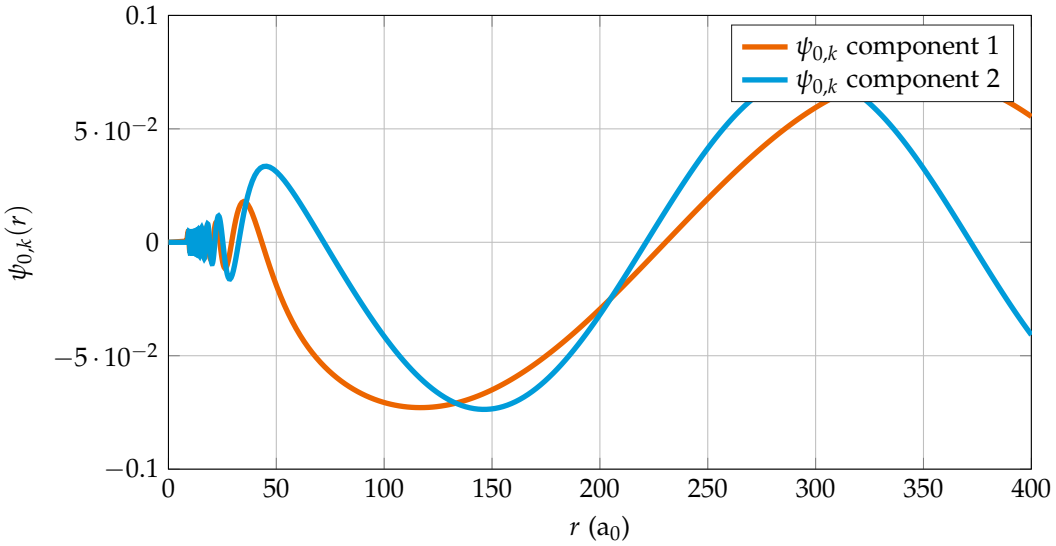

Figure 8.2: Two components of the scattering wave function $\psi_{0,k}$ for ^{20}Ne where the coupling is given by $V_{12}^{\text{pol,20}}$. The relative collision energy reads $E_{\text{rel}} = 1.6$ mK.

Multiplying equation (8.18) with h_2/h_1 and adding equation (8.17) leads to

$$\begin{aligned} &y(x+h_2) - \left(1 + \frac{h_2}{h_1}\right) y(x) + \frac{h_2}{h_1} y(x-h_1) \\ &= \frac{1}{2}\left(h_2^2 + h_1 h_2\right) y''(x) + \frac{1}{3!}\left(h_2^3 - h_2 h_1^2\right) y'''(x) + \frac{1}{4!}\left(h_2^4 + h_2 h_1^3\right) y^{(4)}(x) + \mathcal{O}(h^5), \end{aligned} \tag{8.19}$$

with $h = \max(h_1, h_2)$. Using again three-point approximations for $y'''(x)$ and $y^{(4)}(x)$ we can write

$$A + B + C = 0, \tag{8.20}$$

with

$$A = y(x+h_2) + \frac{1}{12}\left(-h_2^2 - h_1 h_2 + h_1^2\right) f\left(x + h_2, y(x+h_2)\right), \tag{8.21}$$

$$B = \left(-1 - \frac{h_2}{h_1}\right) y(x) - \left(\frac{h_2^3 + 4h_2^2 h_1 + 4h_2 h_1^2 + h_1^3}{12 h_1}\right) f(x, y(x)), \tag{8.22}$$

$$C = \frac{h_2}{h_1} y(x-h_1) + \left(\frac{h_2^3 - h_2^2 h_1 - h_2 h_1^2}{12 h_1}\right) f\left(x - h_1, y(x-h_1)\right). \tag{8.23}$$

Equation (8.20) is a generalization of the *Numerov method* (8.15) for unequal step sizes h_1, h_2. For $h_1 = h_2$ equation (8.20) reduces to (8.15). The error per step size here is given by $\mathcal{O}(h^5)$ which is worse compared to the step size error on the order $\mathcal{O}(h^6)$ by the *Numerov method*. However, this generalization allows for a complete variable step size. To set up the grid for the two-channel model we distinguish between the classically allowed region $E > V(r)$ and the classically forbidden region $E < V(r)$. These regions are separated by the turning points r_{tp} where $E = V(r)$. In the inner, classically forbidden region the wave function decreases exponentially for $r \to 0$. For the potentials of the two-channel model we start integration from $\sim 0.5\ a_0$ inside the inner turning point with a fixed step size up to r_{tp}. For $r > r_{\text{tp}}$ the wave function shows oscillatory behavior. We define the integration step size in the classically allowed region by

$$h(r) = 10 \cdot 2\pi / k(r), \tag{8.24}$$

with the local wave number $k(r) = \sqrt{E - V_{\text{ion}}(r)}$. The factor 10 arises as we resolve the wave function with 10 grid points per wave length $\lambda = 2\pi/k$ and the local wave number $k(r)$ is given in terms of V_{ion} in order to resolve the wave function of the lower channel properly. As this

channel lies lower energetically, the wave function in this channel has a shorter wave length for a given energy than the wave function in the upper channel.

Matching procedure

We employ the adapted version (8.20) of the Numerov method to the Schrödinger equation (8.1). The numerical solution can be written as

$$\psi_{l,k}^{\text{num}}(r) = M_l(Kr)\phi_l, \tag{8.25}$$

where $K_{ij} = k_i\delta_{ij}$ with $k_1 = k$ and $k_2 = \sqrt{k^2 - \Delta}$ and where ϕ_l is a constant 2×2 coefficient matrix. The 2×2 matrix $M_l(Kr)$ describes the radial dependence of $\psi_{l,k}^{\text{num}}(r)$. In the asymptotic region, $r \to \infty$, the numerical solution (8.25) is identical to the analytic asymptotic solution which is given by

$$\psi_{l,k}^{\text{asymp}} \underset{r\to\infty}{\longrightarrow} \frac{i}{2}\left[\hat{h}_l^-(Kr) + \hat{h}_l^+(Kr)K^{-1/2}S_lK^{1/2}\right]. \tag{8.26}$$

We solve the Schrödinger equation (8.1) numerically up to $r_{\max} = 1000\ a_0$ and utilize the last two points $(r_{\max-1}, r_{\max})$ of the variable grid as matching points

$$\psi_{l,k}^{\text{num}}(r_{\max-1}) = \psi_{l,k}^{\text{asymp}}(r_{\max-1}), \quad \psi_{l,k}^{\text{num}}(r_{\max}) = \psi_{l,k}^{\text{asymp}}(r_{\max}). \tag{8.27}$$

The scattering matrix S_l is then given by

$$S_l = K^{1/2}\left[\left(L_l^{\text{out}}\right)^{-1} L_l^{\text{in}}\right] K^{-1/2}, \tag{8.28}$$

where we have introduced the matrices

$$L_l^{\text{in}} = \hat{h}_l^-(Kr_{\max}) - M_l(Kr_{\max})M_l(Kr_{\max-1})^{-1}\hat{h}_l^-(Kr_{\max-1}), \tag{8.29}$$

$$L_l^{\text{out}} = \hat{h}_l^+(Kr_{\max}) - M_l(Kr_{\max})M_l(Kr_{\max-1})^{-1}\hat{h}_l^+(Kr_{\max-1}). \tag{8.30}$$

From the S matrix, the elastic and inelastic cross sections σ_l^{el}, σ_l^{inel} are calculated by the equations (5.135), (5.136), respectively.

8.3 TWO-BODY LOSS RATE COEFFICIENTS AND ELASTIC CROSS SECTIONS

Here, we show how we calculate from the inelastic cross sections the two-body loss rate coefficients of the two-channel model for different isotope mixtures. In section 5.8.5 and 5.8.6 we derived the two-body loss rate coefficients for a two-channel model with the loss channel α'. The loss channel α' for the two-channel model presented here is given by the potential V_{ion} and inelastic collisions are given by the transitions from the scattering potential V_{int} to the ionization potential V_{ion}. The integral in equation (5.168) is solved numerically by the *Gauss-Legendre quadrature* [13] for the intervals $[v_{i-1}, v_i]$ with $i \in 1, \ldots, n$ and $v_0 = 0$. Here the $v_{i>0}$ are the roots of the Laguerre polynomial $L_n(v)$. The division of the full integration range $[0, \infty]$ to the intervals $[v_{i-1}, v_i]$ results from applying the *generalized Gauss-Laguerre quadrature* method [13]. It was found that $n = 10$ is sufficient to find a good approximation to the integral (5.168).

For Ne*, the species are $F, G = 20, 21, 22$ for the ^{20}Ne, ^{21}Ne, ^{22}Ne isotopes and the internal spin states read $m_1, m_2 = -2, \ldots, +2$ for the sublevels of the $^3P_2$ manifold. For homonuclear collisions of ^{20}Ne and ^{22}Ne, when the atoms are in the internal, spin-aligned state $m_1 = m_2 = 2$, we solve the Schrödinger equation (8.1) with the coupling strength $V_{12}^{\text{pol},F}$ with $F = 20, 22$, respectively. As the atoms are identical in identical internal states we find from equation (5.170) the overall two-body loss rate coefficients for polarized homonuclear ensembles as

$${}^{FF}\beta_{\text{pol}} = {}^{FF}\beta_{22} = \sum_{l\ \text{even}} {}^{FF}\beta_{l,22}. \tag{8.31}$$

For homonuclear collisions in all other possible substates $(m_1m_2) \neq (22)$, we solve the Schrödinger equation (8.1) with the coupling strength V_{12}^{unp}. We obtain from the equations (5.170), (5.172) the homonuclear two-body loss rate coefficients as

$${}^{FF}\beta_{m_1m_1} = \sum_{l\ \text{even}} {}^{FF}\beta_{l,m_1m_1}, \quad {}^{FF}\beta_{m_1\neq m_2} = \frac{1}{2}\sum_{l} {}^{FF}\beta_{l,m_1\neq m_2}, \tag{8.32}$$

with $m_1 \neq 2$ in the first equation. As the interaction potential is not dependent on the internal sublevels of the atoms we obtain identical partial two-body loss rate coefficients and write ${}^{FF}\beta_l \equiv {}^{FF}\beta_{l,m_1m_1} = {}^{FF}\beta_{l,m_1\neq m_2}$. Note that this identity is not true for $(m_1m_2) = (22)$ as in this case the Schrödinger equation is solved with the coupling matrix element $V_{12}^{\mathrm{pol},F}$ with $F = 20, 22$. The unpolarized two-body loss rate coefficient for homonuclear collisions is given in equation (5.176). For our coupled two-channel model, we find, that the unpolarized two-body loss rate coefficient is given by

$$ {}^{FF}\beta_{\mathrm{unp}} = \frac{1}{(2j+1)^2} \sum_{l\,\mathrm{even}} {}^{FF}\beta_{l,22} + \frac{2j}{(2j+1)^2} \sum_{l\,\mathrm{even}} {}^{FF}\beta_l + \frac{2j(2j+1)}{(2j+1)^2} \frac{1}{2} \sum_l {}^{FF}\beta_l. \tag{8.33} $$

PI collisions are suppressed in spin-aligned [i.e. $(m_1m_2) = (22)$] samples compared to unpolarized ensembles. The suppression factor is given by the ratio

$$ {}^{FF}\eta^{-1} = {}^{FF}\beta_{\mathrm{unp}}/{}^{FF}\beta_{22}. \tag{8.34} $$

The definition of the suppression of polarized samples loss rates as the inverse of η follows the definition of [57].

In heteronuclear collisions, only polarized [$(m_1m_2) = (22)$] two-body loss rate coefficients have been measured in the experiment. For the coupled two-channel model we solve the Schrödinger equation (8.1) with the coupling strength $V_{12}^{\mathrm{pol,het}}$ and obtain the two-body loss rate coefficients for polarized collisions from equation (5.173) as

$$ {}^{F\neq G}\beta_{22} = \frac{1}{2} \sum_l {}^{F\neq G}\beta_{l,22}. \tag{8.35} $$

We also calculate elastic cross sections for polarized collisions [$(m_1m_2) = (22)$]. In the case of homonuclear collisions of bosons they are given by

$$ {}^{FF}\sigma_{22}^{\mathrm{el}} = 2 \sum_{l\,\mathrm{even}} {}^{FF}\sigma_{l,22}^{\mathrm{el}}, \tag{8.36} $$

and in the case of heteronuclear collisions we have

$$ {}^{F\neq G}\sigma_{22}^{\mathrm{el}} = \sum_l {}^{F\neq G}\sigma_{l,22}^{\mathrm{el}}. \tag{8.37} $$

So far, nothing has been said about the numerical values of the potential parameters we use. The free potential parameters are found from an optimization in order to find the best match of the numerical results with the experimental measurements. This optimization is described in more detail in the next section.

8.4 DETERMINATION OF THE FREE POTENTIAL PARAMETERS

In order to find the best potential parameters of the coupled two-channel model we include 17 experimental data points on homonuclear and heteronuclear collision rates. The data points read

$$ \begin{aligned} y_{\mathrm{exp}} = \Big\{ & {}^{FF}\beta_{20}(T = 315\ \mu\mathrm{K}),\ {}^{FF}\beta_{11}(T = 350\ \mu\mathrm{K}),\ {}^{FF}\beta_{\mathrm{unp}}(T = 315\ \mu\mathrm{K}),\ {}^{FF}\beta_{\mathrm{unp}}(T = 1.5\ \mathrm{mK}), \\ & {}^{FF}\beta_{22}(T = 670, 730\ \mu\mathrm{K}),\ {}^{FF}\sigma_{22}^{\mathrm{el}}(T = 200\ \mu\mathrm{K}),\ {}^{FF}\sigma_{22}^{\mathrm{el}}(T = 500\ \mu\mathrm{K}),\ {}^{F\neq G}\beta_{22} \Big\}, \end{aligned} \tag{8.38} $$

with $F = 20, 22$ and ${}^{F\neq G}\beta_{22}$ for all three heteronuclear collision types. The temperature in the brackets indicates at what atomic ensemble temperature the measurement was performed. For ${}^{FF}\beta_{22}$ the ensemble temperature reads $T = 670\ \mu\mathrm{K}$ for ^{20}Ne and $T = 730\ \mu\mathrm{K}$ for ^{22}Ne. The measurements of the heteronuclear rates were performed at $T = 500\ \mu\mathrm{K}$ for ^{21}Ne–^{20}Ne, $T = 750\ \mu\mathrm{K}$ for ^{22}Ne–^{20}Ne and $T = 600\ \mu\mathrm{K}$ for ^{21}Ne–^{22}Ne.

The free potential parameters of the coupled two-channel model are given by

$$x = \left\{ V_{12}^{\mathrm{pol},20},\ V_{12}^{\mathrm{pol},22},\ V_{12}^{\mathrm{pol,het}},\ V_{12}^{\mathrm{unp}},\ r_\Omega,\ r_\Delta,\ \Delta,\ c_6,\ c_6^{\mathrm{ion}},\ c_5,\ c_5^{\mathrm{ion}} \right\}. \tag{8.39}$$

We calculate numerically the minimum of the function

$$f(x) = \sum_i \left(\frac{y_i(x) - y_{i,\mathrm{exp}}}{y_{i,\mathrm{exp}}} \right)^2, \tag{8.40}$$

where $y(x)$ calculates the two-body loss rate coefficients and elastic cross sections as a function of the free potential parameters. The first component $y_1(x)$ is the numerical result for ${}^{FF}\beta_{20}$ at $T = 315\ \mu\mathrm{K}$ for ^{20}Ne and so forth. We minimize the function $f(x)$ under the constraints

$$\begin{aligned}
2\ \mathrm{K} \leq & V_{12} \leq 200\ \mathrm{K}, \\
9.5\ \mathrm{a_0} \leq & r_\Omega \leq 11\ \mathrm{a_0}, \\
0.05\ \mathrm{a_0} \leq & r_\Delta \leq 1.0\ \mathrm{a_0}, \\
-0.1\ \mathrm{K} \leq & \Delta \leq -0.001\ \mathrm{K}, \\
-0.37\ \mathrm{a.u.} \leq & c_5 \leq +0.47\ \mathrm{a.u.}, \\
1820\ \mathrm{a.u.} \leq & c_6 \leq 2079\ \mathrm{a.u.} \\
-0.37\ \mathrm{a.u.} \leq & c_5^{\mathrm{ion}} \leq +0.47\ \mathrm{a.u.}, \\
200\ \mathrm{a.u.} \leq & c_6^{\mathrm{ion}} \leq 5000\ \mathrm{a.u.},
\end{aligned} \tag{8.41}$$

where the boundaries on V_{12} were set for all different coupling strength

$$\left\{ V_{12}^{\mathrm{pol},20},\ V_{12}^{\mathrm{pol},22},\ V_{12}^{\mathrm{pol,het}},\ V_{12}^{\mathrm{unp}} \right\}.$$

The boundaries on the c_5 and the c_6 coefficients are due to the anisotropy in the long-range interactions of Ne*. This corresponds to the maximum and minimum value of the coefficients in table 6.2. For the boundaries of the c_6 coefficient we have also included the 4 % uncertainty, indicated in [9]. The boundaries on r_Ω were chosen in order to allow PI to start when the electron orbitals overlap. The other boundary conditions were chosen due to numerical reasons.

parameter	numerical value	unit
$V_{12}^{\mathrm{pol},20}$	6.4	K
$V_{12}^{\mathrm{pol},22}$	9.8	K
$V_{12}^{\mathrm{pol,het}}$	91.9	K
V_{12}^{unp}	145.6	K
r_Ω	9.76	$\mathrm{a_0}$
r_Δ	0.05	$\mathrm{a_0}$
Δ	-0.002	K
c_6	1832.5	a.u.
c_6^{ion}	527.0	a.u.
c_5	0.47	a.u.
c_5^{ion}	-0.35	a.u.

Table 8.1: Resulting parameters of optimization of $f(x)$ (8.40) for the two-channel model. The boundaries of the optimization are given in (8.41).

The resulting potential parameters from the minimization of the function $f(x)$ are given in table 8.1. One has to highlight that the found coupling parameters $V_{12}^{\mathrm{pol},20}$, $V_{12}^{\mathrm{pol},22}$ are much lower than V_{12}^{unp}. Thus, coupling from the interaction channel to the loss channel is weaker for collisions in the sublevels $(m_1 m_1) = (22)$ than in collisions in the other states. This is consistent

with the prediction, that PI is suppressed in collisions of spin-aligned atoms. Note, that these couplings strengths result from the minimization of $f(x)$, the suppression of $V_{12}^{\mathrm{pol},F}$ was not included explicitly in the calculation.

In order to fit 17 data points we have used 11 potential parameters. In total, there are 31 experimental data points available. We show in the next section that most of them are matched with the potential parameters of table 8.1.

8.5 RESULTS

Given the potential parameters in table 8.1 we calculate two-body loss rate coefficients, elastic cross sections for homonuclear ^{20}Ne and ^{22}Ne collisions and for heteronuclear ^{21}Ne–^{20}Ne, ^{22}Ne–^{20}Ne, ^{21}Ne–^{22}Ne collisions in the temperature range $T = 1\ \mathrm{nK} - 100\ \mathrm{mK}$. In table 8.2 and in table 8.3 the numerical results are compared to corresponding experimental data points.

quantity	unit	^{20}Ne		^{22}Ne	
		num	exp	num	exp
σ^{el} (200 μK)	$[10^{-17}\ \mathrm{m}^2]$	6.0	8(2)	7.7	30(8)
σ^{el} (550 μK)	$[10^{-17}\ \mathrm{m}^2]$	3.0	2.8(7)	8.4	13(3)
β_{pol}	$[10^{-12}\ \mathrm{cm}^3/\mathrm{s}]$	6.5	6.5(18)	12.14	12(3)
β_{unp} (315 μK)	$[10^{-12}\ \mathrm{cm}^3/\mathrm{s}]$	100.0	78(47)	27.5	36(16)
$\beta_{\mathrm{unp}}/\beta_{\mathrm{pol}}$		15.38	12.0(65)	2.27	3.0(11)
β_{11} (350 μK)	$[10^{-12}\ \mathrm{cm}^3/\mathrm{s}]$	165.30	177(78)	35.84	58(15)
β_{00} (315 μK)	$[10^{-12}\ \mathrm{cm}^3/\mathrm{s}]$	170.85	144(59)	35.90	43(15)
β_{21} (350 μK)	$[10^{-12}\ \mathrm{cm}^3/\mathrm{s}]$	90.38	41(18)	26.76	6(6)
β_{res} (315 μK)	$[10^{-12}\ \mathrm{cm}^3/\mathrm{s}]$	90.38	100(68)	26.76	41(14)

Table 8.2: Homonuclear collisions: relaxation cross sections and two-body loss rate coefficients. Temperatures for the loss rates of the polarized samples are $T = 670$ μK and $T = 730$ μK for ^{20}Ne and ^{22}Ne collisions, respectively. The experimental data points are given in [5]. β_{res} is the average value of β_{2-1}, β_{1-1} and β_{2-2}.

quantity	unit	^{21}Ne–^{20}Ne		^{22}Ne–^{20}Ne		^{21}Ne–^{22}Ne	
		num	exp	num	exp	num	exp
σ^{el}	$[10^{-17}\ \mathrm{m}^2]$	6.76	7	1.79	4	8.46	20
β_{pol}	$[10^{-12}\ \mathrm{cm}^3/\mathrm{s}]$	31.26	39(27)	26.56	26(7)	44.42	39(19)

Table 8.3: Heteronuclear collisions of Ne*. Relaxation cross sections σ^{el} and two-body loss rate coefficients β_{pol} of spin-aligned atomic ensembles. The temperatures of these samples are $T = 500, 750, 600$ μK for ^{21}Ne–^{20}Ne, ^{22}Ne–^{20}Ne and ^{21}Ne–^{22}Ne collisions, respectively. Experimental values were published in [4] and are also given in [5]. The experimental values for the relaxation cross sections are upper bounds.

In figure 8.3 and in figure 8.4 the numerical results for two-body loss rate coefficients of homonuclear ^{20}Ne and ^{22}Ne are shown. In both cases the significant difference of polarized loss rates to loss rates of other spin-combinations is visible. Especially in the case of ^{20}Ne collisions, a large difference of one order of magnitude for scattering rates of polarized and unpolarized atomic ensembles for s-wave collisions is observed. Almost all of the experimental data points are matched for homonuclear collisions. The most striking deviation is observed for β_{unp} of ^{20}Ne collisions at $T = 1.5$ mK. This has to be further investigated.

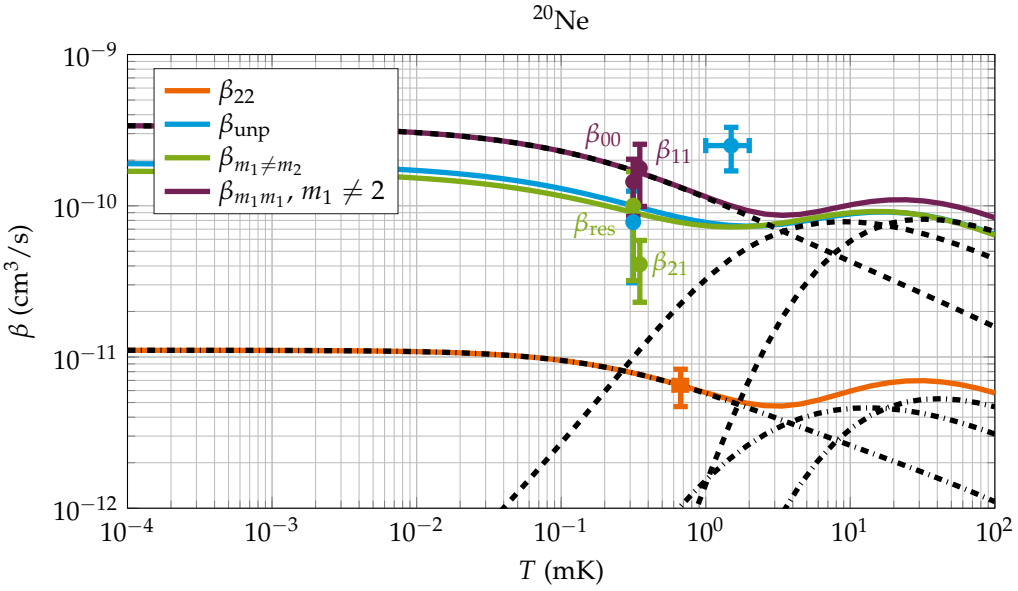

Figure 8.3: Two-body loss rate coefficients β for homonuclear ensembles of ^{20}Ne versus temperature. In addition to the legend, we also show the partial-wave contributions β_{l,m_1m_1} with $(m_1m_1) = (22)$ (black dashed lines) and β_{l,m_1m_2} with $(m_1m_2) \neq (22)$ (black dashed-dotted lines). Experimental data points and error bars are indicated in the corresponding colors.

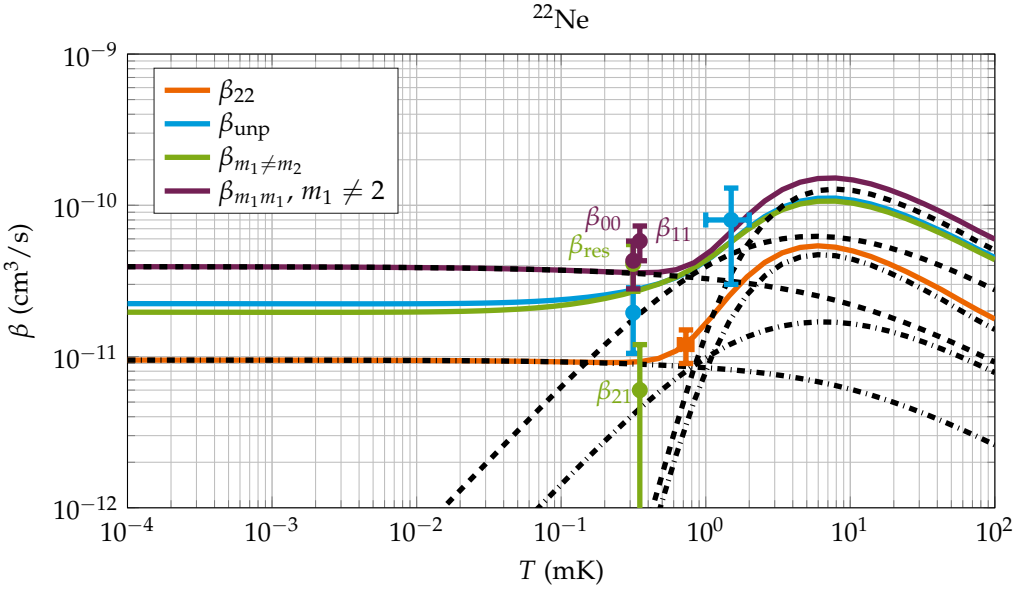

Figure 8.4: Two-body loss rate coefficients β for homonuclear ensembles of ^{22}Ne versus temperature. In addition to the legend, we also show the partial-wave contributions β_{l,m_1m_1} with $(m_1m_1) = (22)$ (black dashed lines) and β_{l,m_1m_2} with $(m_1m_2) \neq (22)$ (black dashed-dotted lines). Experimental data points and error bars are indicated in the corresponding colors.

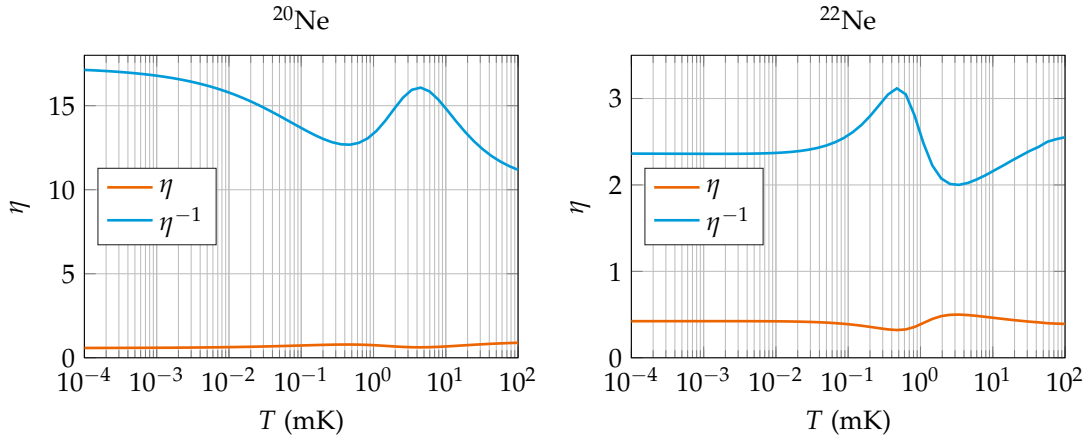

Figure 8.5: Ratio $\eta = \beta_{\mathrm{pol}}/\beta_{\mathrm{unp}}$ and suppression ratio $\eta^{-1} = \beta_{\mathrm{unp}}/\beta_{\mathrm{pol}}$ for homonuclear ensembles of ^{20}Ne in the left subfigure and of ^{22}Ne in the right subfigure versus temperature.

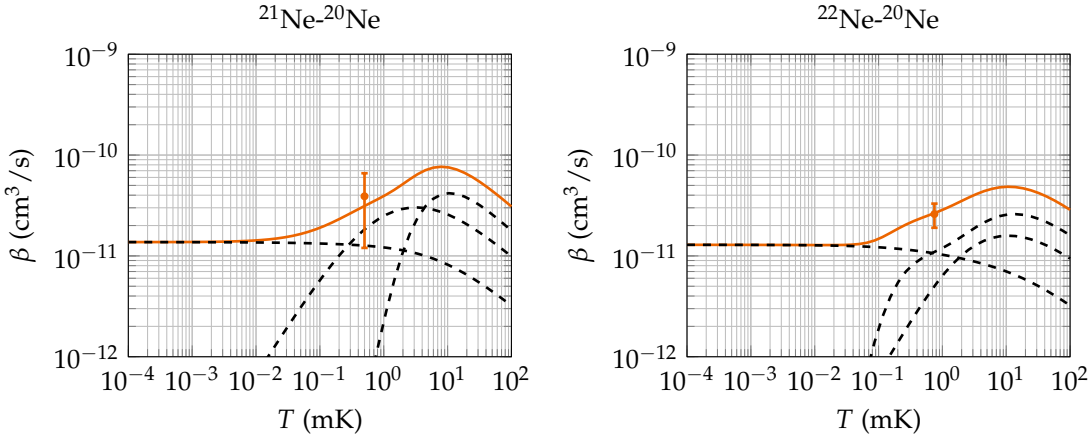

Figure 8.6: Two-body loss rate coefficients β_{22} of ^{21}Ne–^{20}Ne in the left subfigure and of ^{22}Ne–^{20}Ne in the right subfigure versus temperature. The orange solid lines indicate the total two-body loss rate coefficients and the partial wave contributions $\beta_{l,22}$ are shown as black dashed lines. Experimental data points and error bars are indicated in orange color.

In figure 8.5 the calculated suppression ratios η^{-1} and η are shown for homonuclear ensembles. It can be seen that for the full temperature range, the suppression ratio $\eta^{-1} > 1$. Therefore, suppression of PI due to spin-alignment of the atoms is successfully implemented in the two-channel model. In addition, the suppression ratio η^{-1} of ^{20}Ne is higher than for ^{22}Ne which is consistent with the experimental results.

In figure 8.6 and in the left subfigure of figure 8.7 the numerical two-body loss rate coefficients for heteronuclear Ne* collisions are shown. Unfortunately, there are only three experimental data points available. These data points are perfectly matched by the numerical calculation. The heteronuclear scattering rates were all calculated with the same coupling strength $V_{12}^{\mathrm{pol,het}}$. Thus, the different behavior of the scattering rates is solely due to the mass scaling of the interaction potentials.

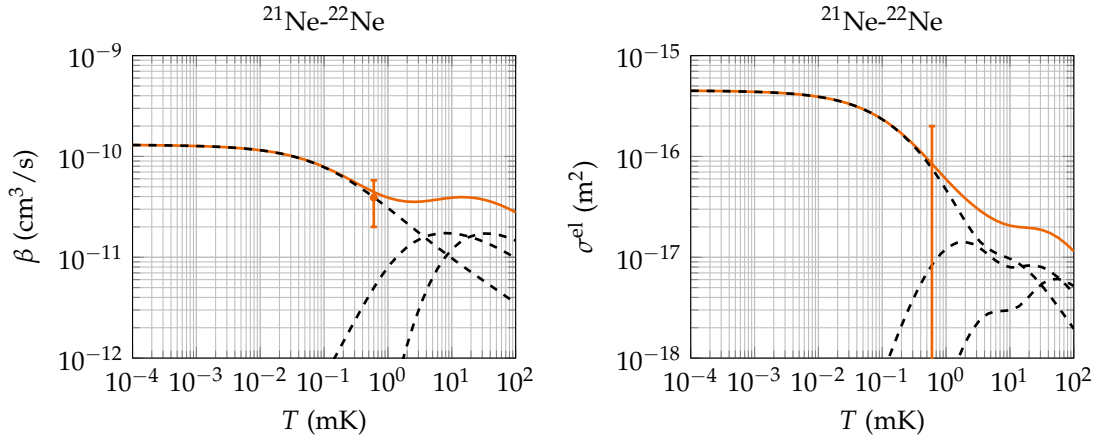

Figure 8.7: ^{21}Ne–^{22}Ne: two-body loss rate coefficient β_{22} in the left subfigure and elastic cross section $\sigma_{22}^{\mathrm{el}}$ in the right subfigure versus temperature. The partial-wave contributions $\sigma_{l,22}^{\mathrm{el}}$, $\beta_{l,22}$ are shown as black dashed lines. Experimental upper bounds and data points are indicated in orange color.

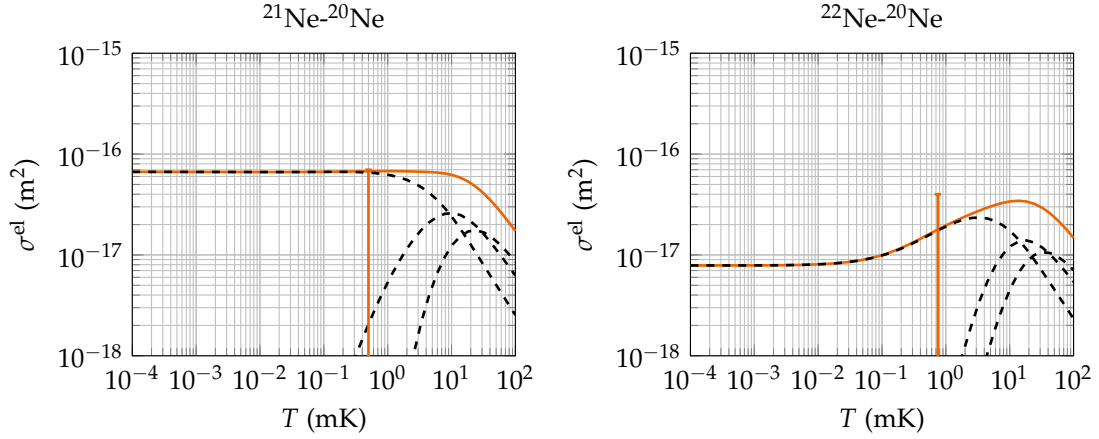

Figure 8.8: Elastic cross section $\sigma_{22}^{\mathrm{el}}$ of ^{21}Ne–^{20}Ne in the left subfigure and of ^{22}Ne–^{20}Ne in the right subfigure versus temperature. The solid orange lines display the total elastic cross sections and the black dashed lines indicate the partial-wave contributions $\sigma_{l,22}^{\mathrm{el}}$. Experimental upper bounds are indicated by the vertical solid orange lines.

In the right subfigure of figure 8.7 and in figure 8.8 the numerical results of the elastic cross sections for heteronuclear collisions of Ne* are shown. It is seen in the figures that the calculated cross sections match the boundaries for all observed isotope-combinations. It is important to mention again, that these results are solely due to the mass scaling effect of the potentials as only a single coupling strength $V_{12}^{\mathrm{pol,het}}$ is assumed.

In figure 8.9 the numerical results for the elastic cross sections of polarized ^{20}Ne and ^{22}Ne collisions are shown. The elastic cross section for ^{20}Ne is consistent with the experimental measurements which is not the case for ^{22}Ne collisions. We have performed calculations with different potential parameters but it was found, that it is not possible to obtain good agreement with the experiment for both, the elastic cross section and the two-body loss rate coefficient β_{22} of ^{22}Ne at the same time.

In figure 8.10 the real and imaginary part of the complex energy-dependent scattering length are shown for spin-aligned collisions of ^{20}Ne and ^{22}Ne and $l = 0$. The complex energy-dependent scattering length was given in equation (5.139). For the real part $\tilde{\alpha}_0$ one can observe in the threshold regime a negative value for ^{20}Ne and positive value for ^{22}Ne on the order of $\tilde{\alpha}_0 \simeq \pm 40\ \mathrm{a}_0$. The numerical result of a negative scattering length for ^{20}Ne and a positive

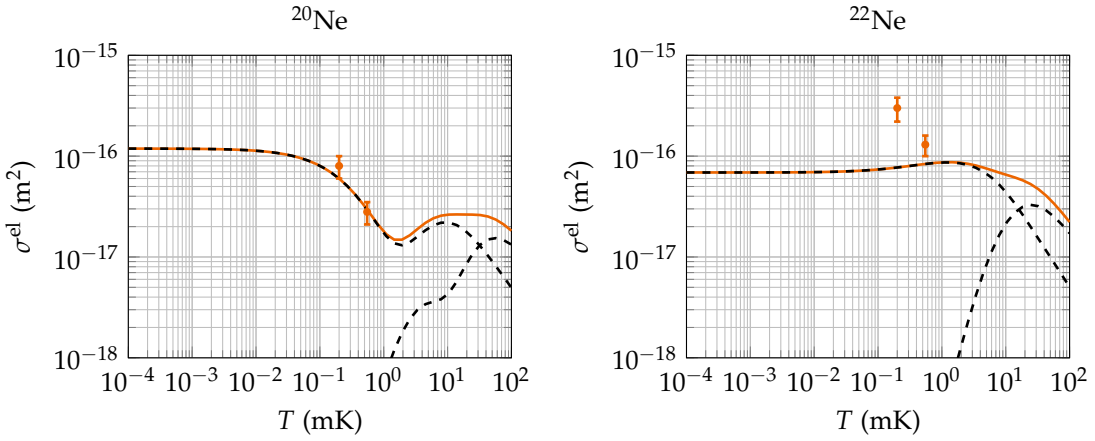

Figure 8.9: Elastic cross section $\sigma^{\mathrm{el}}_{22}$ for homonuclear ensembles of ^{20}Ne in the left subfigure and for ^{22}Ne in the right subfigure versus temperature. The solid orange lines indicate the total elastic cross sections and the black dashed lines display the s-wave and d-wave contributions $\sigma^{\mathrm{el}}_{l,22}$. Experimental data points and error bars are indicated in orange color.

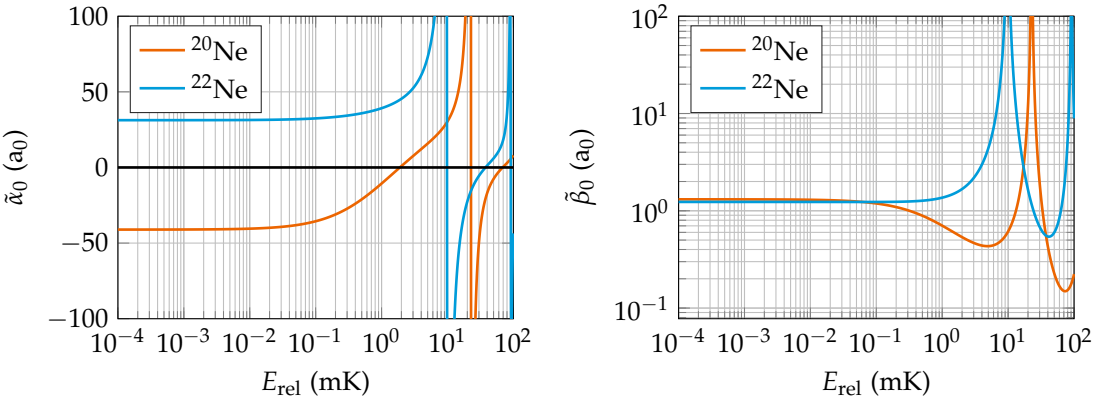

Figure 8.10: Complex scattering length for $l = 0$. Shown are the real part $\tilde{\alpha}_0$ in the left subfigure and the imaginary part $\tilde{\beta}_0$ in the right subfigure versus relative collision energy E_{rel} for ^{20}Ne and ^{22}Ne collisions.

scattering length for ^{22}Ne is consistent with the determination of the s-wave scattering lengths in the experiment, given by [2]

$$a_{sc} = -180\ \mathrm{a_0} \quad (^{20}\mathrm{Ne}), \quad a_{sc} = +150\ \mathrm{a_0} \quad (^{22}\mathrm{Ne}). \tag{8.42}$$

Even though the absolute values are not correct, the qualitative behavior of the scattering length is in good agreement with the experimental observations.

In total, the results of the two-channel model are in very good agreement with the experimental measurements, including all different isotopes. This is remarkable, as the scattering of Ne* in the two-channel model is described by a single interaction potential instead of the multitude of potentials which occur in the full *coupled-channel equations* for Ne* interactions. From the results shown in this section we conclude that the coupled two-channel model is an effective model for cold collisions of Ne*. In order to discuss its validity, we compare it in the next section to different approaches for cold reactive collisions of atoms.

8.6 COMPARISON TO THE DIFFERENT MODELS

Here we compare our two-channel model of this chapter to the *quantum reflection model*, the *non-universal* approach and also to the results of the coupled two-channel model with square-well potentials, which was introduced in the previous chapter.

8.6.1 *Quantum reflection model*

The *quantum reflection model* is a widely used model to describe cold reactive collisions of metastable rare gases [56–59]. It is shown in figure 8.11 for a interaction potential with rotational barrier ($l > 0$).

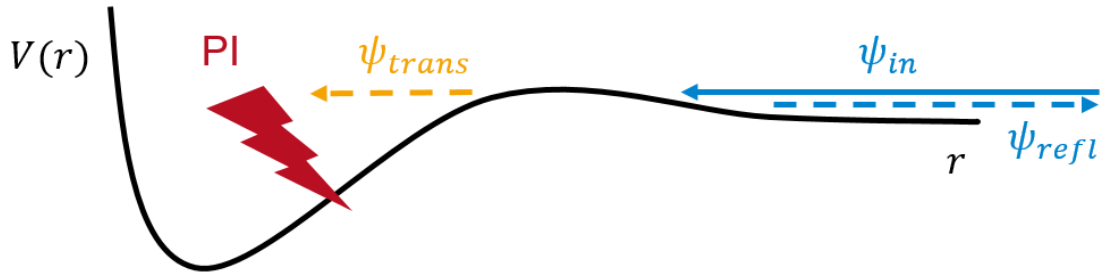

Figure 8.11: The *quantum reflection model*. A potential with rotational barrier is depicted. The solid blue line indicates an incoming wave, the blue dashed line is the reflected fraction and the dashed orange line is the transmitted fraction of the incoming wave. The red bolt indicates ionization at short-range.

A fraction ψ_{trans} of the incoming scattering wave function ψ_{in} is transmitted through the rotational barrier and a fraction ψ_{refl} is reflected. The *quantum reflection model* assumes, that the particles at short-range ionize with 100 % probability. Therefore, the transmitted fraction of the wave function is not back-reflected and the complete scattering physics is governed by the long-range part of the potential only. In [57] the *quantum reflection model* was employed successfully to explain cold collisions of Xe*. In this specific version of the *quantum reflection model*, the potential was given by

$$V(r) = \begin{cases} -c_6/r^6 & r > r_{\text{cut}} \\ V(r_{\text{cut}}) & r \leq r_{\text{cut}} \end{cases}, \tag{8.43}$$

and the radial distance was extended to $r \to -\infty$. By solving the radial Schrödinger equation one obtains the transmitted probability current j_{trans} of the scattering wave function and can calculate the transmission probability P_T through the potential barrier as

$$P_T = j_{\text{trans}}/j_{\text{in}}, \tag{8.44}$$

where j_{in} is the incoming probability current of the scattering wave function. The inelastic scattering cross section of the *quantum reflection model* then reads

$$\sigma_l^{\text{inel}}(E) = \frac{\pi}{k^2}(2l+1)P_T(E,l). \tag{8.45}$$

The transmission probability only depends on the c_6 coefficient and on the reduced mass μ of the colliding particles. Small changes in the reduced mass for different isotope combinations only influence weakly the inelastic cross section σ^{inel}. Therefore, the *quantum reflection model* predicts universal scattering rates for collisions of different isotopes. In [57] it was demonstrated experimentally that for 5 different isotopes of Xe*, the scattering rates were almost identical. This observation agrees with the predictions of the *quantum reflection model*. The independence of the scattering rates on different isotope combinations is called *universal* behavior. Therefore, the *quantum reflection model* is also called the *universal model* [60].

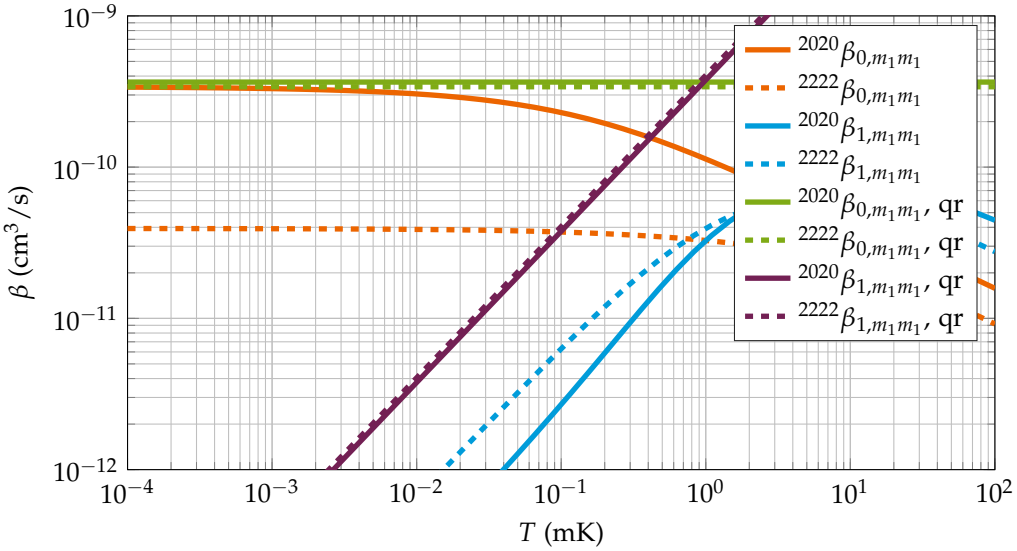

Figure 8.12: Partial two-body loss rate coefficients β_{l,m_1m_1} obtained by the two-channel model with $m_1 \neq 2$ and the threshold rates of the *quantum reflection model* (qr) (8.46) for ^{20}Ne collisions and for ^{22}Ne collisions.

A similar approach to the Xe* case has been employed successfully to explain cold collisions of He* [58, 59]. In [56] the *quantum reflection model* was employed to explain scattering rates of Kr*. Further developments of the *quantum reflection model* in [60] and in [137] gave analytic expressions of the two-body loss rate coefficients in the $E \to 0$ limit in terms of the c_6 coefficients. This makes it unnecessary to calculate the Schrödinger potential numerically for model potentials such as in equation (8.43). The rate constants given in [60] read

$$\beta_0 \xrightarrow[E\to 0]{} 2g\frac{h}{\mu}\bar{a}, \tag{8.46a}$$

$$\beta_1 \xrightarrow[E\to 0]{} 2g\frac{h}{\mu}\bar{a}_1(k\bar{a})^2., \tag{8.46b}$$

Here, $\bar{a}$ is the mean scattering length for the *van der Waals potential* given in equation (6.43) and $\bar{a}_1 = \bar{a}\Gamma(1/4)^6/[144\pi^2\Gamma(3/4)^2]$ with $\Gamma(x)$ the Gamma function. The factor g is a symmetrization factor which is 2 for identical atoms in identical states and 1 otherwise. The rate constants in (8.46) are only dependent on the reduced mass μ and the dispersion coefficient c_6. With $c_6 = 1832.5$ a.u. given in table 8.1, we calculate the two-body loss rate coefficients (8.46) of the *quantum reflection model* .

In figure 8.12 the resulting scattering rates are compared to the partial two-body loss rate coefficients β_{l,m_1m_1} with $m_1 \neq 2$ for ^{20}Ne, ^{22}Ne collisions, obtained by the two-channel model. Two important observations can be made. First, the s-wave threshold constant of ^{20}Ne collisions of the *quantum reflection model* agrees very well with the s-wave loss rate in the low-temperature regime calculated by the two-channel model. Second, a change of isotopic mass from ^{20}Ne to ^{22}Ne collisions does not change the rate constants of the *quantum reflection model* sufficiently to give good agreement with the differences for the different isotopes obtained by the two-channel model. As the *quantum reflection model* only takes into account long-range physics, the rate coefficients are only weakly sensitive to small changes in isotopic mass. In the two-channel model, however, a difference of almost one order of magnitude can be observed in the s-wave rate constants. The p-wave rate constants of the *quantum reflection model* and of the two-channel model do not agree at all. The results of the two-channel model for $^{FF}\beta_{m_1m_1}$ were in good agreement with the experimental measurements of $^{FF}\beta_{11}$, $^{FF}\beta_{00}$ for $F = 20, 22$. Therefore, and as already demonstrated in [5], it is shown, that the *quantum reflection model* is not a good description for reactive collisions of Ne*.

8.6.2 *Non-universal model*

Within the framework of *Multichannel Quantum Defect Theory* (MCQDT) [63–66], the *non-universal model* has been developed [60, 61] and explicit expressions for s-wave and p-wave two-body loss rate coefficients in the threshold limit in terms of two parameters (y, s) were given in [61]. These *non-universal* two-body loss rate coefficients for $E \to 0$ read

$$\beta_0 \xrightarrow[E\to 0]{} 2g\frac{h}{\mu}\bar{a}y\frac{1+(s-\nu)^2}{1+y^2(s-\nu)^2}, \tag{8.47a}$$

$$\beta_1 \xrightarrow[E\to 0]{} 2g\frac{h}{\mu}\bar{V}k^2y\frac{1+\nu^2}{\nu^2}\times\frac{1+(s-\nu)^2}{y^2(s-\nu+\nu^{-1})^2+(s\nu^{-1}-2)^2}, \tag{8.47b}$$

where $\nu = \cot(\pi/n-2)$ and $\bar{V}$ is the characteristic p-wave volume

$$\bar{V} = \frac{\pi}{9}\frac{(n-2)^{(n-8)/(n-2)}}{\Gamma^2(\frac{3}{n-2})}R_n^3. \tag{8.48}$$

The characteristic length is given by

$$R_n = \left(2\mu C_n/\hbar^2\right)^{1/(n-2)}, \tag{8.49}$$

and for *van der Waals* interactions $(n = 6)$ we obtain the *van der Waals* length R_6 which was given in equation (6.43). Note that there is a factor of $1/2$ between equation (6.43) of [60] and equation (8.49) of [61].

The basic assumption of MQDT and the *non-universal model* is the separation of short-range and long-range physics. A physical interpretation of the parameter y is given if one assumes the *WKB*-form of the scattering wave function at short distances

$$\psi(r) \sim \frac{\exp\left[-i\int^r k(x)dx\right]}{\sqrt{k(r)}} - \left(\frac{1-y}{1+y}\right)\frac{\exp\left[+i\int^r k(x)dx\right]}{\sqrt{k(r)}}, \tag{8.50}$$

with the local wave number $k(r) = \sqrt{2\mu(E-V(r)}/\hbar$. The first term of equation (8.50) describes the incoming part of the scattering wave and the second term the outgoing part. The parameter y is restricted to $0 \le y \le 1$. One can see that for $y = 1$ there is no outgoing or reflected term in equation (8.50). For $y = 0$ however, the incident and outgoing fluxes are equal. This means, that for $y = 1$ nothing is reflected and for $y = 0$ vice versa. The parameter y is thus a parametrization of the probability of loss at short-range and this probability is given by [61]

$$P_{\mathrm{ls}} = 4y/(1+y)^2. \tag{8.51}$$

For $y = 1$, the expressions of the rate coefficients in [61] reduce to those of the *quantum reflection model*, given by equation (8.46) and become independent of the parameter s. The dimensionless parameter s is given by $s = a_{sc}/\bar{a}$, where a_{sc} is the s-wave scattering length of the potential and $\bar{a}$ again the mean scattering length. It contains the information about the short-range part of the potential. For $y = 1$, this information does not influence the scattering wave function.

When two-body loss rate coefficients have been established experimentally or numerically, the parameters (y, s) serve as fit parameters to the results. We fit these parameters to the two-body loss rate coefficients obtained by the two-channel model of this chapter, in the threshold limit. As these equations are non-linear in (y, s), multiple solutions are obtained. However, $0 \le y \le 1$ must hold. The parameter s is the scaled scattering length and must agree with the experimental observations. We perform a fit of (y, s) of (8.47) with the calculated coefficient $c_6 = 1832.5$ a.u. in the threshold limit to the scattering rates $\beta_{m_1 m_1}$ with $m_1 \neq 2$ for ^{20}Ne and for ^{22}Ne and obtain the set of parameters

$$\begin{aligned}(^{20}y = 0.06,\ ^{20}s = -4.14),\\ (^{22}y = 0.07,\ ^{22}s = +0.66).\end{aligned} \tag{8.52}$$

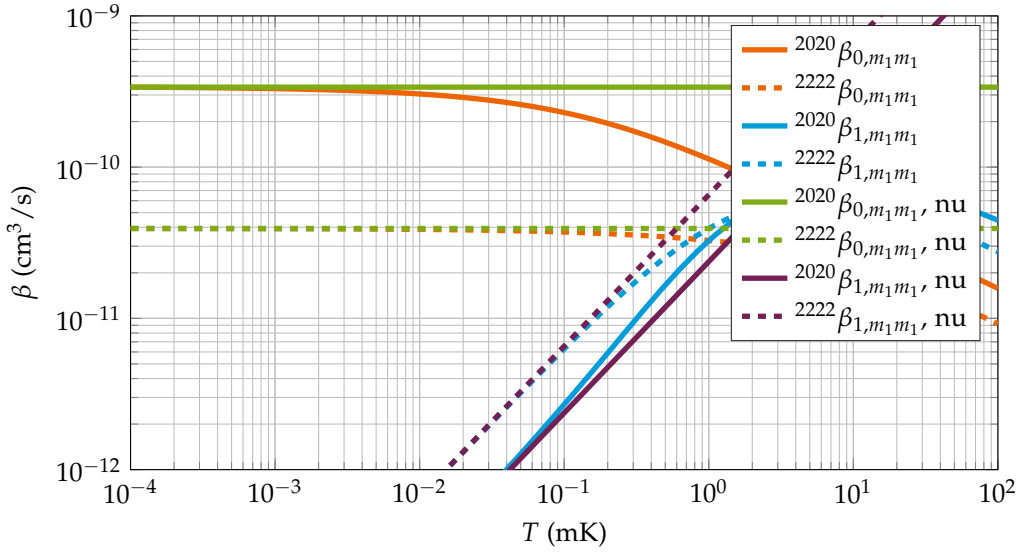

Figure 8.13: Partial two-body loss rate coefficients β_{l,m_1m_1} obtained by the two-channel model and obtained by the *non-universal model* (nu) for ^{20}Ne and for ^{22}Ne for collisions in $m_1 \neq 2$. The rates of the *non-universal model* are given for $c_6 = 1832.5$ a.u. and with the fit parameters of (8.52).

From the values of y one can calculate the loss probabilities (8.51) as $P_{\text{ls}} = 20.11\,\%$ for ^{20}Ne and $P_{\text{ls}} = 25.67\,\%$ for ^{22}Ne. The obtained values for s lead to the scattering lengths $a_{sc} = -179\ a_0$ for ^{20}Ne and $a_{sc} = +29\ a_0$ for ^{22}Ne, where we have used, that the mean scattering lengths $\bar{a}$ are given by $\bar{a} = 43.21\ a_0$ for ^{20}Ne and $\bar{a} = 44.25\ a_0$ for ^{22}Ne with $c_6 = 1832.5$ a.u. While the scattering length matches perfectly the experimental result for ^{20}Ne it underestimates the scattering length of ^{22}Ne [see (8.42)]. This error is systematical as the parameter s was found from a fit to the two-channel model of this chapter which itself did not describe accurately the elastic scattering in ^{22}Ne (see figure 8.9). It is thus consistent with the error of the two-channel model, that the scattering length obtained by a fit of the *non-universal model* gives a lower value for the scattering length.

A second fit was made to the two-body loss rate coefficients obtained by the two-channel model of this chapter for polarized ensembles β_{22} for ^{20}Ne and ^{22}Ne. Again, from the equations (8.47) with $c_6 = 1832.5$ a.u. we obtain a set of parameters (y, s) which read

$$\begin{aligned} &(^{20}y_{\text{pol}} = 0.002,\ ^{20}s_{\text{pol}} = -3.5),\\ &(^{22}y_{\text{pol}} = 0.02,\ ^{22}s_{\text{pol}} = +0.7). \end{aligned} \tag{8.53}$$

From the parameters (y, s) one can calculate the loss probabilities from equation (8.51) which leads to $P_{\text{ls}} = 0.96\,\%$ for ^{20}Ne and $P_{\text{ls}} = 6.63\,\%$ for ^{22}Ne. We can see that these loss probabilities are much lower than for the y parameters in (8.52). If we calculate the ratios $\beta_{22}/\beta_{m_1m_2}$ with $(m_1m_2) \neq (22)$ of the loss probabilities, we find $20.11\,\%/0.96\,\% \simeq 20.95$ for ^{20}Ne and $25.67\,\%/6.63\,\% \simeq 3.87$ for ^{22}Ne. Therefore, the suppression of loss in the *non-universal model* is higher in ^{20}Ne than in ^{22}Ne, which is consistent with the experimental observations. Calculating the scattering lengths from the parameter s of (8.53) leads to $a_{sc} = -151\ a_0$ for ^{20}Ne and $a_{sc} = +30\ a_0$ for ^{22}Ne. Again, the scattering length agrees well with the experimental measurement for ^{20}Ne but underestimates the magnitude of the scattering length for ^{22}Ne. Strikingly, the parameter values of s in (8.52) and in (8.53) are very similar and lead to similar scattering lengths for ^{20}Ne and ^{22}Ne.

In figure 8.13 and in figure 8.14 the scattering rates of the two-channel model of this chapter are compared to the threshold rates of the *non-universal model* with the fit parameters in (8.52) and in (8.53). It can be seen in the graphs, that in both cases, the scattering rates of the *non-universal model* are in very good agreement with the threshold scattering rates of the two-channel

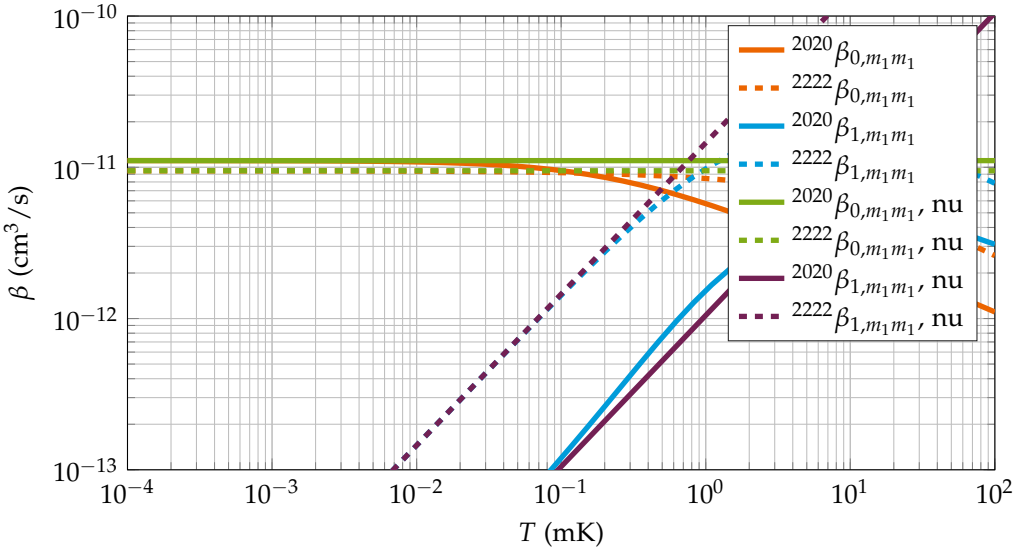

Figure 8.14: Partial two-body loss rate coefficients β_{l,m_1m_1} obtained by the two-channel model and obtained by the *non-universal model* (nu) for ^{20}Ne and for ^{22}Ne for spin-aligned collisions with $m_1 = 2$. The rates of the *non-universal model* are given for $c_6 = 1832.5$ a.u. and with the fit parameters of (8.53).

model in the limit $T \to 0$. Additionally, the physical interpretation of the parameters (y, s), found from the fit to match the scattering rates, is in good agreement with the experimental observations. Therefore, comparing the results of the two-channel model of this chapter to the *non-universal model* gives additional insight about the importance of short-range physics and the scattering lengths in Ne* collisions.

8.6.3 *Two-channel model with square-well potentials*

After the comparison of the two-channel model of this chapter to the *quantum reflection model* and the *non-universal model* we compare it with the coupled two-channel model with square-well potentials of the previous chapter. As an example we choose heteronuclear collisions of ^{20}Ne–^{21}Ne. The procedure of this subsection can of course be applied to different types of Ne* collisions.

The parametrized unaveraged two-body loss rate coefficients for the analytic square-well potentials were given in equation (7.60). They have been derived from a Taylor series of the background scattering phases in equation (7.58) up to first order in k. In order to fit the results of the simulations for $^{2120}\beta$ we found, that the background scattering phases have to include higher order terms, reading

$$\eta_0^{\mathrm{bg}}(k) = \log a_0 + b_0 k + c_0 k^2 + \ldots, \tag{8.54a}$$

$$\eta_1^{\mathrm{bg}}(k) = \log a_1 + b_1 k + c_1 k^2 + \ldots, \tag{8.54b}$$

$$\eta_2^{\mathrm{bg}}(k) = \log a_2 + b_2 k + c_2 k^2 + d_2 k^3 + d_3 k^4 + \ldots. \tag{8.54c}$$

Inserting these expansions for the background scattering phases in the equations (7.57) and the results in the equations (7.59) we calculate the two-body loss rate coefficients.

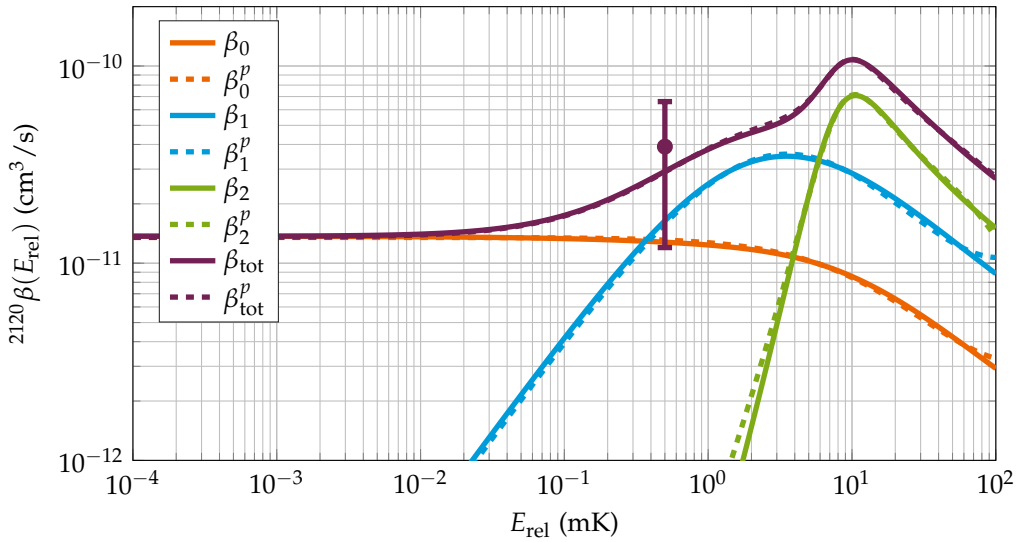

Figure 8.15: Partial and total two-body loss rate coefficients β_l, β as functions of the relative collision energy E_{rel} of the two-channel model of this chapter (solid lines) and of the model with square-well potentials (8.55) (dashed lines) with the fit parameters given in the equations (8.56), (8.57), (8.58).

As the coefficients b_l and d_2 are purely imaginary, we obtain

$$\beta_0^p(k) = \frac{2\pi|a_0|^2}{k^2 + \varkappa_1^2} e^{-c_0 k^2}, \tag{8.55a}$$

$$\beta_1^p(k) = \frac{6\pi|a_1|^2 e^{-c_1 k^2}}{\left(k^2 - \varkappa_1^2\right)^2 + 4\,\mathrm{Re}^2\,\kappa_1\,\mathrm{Im}^2\,\kappa_1} k^2, \tag{8.55b}$$

$$\beta_2^p(k) = \frac{10\pi|a_2|^2 e^{-c_2 k^2} e^{-e_2 k^4}}{\left(k^2 - \varkappa_2^2\right)^2 + 4\,\mathrm{Re}^2\,\kappa_2\,\mathrm{Im}^2\,\kappa_2} k^4. \tag{8.55c}$$

A least-square fit of these two-body loss parameters to the results of the simulations for the unaveraged partial two-body loss rate coefficients β_l for ^{20}Ne–^{21}Ne collisions leads for $l = 0$ to the coefficients

$$a_0 = 0.1477, \quad c_0 = -57.3641, \quad \varkappa_1 = 0.0408, \tag{8.56}$$

for $l = 1$ to the coefficients

$$a_1 = 0.1326, \quad c_1 = -76.8736, \tag{8.57a}$$

$$\mathrm{Re}\,\kappa_1 = 1.5e-10, \quad \mathrm{Im}\,\kappa_1 = -0.0198, \tag{8.57b}$$

and for $l = 2$ to the coefficients

$$a_2 = 2.3141, \quad c_2 = 64.7843, \quad e_2 = 642.3825, \tag{8.58a}$$

$$\mathrm{Re}\,\kappa_2 = 0.0304, \quad \mathrm{Im}\,\kappa_2 = -0.0100. \tag{8.58b}$$

Note, that the fit parameters $a_l, b_l, \ldots$ are the expansion coefficients of equation (8.54) and the positions $\varkappa_1$, κ_1, $\ldots$ are the pole positions of the S matrix in the complex k plane due to bound states and resonant states in the interaction channel of the coupled square-well potential.

In figure 8.15 the unaveraged two-body loss rate coefficients of the two-channel model with a realistic interaction potential and the two-body loss rate coefficients of the two-channel model with square-well potentials (8.55) are compared for ^{20}Ne–^{21}Ne collisions. It can be seen that both results agree very well. In figure 8.15 also the experimental data point is given even though it was obtained in a thermal ensemble of Ne atoms with temperature T. However, as the width of the Maxwell-Boltzmann distribution (5.169) of the relative velocities is large compared with

the widths of the resonances of the unaveraged two-body loss rate coefficients, the scattering rates are not very sensitive to the effect of averaging. As the errors bars for the two-body loss rate coefficients obtained in experiment are large compared with the effect of averaging on the loss rates, we can compare the calculated unaveraged two-body loss rate coefficients with the experimental measurement. It can be seen, that the two-body loss rate coefficients of both models as well as the experimental measurement agree very well for ^{20}Ne–^{21}Ne collisions. Therefore, we conclude that the physics of the coupled two-channel model is independent of the exact details of the potentials.

CONCLUSION

In this chapter we presented the coupled two-channels with a realistic interaction potential of Ne* as a model for cold collisions of Ne*. The two-channel model of this chapter describes elastic scattering and PI in Ne* collisions in terms of a single realistic interaction potential of Ne_2 and a single ionization potential. The effect of the suppression of PI due to spin-polarization of the atoms is included by the assumption of different coupling strengths for collisions in different internal states. We optimized the free potential parameters of this model in order to fit the experimental data and found, that the resulting scattering rates agree very well with the experimental measurements for the different isotope mixtures and internal spin-states. Furthermore, we compared the results to the *quantum reflection model* and the *non-universal model*. We found that the *quantum reflection model* cannot reproduce the results of the two-channel model and the experiment. With the *non-universal model*, we obtained agreement of the threshold behavior of the scattering rates of the two-channel model and the results for the fit parameters (y, s) agreed with the experimental observations. Finally, we demonstrated, that the two-body loss rate coefficients, which we have derived in the previous chapter for the analytic coupled square-well model from the pole expansion of the S matrix, agree with the results of the two-channel model of this chapter.

9

CONCLUSION

In this thesis we investigated theoretically the properties of cold gases of Ne*. These gases are dilute and the behavior is dominated by the binary interaction physics of Ne*. The collision physics is given by the short-range interactions and the long-range interactions between the atoms. The interaction energies were calculated for short-range interactions of Ne* in [6] and for long-range interactions of Ne* in [7–9] in the molecular bases of *Hund's case* (a) and *Hund's case* (c), respectively.

For employing these interaction potentials in the scattering equations for Ne* we examined the short-range and long-range interactions for simpler atomic systems in order to introduce the notation and in order to illuminate the symmetries and the spectroscopic notation for these interaction potentials. This has been done in this work by calculating the molecular potential energies of H_2^+ and H_2 as examples for the short-range interaction potentials and by calculating the *van der Waals* interaction energy of hydrogen and helium as examples for long-range interactions. We introduced the different molecular basis states in terms of the results of the calculated molecular potentials.

The scattering equations are solved by quantum scattering theory. Therefore, we introduced the basic concepts and operators of quantum scattering before we introduced the interaction potentials of Ne* at short- and long-range and set up the scattering equations for Ne* in terms these potentials.

Instead of solving the full scattering equations of Ne* by taking into account all the molecular potentials involved we introduced a coupled two-channel system as a model for cold reactive collisions of Ne*. In this model, the elastic scattering channel is given by a single interaction potential only and ionizing collisions are described by transitions from the elastic scattering channel to the second channel which represents the loss channel. We studied this two-channel model in a version, where both channels were given by square-well potentials. The Schrödinger equation for this model can be solved analytically and we examined the analytic solutions in the complex k plane. We found that the pole expansion of the S matrix is given in terms of a single term only if a bound state or a quasi-bound state is present in the scattering channel. With the single-pole expansion of the transition S matrix element we parametrized the two-body loss rate coefficients within this model for the lowest partial-waves.

In the second version of the two-channel model we employed a realistic interaction potential of Ne*, given by the calculated short-range and long-range interaction potentials for Ne* and a model ionization potential. We found that within this model we can describe the elastic and ionizing collisions of homonuclear and heteronuclear collisions of Ne* very well. The experimental data was used for a fit of the free potential parameters of the model which resulted in very good agreement of the calculations and the experiment. We understood the suppression of PI for spin-aligned collisions, which is observed in the experiment, in terms of a weaker coupling from the scattering channel to the ionization channel than the coupling for collisions in other states. The suppression ratios measured in the experiment were very well described with this mechanism for both homonuclear collision types. In heteronuclear collisions, the single set of potential parameters led to very good agreement of the calculations with the experiment for all available isotope mixtures. Therefore, this two-channel model is an accurate description of the Ne* collision properties and gives a simple interpretation of the suppression of PI due to spin-aligned collisions. We introduced this model since the *quantum reflection model*, which was employed successfully for other rare gas collisions, fails to describe Ne* collisions which was demonstrated in this work. We compared the two-channel model with the *non-universal*

model by fitting the free parameters of the rate coefficients of the *non-universal* model, which are valid in the $T \to 0$ limit, to the rate coefficients of the two-channel model and found that these parameters are in good agreement with the experimental observations. Therefore, the *non-universal* model is complementary to the two-channel model in the limit $T \to 0$.

Finally we found from a fit of the parametrized two-body loss rate coefficients of the two-channel model with square-well potentials to the two-body loss rate coefficients of the two-channel model with a realistic interaction potential very good agreement of these models as well as of the experiment. Therefore, we conclude that the coupled two-channel square-well model describes ionizing collisions of Ne*.

OUTLOOK

The two-channel models given in this work assume that Ne* collisions can be approximated by a single elastic scattering channel. In the version with a realistic interaction potential, this approximation explains very well the experimentally obtained scattering rates and covers the main features of Ne* collisions. However, it does not cover all the measured data points as it does not take into account all the details of the microscopic interactions. Therefore, one would need to solve the full *coupled channel equations* which were given in chapter 6 for a specific coupling scheme. Unfortunately, the short-range molecular interaction potentials are only known to a certain precision which is not sufficient to describe cold Ne* collisions accurately. Therefore, there is a need to calculate the short-range *Born-Oppenheimer* potentials of Ne_2 to a greater extent of accuracy. The information about auto-ionization widths and ionization potentials is also rare in the case of Ne*. A detailed study of the PI processes in Ne* is very challenging but mandatory to obtain more insight into the ionization properties of Ne*.

Most recently, the analysis of the experimental scattering data showed a dependency of the scattering rates of the temperature and of the magnetic field. The magnetic field dependence suggests lower ionization rates for higher magnetic fields in the case of ^{22}Ne collisions. It would prove interesting to investigate the behavior of the scattering rates for even higher magnetic fields as with lower ionization rates lower temperatures in atomic gases of Ne*, closer to T_c, could be achieved. Therefore, the quest still remains open if a phase transition of the thermal Ne* gas to a BEC can be observed. In addition to the suggested lower rates of ionization for higher magnetic fields, the isotope ^{22}Ne possesses the promising property of having a positive scattering length which is crucial for obtaining a stable BEC.

A

UNITS

Here we introduce atomic units and give numerical values for the fundamental constants of physics. In atomic units the energy scale is defined in terms of the Hartree energy E_h given by [42, 138]

$$\mathcal{E} \equiv E_h = \frac{\hbar^2}{m_e \mathrm{a}_0^2}, \tag{A.1}$$

where the physical constants are given in table A1. The length scale in atomic units is the Bohr radius

$$\mathcal{L} \equiv \mathrm{a}_0 = \frac{4\pi\varepsilon_0\hbar^2}{m_e e^2}. \tag{A.2}$$

The lengths and energies are scaled in these units

$$\tilde{r} = r/\mathrm{a}_0, \quad \tilde{E} = E/E_h. \tag{A.3}$$

quantity	symbol	numerical value	unit
Bohr radius	a_0	0.529 177 210 67(12)	Å
Hartree energy	E_h	$4.359\,744\,650(54) \times 10^{-18}$	J
Planck constant	h	$6.626\,070\,040(81) \times 10^{-34}$	Js
reduced Planck constant	$\hbar$	$1.054\,571\,800(13) \times 10^{-34}$	Js
electron mass	m_e	$9.109\,383\,56(11) \times 10^{-31}$	kg
electric constant	ε_0	$8.854\,187\,817\ldots \times 10^{-12}$	Fm^{-1}
elementary charge	e	$1.602\,176\,6208(98) \times 10^{-19}$	C
Boltzmann constant	k_B	$1.380\,648\,52(79) \times 10^{-23}$	JK^{-1}

Table A1: Fundamental constants of physics. We use the CODATA recommended values 2014 [139].

Single-particle Schrödinger equation

The advantage of using atomic units may be illustrated by introducing them to the Schrödinger equation for the electron in hydrogen which in SI units is given by

$$\left[-\frac{\hbar^2}{2m_e}\nabla_{\mathbf{r}}^2 - \frac{e^2}{4\pi\varepsilon_0 r}\right]\Psi(\mathbf{r}) = E\Psi(\mathbf{r}), \tag{A.4}$$

Substituting $\mathbf{r}$ with $\tilde{\mathbf{r}}$ results in

$$\left[-\frac{\hbar^2}{2m_e a_0^2}\nabla_{\tilde{\mathbf{r}}}^2 - \frac{e^2}{4\pi\varepsilon_0 \tilde{r} a_0}\right]\Psi(\tilde{\mathbf{r}}) = E\Psi(\tilde{\mathbf{r}}). \tag{A.5}$$

Further rearrangement of equation (A.5) leads to

$$\frac{\hbar^2}{m_e a_0^2}\left[-\frac{1}{2}\nabla_{\tilde{\mathbf{r}}}^2 - \frac{m_e a_0^2}{\hbar^2}\frac{e^2}{4\pi\varepsilon_0 \tilde{r} a_0}\right]\Psi(\tilde{\mathbf{r}}) = E\Psi(\tilde{\mathbf{r}}), \tag{A.6}$$

which finally can be expressed in terms of atomic units only as

$$\left[-\frac{1}{2}\nabla_{\tilde{\mathbf{r}}}^2 - \frac{1}{\tilde{r}}\right]\Psi(\tilde{\mathbf{r}}) = \tilde{E}\Psi(\tilde{\mathbf{r}}). \tag{A.7}$$

Two-particle radial Schrödinger equation

For two-particle scattering, with the wave function in the center-of-mass frame

$$\Psi(\mathbf{r}_1, \mathbf{r}_2) = \Psi_{\text{com}}(\mathbf{R}_{\text{com}}) \cdot \Psi_{\text{rel}}(\mathbf{r}), \tag{A.8}$$

the radial Schrödinger equation for the relative motion in atomic units reads

$$\left[-\frac{1}{2\tilde{\mu}}\nabla_{\tilde{r}}^2 + \tilde{V}(\tilde{r}) + \frac{l(l+1)}{2\tilde{\mu}\tilde{r}^2}\right]\Psi_{\text{rel}}(\tilde{r}) = \tilde{E}\Psi_{\text{rel}}(\tilde{r}). \tag{A.9}$$

Here the reduced mass $\tilde{\mu}$ in atomic units reads

$$\tilde{\mu} = \frac{1}{m_e}\frac{m_1 m_2}{m_1 + m_2} = \frac{\mu}{m_e}, \tag{A.10}$$

where m_1, m_2 are the particle masses. The interaction potential $\tilde{V}$ is scaled by the Hartree energy $\tilde{V} = V/E_h$. Multiplication of (A.9) with $2\tilde{\mu}$ leads to

$$\left[-\nabla_{\tilde{r}}^2 + 2\tilde{\mu}\tilde{V}(\tilde{r}) + \frac{l(l+1)}{\tilde{r}^2}\right]\Psi_{\text{rel}}(\tilde{r}) = \tilde{k}^2\Psi_{\text{rel}}(\tilde{r}), \tag{A.11}$$

where $\tilde{k}^2 = \tilde{E}$. This is the reduced radial Schrödinger equation for $\Psi_{\text{rel}}(\tilde{r})$ in atomic units.

B

ANGULAR MOMENTUM ALGEBRA

B.1 CLEBSCH-GORDAN COEFFICIENTS AND WIGNER nj SYMBOLS

Coupling of two angular momenta

Consider two states $|j_1 m_1\rangle$ and $|j_2 m_2\rangle$ which are eigenstates of the angular momenta $\mathbf{J}_1^2$ and $\mathbf{J}_2^2$ [140], We have

$$\mathbf{J}_1^2 |j_1 m_1\rangle = j_1(j_1+1) |j_1 m_1\rangle , \qquad \mathbf{J}_2^2 |j_2 m_2\rangle = j_2(j_2+1) |j_2 m_2\rangle , \tag{B.1}$$

$$J_{1z} |j_1 m_1\rangle = m_1 |j_1 m_1\rangle , \qquad J_{2z} |j_2 m_2\rangle = m_2 |j_2 m_2\rangle , \tag{B.2}$$

where J_{1z}, J_{2z} are the z components of $\mathbf{J}_1$, $\mathbf{J}_2$. In the uncoupled representation $|j_1 m_1\rangle |j_2 m_2\rangle$ the operators $\mathbf{J}_1^2$, $\mathbf{J}_2^2$, J_{1z}, J_{2z} are diagonal. Consider the total angular momentum operator

$$\mathbf{J} = \mathbf{J}_1 + \mathbf{J}_2. \tag{B.3}$$

We seek a representation in which $\mathbf{J}^2$ and J_z are also diagonal with eigenvalues $j(j+1)$ and m. This coupled representation is given by a unitary transformation of the uncoupled basis

$$|jm\rangle = \sum_{m_1,m_2} \langle j_1 m_1 j_2 m_2 | jm\rangle \, |j_1 m_1\rangle \, |j_2 m_2\rangle . \tag{B.4}$$

The numbers $\langle j_1 m_1 j_2 m_2 | jm\rangle$ are the Clebsch-Gordan coefficients and may be written in various forms for example as

$$\langle j_1 m_1 j_2 m_2 | jm\rangle = C(j_1 j_2 j; m_1 m_2 m). \tag{B.5}$$

The Clebsch-Gordan coefficients are non-zero only if $|j_1 - j_2| \leq j \leq j_1 + j_2$ and if $m_1 + m_2 = m$ is fulfilled. They possess important symmetry properties, in particular

$$C(j_1 j_2 j; m_1 m_2 m) = (-1)^{j_1+j_2-j_3} C(j_2 j_1 j; m_2 m_1 m), \tag{B.6}$$

which has been used explicitly in section 6.9 to obtain properly symmetrized wave functions under the exchange of nuclei which possess angular momenta j_1 and j_2.

The Clebsch-Gordan coefficients may be written in terms of Wigner $3j$ symbols [141]

$$\begin{pmatrix} j_1 & j_2 & j \\ m_1 & m_2 & m \end{pmatrix} = (-1)^{j_1-j_2-m} (2j+1)^{-\frac{1}{2}} \langle j_1 m_1 j_2 m_2 | j - m\rangle. \tag{B.7}$$

The advantage of the Wigner $3j$ symbols over the Clebsch-Gordan coefficients is the easier way of deducing the symmetries. An even number of permutations of the rows of the Wigner $3j$ symbols is not leading to a change in sign

$$\begin{pmatrix} j_1 & j_2 & j \\ m_1 & m_2 & m \end{pmatrix} = \begin{pmatrix} j_2 & j & j_1 \\ m_2 & m & m_1 \end{pmatrix} = \begin{pmatrix} j & j_1 & j_2 \\ m & m_1 & m_2 \end{pmatrix}, \tag{B.8}$$

whereas an odd number of permutations leads to a factor $(-1)^{j_1+j_2+j}$

$$(-1)^{j_1+j_2+j} \begin{pmatrix} j_1 & j_2 & j \\ m_1 & m_2 & m \end{pmatrix} = \begin{pmatrix} j_2 & j_1 & j \\ m_2 & m_1 & m \end{pmatrix} = \begin{pmatrix} j_1 & j & j_2 \\ m_1 & m & m_2 \end{pmatrix} = \begin{pmatrix} j & j_2 & j_1 \\ m & m_2 & m_1 \end{pmatrix}. \tag{B.9}$$

Coupling of three angular momenta

Consider now three angular momenta $\mathbf{J}_1$, $\mathbf{J}_2$, $\mathbf{J}_3$. These angular momenta may be coupled in various ways to obtain the total angular momentum $\mathbf{J}$. One way is given by

$$\mathbf{J}_{12} = \mathbf{J}_1 + \mathbf{J}_2, \quad \mathbf{J} = \mathbf{J}_{12} + \mathbf{J}_3, \tag{B.10}$$

where first $\mathbf{J}_1$ and $\mathbf{J}_2$ couple to $\mathbf{J}_{12}$ which then couples with $\mathbf{J}_3$ to give $\mathbf{J}$. A second way is given by

$$\mathbf{J}_{23} = \mathbf{J}_2 + \mathbf{J}_3, \quad \mathbf{J} = \mathbf{J}_{23} + \mathbf{J}_1, \tag{B.11}$$

where first $\mathbf{J}_2$ and $\mathbf{J}_3$ couple to $\mathbf{J}_{23}$ which then couples with $\mathbf{J}_1$ to give $\mathbf{J}$. Both coupling schemes lead to a coupled representation $|((j_1j_2)j_{12}j_3)jm\rangle$ for (B.10) and $|((j_2j_3)j_{23}j_1)jm\rangle$ for (B.11). It is important to note that the states $|jm\rangle$ obtained from coupling three angular momenta are not uniquely determined but depend on the details of the specific coupling scheme so that in general $|((j_1j_2)j_{12}j_3)jm\rangle \neq |((j_2j_3)j_{23}j_1)jm\rangle$. The two states are however related by a unitary transformation [40]

$$|((j_2j_3)j_{23}j_1)jm\rangle = \sum_{j_{12}} |((j_1j_2)j_{12}j_3)jm\rangle \, \langle((j_1j_2)j_{12}j_3)j|((j_2j_3)j_{23}j_1)j\rangle. \tag{B.12}$$

The coefficient $\langle((j_1j_2)j_{12}j_3)j|((j_2j_3)j_{23}j_1)j\rangle$ is given in terms of the Wigner $6j$ symbol as

$$\langle((j_1j_2)j_{12}j_3)j|((j_2j_3)j_{23}j_1)j\rangle = \sqrt{(2j_{12}+1)(2j_{23}+1)}(-1)^{j_1+j_2+j_3+j} \begin{Bmatrix} j_1 & j_2 & j_{12} \\ j_3 & j & j_{23} \end{Bmatrix}. \tag{B.13}$$

The $6j$ symbol is invariant under an interchange of columns and an interchange of two numbers in the bottom row with the respective two numbers in the top row [98]

$$\begin{Bmatrix} a & b & e \\ d & c & f \end{Bmatrix} = \begin{Bmatrix} a & e & b \\ d & f & c \end{Bmatrix} = \begin{Bmatrix} e & b & a \\ f & c & d \end{Bmatrix} = \begin{Bmatrix} a & c & f \\ d & b & e \end{Bmatrix} = \begin{Bmatrix} d & c & e \\ a & b & f \end{Bmatrix} = \dots \tag{B.14}$$

The Wigner $6j$ symbols can be expressed by the Racah W-coefficient [98]

$$\begin{Bmatrix} j_1 & j_2 & j_3 \\ l_1 & l_2 & l_3 \end{Bmatrix} = (-1)^{j_1+j_2+l_1+l_2} W(j_1j_2l_2l_1; j_3l_3). \tag{B.15}$$

Coupling of four angular momenta

Assume now the coupling of four angular momenta $\mathbf{J}_1$, $\mathbf{J}_2$, $\mathbf{J}_3$, $\mathbf{J}_4$. Again, there are various ways of coupling these four momenta to a total angular momentum $\mathbf{J}$. Assume again two different ways of coupling the four angular momenta

$$\mathbf{J}_{12} = \mathbf{J}_1 + \mathbf{J}_2, \quad \mathbf{J}_{34} = \mathbf{J}_3 + \mathbf{J}_4, \quad \mathbf{J} = \mathbf{J}_{12} + \mathbf{J}_{34}, \tag{B.16}$$

$$\mathbf{J}_{13} = \mathbf{J}_1 + \mathbf{J}_3, \quad \mathbf{J}_{24} = \mathbf{J}_2 + \mathbf{J}_4, \quad \mathbf{J} = \mathbf{J}_{13} + \mathbf{J}_{24}. \tag{B.17}$$

The unitary transformation between the states $|((j_1j_2)j_{12}(j_3j_4)j_{34})jm\rangle$ and $|((j_1j_3)j_{13}(j_2j_4)j_{24})jm\rangle$ is given by

$$|((j_1j_3)j_{13}(j_2j_4)j_{24})jm\rangle = \sum_{j_{12},j_{34}} |((j_1j_2)j_{12}(j_3j_4)j_{34})jm\rangle \, \langle((j_1j_2)j_{12}(j_3j_4)j_{34})j|((j_1j_3)j_{13}(j_2j_4)j_{24})j\rangle, \tag{B.18}$$

where the coefficients $\langle((j_1j_2)j_{12}(j_3j_4)j_{34})j|((j_1j_3)j_{13}(j_2j_4)j_{24})j\rangle$ may be written in terms of the Wigner $9j$ symbols

$$\begin{aligned} \langle((j_1j_2)j_{12}(j_3j_4)j_{34})j|((j_1j_3)j_{13}(j_2j_4)j_{24})j\rangle = & \begin{Bmatrix} j_1 & j_2 & j_{12} \\ j_3 & j_4 & j_{34} \\ j_{13} & j_{24} & j \end{Bmatrix} \\ & \times \sqrt{(2j_{12}+1)(2j_{34}+1)(2j_{13}+1)(2j_{24}+1)}. \end{aligned} \tag{B.19}$$

The symmetries of the Wigner 9j symbols were investigated in [142]. The Wigner 9j symbol is invariant under the interchange of rows and columns. Upon the interchange of two adjacent rows or columns it is multiplied by $(-1)^{j_1+j_2+j_{12}+j_3+j_4+j_{34}+j_{13}+j_{24}+j}$. A contraction in terms of Racah coefficients is given by

$$\begin{Bmatrix} a & b & c \\ d & e & f \\ g & h & i \end{Bmatrix} = \sum_k (2k+1) W(aidh;kg) W(bfhd;ke) W(aibf;kc). \tag{B.20}$$

Coupling of five angular momenta

To conclude the discussion of Wigner symbols we look at the coupling of five angular momenta $\mathbf{J}_1$, $\mathbf{J}_2$, $\mathbf{J}_3$, $\mathbf{J}_4$, $\mathbf{J}_5$. Two different ways of coupling these momenta to a total angular momentum $\mathbf{J}$ read

$$\mathbf{J}_{12} = \mathbf{J}_1 + \mathbf{J}_2, \quad \mathbf{J}_{123} = \mathbf{J}_{12} + \mathbf{J}_3, \quad \mathbf{J}_{45} = \mathbf{J}_4 + \mathbf{J}_5, \quad \mathbf{J} = \mathbf{J}_{123} + \mathbf{J}_{45} \tag{B.21}$$

$$\mathbf{J}_{14} = \mathbf{J}_1 + \mathbf{J}_4, \quad \mathbf{J}_{143} = \mathbf{J}_{14} + \mathbf{J}_3, \quad \mathbf{J}_{25} = \mathbf{J}_2 + \mathbf{J}_5, \quad \mathbf{J} = \mathbf{J}_{143} + \mathbf{J}_{25}. \tag{B.22}$$

The states $|(((j_1 j_2) j_{12}, j_3) j_{123} (j_4 j_5) j_{45}) jm\rangle$ and $|(((j_1 j_4) j_{14}, j_3) j_{143} (j_2 j_5) j_{25}) jm\rangle$ are related by a unitary transformation

$$\begin{aligned} |(((j_1 j_4) j_{14}, j_3) j_{143} (j_2 j_5) j_{25}) jm\rangle = \sum_{j_{12}, j_{123}, j_{45}} & |(((j_1 j_2) j_{12}, j_3) j_{123} (j_4 j_5) j_{45}) jm\rangle \\ & \times \langle (((j_1 j_2) j_{12}, j_3) j_{123} (j_4 j_5) j_{45}) j | (((j_1 j_4) j_{14}, j_3) j_{143} (j_2 j_5) j_{25}) j\rangle. \end{aligned} \tag{B.23}$$

The coefficients $\langle (((j_1 j_2) j_{12}, j_3) j_{123} (j_4 j_5) j_{45}) j | (((j_1 j_4) j_{14}, j_3) j_{143} (j_2 j_5) j_{25}) j\rangle$ are expressed in terms of the Wigner 12j symbol [143]

$$\begin{aligned} &\langle (((j_1 j_2) j_{12}, j_3) j_{123} (j_4 j_5) j_{45}) j | (((j_1 j_4) j_{14}, j_3) j_{143} (j_2 j_5) j_{25}) j\rangle = \\ &\sqrt{(2j_{12}+1)(2j_{45}+1)(2j_{14}+1)(2j_{25}+1)(2j_{123}+1)(2j_{143}+1)} \begin{Bmatrix} j_1 & j_2 & j_{12} & j_{123} \\ j_4 & j_5 & j_{45} & j_{143} \\ j_{14} & h & j_3 & j \end{Bmatrix}. \end{aligned} \tag{B.24}$$

The decomposition of the Wigner 12j symbol in terms of the Wigner 6j symbols reads

$$\begin{Bmatrix} a & b & e & p \\ c & d & f & q \\ g & h & r & s \end{Bmatrix} = (-1)^R \sum_x (-1)^{-x} \begin{Bmatrix} b & c & x \\ g & e & a \end{Bmatrix} \begin{Bmatrix} g & e & x \\ p & q & r \end{Bmatrix} \begin{Bmatrix} p & q & x \\ h & f & s \end{Bmatrix} \begin{Bmatrix} h & f & x \\ c & b & d \end{Bmatrix}, \tag{B.25}$$

where R is the sum over all twelve elements of the 12j symbol.

B.2 WIGNER D-MATRIX

In scattering calculations very often the basis states are transformed from the atomic basis in space-fixed coordinates to the molecular basis in body-fixed coordinates. Different coordinate systems are the systems in $\mathbf{k}$-direction or in $\mathbf{k}'$-direction. Figure 2.1 shows these various kinds of coordinate systems with respect to a space-fixed system.
The rotation of the basis states is performed by the Wigner D matrix [144]. Assume that J_x, J_y, J_z are the generators of the Lie algebra of SU(2) and SO(3). They are the components of the angular momentum operator $\mathbf{J}$ and the following commutation relations hold

$$[J_x, J_y] = iJ_z, \quad [J_z, J_x] = iJ_y, \quad [J_y, J_z] = iJ_x. \tag{B.26}$$

The eigenvalue equation for $\mathbf{J}^2 = J_x^2 + J_y^2 + J_z^2$ and J_z read

$$\mathbf{J}^2 |jm\rangle = j(j+1) |jm\rangle, \quad J_z |jm\rangle = m |jm\rangle, \tag{B.27}$$

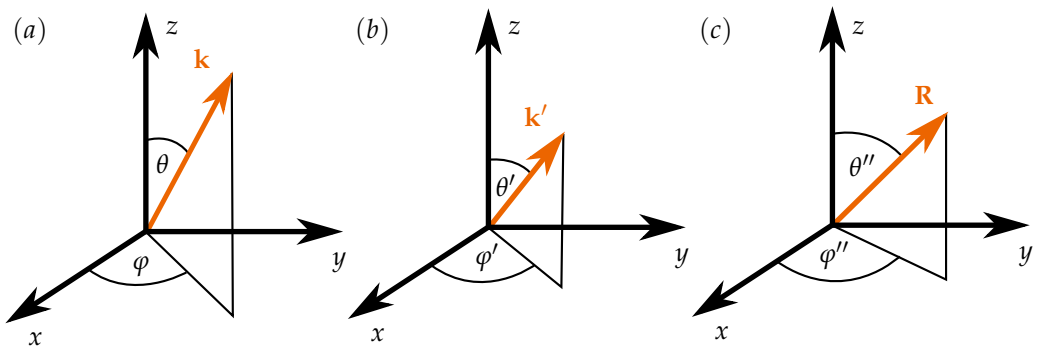

Figure 2.1: In subfigure (a) the polar angles (θ, φ) of the incident wave number $\mathbf{k}$ with respect to the space-fixed frame xyz is shown. Subfigure (b) shows a different set of polar angles (θ', φ') which are the polar angles of the scattered wave number $\mathbf{k}'$. Subfigure (c) shows the polar angles (θ'', φ'') of the internuclear axis $\mathbf{R}$.

with $|jm\rangle$ the total angular momentum states. For an arbitrary rotation of coordinate system a rotation operator can be defined in terms of the components of $\mathbf{J}$ as [145]

$$R(\alpha, \beta, \gamma) = e^{-i\alpha J_z} e^{-i\beta J_y} e^{-i\gamma J_z}, \tag{B.28}$$

where (α, β, γ) are the Euler angles. The Wigner D-matrix is defined by [84]

$$D^j_{m'm}(\alpha, \beta, \gamma) \equiv \langle jm'| R(\alpha, \beta, \gamma) |jm\rangle = e^{-im'\alpha} d^j_{m'm}(\beta) e^{-im\gamma}, \tag{B.29}$$

which is a $2j+1$ dimensional matrix and where m, m' are the projections of $\mathbf{J}$ on the unrotated and rotated axis, respectively. Here we have introduced the element of the Wigner (small) D-matrix

$$d^j_{m'm}(\beta) = D^j_{m'm}(0, \beta, 0) = \langle jm'| e^{-i\beta J_y} |jm\rangle . \tag{B.30}$$

One may write out the Wigner (small) D-matrix more explicitly

$$d^j_{m'm}(\beta) = \sum_t (-1)^t \frac{\sqrt{(j+m')!(j-m')!(j+m)!(j-m)!}}{(j+m'-t)!(j-m-t)!t!(t-m'+m)!} \tag{B.31}$$

$$\times \left(\cos \tfrac{1}{2}\beta\right)^{2j+m'-m-2t} \times \left(\sin \tfrac{1}{2}\beta\right)^{2t-m'+m}. \tag{B.32}$$

A rotation of the state in equation (B.27) through the Euler angles (α, β, γ) is given by

$$R(\alpha, \beta, \gamma) |jm\rangle = \sum_{m'} |jm'\rangle \langle jm'| R(\alpha, \beta, \gamma) |jm\rangle = \sum_{m'} D^j_{m'm}(\alpha, \beta, \gamma) |jm'\rangle , \tag{B.33}$$

The following orthogonality relation is fulfilled by the Wigner D-matrices [145]

$$\int_0^{2\pi} d\alpha \int_0^{\pi} \sin\beta d\beta \int_0^{2\pi} d\gamma D^{j'}_{m'k'}(\alpha, \beta, \gamma)^* D^j_{mk}(\alpha, \beta, \gamma) = \frac{8\pi^2}{2j+1} \delta_{m'm} \delta_{k'k} \delta_{j'j}, \tag{B.34}$$

and for integer $j = l$ the rotation matrices are related to the spherical harmonics $Y_{lm}(\beta, \alpha)$ as

$$D^l_{m0}(\alpha, \beta, 0)^* = \sqrt{\frac{4\pi}{2l+1}} Y_{lm}(\beta, \alpha) \tag{B.35}$$

and to the associated Legendre functions $P^m_l(\cos\beta)$ as

$$d^l_{m0}(\beta) = (-1)^m \left[\frac{(l-m)!}{(l+m)!}\right]^{\frac{1}{2}} P^m_l(\cos\beta). \tag{B.36}$$

C

BESSEL FUNCTIONS

C.1 BESSEL FUNCTIONS

An overview of the properties of the Bessel functions may be found in [146]. The Bessel functions are solutions to the differential equation [13]

$$z^2\frac{d^2w}{dz^2}+z\frac{dw}{dz}+\left(z^2-\nu^2\right)w=0, \tag{C.1}$$

which has a regular singularity at $z=0$ with indices $\pm\nu$ and an irregular singularity at $z=\infty$ of rank 1. The solutions are given in terms of the Bessel functions of the First Kind

$$J_\nu(z)=\left(\tfrac{1}{2}z\right)^\nu\sum_{k=0}^{\infty}(-1)^k\frac{(\frac{1}{4}z^2)^k}{k!\Gamma(\nu+k+1)}, \tag{C.2}$$

where $\Gamma(x)$ is the Gamma function. These functions are analytic functions of $z\in\mathbb{C}$ except at $z=0$ if ν is not an integer. If ν is an integer, the functions $J_\nu(z)$ are entire functions of z. The Bessel functions of the Second Kind which are also known as Weber's function are given in terms of the Bessel functions of the First Kind

$$Y_\nu(z)=\frac{J_\nu(z)\cos\nu\pi-J_{-\nu}(z)}{\sin\nu\pi} \tag{C.3}$$

The Bessel functions of the First Kind an the Second Kind are both real-valued functions when $\nu\in\mathbb{R}$ and $\operatorname{ph} z=0$. The complex-valued functions are superpositions of $J_\nu(z)$ and $Y_\nu(z)$ and given by

$$H_\nu^{\pm}(z)=J_\nu(z)\pm iY_\nu(z), \tag{C.4}$$

and are called the Bessel functions of the Third Kind or the Hankel functions. For $z\to\infty$ the Hankel functions behave as

$$H_\nu^{+}(z)\sim\sqrt{\frac{2}{\pi z}}e^{i(z-\nu\pi/2-\pi/4)}, \tag{C.5}$$

$$H_\nu^{+}(z)\sim\sqrt{\frac{2}{\pi z}}e^{-i(z-\nu\pi/2-\pi/4)}. \tag{C.6}$$

C.2 SPHERICAL BESSEL FUNCTIONS

The spherical Bessel functions are solutions to the differential equation

$$z^2\frac{d^2w}{dz^2}+2z\frac{dw}{dz}+\Big(z^2-n(n+1)\Big)w=0, \tag{C.7}$$

where n is an integer in contrast to ν in (C.1) which may take any complex value. The solutions are the spherical Bessel functions of the First Kind $j_n(z)$ and of the Second Kind $y_n(z)$ and given by

$$j_n(z)=\sqrt{\frac{\pi}{2z}}J_{n+\frac{1}{2}}(z), \tag{C.8a}$$

$$y_n(z)=\sqrt{\frac{\pi}{2z}}Y_{n+\frac{1}{2}}(z)=(-1)^{n+1}\sqrt{\frac{\pi}{2z}}J_{-n-\frac{1}{2}}. \tag{C.8b}$$

The spherical Bessel functions of the Third Kind or the spherical Hankel functions are superpositions of $j_n(z)$ and $y_n(z)$ as in (C.4)

$$h_n^{\pm}(z) = \sqrt{\frac{\pi z}{2}} H^{\pm}_{n+\frac{1}{2}}(z). \tag{C.9}$$

C.3 RICCATI-BESSEL FUNCTIONS

The Riccati-Bessel functions are solutions to the differential equation

$$\frac{d^2w}{dz^2} + \left(1 - \frac{n(n+1)}{z^2}\right) w = 0, \tag{C.10}$$

where again, as in the differential equation (C.7), n is an integer number. There are slightly different definitions and notations in the literature regarding the solutions of (C.10). Therefore, we give an overview over these different definitions in the literature.

Abramowitz

The solutions to (C.10) given by [13] read

$$\hat{\jmath}_n(z) = z j_n(z) = \sqrt{\frac{\pi z}{2}} J_{n+\frac{1}{2}}(z), \quad \hat{y}_n(z) = z y_n(z) = \sqrt{\frac{\pi z}{2}} Y_{n+\frac{1}{2}}(z), \tag{C.11}$$

for the Riccati-Bessel functions of the First Kind and Second Kind and for the Riccati-Hankel functions

$$\hat{h}_n^{\pm}(z) = z h_n^{\pm}(z) = \hat{\jmath}_n(z) \pm i\hat{y}_n(z). \tag{C.12}$$

Taylor

In [38] the Riccati-Neumann function is introduced as

$$\hat{n}_n(z) = z n_n(z) = -\sqrt{\frac{\pi z}{2}} Y_{n+\frac{1}{2}}(z), \tag{C.13}$$

which differs from $\hat{y}_n(z)$ of [13] by a minus sign. The Riccati-Bessel function of the First Kind $\hat{\jmath}_n(z)$ is identical to (C.11). The Riccati-Hankel functions in [38] are defined in terms of the Riccati-Neumann functions (C.13) and the Riccati-Bessel functions and read

$$\hat{h}_n^{\pm}(z) = \hat{n}_n(z) \pm i\hat{\jmath}_n(z), \tag{C.14}$$

which is a different definition than in [13]. The low z behavior of $\hat{\jmath}_n(z)$ and $n_n(z)$ are given by

$$\hat{\jmath}_n(z) = \frac{z^{n+1}}{(2n+1)!!}\left[1 + \mathcal{O}(z^2)\right], \quad [z \to 0] \tag{C.15}$$

$$\hat{n}_n(z) = z^{-n}(2n-1)!!\left[1 + \mathcal{O}(z^2)\right]. \quad [z \to 0] \tag{C.16}$$

For large z the functions $\hat{\jmath}_n(z)$, $\hat{n}_n(z)$ behave as

$$\hat{\jmath}_n(z) \underset{z\to\infty}{\simeq} \sin(z - n\pi/2), \tag{C.17}$$

$$\hat{n}_n(z) \underset{z\to\infty}{\simeq} \cos(z - n\pi/2), \tag{C.18}$$

and the Riccati-Hankel functions defined by (C.14) as

$$\hat{h}_n^{\pm}(z) \underset{z\to\infty}{\simeq} e^{\pm i(z - n\pi/2)}\left[1 + \mathcal{O}(z^{-1})\right]. \tag{C.19}$$

Important relation between $\hat{h}_n^+$ and $\hat{h}_n^-$ read

$$\hat{h}_n^{\pm}(-z) = (-1)^l \hat{h}_n^{\mp}(z), \tag{C.20}$$

$$\hat{h}_n^{\pm}(z)^* = \hat{h}_n^{\mp}(z), \quad z \text{ real}. \tag{C.21}$$

Newton

In [37] the Riccati-Bessel functions are defined by

$$u_n(z) = z j_n(z) = \sqrt{\frac{\pi z}{2}} J_{n+\frac{1}{2}}(z), \tag{C.22}$$

$$v_n(z) = \sqrt{\frac{\pi z}{2}} N_{n+\frac{1}{2}}(z) = z n_n(z), \tag{C.23}$$

where $N_n(z)$ are the Neumann functions. The definition for $v_n(z)$ is equivalent to the definition (C.11) but differs by a minus sign from (C.13). The Riccati-Bessel function of the First Kind $\hat{\jmath}_n(z)$ and $u_n(z)$ are equivalent. The Riccati-Hankel functions in [37] read

$$w_n^+(z) = i e^{i\pi n} \sqrt{\frac{\pi z}{2}} H^{(+)}_{n+\frac{1}{2}}(z) = i e^{i\pi n} z h_n^{(+)}(z), \tag{C.24a}$$

$$w_n^-(z) = w_n^+(-z) = e^{i\pi n} w_n^+(z)^* = -i \sqrt{\frac{\pi z}{2}} H^{(-)}_{n+\frac{1}{2}}(z). \tag{C.24b}$$

The different phase factors introduced in (C.24) compared to (C.14) leads to a different asymptotic behavior for the Riccati-Hankel functions, reading

$$w_n^\pm(z) \underset{z\to\infty}{\simeq} e^{i(\pm z + 1/2\pi n)}. \tag{C.25}$$

In this work we use exclusively the definitions of [38].

D

EULER-MASCHERONI CONSTANT AND EXPONENTIAL INTEGRAL

γ is the *Euler-Mascheroni constant* [147] and $\mathrm{Ei}(x)$ is the *exponential integral* [13]. The *Euler-Mascheroni constant* is defined by

$$\gamma \equiv \lim_{n\to\infty}\left(-\ln n + \sum_{k=1}^{n} 1/k\right), \tag{D.1}$$

and has the numerical value $\gamma = 0.5772\ldots$ The *exponential integral* is given by

$$\mathrm{Ei}(x) = -\int_{-x}^{\infty} \frac{e^{-}t}{t} dt, \tag{D.2}$$

which for positive values has to be understood in the Cauchy principal value sense [114].

E

LIST OF ABBREVIATIONS AND ACRONYMS

List of abbreviations and acronyms used throughout this thesis:

AI	Associative Ionization
BEC	Bose-Einstein Condensate
CC	Coupled Cluster
CI	Configuration Interaction
CODATA	Comittee on Data for Science and Technology
DWBA	Distorted-Wave Born Approximation
GAMESS	General Atomic and Molecular Electronic Structure System
GTO	Gaussian-Type Orbital
GVB	Generalized Valence Bond
HBT	Hanbury-Brown-and-Twiss
HF	Hartree-Fock
HL	Heitler-London
LCAO	Linear Combination of Atomic Orbitals
MCQDT	Multichannel Quantum Defect Theory
MCSCF	Multi-Configurational Self-Consistent Field
MP	Møller-Plesset perturbation theory
PGTO	Primitive Gaussian-Type Orbital
PI	Penning Ionization
Rg	Rare gas
RHF	Restricted Hartree-Fock
ROHF	Restricted Open-Shell Hartree-Fock
STO	Slater-Type Orbital
(TD)DFT	(Time-Dependent) Density Functional Theory
UHF	Unrestricted Hartree-Fock

BIBLIOGRAPHY

[1] W. Vassen, C. Cohen-Tannoudji, M. Leduc, D. Boiron, C. I. Westbrook, A. Truscott, K. Baldwin, G. Birkl, P. Cancio, and M. Trippenbach. Cold and trapped metastable noble gases. *Reviews of Modern Physics*, 84(1):175–210, February 2012.

[2] P. Spoden, M. Zinner, N. Herschbach, W. J. van Drunen, W. Ertmer, and G. Birkl. Collisional properties of cold spin-polarized metastable neon atoms. *Physical Review Letters*, 94(22):223201, June 2005.

[3] T. Feldker, J. Schuetz, H. John, and G. Birkl. Magneto-optical trapping of bosonic and fermionic neon isotopes and their mixtures: isotope shift of the P-3(2) <-> D-3(3) transition and hyperfine constants of the D-3(3) state of Ne-21. *European Physical Journal D*, 65(1-2):257–262, November 2011.

[4] J. Schuetz, T. Feldker, H. John, and G. Birkl. Heteronuclear collisions between laser-cooled metastable neon atoms. *Physical Review A*, 86(2):022713, August 2012.

[5] J. Schuetz. *Collisional interactions in isotope and spin mixtures of laser-cooled metastable neon atoms*. PhD thesis, TU Darmstadt, 2013.

[6] S. Kotochigova, E. Tiesinga, and I. Tupitsyn. Nonrelativistic ab initio calculation of the interaction potentials between metastable Ne atoms. *Physical Review A*, 61(4):042712, April 2000.

[7] M. R. Doery, E. J. D. Vredenbregt, J. G. C. Tempelaars, H. C. W. Beijerinck, and B. J. Verhaar. Long-range diatomic s+p potentials of heavy rare gases. *Physical Review A*, 57y(5):3603–3620, May 1998.

[8] M. R. Doery, E. J. D. Vredenbregt, S. S. O. de Beek, H. C. W. Beijerinck, and B. J. Verhaar. Limit on suppression of ionization in metastable neon traps due to long-range anisotropy. *Physical Review A*, 58(5):3673–3682, November 1998.

[9] A. Derevianko and A. Dalgarno. Long-range interaction of two metastable rare-gas atoms. *Physical Review A*, 62(6):062501, December 2000.

[10] Bose. Plancks Gesetz und Lichtquantenhypothese. *Zeitschrift für Physik*, 26(1):178–181, 1924.

[11] *Sitzungsberichte der Preussischen Akademie der Wissenschaften. Physikalisch-mathematische Klasse.*, 1924.

[12] C.J. Pethick and H. Smith. *Bose-Einstein Condensation in Dilute Gases*. Cambridge University Press, 2002.

[13] M. Abramowitz and I. Stegun. *Handbook of mathematical functions*. Dover Publications, Inc., 1965.

[14] K.B. Davis et al. Bose-Einstein Condensation in a Gas of Sodium Atoms. *Phys. Rev. Lett.*, 75(3969), 1995.

[15] Isaac F. Silvera and J. T. M. Walraven. Stabilization of Atomic Hydrogen at Low Temperature. *Phys. Rev. Lett.*, 44:164–168, Jan 1980.

[16] Harald F. Hess. Evaporative cooling of magnetically trapped and compressed spin-polarized hydrogen. *Phys. Rev. B*, 34:3476–3479, Sep 1986.

[17] H.J. Metcalf and P. van der Straten. *Laser cooling and trapping (corr. 2nd print)*. Springer, 2002.

[18] M.H. Anderson et al. Observation of Bose-Einstein Condensation in a Dilute Atomic Vapor. *Science*, 269(198), 1995.

[19] Steven Chu. Nobel lecture: The manipulation of neutral particles. *Rev. Mod. Phys.*, 70:685–706, Jul 1998.

[20] Claude N. Cohen-Tannoudji. Nobel lecture: Manipulating atoms with photons. *Rev. Mod. Phys.*, 70:707–719, Jul 1998.

[21] William D. Phillips. Nobel lecture: Laser cooling and trapping of neutral atoms. *Rev. Mod. Phys.*, 70:721–741, Jul 1998.

[22] E. A. Cornell and C. E. Wieman. Nobel Lecture: Bose-Einstein condensation in a dilute gas, the first 70 years and some recent experiments. *Rev. Mod. Phys.*, 74:875–893, Aug 2002.

[23] Wolfgang Ketterle. Nobel lecture: When atoms behave as waves: Bose-Einstein condensation and the atom laser. *Rev. Mod. Phys.*, 74:1131–1151, Nov 2002.

[24] A. Aspect, E. Arimondo, R. Kaiser, N. Vansteenkiste, and C. Cohen-Tannoudji. Laser cooling below the one-photon recoil energy by velocity-selective coherent population trapping. *Phys. Rev. Lett.*, 61:826–829, Aug 1988.

[25] Fujio Shimizu, Kazuko Shimizu, and Hiroshi Takuma. Laser cooling and trapping of Ne metastable atoms. *Phys. Rev. A*, 39:2758–2760, Mar 1989.

[26] F.M. Penning. Ueber Ionisation durch metastabile Atome. *Naturwissenschaften*, 15(40):818–818, 1927.

[27] P. E. Siska. Molecular-beam Studies of Penning Ionization. *Reviews of Modern Physics*, 65(2):337–412, April 1993.

[28] Masami Yasuda and Fujio Shimizu. Observation of two-atom correlation of an ultracold neon atomic beam. *Phys. Rev. Lett.*, 77:3090–3093, Oct 1996.

[29] M. Schellekens, R. Hoppeler, A. Perrin, J. Viana Gomes, D. Boiron, A. Aspect, and C. I. Westbrook. Hanbury brown twiss effect for ultracold quantum gases. *Science*, 310(5748):648–651, 2005.

[30] F. P. Dos Santos, J. Leonard, J. M. Wang, C. J. Barrelet, F. Perales, E. Rasel, C. S. Unnikrishnan, M. Leduc, and C. Cohen-Tannoudji. Bose-Einstein condensation of metastable helium. *Physical Review Letters*, 86(16):3459–3462, April 2001.

[31] F. P. Dos Santos, J. Leonard, J. M. Wang, C. J. Barrelet, F. Perales, E. Rasel, C. S. Unnikrishnan, M. Leduc, and C. Cohen-Tannoudji. Production of a Bose Einstein condensate of metastable helium atoms. *European Physical Journal D*, 19(1):103–109, April 2002.

[32] A. Robert, O. Sirjean, A. Browaeys, J. Poupard, S. Nowak, D. Boiron, C. I. Westbrook, and A. Aspect. A Bose-Einstein condensate of metastable atoms. *Science*, 292(5516):461–464, April 2001.

[33] J. M. McNamara, T. Jeltes, A. S. Tychkov, W. Hogervorst, and W. Vassen. Degenerate Bose-Fermi Mixture of Metastable Atoms. *Phys. Rev. Lett.*, 97:080404, Aug 2006.

[34] H.S.W. Massey. *Electronic and Ionic Impact Phenomena (Vol. 3)*. Oxford University Press, New York, 1973.

[35] G. V. Shlyapnikov, J. T. M. Walraven, U. M. Rahmanov, and M. W. Reynolds. Decay Kinetics and Bose-condensation In A Gas of Spin-polarized Triplet Helium. *Physical Review Letters*, 73(24):3247–3250, December 1994.

[36] Oleksij H. Sytenko. *Scattering theory*. Springer series in nuclear and particle physics. Springer, Berlin [u.a.], 1991.

[37] R.G. Newton. *Scattering Theory of Waves and Particles (2nd edition)*. New York: Dover Publications, Inc., 2002.

[38] J.R. Taylor. *Scattering Theory: The Quantum Theory of Nonrelativistic Collisions*. New York: Dover Publications, 2006.

[39] N.F. Mott and H.S.W. Massey. *The theory of atomic collisions (3rd edition)*. Clarendon Press, 1965.

[40] M. Weissbluth. *Atoms and Molecules*. Academic Press New York San Francisco London, 1978.

[41] H. Friedrich. *Theoretische Atomphysik*. Springer Verlag Berlin Heidelberg, 1990.

[42] B.H. Bransden and C.J. Joachain. *Physics of Atoms and Molecules (2nd edition)*. Pearson education limited, 2003.

[43] C.J. Foot. *Atomic Physics*. Oxford University Press, 2006.

[44] F. H. Mies. Molecular Theory of Atomic Collisions - Fine-structure Transitions. *Physical Review A*, 7(3):942–957, 1973.

[45] W. E. Baylis, J. Pascale, and F. Rossi. Polarization and electronic excitation in nonreactive collisions: Basic formulation for quantum calculations of collisions between ^{2}state alkali-metal atoms and h_2 or d_2. *Phys. Rev. A*, 36:4212–4218, Nov 1987.

[46] B. Zygelman, A. Dalgarno, and R. D. Sharma. Molecular theory of collision-induced fine-structure transitions in atomic oxygen. *Physical Review A*, 49(4):2587–2606, April 1994.

[47] W. Demtröder. *Molecular Physics*. Wiley-VCH Verlag, 2005.

[48] A. Dalgarno. New methods for calculating long-range intermolecular forces. In *Advances in Chemical Physics*, pages 143–166. John Wiley & Sons, Inc., 2007.

[49] H. T. C. Stoof, J. M. V. A. Koelman, and B. J. Verhaar. Spin-exchange and dipole relaxation rates in atomic hydrogen: Rigorous and simplified calculations. *Phys. Rev. B*, 38:4688–4697, Sep 1988.

[50] P. S. Julienne and F. H. Mies. Collisions of Ultracold Trapped Atoms. *J. Opt. Soc. Am. B*, 6(11):2257–2269, November 1989.

[51] J. Weiner, V. S. Bagnato, S. Zilio, and P. S. Julienne. Experiments and theory in cold and ultracold collisions. *Reviews of Modern Physics*, 71(1):1–85, January 1999.

[52] E.E. Nikitin and S.Ya. Umanskii. *Theory of Slow Atomic Collisions*. Springer Verlag Berlin Heidelberg, 1984.

[53] Bo Gao. Theory of slow-atom collisions. *Phys. Rev. A*, 54:2022–2039, Sep 1996.

[54] H. A. Bethe. Theory of disintegration of nuclei by neutrons. *Phys. Rev.*, 47:747–759, May 1935.

[55] E. P. Wigner. On the Behavior of Cross Sections Near Thresholds. *Physical Review*, 73(9):1002–1009, 1948.

[56] H. Katori, H. Kunugita, and T.Wal Ido. Quantum-statistical Effect On Ionizing Collisions of Ultracold Metastable Kr Isotopes. *Physical Review A*, 52(6):R4324–R4327, December 1995.

[57] C. Orzel, M. Walhout, U. Sterr, P. S. Julienne, and S. L. Rolston. Spin polarization and quantum-statistical effects in ultracold ionizing collisions. *Physical Review A*, 59(3):1926–1935, March 1999.

[58] R. J. W. Stas, J. M. McNamara, W. Hogervorst, and W. Vassen. Homonuclear ionizing collisions of laser-cooled metastable helium atoms. *Physical Review A*, 73(3):032713, March 2006.

[59] J. M. McNamara, R. J. W. Stas, W. Hogervorst, and W. Vassen. Heteronuclear ionizing collisions between laser-cooled metastable helium atoms. *Phys. Rev. A*, 75:062715, Jun 2007.

[60] Z. Idziaszek and P. S. Julienne. Universal Rate Constants for Reactive Collisions of Ultracold Molecules. *Physical Review Letters*, 104(11):113202, March 2010.

[61] K. Jachymski, M. Krych, P. S. Julienne, and Z. Idziaszek. Quantum Theory of Reactive Collisions for 1/r(n) Potentials. *Physical Review Letters*, 110(21):213202, May 2013.

[62] K. Jachymski, M. Krych, P. S. Julienne, and Z. Idziaszek. Quantum-defect model of a reactive collision at finite temperature. *Physical Review A*, 90(4):042705, October 2014.

[63] C. Greene, U. Fano, and G. Strinati. General form of the quantum-defect theory. *Phys. Rev. A*, 19:1485–1509, Apr 1979.

[64] Chris H. Greene, A. R. P. Rau, and U. Fano. General form of the quantum-defect theory. II. *Phys. Rev. A*, 26:2441–2459, Nov 1982.

[65] F. H. Mies. A Multichannel Quantum Defect Analysis of Diatomic Predissociation and Inelastic Atomic Scattering. *Journal of Chemical Physics*, 80(6):2514–2525, 1984.

[66] F. H. Mies and P. S. Julienne. A Multichannel Quantum Defect Analysis of 2-state Couplings In Diatomic-molecules. *Journal of Chemical Physics*, 80(6):2526–2536, 1984.

[67] Bo Gao, Eite Tiesinga, Carl J. Williams, and Paul S. Julienne. Multichannel quantum-defect theory for slow atomic collisions. *Phys. Rev. A*, 72:042719, Oct 2005.

[68] Bo Gao. General form of the quantum-defect theory for $-1/r^{\alpha}$ type of potentials with α>2. *Phys. Rev. A*, 78:012702, Jul 2008.

[69] James F. E. Croft, Alisdair O. G. Wallis, Jeremy M. Hutson, and Paul S. Julienne. Multichannel quantum defect theory for cold molecular collisions. *Phys. Rev. A*, 84:042703, Oct 2011.

[70] Gerhard Herzberg. *Molecular spectra and molecular structure : 1. Spectra of diatomic molecules*. Krieger, Malabar, Fla., 2. ed., reprint ed. w/corr. [der ausg.] new york 1950, 5. [dr.] edition, 1989.

[71] N. F. Stepanov and Zhilinsk.BI. When and Why Hunds Cases Arise. *Journal of Molecular Spectroscopy*, 52(2):277–286, 1974.

[72] Claude Cohen-Tannoudji, Bernard Diu, and Franck Laloë. *Quantum mechanics : 1*. Wiley [u.a.], New York [u.a.], 1977.

[73] I.I. Sobelman. *Atomic Spectra and Radiative transitions (2nd edition)*. Springer Verlag Berlin Heidelberg New York, 1992.

[74] Wolfgang Demtröder. Atoms, molecules and photons : An introduction to atomic-, molecular- and quantum physics, 2010.

[75] John A. Pople. Nobel lecture: Quantum chemical models. *Rev. Mod. Phys.*, 71:1267–1274, Oct 1999.

[76] W. Kohn. Nobel lecture: Electronic structure of matter—wave functions and density functionals. *Rev. Mod. Phys.*, 71:1253–1266, Oct 1999.

[77] Ira N. Levine. *Quantum chemistry*. Prentice Hall, Upper Saddle River, NJ, 5. ed. edition, 2000.

[78] H. Haken and H.C. Wolf. *Molekuelphysik und Quantenchemie (5. Auflage)*. Springer Verlag Berlin Heidelberg New York, 2006.

[79] F. Jensen. *Introduction to Computational Chemistry (2nd edition)*. John Wiley & Sons, Inc., 2007.

[80] E. E. Salpeter H. A. Bethe. *Quantum mechanics of one- and two-electron atoms*. Plenum Publishing Corporation, New York, 1977.

[81] Claude Cohen-Tannoudji, Bernard Diu, and Franck Laloë. *Quantum mechanics : 2.* Wiley [u.a.], New York [u.a.], 1977.

[82] Edward Uhler Condon and George Shortley. *The theory of atomic spectra*. Cambridge Univ. Press, Cambridge, repr. edition, 1957.

[83] G. W. F. Drake. *Springer handbook of atomic, molecular, and optical physics*. Springer, 2006.

[84] Albert Messiah. *Quantenmechanik : 2.* de Gruyter, Berlin [u.a.], 3., verb. aufl. edition, 1990.

[85] J.C. Slater. The theory of complex spectra. *The Physical Review*, 34:1293–1322, 1929.

[86] E.U. Condon. The theory of complex spectra. *The Physical Review*, 36:1121–1133, 1930.

[87] C. C. J. Roothaan. Self-consistent field theory for open shells of electronic systems. *Rev. Mod. Phys.*, 32:179–185, Apr 1960.

[88] R. McWeeny. *Methods of Molecular Quantum Mechanics*. 1969.

[89] M. W. Schmidt, K. K. Baldridge, J. A. Boatz, S. T. Elbert, M. S. Gordon, J. H. Jensen, S. Koseki, N. Matsunaga, K. A. Nguyen, S. J. Su, T. L. Windus, M. Dupuis, and J. A. Montgomery. General Atomic and Molecular Electronic-structure System. *Journal of Computational Chemistry*, 14(11):1347–1363, November 1993.

[90] Clifford E. Dykstra and Gernot Frenking. Theory and applications of computational chemistry : the first forty years, 2005.

[91] H. Friedrich. *Scattering Theory*. Springer Verlag Berlin Heidelberg, 2013.

[92] C. C. J. Roothaan. New Developments In Molecular Orbital Theory. *Reviews of Modern Physics*, 23(2):69–89, 1951.

[93] John C. Slater. *Quantum theory of molecules and solids : 1. Electronic Structure of Molecules*. McGraw-Hill Book Co., New York [u.a.], 1963.

[94] Marius Gellrich. Vom Di-Atom zum Molekül: Einfache Modelle der paarweisen Wechselwirkung von komplexen Atomen. Bachelor's thesis, Technical University Darmstadt, 2014.

[95] Martin Birkholz. Di-Atomare Molekülzustände und deren Symmetrieeigenschaften. Bachelor's thesis, Technical University Darmstadt, 2015.

[96] J.D. Jackson. *Classical Electrodynamics (3rd edition)*. John Wiley & Sons, Inc., 1999.

[97] E. Steinborn and K. Ruedenberg. Rotation and translation of regular and irregular solid spherical harmonics. *Advances in quantum chemistry*, 7, 1973.

[98] D.M. Brink and G.R. Satchler. *Angular Momentum (2nd edition)*. Clarendon Press, 1968.

[99] Julian K. Knipp. Quadrupole-quadrupole interatomic forces. *Phys. Rev.*, 53:734–745, May 1938.

[100] T. Y. Chang. Moderately Long-range Interatomic Forces. *Reviews of Modern Physics*, 39(4):911–&, 1967.

[101] A. Galindo and P. Pascual. *Quantum mechanics II (2nd edition)*. Springer Verlag Berlin Heidelberg New York, 1989.

[102] Tosio Kato. *Perturbation theory for linear operators*. Classics in mathematics. Springer, Berlin [u.a.], reprint of the 1980 ed., corr. printing of the 2. ed. edition, 1995.

[103] J.J. Sakurei. *Modern Quantum Mechanics*. The Benjamin/Cummings Publishing Company, Inc., 1985.

[104] Hans Albrecht Bethe and Roman W. Jackiw. *Intermediate quantum mechanics*. Advanced book classics. Addison-Wesley, Reading, Mass., 3. ed. edition, 1997.

[105] A. Dalgarno. Sum rules and atomic structure. *Rev. Mod. Phys.*, 35:522, 1963.

[106] M. H. Mittleman and Fred A. Wolf. Coherent scattering of photons by atomic hydrogen. *Phys. Rev.*, 128:2686, 1962.

[107] Albrecht Unsöld. Quantentheorie des Wasserstoffmolekülions und der Born-Landéschen Abstoßungskräfte. *Zeitschrift für Physik*, 43(8):563–574, 1927.

[108] Z. C. Yan, J. F. Babb, A. Dalgarno, and G. W. F. Drake. Variational calculations of dispersion coefficients for interactions among H, He, and Li atoms. *Physical Review A*, 54(4):2824–2833, October 1996.

[109] A. Kramida, Yu. Ralchenko, J. Reader, and and NIST ASD Team. NIST Atomic Spectra Database (ver. 5.3), [Online]. Available: http://physics.nist.gov/asd [2016, October 12]. National Institute of Standards and Technology, Gaithersburg, MD., 2015.

[110] H.N.W. Lekkerkerker, Ph. Coulon, and R. Luyckx. Dispersion forces between closed shell atoms. *Physica A: Statistical Mechanics and its Applications*, 88(2):375 – 384, 1977.

[111] C. Cop. Multichannel scattering theory of atoms with applications. Master's thesis, Technical University Darmstadt, 2012.

[112] B. A. Lippmann and Julian Schwinger. Variational principles for scattering processes. i. *Phys. Rev.*, 79:469–480, Aug 1950.

[113] John B. Conway. *Functions of one complex variable : 1.*, volume 11 of *Graduate texts in mathematics*. Springer, New York [u.a.], 2. ed., 13. print. edition, 2010.

[114] Eberhard Freitag and Rolf Busam. *Complex analysis*. Universitext. Springer, Berlin [u.a.], 2. ed. edition, 2009.

[115] N. Balakrishnan, V. Kharchenko, R.C. Forrey, and A. Dalgarno. Complex scattering lengths in multi-channel atom-molecule collisions. *Chemical Physics Letters*, 280(1-2):5–9, 1997.

[116] J. L. Bohn and P. S. Julienne. Prospects for influencing scattering lengths with far-off-resonant light. *Physical Review A*, 56(2):1486–1491, August 1997.

[117] Jeremy M Hutson. Feshbach resonances in ultracold atomic and molecular collisions: threshold behaviour and suppression of poles in scattering lengths. *New Journal of Physics*, 9(5):152, 2007.

[118] J.T.M. Walraven. *Elements of Quantum Gases: Thermodynamic and Collisional Properties of Trapped Atomic Gases*. Lecture Notes, 2009.

[119] M. Berglund and M.E. Wieser. Isotopic compositions of the elements 2009. *Pure and Applied Chemistry*, 83(1):397–410, January 2009.

[120] Frank L. Pilar. Elementary quantum chemistry, second edition, 2013.

[121] Norma E. Small-Warren and Lue-Yung Chow Chiu. Lifetime of the metastable $^3p_2$ and $^3p_0$ states of rare-gas atoms. *Phys. Rev. A*, 11:1777–1783, Jun 1975.

[122] M. Zinner, P. Spoden, T. Kraemer, G. Birkl, and W. Ertmer. Precision measurement of the metastable P-3(2) lifetime of neon. *Physical Review A*, 67(1):010501, January 2003.

[123] W. A. Goddard and L. B. Harding. Description of chemical bonding from abinitio calculations. *Annual Review of Physical Chemistry*, 29:363–396, 1978.

[124] M. Wang et al. The AME2012 atomic mass evaluation. *Chinese Phys. C*, 36(12), 2012.

[125] F. H. Mies. Molecular Theory of Atomic Collisions - Calculated Cross-sections For H^+ + $F(^2P)$. *Physical Review A*, 7(3):957–967, 1973.

[126] S. J. M. Kuppens, J. G. C. Tempelaars, V. P. Mogendorff, B. J. Claessens, H. C. W. Beijerinck, and E. J. D. Vredenbregt. Approaching Bose-Einstein condensation of metastable neon: Over 10^9 trapped atoms. *Phys. Rev. A*, 65:023410, Jan 2002.

[127] van Drunen. *Collisional interactions between metastable neon Atoms*. PhD thesis, TU Darmstadt, Germany, 2008.

[128] Z. C. Yan and J. F. Babb. Long-range interactions of metastable helium atoms. *Physical Review A*, 58(2):1247–1252, August 1998.

[129] P. J. Leo, V. Venturi, I. B. Whittingham, and J. F. Babb. Ultracold collisions of metastable helium atoms. *Physical Review A*, 64(4):042710, October 2001.

[130] B. Numerov. A method of extrapolation of perturbations. *Monthly notices of the Royal Astronomical Society*, 84:592–601, 1924.

[131] B. Numerov. Note on the numerical integration of $d^2x/dt^2 = f(x,t)$. *Astron. Nachrichten*, 230:359–364, 1927.

[132] John M. Blatt. Practical points concerning the solution of the Schrödinger equation. *Journal of Computational Physics*, 1:382–396, 1967.

[133] A.C. Allison. The numerical solution of coupled differential equations arising from the Schrödinger equation. *Journal of Computational Physics*, 6:378–391, 1970.

[134] B.R. Johnson. The multichannel log-derivative method for scattering calculations. *Journal of Computational Physics*, 13:445–449, 1973.

[135] B.R. Johnson. New numerical methods applied to solving the onedimensional eigenvalue problem. *The Journal of Chemical Physics*, 67(4086), 1977.

[136] B.R. Johnson. The renormalized Numerov method applied to calculating bound states of the coupledchannel Schrödinger equation. *The Journal of Chemical Physics*, 69(4678), 1978.

[137] A. S. Dickinson. Quantum reflection model for ionization rate coefficients in cold metastable helium collisions. *Journal of Physics B-atomic Molecular and Optical Physics*, 40(16):F237–F240, August 2007.

[138] H. Shull and G.G. Hall. Atomic units. *Nature*, 184(4698):1559–1560, November 1959.

[139] P.J. Mohr, D.B. Newell, and B.N. Taylor. CODATA Recommended Values of the Fundamental Physical Constants: 2014. *45*, 45(043102), 2016.

[140] M.E. Rose. *Elementary theory of angular momentum*. John Wiley & Sons, Inc., 1961.

[141] A.R. Edmonds. *Angular momenta and quantum mechanics*. Princeton University Press, 1960.

[142] H. A. Jahn and J. Hope. Symmetry properties of the wigner 9j symbol. *Phys. Rev.*, 93:318–321, Jan 1954.

[143] R. J. Ord-Smith. The symmetry relations of the 12j symbol. *Phys. Rev.*, 94:1227–1228, Jun 1954.

[144] E.P. Wigner. *Group theory and its applications to the quantum mechanics of atomic spectra*. Academic Press New York and London, 1959.

[145] Lawrence C. Biedenharn and James D. Louck. *Angular momentum in quantum physics : theory and application*, volume 8 of *Encyclopedia of mathematics and its applications*. Addison-Wesley, Reading, Mass. [u.a.], 1981.

[146] George N. Watson. *A Treatice on the Theory of Bessel Functions*. Cambridge University Press, Cambridge, 1958.

[147] Edmund T. Whittaker and George N. Watson. *A course of modern analysis : an introduction to the general theory of infinite processes and of analytical functions*. Cambridge mathematical library. Cambridge Univ. Press, Cambridge, 4th ed., repr. edition, 2004.

LIST OF PUBLICATIONS

- C. Cop, A. Martin, G. Birkl and R. Walser,
  Cold collisions of metastable neon atoms,
  to be published

- C. Cop and R. Walser,
  Two-body loss rates for reactive collisions of cold atoms,
  to be published

- J. Schütz, A. Martin, S. Altenburg, C. Cop, R. Walser and G. Birkl,
  Zeeman state dependence of ionizing collision rates in metastable neon,
  to be published

CONFERENCE CONTRIBUTIONS AND RESEARCH VISITS

CONFERENCE CONTRIBUTIONS

- **Talk**,
  Effective two-channel model for cold reactive collisions,
  DPG Frühjahrstagung, Mainz, Germany, 2017
- **Poster**,
  Two-channel model for cold collisions of metastable neon atoms,
  12th European Conference on Atoms Molecules and Photons, Frankfurt, Germany, 2016
- **Talk**,
  Two-channel model for cold collisions of metastable neon atoms,
  DPG Frühjahrstagung, Hannover, Germany, 2016
- **Talk**,
  Two-channel model of Penning ionization of cold metastable neon atoms,
  DPG Frühjahrstagung, Heidelberg, Germany, 2015
- **Poster**,
  Cold atomic collisions of metastable neon atoms,
  DPG Frühjahrstagung, Berlin, Germany, 2014
- **Poster**,
  Atomic scattering of metastable neon atoms,
  DPG Frühjahrstagung, Stuttgart, Germany, 2012

RESEARCH VISITS

- **National Institute of Standards and Technology (NIST)**, U.S. Department of Commerce,
  Gaithersburg, USA, supervisor: Eite Tiesinga,
  March 25–April 05, 2013
- **National Institute of Standards and Technology (NIST)**, U.S. Department of Commerce,
  Gaithersburg, USA, supervisor: Eite Tiesinga,
  January 20–February 6, 2015

SUPERVISED THESES

- Martin Birkholz,
  Di-Atomare Molekülzustände und deren Symmetrieeigenschaften,
  Bachelorthesis, Oktober 2015
- Marius Gellrich,
  Vom Di-Atom zum Molekül: Einfache Modelle der paarweisen Wechselwirkung von komplexen Atomen,
  Bachelorthesis, Januar 2014

DANKSAGUNG

An dieser Stelle danke ich allen, die zum Entstehen und Gelingen dieser Arbeit beigetragen haben:

Zuvorderst geht mein Dank an *Herrn Prof. Dr. Walser*, der mir die tolle Möglichkeit bot, an der Forschung zur Streutheorie, den kalten atomaren Stößen und nicht zuletzt an einer spannenden Kollaboration mit den Experimentatoren teilzuhaben. Sehr zu schätzen weiß ich neben der alltäglichen persönlichen Betreuung, den Hilfestellungen und den Korrekturvorschlägen auch die Möglichkeit des regelmäßigen Austauschs mit der experimentellen Gruppe. Des Weiteren bedanke ich mich für die Gelegenheiten, an internationalen Konferenzen teilnehmen zu können und für die gemeinsamen Gastaufenthalte am NIST in Gaithersburg, die für mich starke, positive Eindrücke hinterließen. Nicht zuletzt bedanke ich mich für die Unterstützung und das immer offene Ohr für alle Themen auch abseits universitärer Belange.

Bedanken möchte ich mich bei *Herrn Prof. Dr. Birkl* für die Gelegenheit direkt mit der experimentellen Gruppe arbeiten zu können und für die unzähligen gemeinsamen Treffen zum Neon-Projekt, die sehr aufschlussreich waren und wesentlich zum Fortschritt dieser Arbeit beitrugen. Bedanken möchte ich mich auch hier für die sehr angenehme Atmosphäre, in der all diese Treffen stattfanden sowie für die Bereitschaft, das Zweitgutachten für diese Arbeit anzufertigen.

I am grateful to *Mr. Prof. Dr. Tiesinga* who invited and welcomed us warmly for two times at the National Institute of Standards and Technology in Gaitherburg. During our stays *Mr. Prof. Dr. Tiesinga* was always available for discussions of physics and in particular of scattering physics and aspects of cold collisions. These discussions were always very helpful and had a big impact on the progress of this thesis. Furthermore, I thank *Mr. Prof. Dr. Tiesinga* for providing us with the *close-coupling code*. I am also thankful to *Ms. Prof. Dr. Kotochigova*, *Mr. Prof. Dr. Julienne* und *Mr. Prof. Dr. Williams* for the many fruitful discussions and in particular to *Ms. Prof. Dr. Kotochigova* for providing us with the molecular interaction potentials for Ne*.

Mein Dank geht an *Jan Schütz* und *Alexander Martin*, die in jahrelanger intensiver Arbeit die Daten zu Neon zusammentrugen, in den Diskussionen immer hilfsbereit zur Seite standen und mit denen ich sehr gerne zusammenarbeitete.

Ich bedanke mich bei der *Arbeitsgruppe Walser* für die angenehme Arbeitsatmosphäre. Insbesondere danke ich *Johannes Battenberg*, *Oliver Gabel* und *Srihari Srinivasan* die sehr viel Zeit investierten, den anderen Mitgliedern ein funktionierendes Netzwerk bereitzustellen. Bei allen Fragen zu Backup-, LDAP-, Server-Einrichtung wurde ich jederzeit und tatkräftig unterstützt.

Ich danke *Frau Christine Schütze*, die trotz zeitweiliger Doppel-Belastung der Betreuung zweier Arbeitsgruppen immer gut gelaunt für eine nette Arbeitsatmosphäre sorgte und maßgeblich daran beteiligt war, dass immer alles funktionierte.

Ich danke *Franziska Friedrich*, *Antje Neumann*, *Oliver Gabel*, *Matthias Hansli*, *Srihari Srinivasan*, *Martin Sturm*, *Roman Sulzbach* und *Jan Teske* für Ihre Anmerkungen zu den Korrekturtätigkeiten an dieser Arbeit.

Ich bedanke mich bei meiner Freundin *Michèle Klein* für ihre Geduld, Unterstützung und großen Rückhalt während des Anfertigens dieser Arbeit.

Last but not least bedanke ich mich bei meiner Familie: Ich danke meinem Vater *Fryderyk Cop*, meiner Mutter *Hedwig Cop*, meiner Schwester *Angelika Cop* und meinem Onkel *Martin Cop*. All diese Personen haben mich seit jeher in allen Lebenslagen und Lebensbelangen gefördert, beraten und unterstützt. Im Wissen darum schätze ich mich sehr glücklich.

DECLARATION

Hiermit versichere ich, die vorliegende Dissertation ohne Hilfe Dritter, nur mit den angegebenen Quellen und Hilfsmitteln angefertigt zu haben. Alle Stellen, die aus Quellen entnommen wurden, sind als solche kenntlich gemacht. Diese Arbeit hat in gleicher oder ähnlicher Form noch keiner Prüfungsbehörde vorgelegen.

Darmstadt, 18. April 2017

Christian Cop